GAS TRANSPORT PROPERTIES IN POLYCARBONATE

INFLUENCE OF THE COOLING RATE, PHYSICAL AGING, AND ORIENTATION

by

Christelle M. Laot

Dissertation submitted to the Faculty of the

Virginia Polytechnic Institute and State University

in partial fulfillment of the requirements for the degree of

Doctor of Philosophy

in

Chemical Engineering

Dr. Eva Marand, Chair

Dr. Richey M. Davis

Dr. Hervé Marand

Dr. Ravi Saraf

Dr. Garth L. Wilkes

October 17th, 2001

Blacksburg, Virginia

Keywords: polycarbonate, gas transport, free volume, permeation, permeability, solubility, diffusion, cooling rate, physical aging.

GAS TRANSPORT PROPERTIES IN POLYCARBONATE

INFLUENCE OF THE COOLING RATE, PHYSICAL AGING, AND ORIENTATION

Christelle M. Laot
Department of Chemical Engineering
Virginia Polytechnic Institute and State University
Blacksburg, VA 24061-0211

ABSTRACT

The objective of this research work was to understand the molecular mechanism of gas transport through amorphous glassy polymers. Especially, emphasis was placed on determining whether or not gas transport in amorphous glassy polymers is directly correlated with the free volume content. Free volume arguments are indeed commonly used to explain the gas transport process.

The gas transport properties of bisphenol-A polycarbonate films were examined as a function of the cooling rate, physical aging, and orientation. Such conditions affect the free volume content and its size and shape distribution. Results obtained from permeation experiments were accompanied with dynamic mechanical and density measurements.

The experimental results suggest that the diffusion coefficient of small gas molecules in glassy polycarbonate is influenced by the local dynamics or mobility of the polymer chains rather than by the overall free volume content. Indeed, the diffusion coefficient of N_2 for instance was reduced in fast-cooled samples, despite of the fact that those samples possessed a greater overall free volume content. Fast cooling rates may generate highly restricted conformations which hinder local motions, and therefore tend to increase the activation energy of diffusion. As expected, the greater the free volume content, the greater was the solubility coefficient. The increase in the polymer relaxation times with aging time is believed to restrict the local chain motions, leading to enhanced activation energies of diffusion, and therefore to reduced diffusion coefficients. The change in the solubility coefficients with physical aging revealed that the aging process

might not affect all the cavity sizes in polycarbonate equally. According to free volume arguments, one would anticipate that the physical aging of fast-cooled samples (which possess more free volume) should be enhanced compared to that of slowly-cooled samples. Quite interestingly, the decrease in the diffusion coefficient with aging was found to occur much slower in fast-cooled samples, despite of the higher initial free volume content. In contrast, properties directly related to the free volume content, such as density or isothermal DMTA measurements actually showed a greater aging rate in the sample containing the greatest amount of free volume. Slow-cooled samples that are in a low energy conformational state may loose their internal degrees of freedom more rapidly, due to the closer interchain packing and the possibly restricted segmental motions. Studies dealing with orientation and gas transport were complicated by several factors. For instance the fact that the permeation experiments were performed perpendicularly to the orientation of the chains and not along the orientation axis limited the sensitivity of the gas transport properties to orientation.

This work points out that dynamic rather than static models should be developed to predict the gas transport phenomenon.

Acknowledgments

I would like to thank the following people for their help and support in conducting this research:

- Dr. Eva Marand, my advisor at Virginia Tech, for her support throughout the five years I have spent in the United States. I acknowledge Dr. Marand's efforts to provide the funding for this research project. I have especially appreciated the freedom she gave me to perform the research that interested me, and to allow me to finish my dissertation in Europe.
- Dr. Chris Cornelius for his many excellent comments and suggestions, for his continuing interest in this research project, and most of all for his friendship.
- Dr. Richey M. Davis, Dr. Hervé Marand, Dr. Ravi Saraf, and Dr. Garth L. Wilkes for all their constructive critique which helped me to improve my work.
- I thank all other colleagues and fellow students who have to remain unnamed here.

I owe much to Bayer AG (Leverkusen, Germany) for giving me the opportunity of working as a research scientist in polymer physics. They put their trust in me before I received the doctorate.

Finally I would like to thank the following people:

- My friends, especially Xianqin, for all their encouragements and friendship.
- My parents and my brothers Philippe and Gérald for their support and love throughout my studies over the years.
- Thomas for his support, encouragements, patience, and love while writing this dissertation.

Table of Contents

List of Figures

Chapter 1

Chapter 2

Chapter 3

Chapter 4

Chapter 5

Chapter 6

Chapter 7

Chapter 8

List of Tables

Chapter 4

Chapter 5

Chapter 6

Chapter 7

Chapter 8

Chapter 1

Introduction

1.1. Motivation and objectives

Polymers come into contact with gases in several applications such as packaging, polymer processing, production of foam, protective coatings, contact lenses, sensors, gas separations using non-porous polymeric membranes, etc [1-4]. Therefore there is a need to understand gas transport through polymers. For instance, polymers used for carbonated beverages should be capable of keeping carbon dioxide inside the bottle and at the same time be permeable to oxygen. While both high permeability and high permselectivity are necessary for polymeric membranes used in gas separations, an enhancement of one of the parameters commonly results in a decrease in the other parameter, and vice-versa. The chemical structure / permeation properties are not straightforward and the development of a suitable glassy polymeric membrane for a given application is still, to a large extent, empirical. Once the gas transport phenomenon is better understood, predictive tools may be further developed to select or create appropriate polymers.

Gas transport properties are defined by three transport coefficients, which are the permeability, solubility, and diffusion coefficients. The permeability coefficient P indicates the rate at which a permeant traverses a membrane. It corresponds to the product of the solubility coefficient and the diffusion coefficient. The solubility coefficient S is a measure of the amount of gas sorbed by the membrane when

equilibrated with a given pressure of gas at a particular temperature. It is a thermodynamic parameter that is believed to be dependent on the amount of free volume, on the condensability of the penetrant, and on the degree to which the permeant interacts with the polymeric matrix. The diffusion coefficient D indicates how fast a penetrant is transported through the membrane. It is a kinetic parameter, which is related to the polymer chain mobility or flexibility and to that of the permeant. D is also believed to relate to the free volume content, as apparent from the correlations showing an increase in the diffusion coefficient with an increase in the free volume content [5-10].

Emphasis is usually placed on developing new materials for gas separation applications. Structure-property relationships are studied for those new materials. However, the trends seen for a family of polymers may be different for a particular polymer with different thermal histories. Therefore, studies have to be conducted in order to understand how the gas transport properties are affected by morphology, free volume, orientation, thermal processing history, degree of crystallization, types of crystallites, annealing, composition, defects, cross-linking, temperature, molecular weight, molecular weight distribution, etc. Gas transport is expected to be highly complicated by the presence of the crystalline domains, which add a tortuosity factor to the gas diffusion process. As a consequence, this study will be focused on the amorphous state only.

Gas transport through amorphous glassy polymers is commonly explained from the free volume concept point of view [4-9, 11-16]. The free volume present in polymers can be visualized as dynamic microvoids or holes, with a distribution of sizes and shapes, dispersed inside the polymeric matrix. One would expect that as the free volume content increases, the permeability and the diffusion coefficients increase, and that the activation energies of permeation and diffusion decrease. Actually, this trend summarized in Figure 1.1 has been verified in the literature for amorphous glassy polymers with different structures [10, 11]. Nevertheless, with some deeper thinking, one may also wonder whether or not gas transport through amorphous glassy polymers is directly related to the amount of free volume for a particular polymer at given conditions. Indeed, two samples of the same polymer may possess the same free volume content, but completely different

free volume distributions, as sketched in Figure 1.2. This should lead to significant differences in the properties of the material. Furthermore the way the free volume is arranged in the matrix may allow or prevent molecular motions.

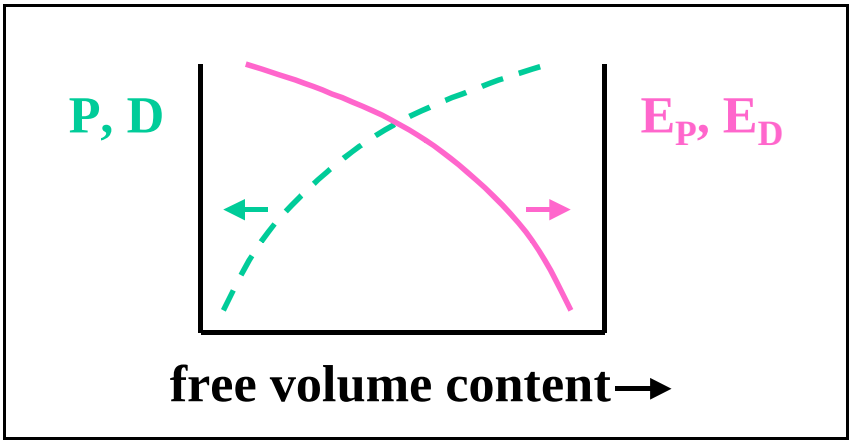

Figure 1.1: Trends reported in the literature for polymers with different structures. As the free volume content increases, P and D increase, and E_P and E_D decrease.

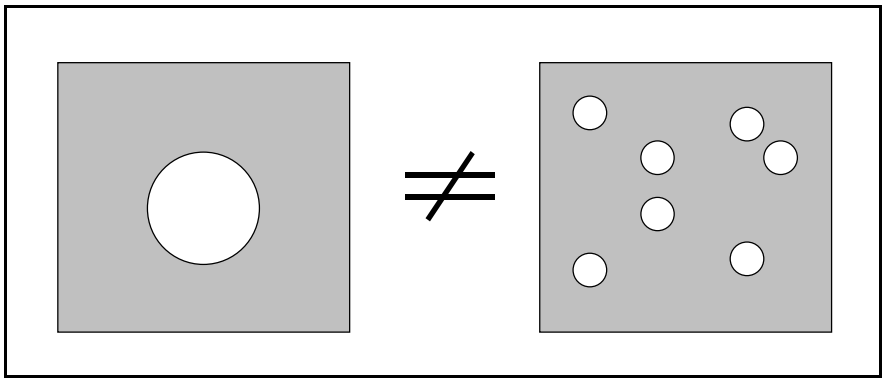

Figure 1.2: Schematic showing that two specimens can have the same free volume content, but completely different distributions. For instance, a volume of 21cm^3 can be represented by 1 hole of 21cm^3, or by 7 holes of 3cm^3 each.

In order to answer the question as to whether or not gas transport in polymers is directly correlated with the free volume content, three polymer physical parameters were picked. Those parameters were chosen as:

- the cooling rate,
- physical aging,
- and orientation.

The above parameters should affect the free volume content and its distribution, and hopefully provide an answer to the central question of this research, which is to understand the molecular mechanism of gas transport through amorphous glassy polymers (see Figure 1.3). The same phenomena should indeed govern gas transport in different types of samples (freshly processed / physically aged / oriented).
From the polymer film applications point of view, it is important to understand the molecular aspects of polymer physical aging and orientation. This can be achieved by using inert gases with different kinetic diameters in order to probe the free volume of polymers.

As the focus of this research project is on the amorphous state, a polymer which does not readily crystallize under normal conditions and under hydrostatic pressure, and which does not show any signs of strain-induced crystallization had to be selected. A commercial 34,000g/mol weight average molecular weight of bisphenol-A polycarbonate was chosen in this research. In addition, polycarbonate is a polymer of major importance because of its transparency, toughness, thermal stability, and low birefringence. It has found applications in optical data storage, plastic bottles, and is used in electric, automotive, and architectural industries.

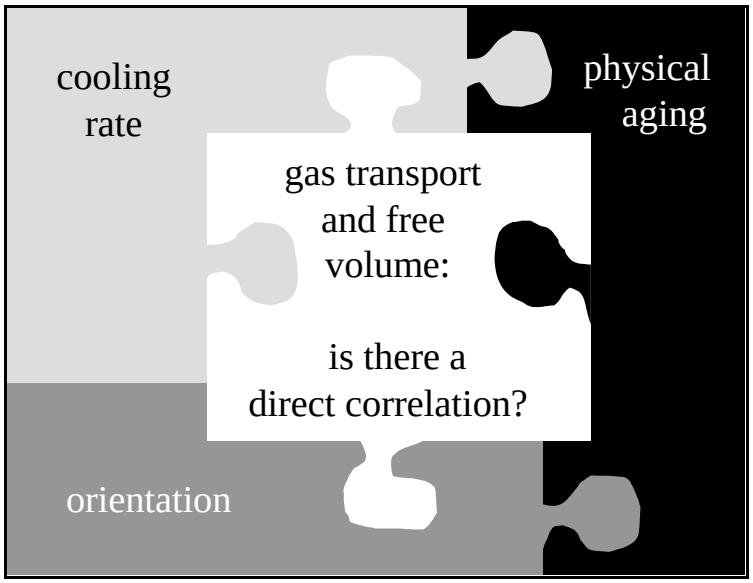

Figure 1.3: Puzzle showing the strategy adopted in this research to solve the research objective.

1.2. Proposal

Specifically, here are the questions that tried to be answered in this research work:

1. What is the effect of the free volume on gas transport in freshly processed polycarbonate?

The transport of gas molecules through dense polymers is believed to be due to the thermal motion of the polymer chains facilitated by the presence of free volume in the material. This free volume originates from imperfect packing in the material. One would expect that the greater the amount of free volume in a freshly processed polymer, the more permeable is the material, and the lower are the activation energies. Nevertheless this trend commonly observed for the transport of gas molecules through various glassy polymer families or classes [10, 11] has to be confirmed for the gas transport process through a particular polymer with different amounts of free volume. Although the diffusion coefficient should really indicate a measure of the polymer chain mobility, it is often related to the free volume content of the materials [4, 11, 13-15]. Theories have been developed to relate the increase in the diffusion coefficient to the increase in the free volume content [5-9]. Nevertheless the experimental results originated from studies carried out on polymer families and need to be confirmed for a particular polymer at given conditions. The two parameters that are the diffusion coefficient and the free volume may not be directly correlated. The free volume content and its distribution in freshly processed polycarbonate can be varied by changing the cooling rate from the liquid state for instance.

2. What is the effect of physical aging on gas transport?

The excess free volume trapped in glassy polymers is at the origin of the non-equilibrium nature of the glassy state. The time-dependent structural changes affect any property that is a function of molecular mobility [17-27]. The behavior of polymeric materials with time is an important parameter to consider for future industrial

applications. Polymeric membranes used for gas separation for instance should have a long durability, otherwise the process may not be economically better than other separation processes.

The effects of physical aging on the gas transport properties have been reported in the literature [28-35]. The gas transport parameters (P, D, and S) were generally observed to decrease with aging, and the difference was attributed to the loss of free volume with annealing. However, most of the published data were complicated by several factors: conditioning, samples used as-received or cast from solution, plasticization induced by carbon dioxide, and sorption experiments themselves. New studies free of the above factors should be conducted in order to confirm the trends reported in the literature. Determining how the relative permeability coefficients between two gases, or the permselectivity, is affected by aging is crucial in food packaging or gas separation for instance, as one gas may be desired and another one not. Ideally, the separation properties of polymer films should not change with time in order to insure good durability of the polymer films.

However, there still remains some unanswered questions, such as which cavity sizes are more likely to be affected by the aging phenomena. Contradictions can be found in the literature about the changes in the cavity sizes of polycarbonate with aging. According to small angle X-ray scattering (SAXS) results [36], although the amount of free volume in polycarbonate decreases with aging at sub-T_g annealing temperatures below the glass transition range, the average free volume hole size increases. In contrast, positron annihilation lifetime spectroscopy (PALS) studies of physical aging found that on aging at temperatures below the glass transition range, the holes in polycarbonate did not decrease in size but in number [37-42]. Similar conclusions were reached by studying physical aging in polycarbonate with photochromic probes [43].

Probing the free volume with gas molecules of different sizes can give information on the structural scale of changes occurring during physical aging. Gas permeation can be used as a tool to probe the free volume of polymeric materials. Gas molecules with different kinetic diameters can be used to access the size of the microvoids.

3. What is the effect of orientation on gas transport?

Commercial polymeric films are often oriented to some extent due to the processing techniques. There is therefore a need to investigate the influence of molecular orientation of amorphous glassy polymers on gas transport.

The literature is relatively sparse on the effect of molecular orientation on the gas transport properties of amorphous glassy polymers. The few papers [44-48] dealing with this subject are most of the time complicated by the presence of strain-induced crystallinity in the polymeric samples. The various results suggest that the influence of orientation on the gas transport parameters is rather complex. Especially, a polymer that does not show any signs of strain-induced crystallization has to be selected in order to isolate the effect of the amorphous orientation only. Moreover, gases that do not induce any plasticization effects have to be chosen.

When aging studies are conducted on uniaxially oriented amorphous glassy polymers, volume relaxation is enhanced by one order of magnitude in both cold- and hot-drawn samples, despite of the much higher density [49-55]. These results suggest that the concept of free volume commonly used to provide a physical picture of physical aging [18] may not be adequate. According to the free volume theory, a higher density should result in a lower mobility, and thus in a lower aging rate. Instead, enhancement of physical aging is observed in oriented polymers. Another order parameter, such as the distribution of free volume, or degree of short-range structural order, as well as the shape of the holes, or even the polymer chain dynamics, may be also important in determining the mechanical properties of glassy materials.

The effects of orientation on polymer physical aging and the corresponding gas transport properties of polymers have not been examined in the literature. Using gas transport to probe the free volume of polymers should provide information on how physical aging is affected by orientation from a molecular point of view.

1.3. Outline

The dissertation has been written as a collection of chapters which deal with the research objectives previously stated.

The first chapters provide a critical background about the subjects treated in the research work. Chapter 2 offers a background on gas transport. The transport parameters are explained, and the influence of the polymer structure on gas transport is discussed. Gas sorption and permeation experiments are also presented. In Chapter 3, backgrounds about physical aging and orientation are first given, before discussing the work that has been reported in the literature about gas transport and physical aging, and gas transport and orientation, respectively.

The experimental details are provided in Chapter 4.

The research results are then presented and discussed in the following chapters. Pertinent literature reviews are provided in those chapters whenever needed. Note that the use of “we” will then be seen throughout those chapters since the chapters dealing with experimental results do correspond to manuscripts. Chapter 5 tries to answer the question of whether or not the gas transport of gas molecules through polymers is directly related to the amount of free volume by comparing two commercial grades of polycarbonates obtained from two different suppliers. Chapter 6 deals with the effect of the cooling rate on the gas transport properties of polycarbonate. Chapter 7 investigates how physical aging in polycarbonate is revealed by gas transport measurements. The influence of the cooling rate on the physical aging rate is also discussed. The effect of orientation on the transport of gas molecules through amorphous glassy bisphenol-A polycarbonate is reported in Chapter 8.

Finally, the results obtained in this research are summarized in the last chapter and suggestions are given for future research work.

1.4. References

1. X. Wang and H. G. Spencer, Polymer Membranes for Use in Food Processing, *TRIP*, 5, 2, 38 (1997).
2. W. J. Koros and R. T. Chern, Separation of Gaseous Mixtures using Polymer Membranes, *Handbook of Separation Process Technology*, edit. R. W. Rousseau, (1987).
3. K. Ghosal and B. D. Freeman, Gas Separation Using Polymer Membranes: An Overview, *Polymer for Advanced Technologies*, 5, 673-697 (1994).
4. D. R. Paul, Yuri P. Yampol'skii, editors, *Polymeric gas separation membranes*, CRC Press, Boca Raton, 1994.
5. J. L. Duda and J. M. Zielinski, Free-Volume Theory, *Plastics Engineering*, 32, 143 (1996).
6. M. H. Cohen and D. Turnbull, *J. Chem. Phys.*, 31, 1164 (1959).
7. J. S. Vrentas and J. L. Duda, *J. Polym. Sci.*, 15, 403 (1977).
8. J. S. Vrentas and J. L. Duda, *J. Polym. Sci.*, 15, 417 (1977).
9. H. Fujita, *Fortschr. Hochpolym. Forsch.*, 3, 1 (1961).
10. Y. Yampolskii, S. Shishatskii, A. Alentiev, K. Loza, Correlations with and prediction of activation energies of gas permeation and diffusion in glassy polymers, *Journal of Membrane Science*, 148, 59-69 (1998).
11. J. Y. Park, D. R. Paul, Correlation and prediction of gas permeability in glassy polymer membrane materials via a modified free volume based group contribution method, *Journal of Membrane Science*, 125, 23-39 (1997).
12. W. M. Lee, Selection of barrier materials from molecular structure, *Polym. Eng. Sci.*, 20, 65-69 (1980).
13. Y. Kobayashi, K. Haraya, S. Hattori, *Polymer*, 35, 925-928 (1994).
14. S. Trohalaki, L. C. DeBolt, J. E. Mark, H. L. Frisch, *Macromolecules*, 23, 813-816 (1990).
15. Y. Maeda and D. R. Paul, Effect of AntiPlasticization on Gas Sorption and Transport. III. Free Volume Interpretation, *Journal of Polymer Science: Part B: Polymer Physics*, 25, 1005 (1987).
16. A. Thran, G. Kroll, F. Faupel, Correlation between fractional free volume and diffusivity of gas molecules in glassy polymers, *Journal of Polymer Science: Part B: Polymer Physics*, 37, 3344-3358 (1999).
17. J. M. Hutchinson, Physical aging of polymers, *Prog. Polym. Sci.* , 20, 703 (1995).
18. L. C. E. Struik, Physical aging in amorphous polymers and other materials, Elsevier, New York, 1978.
19. M. R. Tant and G. L. Wilkes, An overview of the nonequilibrium behavior of polymer glasses, *Polymer Engineering and Science*, 21, 14, 874 (1981).
20. J. M. Hutchinson, Relaxation processes and physical aging, in The Physics of Glassy Polymers, edited by R. N. Haward and R. J. Young, Chapman & Hall, London, 1997.
21. R. P. Chartoff, Thermoplastic polymers, in Thermal characterization of polymeric materials, E. A. Turi, edt, Academic Press, NY, 548-573 (1997).

22. L. C. E. Struik, Aging, Physical, *Encyclopedia of Polymer Science and Engineerin*g, vol 1, 595-611, Wiley, NY (1985).
23. J. M. O'Reilly, Review of structure and mobility in amorphous polymers, *CRC critical reviews in solid state and materials sciences*, 13, 3, 259-277 (1987).
24. J. Mijovic, L. Nicolais, A. D'Amore, J. M. Kenny, Principal features of structural relaxation in glassy polymers- A review, *Polymer Enginering and Science*, 34, 5, 381 (1994).
25. S, Matsuoka, Free volume, excess entropy and mechanical behavior of polymeric glasses, *Polymer Engineering and Science*, mid-october, 21, 14, 907-921 (1981).
26. J.-C. Bauwens, Physical aging: relation between free volume and plastic deformation, in Failure of plastics, W. Brostow and R. D. Corneliussen, edts, Hanser Publishers, Munich (1986).
27. L. C. E. Struik, Physical aging: influence on the deformation behavior of amorphous polymers, in Failure of plastics, W. Brostow and R. D. Corneliussen, edts, Hanser Publishers, Munich (1986).
28. H. Hachisuka, H. Takizawa, T. Tsujita, A. Takizawa, T. Kinoshita, gas transport properties in polycarbonate films with various unrelaxed volumes, *Polymer*, 32, 13, 2383 (1991).
29. A. H. Chan and D. R. Paul, Effect of sub-Tg annealing on CO_2 sorption in polycarbonate, *Polymer Enginering and Science*, 20, 1, 87 (1980).
30. H. Hachisuka, Y. Tsujita, A. Takizawa, T. Kinoshita, Gas transport properties of annealed polyimide films, *Journal of Polymer Science: Part B: Polymer Physics*, 29, 11 (1991).
31. K. Toi, T. Ito, I. Ikemoto, Effect of aging and conditioning on the gas transport of poly(vinyl acetate), *Journal of Polymer Science: Polymer Letters Edition*, 23, 525-529 (1985).
32. K. Nagai, T. Nakagawa, Effects of aging on the gas permeability and solubility in poly(1-trimethylsilyl-1-propyne) membranes synthetized with various catalysts, *Journal of Membrane Science*, 105, 261-272 (1995).
33. Von K.-H. Illers, Einfluss der thermischen Vorgeschichte auf die Eigenschaften von Polyvinylchlorid, *Die Makromolekulare Chemie*, 127, 3032, 1-33 (1969).
34. T. Nakagawa, T. Watanabe, M. Mori, K. Nagai, Aging phenomena of gas permeability of poly[1-(tri-methylsilyl)-1-pripyne] and its blend polymer, *Polym. Mater. Sci. Eng.*, 77, 249 (1997).
35. H. Hachisuka, K. Kito, Y. Tsujita, A. Takizawa, T. Kinoshita, O_2 and N_2 gas permselectivity of alternating copoly(vinylidene cyanide-vinyl acetate), *Journal of Applied Polymer Science*, 35, 1333 (1988).
36. J. J. Curro and R.-J. Roe, Isothermal relaxation of specific volume and density fluctuation in poly(methyl methacrylate) and polycarbonate, *Polymer*, 25, 1424 (1984).
37. A. J. Hill, I. M. Katz and P. L. Jones, Isothermal volume relaxation in aged polycarbonate measured by positron annihilation lifetime spectroscopy, *Polymer Enginering and Science*, 30, 13, 762 (1990).
38. T. C. Sandreczki, X. Hong, and Y. C. Jean, Sub-glass-transition-temperature annealing of polycarbonate studied by positron annihilation spectroscopy, *Macromolecules*, 29, 4015-4018 (1996).

39. A. J. Hill, C. M. Agrawal, Positron lifetime spectroscopy characterization of thermal history effects on polycarbonate, *Journal of Materials Science*, 25, 5036-5042 (1990).
40. J. E. Kluin, H. Moaddel, M. Y. Ruan, Z. Yu, A. M. Jamieson, R. Simha, J. D. McGervey, Probe spectroscopy, free volume concepts, and physical aging of polymer glasses, in Structure-property relations in polymers: spectroscopy and performance, ACS, 236, 535-555 (1993).
41. T. C. Sandreczki, X. Homg, and Y. C. Jean, Sub-glass-transition temperature annealing of polycarbonate studied by positron annihilation spectroscopy, *Macromolecules*, 29, 4015-4018 (1996).
42. J. E. Kluin, Z. Yu, S. Vleeshouwers, J. D. McGervey, A. M. Jamieson, R. Simha, Temperature and time dependence of free volume in bisphenol A polycarbonate studied by positron lifetime spectroscopy, *Macromolecules*, 25, 19, 5089 (1992).
43. J. S. Royal and J. M. Torkelson, Photochromic and fluorescent probe studies in glassy polymer matrices. 5. Effects of physical aging on bisphenol-A polycarbonates and poly(vinyl acetate) as sensed by a size distribution of photochronic probes, *Macromolecules*, 25, 4792 (1992).
44. L. H. Wang, R. S. Porter, On the CO2 permeation of uniaxially drawn polymers, *Journal of Polymer Science: Polymer Physics Edition*, 22, 1645-1653 (1984).
45. M. D. Shelby, G. L. Wilkes, M. R. Tant, J. Zawada, T. J. Bastow and A. J. Hill, Amorphous orientation in glassy polycarbonate, *ACS, Polymeric Materials Science and Engineering, Conference Proceedings*, San Francisco, Spring 1997, 76, 485-6.
46. T. L. Smith and R. E. Adam, Effect of tensile deformations on gas transport in glassy polymer films, *Polymer*, 22, 299-304 (1981).
47. N. Yu. Muzovskaya and A. Ya. Malkin, Influence of orientation on the diffusion characteristics of polycarbonate, *Polymer Science USSR*, 27, 12, 2950-2954 (1985).
48. M. J. El-Hibri and D. R. Paul, Effects of uniaxaial drawing and heat-treatment on gas sorption and transport in PVC, *Journal of Applied Polymer Science*, 30, 3649-3678 (1985).
49. J. Bartos, J. Muller, J. H. Wendorff, Physical ageing of isotropic and anisotropic polycarbonate, *Polymer*, 31, 1678 (1990).
50. M. D. Shelby and G. L. Wilkes, Thermodynamic characterization of the oriented state of bisphenol A polycarbonate as it pertains to enhanced physical aging, *Journal of Polymer Science: Part B: Polymer Physics*, 36, 2111 (1998).
51. R. Pixa, B. Grisoni, T. Gay, and D. Froelich, Influence of deformation on physical aging of polycarbonate- 2 - Volume recovery near ambient temperature, *Polymer Bulletin*, 16, 381-387 (1986).
52. M.-S. S. Wu, Intrinsic birefringence of amorphous poly(bisphenol-A carbonate), *Journal of Applied Polymer Science*, 32, 3263-3275 (1986).
53. M. D. Shelby and G. L. Wilkes, The effect of molecular orientation on the physical ageing of amorphous polymers - dilatometric and mechanical creep behaviour, *Polymer*, 39, 26, 6767-6779 (1998).

54. J. Muller, J. H. Wendorff, Thermal density- Fluctuations in rejuvenated and aged polycarbonate, *Journal of Polymer Science: Part C: Polymer Letters*, 26, 421 (1988).
55. J.-J. Pesce and G. B. McKenna, Prediction of the subyield extension and compression responses of glassy polycarbonate from torsional measurements, *J. Rheol*., 41, 5, 929-942 (1997).

Chapter 2

Background on gas transport

2.1. Introduction

Several books or reviews are available in the literature about gas transport in polymers [1-38]. This chapter serves as a brief background concerning gas transport. The reader is encouraged to consult the references listed above for more insight into the subject. The first section gives an introduction to the topic of gas transport and explains the signification of the transport parameters, namely the permeability, the solubility, and the diffusion coefficients. The second section discusses the influence of the polymer structure on gas transport. The following section is devoted to gas sorption in amorphous polymers and mentions briefly the models found in the literature. Finally, permeation experiments are presented and the time-lag method commonly used in the literature to determine the gas transport coefficients is detailed.

2.2. Transport parameters

Three transport coefficients are commonly used to define gas transport, namely the permeability, the solubility, and the diffusion coefficients. The three following subsections present the characteristics of each of those parameters.

2.2.1. The permeability coefficient P

The permeability coefficient P indicates the rate at which a permeant traverses a membrane. It is therefore the critical parameter that researchers are trying to improve whenever they are involved in the design of new materials. The permeability coefficient is the product of a thermodynamic parameter, the solubility coefficient, and a kinetic parameter, the diffusion coefficient. Those coefficients will be discussed in the following subsections.

For a component i, the permeability coefficient P is given as follows:

$$P_i = D_i S_i \qquad \text{Eq (2.1)}$$

where P_i, D_i, and S_i stand for the permeability, the diffusion, and the solubility coefficients of component i, respectively. The permeability is often expressed in barrers, 1 barrer is equal to 10^{-10} cm^3@STP.cm/cm^2.s.cmHg. The value of the permeability coefficient P depends on operating conditions, such as temperature, pressure, and composition, as well as on structural features of the polymeric material. P is mainly dominated by the diffusion coefficient since variations in D are greater than those in S [39-41].

The permeability coefficient P varies differently with pressure depending on the nature of the gas and that of the polymer. The permeability of permanent gases such as H_2, He, N_2 and O_2 in rubbery or glassy polymeric membranes is not really affected by a variation in pressure, as long as the pressure remains in a reasonable range (typically about 10atm). In a study involving polycarbonate for instance, P was found to remain constant in a pressure range of 3atm to 10atm (the pressure refers to the pressure applied on one side of the membrane in permeation experiments) [42]. The permeability of other gases in glassy polymers decreases with pressure, while it increases in rubbery polymers. A plasticizing behavior is observed sometimes for the permeation of carbon dioxide (CO_2) in glassy polymers [43-63]. The permeability generally decreases as the permeant size increases. P, D, and S are independent of pressure (in the low pressure range where Henry's Law applies) at a given temperature for permanent gases, which have only weak

interactions with a polymer. However, the permeation rate increases for gases that induce swelling and plasticization. The lower the density, or the higher the free volume, the higher is the permeability. Crosslinking, crystallinity and orientation decrease P, and consequently only amorphous thermoplastics polymers are used for gas separation.

P increases with temperature and can be represented by an Arrhenius-type relationship:

$$P = P_o \exp\left(\frac{-E_P}{RT}\right) \qquad \text{Eq (2.2)}$$

with $P_o = S_o D_o$ (S_o and D_o will be defined later), and $E_P = \Delta H_S + E_D$ where E_P is the activation energy of permeation. The quantities ΔH_S and E_D will be defined in subsequent subsections as well.

2.2.2. The solubility coefficient S

The solubility coefficient S, also referred sometimes to as the sorption coefficient, is a measure of the amount of gas sorbed by the membrane. S is a thermodynamics factor related to the specific interactions between the gas molecules and the polymer. S increases with the penetrant condensability (evaluated from the critical temperature, the boiling point, and the Lennard-Jones potential force constant), the permeant size (because of the increase in boiling points), the polymer free volume (within a given family of polymers), the free volume distribution, the polymer/gas interactions and the distribution of the electron density in the polymer matrix. The polymer free volume, which reflects how opened the matrix is, can be determined by the group contribution method [64, 65]. The stronger the interactions between a gas and the functional groups of a polymer, the greater is the solubility. Therefore CO_2 which has a quadrupole moment will be very soluble in polar polymers.

The solubility coefficient S is defined as:

$$S = \frac{C}{f} \qquad \text{Eq (2.3)}$$

where C is the equilibrium concentration of the gas in the polymer in (cm^3_{gas}@STP/$cm^3_{polymer}$) and f is the fugacity in cmHg. S can be expressed in (cm^3@STP/$cm^3_{polymer}$.cmHg). The fugacity of a component i is:

$$f_i = \varphi_i \, y_i \, p \qquad \text{Eq (2.4)}$$

where p is the pressure in cmHg, y_i is the composition and φ_i is the fugacity coefficient. Therefore, $p_i = y_i \, p$ is the partial pressure of penetrant at the surface of the polymer (assuming an ideal gas). S is independent of pressure as long as Henry's Law applies (in the low pressure range C is directly proportional to the applied pressure).

S decreases with temperature and follows a Van't Hoff type relationship expressed as:

$$S = S_o \exp\left(\frac{-\Delta Hs}{RT}\right) \qquad \text{Eq (2.5)}$$

with $\Delta H_S = \Delta H_{cond} + \Delta H_{mix}$. ΔH_S is the enthalpy of sorption or the partial molar heat of solution, ΔH_{cond} is the enthalpy of condensation of the gas, and ΔH_{mix} is the partial molar heat of mixing between the gas and the polymer. For weak interactions, ΔH_{mix} is positive and can be calculated from the following equation:

$$\Delta H_{mix} = V_1 \left(\delta_1 - \delta_2\right)^2 \varphi_2{}^2 \qquad \text{Eq (2.6)}$$

where V_1 is the partial molar volume of the gas, φ_2 is the volume fraction of the polymer, and δ_1 and δ_2 are the solubility parameters of the gas and the polymer, respectively. ΔH_{cond} can be considered as negligible for permanent gases which are well above their critical temperature (i.e. H_2, He, N_2, and O_2). For those gases, ΔH_S is positive and therefore S increases with temperature. This is due to the fact that the gas/polymer interactions are weak. However for condensable gases such as CO_2, SO_2, NH_3 and hydrocarbons, ΔH_{cond} is negative and large. Since ΔH_S is negative, S decreases with temperature. Indeed, as the temperature increases, the penetrants become less condensable.

2.2.3. The diffusion coefficient D

The diffusion or diffusivity coefficient D indicates how fast a penetrant is transported through the membrane. It is a measure of the mobility of the gas molecule within the polymer and therefore a kinetic factor related to polymer-penetrant dynamics and expressed in cm^2/s. It is also commonly correlated with the overall free volume content. D is influenced by the penetrant size and shape, the polymer free volume, the segmental mobility and the rigidity of the polymer chains. It decreases dramatically as the size of the penetrant increases. The size is not however very critical for rubbery polymers. Since rubbery membranes are not very selective, they are generally not utilized for gas separations. The shape of the gas molecule is an important parameter as well. Indeed, spherical molecules do not diffuse as fast as flattened, linear, oblong or elongated molecules. D can be considered as independent of gas concentration for a simple gas, i.e. where the interactions with the polymer are weak. However, it cannot be considered as a constant for plasticized systems or for organic vapors.

For non-plasticizing systems the diffusion coefficient increases as the temperature increases and follows the Arrhenius-type relationship given as:

$$D = D_o \exp\left(\frac{-E_D}{RT}\right) \qquad \text{Eq (2.7)}$$

where D_o is the preexponential factor, and E_D is the activation energy of diffusion. E_D decreases as the volume fraction of gas increases, while it increases as the permeant size increases.

The diffusion coefficient is related to the chain mobility, and therefore is believed to be determined in part by the size of the free volume of the polymer. The thermodynamic diffusion coefficient has been related to the polymer fractional free volume (FFV) using the Doolittle-type relation [66]:

$$D = D_0 \exp\left(\frac{-B}{FFV}\right) \qquad \text{Eq (2.8)}$$

where D_0 and B are constants characteristic of the system. D_0 is equal to (R T A_f) where A_f depends on the size and the shape of the gas molecule. B is an indication of the minimum local free volume necessary to allow a displacement. As the fractional free volume decreases, D decreases.

The fractional free volume is evaluated from the expression:

$$FFV = \left(\frac{V - V_0}{V}\right) \qquad \text{Eq (2.9)}$$

where V is the observed polymer specific volume at a given temperature (which can be obtained from the inverse of the density) and V_o (= 1.3 V_W) is the occupied volume of 1g of the amorphous polymer at 0K. V_W, the Van der Waals volume of a repeating unit, can be calculated from Bondi's group contribution method [64, 65]. Thus $(V - V_0)$ is the free volume.

In the case of plasticization, an empirical relationship has been found for systems which obey Henry's Law (usually when the concentration of sorbed gas is small):

$$D(C) = D_0 \exp(\gamma C) \qquad \text{Eq (2.10)}$$

where γ is a plasticizing parameter depending on the system at a given temperature and D_o is the diffusion coefficient at zero concentration

When Henry's Law cannot be applied anymore because of the strength of the gas/polymer interactions, we have:

$$D(C) = D_0 \exp(A B) \qquad \text{Eq (2.11)}$$

where A is a temperature dependent parameter and B depends on concentration, volume fraction or activity.

2.3. Influence of the polymer structure on gas transport

The relationship between the chemical structure and the permeation properties are not straightforward and the development of a suitable glassy polymeric membrane for a

given application is still to a large extent empirical. Sometimes a minor change in the chemical structure affects the gas transport properties tremendously. Nevertheless, some trends can be distinguished.

2.3.1. Free volume

While considering gas transport data obtained on polymers with various structures, it has been shown that the greater the free volume content or the fractional free volume (FFV), the greater the permeability coefficient P. A linear relationship between ln P and $(FFV)^{-1}$ has been reported [40, 41, 67-74]. Similar trends have been reported for the diffusion coefficient [7, 39, 67, 70, 72, 75-79]. In general, polymers characterized by a high free volume content have high gas solubility coefficients. Nevertheless, the dependence of the free volume on the permeability coefficient has been shown to be problematic for polymers with fluorinated groups [80] or polar substituents [70]. It has been suggested that the diffusion coefficient in polyimides may correlate better with the cohesive energy density [72]. Deviations have also been encountered for materials containing polar groups [70].

2.3.2. Others

The effect of chemical structural variations in various glassy polymers on gas transport has been investigated in many studies [71, 72, 79, 81-83]. In addition to the free volume content (related to the chain packing) the gas transport parameters have been shown to be influenced by the chain rigidity (or flexibility), the segmental mobility, the interchain distance, and the chain interactions. In order to separate the effects of each parameter from one another, studies have focused on the effects of systematic variations in the structure of a given material [40, 70, 71, 73, 81-83]. For instance, the introduction of bulky alkyl substituents opens up the polymer matrix and results in a greater permeability coefficient [81]. Introduction of n-alkyl side groups on a polymer backbone has been shown to increase the side-chain flexibility, to increase the free volume, and

thus the permeability coefficient P [82]. A greater P value has even been observed for branched alkyl chains [82]. However sometimes increasing the side-chain length leads to a better packing and thus to a lower permeability [71]. The substitution of $–C(CH_3)_2$- groups by $–C(CF_3)_2$- groups in the backbone of poly(aryl ether ketone) (PEK) resulted in a higher T_g and thus in a decreased chain mobility due to the hindered molecular rotations brought up by the large fluorine atoms [40]. The increase in free volume resulted in increased permeability, diffusion, and solubility coefficients. Adding a second $–C(CF_3)_2$- group further increased the permeability coefficient. A more attractive interaction of the gas molecules with the $–C(CF_3)_2$- groups was also believed to be responsible for the enhanced solubility coefficient. In addition, the interactions between the gas and the polymer play also a major role in gas transport. Hydrogen bonding for instance, result in a denser material with restricted segmental motion. Hence lower gas permeability and diffusion coefficients are obtained when a particular group is replaced by another one that can form hydrogen bonds [72, 81]. Polarity also tends to lower the permeability coefficient [70, 73, 83]. The same holds true when the interchain interaction is enhanced due to the substitution of one group by another capable of inducing ionic bonds [81]. Nevertheless the permselectivity is then increased.

For gas separation applications a polymer should have both high permeability and high permselectvity. In reality however an increase in permeability results in a decrease in permselectivity, and vice-versa. This “trade-off” relationship is shown in the literature [11, 84]. In order to achieve good membrane performance the polymer should ideally possess two particular characteristics: a high fractional free volume and a narrow free volume distribution. Some exceptions have however been noticed and increases in both permeability and permselectivity have been reported. This is the case for instance for a polymer with bulky substituents and with groups capable of strong intermolecular interactions [81]. Polynorbornenes with aliphatic pendant groups, hence a stiff backbone with flexible side chains, also showed a reversed trade-off [71]. The substitution of $–C(CH_3)_2$- groups by $–C(CF_3)_2$- groups in the backbone of poly(aryl ether ketone) (PEK) shows a simultaneous increase in permselectivity and permeability [40]. The substitution of a longer oligo (phenylene sulfone) segment in the polymer backbone of 6FDA-

poly(phenylene sulfone imide) has been found to decrease both the gas permeability and the permselectivity [85].

In conclusion, high permeability values are likely to be achieved in polymers with a large excess free volume, rigid polymer chains, and low intermolecular interactions.

2.4. Gas sorption in amorphous polymers

2.4.1. Introduction

As explained above, the term “sorption” refers to as the amount of gas molecules that have permeated into a polymer. The objective of this section is to outline the different sorption models presented in the literature. However one has to be aware that a gas molecule can be sorbed by different modes of sorption during an experiment, due to change in concentration, temperature, swelling, and time.

Sorption experiments are usually carried out in pressure decay sorption apparatus [86]. The apparatus allows measurements of the gas uptake inside a polymer as a function of pressure. Briefly, the set-up involves two closed volumes V_1 and V_2 connected by a valve, as sketched in Figure 2.1. A polymer is placed in V_1 and degased. Then some gas is injected in V_2, the valve between V_1 and V_2 is opened and closed rapidly, and the decrease in pressure in V_1 due to the absorption of the gas by the polymer is monitored with time until equilibrium. The procedure is continued by increasing the pressure in V_2, etc.

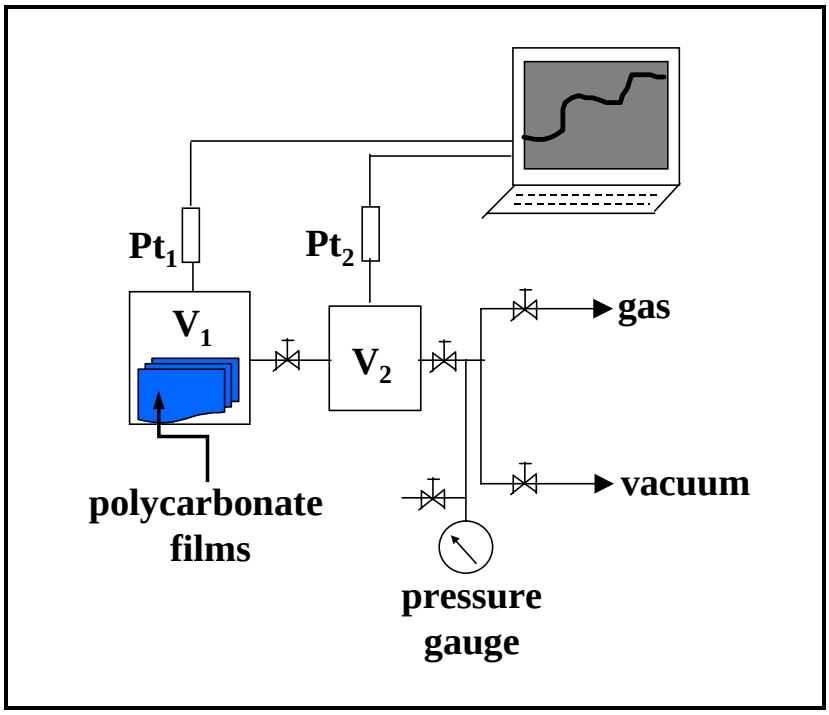

Figure 2.1: Schematic of the sorption apparatus.

The equilibrium concentration of a gas in a polymer is given by the following relation (assuming an ideal gas mixture):

$$C = S\,f = S\,p\,\varphi \cong S\,p \qquad \text{Eq (2.12)}$$

where S is the sorption or the solubility coefficient, φ is the fugacity coefficient and f is the fugacity. S can be a function of temperature, pressure or concentration, but it is usually taken as a constant at a given temperature. φ = 1 only for ideal gases (gases at low pressures), however no significant differences have been observed at high pressures, at least for single gases. C decreases with temperature. It also depends on the nature of the gas. In polycarbonate for instance, C is about 16 times greater in CO_2 than in N_2 for an applied pressure of 0.5 MPa [87].

Several models have been presented in the literature to explain the mechanism of gas transport through non-porous glassy amorphous polymers. The reader can refer to the book written by Paul and Yampol'skii [7] for a deeper insight into the theory behind each model and their limitations. The free volume model [88, 89] applies strictly to rubbery materials. Macroscopic and lattice theories have been derived for glassy polymers [90-

93]. Because of its simplicity, the dual mode sorption (DMS) model [94] remains the model the most used by far in the literature. Therefore only the DMS theory is briefly presented in the present section.

2.4.2. The Dual Mode Sorption (DMS) model

The dual mode sorption (DMS) model is commonly used in the literature to characterize sorption in amorphous glassy polymers. The DMS model consists of a combination of both the Henry's Law and the Langmuir-type sorption. Those two particular behaviors are reviewed in the following subsections before discussing the DMS model itself.

2.4.2.1. The Henry's Law (rubbery polymers)

When the specific interactions between the polymer and the gas molecules themselves are weak compared to the polymer/polymer interactions, the system behaves ideally and Henry's Law is obeyed. Assuming that the solubility coefficient S is constant at a given temperature and that the fugacity and the pressure are equivalent, the equilibrium concentration C of the gas (in cm^3@STP/$cm^3_{polymer}$) in a rubbery polymer is given by the Henry's Law:

$$C = k_D\, p \qquad \text{Eq (2.13)}$$

where p is the pressure and k_D is the Henry's Law dissolution constant. The constant k_D is equivalent to the solubility coefficient S in this case. The concentration of the gas within the polymer is believed to be sufficiently low to obey Henry's Law. This behavior is observed for sorption in rubbery polymers at low pressures ($<10^5$ Pa).

The permeability is independent of pressure, and is expressed as:

$$P = k_D\, D \qquad \text{Eq (2.14)}$$

where D is the diffusion coefficient (taken as a constant).

2.4.2.2. The Langmuir-type sorption

When polymers contain dispersed porous particles such as carbon black or silica gel, or when dyes are sorbed by polymers containing polar groups, a Langmuir-type sorption can be observed at low pressure. The gas molecules are believed to be sorbed in the microvoids of the polymers. The concentration C is given by:

$$C = \frac{C_H' b p}{1 + b p} \qquad \text{Eq (2.15)}$$

where p is the equilibrium pressure in cmHg, C_H' is the hole saturation constant in (cm^3@STP/cm^3) and b is the hole affinity constant in $cmHg^{-1}$.

2.4.2.3. The DMS model

Unlike what is observed in rubbery polymers, the equilibrium concentration of a gas in a glassy polymer is not directly proportional to the applied pressure. Indeed, it has been observed experimentally that the sorption isotherm is linear only at low and high pressure, while the intermediate range is concave to the pressure axis. An empirical model, referred to as the dual mode sorption (DMS) model [94] bases its theory on the excess free volume present in glassy polymers. This excess free volume, which is related to the difference relative to the thermal expansion coefficient of a rubber, is at the origin of the non-equilibrium nature of glassy polymers. Indeed, glassy polymers tend to decrease their excess free volume with time. This phenomenon, known as physical aging, lasts an extremely long time since the polymer below T_g does not have sufficient thermal energy to attain equilibrium rapidly. Some discussion about physical aging is provided in Chapter 3.

The DMS model assumes the existence of two kinds of free volume or holes (or two modes) which are always in equilibrium: the Henry mode in continuous chain matrix and the Langmuir mode in the microvoids of the excess free volume. The two types of sorption associated with those two modes are sometimes referred to as ordinary dissolution and hole-filling, respectively. Therefore the DMS model is a combination of

the Henry's Law and the Langmuir isotherm, as sketched in Figure 2.2. The Henry sites in the dense packing region are smaller whereas the Langmuir sites, which correspond to the packing defects, are larger and more variable in size. Those Langmuir sites arise because of the restricted chain mobility in a glassy material; some holes remain frozen into the material. The original model assumed that the penetrant sorbed in the Langmuir sites were completely immobilized and did not contribute to the diffusive flux. However this given model was modified later and postulates now that the penetrants sorbed under both the Henry and the Langmuir modes are mobile. This model is known as the dual mobility or the partial immobilization model, opposed to the original immobilization model.

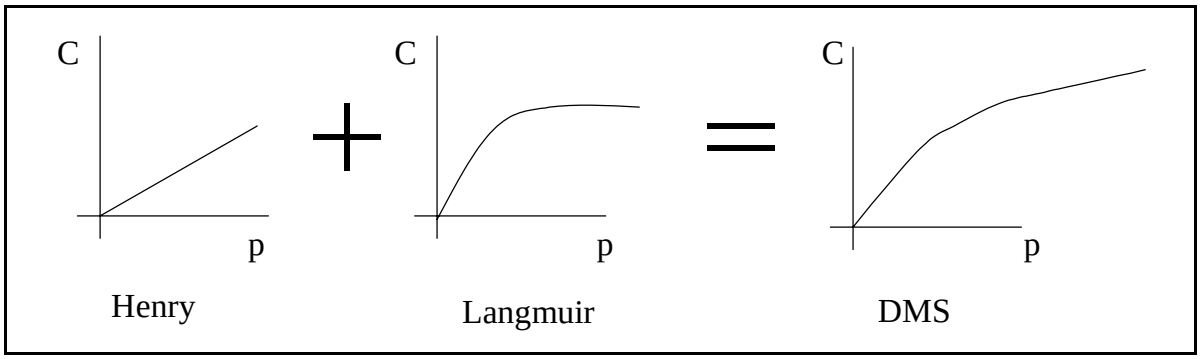

Figure 2.2: The DMS model is a combination of the Henry's law and the Langmuir isotherm

In the absence of strong interactions between the gas and the polymer that may induce plasticization or swelling, the total concentration of the gas in the polymer (in cm^3@STP/cm^3) is given by the sum of the concentration by normal dissolution and the concentration by hole filling (assuming equivalence between pressure and fugacity):

$$C = C_D + C_H = k_D\, p + \frac{C_H' b\, p}{1 + b\, p} \qquad \text{Eq (2.16)}$$

where the subscript D stands for dissolved and refers to the Henry mode, while H stands for holes and refers to the Langmuir mode. p is the equilibrium pressure in cmHg, k_D is the Henry's law dissolution constant in (cm^3@STP/cmHg.cm^3), C_H' is the hole saturation constant in (cm^3@STP/cm^3) and b is the hole affinity constant in $cmHg^{-1}$.

At low pressure, ($bp << 1$) and Eq (2.16) reduces to:

$$C = (k_D + C_H' b)p \qquad \text{Eq (2.17)}$$

The sorbed gas concentration is thus directly proportional to the applied pressure.

At high pressure, (b p > > 1), the Langmuir sites are saturated, and Eq (2.16) reduces to:

$$C = k_D\, p + C_H' \qquad \text{Eq (2.18)}$$

The dual-mode parameters k_D, C_H' and b can be determined as follows. The plot of concentration versus pressure can be obtained experimentally by sorption experiments. The values of k_D, C_H' and b can be obtained by graphical interpolation, as shown in Figure 2.3. Another kind of graphical interpolation is sometimes found in the literature. Since C is obtained experimentally and k_D can be determined from the slope at high pressure, $C_H (= C - k_D p)$ can be plotted versus pressure. From Eq (2.16),

$$\left(\frac{p}{C_H}\right) = \left(\frac{1}{C_H' b}\right) + \left(\frac{p}{C_H'}\right) \qquad \text{Eq (2.19)}$$

The plot of (p/C_H) versus pressure shows a straight line whose intercept is $(1/C_H' b)$ and whose slope is $(1/C_H')$. However the most accurate way to get the parameters is to do a nonlinear regression instead of an extrapolation [87]. Indeed, the true equilibrium is not generally reached at the end of the experiment. The Marquart algorithm for linear least squares is generally used at this purpose.

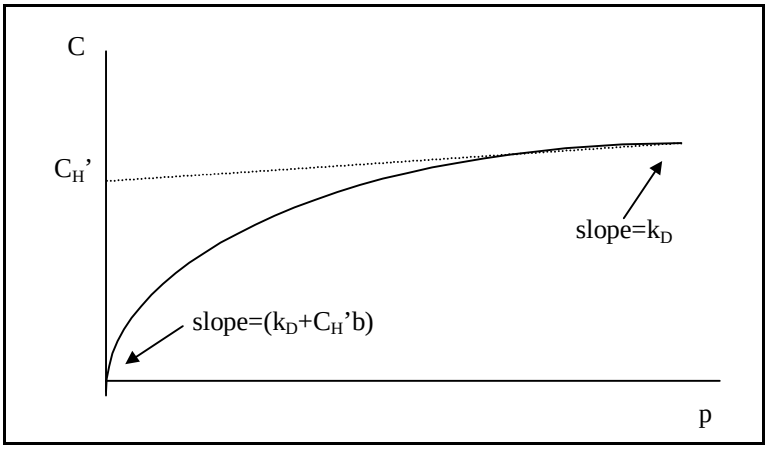

Figure 2.3: C versus p for the DMS model

The DMS model presents an excellent agreement between theory and experiment for glassy polymers up to 20-30 atm for several gases. It is the model the most used in the literature by far. The model seems even applicable for the sorption of vapors through rubbery polymers containing adsorptive fillers.

However, no direct experimental evidence of the two different sorption modes has been observed. Several attempts have been made to confirm the validity of the DMS model and thus the existence of two environments, namely the Henry and the Langmuir modes. However evidence of two different holes has not clearly been confirmed so far. The use of NMR led to conflicting conclusions. The $^{13}CO_2$ NMR results obtained by Cain et al [95] are consistent with the concept of two sorption sites (although no evidence of their existence has been shown) whereas Sefcik and Schaefer [96] believed that two different types of sorption sites did not exist. FTIR has been used by several researchers. Higuchi and Nakagawa [97] did not observe two distinct peaks for CO_2 in a glassy PMMA polymer, suggesting that if indeed the two modes exist, the two modes are similar in the spectroscopic measurements. Murata et al [98] observed two types of desorption, referred to as rapid and slow.

Several comments can be made about the DMS model. The DMS model is only an empirical model, which has been developed without physical interpretation. It is basically a fitting procedure which involves three adjustable parameters k_D, C_H' and b. The values of those parameters depend strongly on the initial curvefitting guess used in a particular algorithm, as well as on the pressure range. The parameters have to be determined for each penetrant at each temperature since no correlations with the properties of the gas or the polymer have been found. No prediction is therefore possible. Furthermore, those parameters have to be different in sorption and in desorption since hysteresis is sometimes observed while doing sorption experiments. The relaxation time of the polymer chains, or physical aging, is not taken into account. The structure and the morphology of the polymer is not considered either. Actually the DMS model assumes that the structure of the polymer remains constant during the experiment, regardless of the duration of the experiment or the pressure used. One complication also arises due to the fact that the polymer is usually conditioned prior to experiments. This procedure may induce irreversible changes inside the polymeric matrix. Comparison with other physical

properties is therefore impossible. Finally, the existence of two different sorption modes for a given polymer is quite difficult to understand on a physical basis. Indeed, it means that there are two distinct populations of gas molecules. The model does not take into consideration the distribution of the holes. It assumes that the expression of the gas concentration is the same near the surface as in the bulk.

2.5. Permeation experiments

Gas permeation through non-porous homogeneous polymeric membranes occurs by the well-known solution-diffusion model [94] suggested by Sir Thomas Graham in 1866. The permeation is believed to occur in three stages, which are sorption/diffusion/desorption. The sorption or solution of gas molecules occurs at the upstream side of the membrane. Because of the concentration gradient, the molecules diffuse across the membrane before finally desorbing on the downstream side of the membrane.

The permeation integral method [13, 99] has been widely used to analyze permeation of a gas through a membrane. A schematic of the experimental set-up for the integral method is given in Figure 2.4. Briefly, a membrane separates a gas at pressure p_f from a closed volume. The system is initially degased by use of a high vacuum. At t = 0, the pressure of the feed or the upstream increases from 0 to p_f. This pressure remains constant throughout the entire experiment. As the gas permeates through the membrane because of the concentration gradient, the pressure in the closed volume p_p will rise. The pressure in the permeate or downstream side is monitored with time, as shown in Figure 2.5.

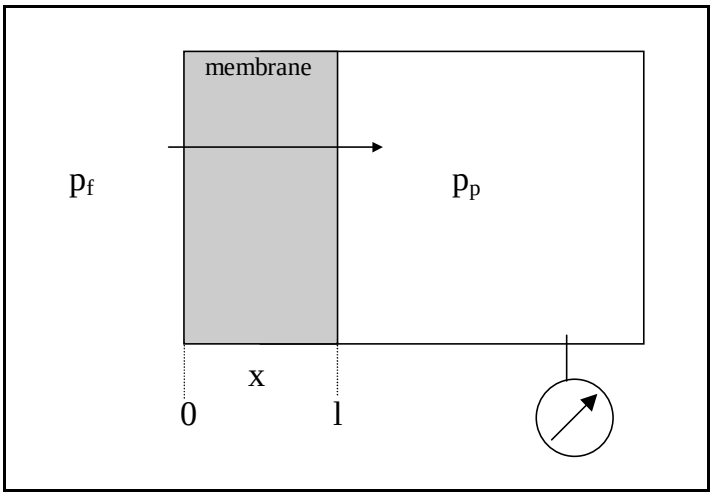

Figure 2.4: Schematic of the integral method ($p_f > p_p$).

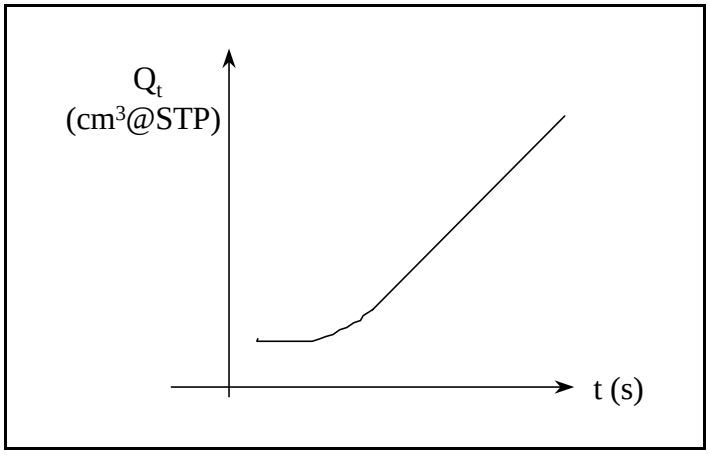

Figure 2.5: Profile obtained by permeation.

Since the thickness of the membrane is very small compared to its surface area (130μm versus 13.36cm^2, respectively, thus corresponding to a ratio of diameter/length of about 317), the flux of gas can be considered a unidirectional and perpendicular to the membrane plane surface. A mass balance can be written on a small volume of thickness dx located at some arbitrary position x, as shown in Figure 2.6. The general expression is:

$$\text{in} + \text{production} = \text{out} + \text{accumulation} + \text{consumption} \qquad \text{Eq (2.20)}$$

Since production = consumption = 0, we have:

$$\text{gas accumulation} = (\text{in at } x) - (\text{out at } (x + dx)) \qquad \text{Eq (2.21)}$$

Neglecting the convection at the top and the bottom of the membrane, the mass balance in the layer is:

$$\frac{\partial}{\partial t}[A\,dx\,C] = A\,J_x - A\,J_{x+dx} \qquad \text{Eq (2.22)}$$

where J is the flux, A is the area, C is the concentration and t is the time.

Dividing by the volume of the layer, one obtains:

$$\frac{\partial C}{\partial t} = -\frac{1}{dx}[J_{x+dx} - J_x] \qquad \text{Eq (2.23)}$$

From the definition of the derivative when $dx \cong 0$,

$$\left(\frac{\partial C}{\partial t}\right) = -\left(\frac{\partial J}{\partial x}\right) \qquad \text{Eq (2.24)}$$

If the appropriate initial and boundary conditions are known, the differential equation can be solved and the concentration profile of the gas within the polymeric membrane can be obtained.

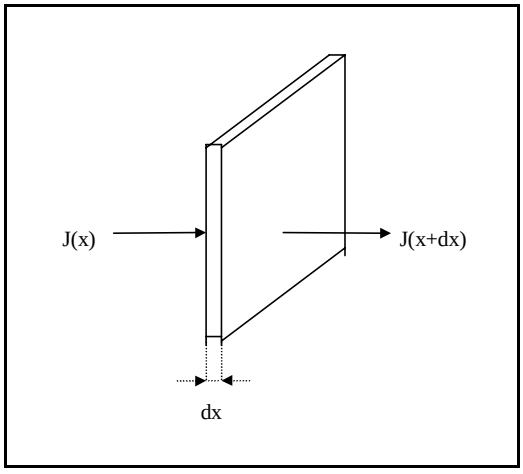

Figure 2.6: Volume of thickness dx considered in the mass balance.

The molecular diffusion of a gas through a membrane is given by the Fick's first law of diffusion (provided that no exceptions occur, such as crystallization or case II diffusion):

$$J = -D(C)\left(\frac{\partial C}{\partial x}\right) \qquad \text{Eq (2.25)}$$

where J is the flux in (cm^3@STP/cm^2 s), D is the mutual diffusion coefficient in cm^2/s, C is the concentration of the gas in the polymer in (cm^3@STP/cm^3) and x is the distance in cm. For weak interactive gases, D can be assumed to be independent of concentration.
The Fick's second law of diffusion can be obtained from Eq (2.24) and Eq (2.25) (assuming a concentration-independent diffusion coefficient D).

$$\left(\frac{\partial C}{\partial t}\right) = D\left(\frac{\partial^2 C}{\partial x^2}\right) \qquad \text{Eq (2.26)}$$

The time-lag method [1] is the method commonly used in the literature to get the values of the diffusion and the solubility coefficients. It is based on the Henry's Law given previously. Although the Henry's Law is strictly verified for rubbery polymers only, estimation of the transport parameters can still be made for glassy polymers at low pressures. The concentration of the gas within the polymer is believed to be sufficiently low to obey Henry's Law. The time lag method is based on the following initial and boundary conditions:

$t < 0$	$0 \le x \le l$	$C = 0$	Eq (2.27)
$t \ge 0$	$x = 0$	$C = C_2$ = a constant	Eq (2.28)
$t \ge 0$	$x = l$	$C = 0$	Eq (2.29)

The concentration profile of the gas within the polymeric membrane can therefore be solved, given the above equations and Eq (2.26).

Unfortunately, the experimental set-up does not allow researchers to monitor directly the concentration profile within the membrane. The permeation integral method measures the increase in pressure in the closed volume. The flux at the end of the membrane and the pressure in the closed volume can be easily related because of the high velocity of gases. The delay between the exit of the gas at the end of the membrane and the reading on the pressure transducer is obviously considered as negligible.

The flux J in (cm^3@STP/cm^2 s) at x = l is equal to (Q_t / A t) where Q_t is the volume of the gas that has permeated in cm^3@STP, A is the area of the membrane in cm^2, t is the time in s and l is the thickness of the membrane in cm. STP stands for standard temperature and pressure conditions (0°C and 1 atm). The volume of the gas that has permeated in a closed volume V_d (in cm^3) at time t is therefore given by:

$$Q_t = A\int_0^t (J)_{x=l}\,dt \qquad \text{Eq (2.30)}$$

The amount of the gas at STP conditions which has permeated in the closed volume can be calculated from Eq (2.30) and compared to the experimental value obtained from the reading of the pressure transducer.

When Eq (2.26) is solved, given Eq (2.27), Eq (2.28) and Eq (2.29), and that the solution is entered into Eq (2.30), we obtain [1, 100]:

$$Q_t = C_2 l\left\{\left(\frac{Dt}{l^2}\right)+\frac{2}{\pi^2}\sum_{n=1}^{\infty}\frac{(-1)^n}{n^2}\left[1-\exp\left(\frac{-Dn^2\pi^2 t}{l^2}\right)\right]\right\} \qquad \text{Eq (2.31)}$$

One can notice by doing computations that if $\frac{2}{\pi^2}\sum_{n=1}^{\infty}\frac{(-1)^n}{n^2}$ is approximated by (-1/6), as what is usually done in the literature [8, 101-103], Q_t differs slightly from zero at t=0.
At sufficient long time, Eq (2.31) reduces to:

$$Q_t = \frac{DC_2}{l}\left[t+\left(\frac{2}{\pi^2}\right)\left(\frac{l^2}{D}\right)\sum_{n=1}^{\infty}\frac{(-1)^n}{n^2}\right] \cong \frac{DC_2}{l}\left[t-\frac{l^2}{6D}\right] \qquad \text{Eq (2.32)}$$

The plot of Q_t versus t will thus be linear at sufficient long time as shown in Figure 2.7 and the slope is equal to (DC_2/l). The time lag θ which is equal to (l^2/6D) can be calculated from the intercept of Q_t with the time-axis. We have:

$$D = \frac{l^2}{6\theta} \qquad \text{Eq (2.33)}$$

While doing experiments, one can notice that Q_t is not necessarily exactly zero at t = 0. The plot has to be corrected for this unaccuracy.

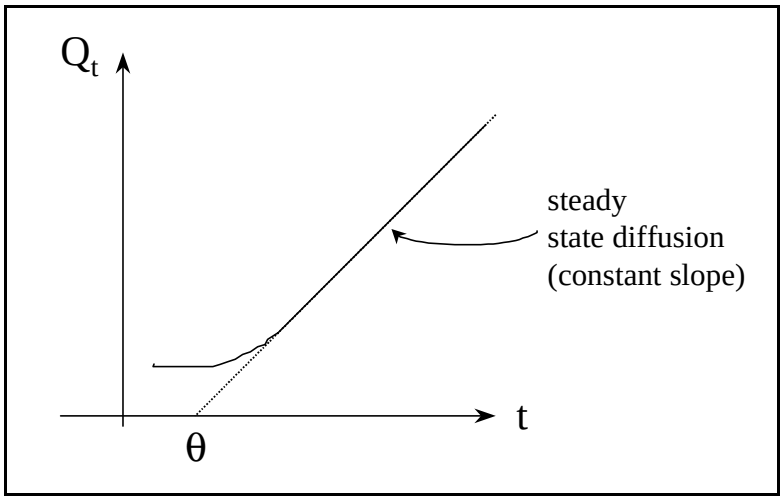

Figure 2.7: Plot of Q_t versus t showing the steady state part and the time lag θ.

If the Henry's Law is verified,

$$C_2 = k_D\, p_f \qquad \text{Eq (2.34)}$$

where p_f is the pressure of the feed. From Eq (2.32), Eq (2.14) and Eq (2.34), we obtain

$$Q_t = \frac{Pp_f}{l}\left(t - \frac{l^2}{6D}\right) \qquad \text{Eq (2.35)}$$

Since the plot is linear at a sufficiently long time, the permeation rate is constant.

$$\text{slope} = \frac{\partial Q_t}{\partial t} = \text{constant} = \frac{Pp_f}{l} = JA \qquad \text{Eq (2.36)}$$

And

$$P = \frac{l}{p_f}\left(\frac{\partial Q_t}{\partial t}\right) \qquad \text{Eq (2.37)}$$

Finally the solubility is:

$$S = k_D = \frac{P}{D} \qquad \text{Eq (2.38)}$$

The time lag method [1] provides usually a good approximation of the transport parameters. However, this method is based on the assumption that the pressure in the closed volume remains negligible throughout the entire permeation process. This assumption can be satisfied in the early part of the experiment only. Indeed, even with a

large closed volume and a slowly permeating gas, this assumption cannot be valid as equilibrium on both sides of the membrane is being achieved, since as the gas permeates through the membrane the pressure in the closed volume will rise. The time lag solution shows that the permeation rate will keep increasing indefinitely (hence the expression steady state), which cannot be true for a closed volume since the pressure will reach a limit when equilibrium will be attained on both sides of the membrane. The procedure to obtain the gas transport coefficients in case of a non-negligible building-up pressure in the closed volume has been detailed elsewhere [104]. Nevertheless, it was confirmed from computer simulations that for the maximum pressure allowed in the closed volume in this research project the concentration at x=l could be assumed to be negligible.

2.6. References

1. J. Crank, *The Mathematics of Diffusion*, second edition, Oxford Science Publications, 1975.
2. J. Comyn, editor, *Polymer Permeability*, Elsevier Applied Science, London, 1985.
3. W. R. Vieth, *Diffusion In and Through Polymers: Principles and Applications*, Hanser, New York, 1991.
4. W. J. Koros and R. T. Chern, Separation of Gaseous Mixtures using Polymer Membranes, *Handbook of Separation Process Technology*, edit. R. W. Rousseau, (1987).
5. W. J. Koros and G. K. Fleming, Membrane-based Gas Separation, *Journal of Membrane Science*, 83, 1-80, (1993).
6. K. Ghosal and B. D. Freeman, Gas Separation Using Polymer Membranes: An Overview, *Polymer for Advanced Technologies*, 5, 673-697 (1994).
7. D. R. Paul, Yuri P. Yampol'skii, editors, *Polymeric gas separation membranes*, CRC Press, Boca Raton, 1994.
8. J. Crank and G. S. Park (editors), *Diffusion in Polymers*, Academic Press, 1968.
9. R. E. Kesting and A. K. Fritzsche, *Polymeric Gas Separation Membranes*, John Wiley & Sons, Inc.,1993.
10. V. Stannett, The Transport of Gases in Synthetic Polymeric Membranes- an Historic Perspective, *Journal of Membrane Science*, 3, 97 (1978).
11. S. A. Stern, Polymers for Gas Separations: the Next Decade, *Journal of Membrane Science*, 94, 1 (1994).
12. I. Blume, E. Smit, M. Wessling and C. A. Smolders, Diffusion Through Rubbery and Glassy Polymer Membranes, *Die Makromolekulare Chemie. Macromolecular Symposia*, 45, 237 (1991).
13. R. M. Felder, Estimation of Gas Transport Coefficients from Differential Permeation, Integral Permeation, and Sorption Rate Data, *Journal of Membrane Science*, 3, 15 (1978).

14. H. L. Frisch, Sorption and Transport in Glassy Polymers - A Review, *Polymer Engineering and Science*, 20, 1, 2 (1980).
15. W. J. Koros, Y. H. Ma and T. Shimidzu, Terminology for membranes and membrane processes, *Journal of Membrane Science*, 120, 149 (1996).
16. H. C. Silvis, Recent Advances in Polymers for Barrier Applications, *TRIP*, 5, 3, 75 (1997).
17. T. deV. Naylor, Permeation Properties, Comprehensive Polymer Science, edit. S. G. Allen and J. C. Bevington, Pergamon Press, New York.
18. B. Freeman and I. Pinnau, Separation of Gases using Solubility-selective Polymers, *TRIP*, 5, 5, 167 (1997).
19. X. Wang and H. G. Spencer, Polymer Membranes for Use in Food Processing, *TRIP*, 5, 2, 38 (1997).
20. W. R. Vieth, *Membrane Systems: Analysis and Design: applications in biotechnology, biomedicine, and polymer science*, Oxford University Press, 1988.
21. R.W. Baker, E. L. Cussler, W. Eykamb, W. J. Koros, R. L. Riley and H. Strathmann, *Membrane Separation Systems: Recent Development and Future Directions*, Noyes Data Corporation, Park Ridge, NJ, 1991.
22. J. G. A. Bitter, *Transport Mechanisms in Membrane Separation Processes*, Plenum Chemical Engineering Series, Plenum Press, New York, 1991.
23. R. D. Noble and S. A. Stern (editors), *Membrane Separations Technology: Principles and Applications*, Elsevier, 1995.
24. Starzak, M. E., The physical chemistry of membranes, Academic press, Orlando, 1984.
25. P. Neogi, editor, Diffusion in Polymers, Marcel Dekker, Inc., New York, 1996.
26. W. J. Koros, editor, *Barrier Polymers and Structures*, *ACS Symposium Series, vol. 423*, American Chemical Society, Washington D.C., 1990.
27. T. Matsuura, *Synthetic Membranes and Membrane Separation Processes*, CRC press Inc.,1994.
28. K. W. Boddeker, editor, The early History of Membrane Science: Selected papers, *Journal of Membrane Science*, 100, 1 (1995).
29. R. M. Felder and G. S. Huvard, Permeation, Diffusion, and Sorption of Gases and Vapors, *Methods of Experimental Physics*, 16c, Chapter 17, Academic Press, NY (1980).
30. W. J. Koros and M. W. Hellums, Transport Properties, Encyclopedia of Polymer Science and Engineering, 2nd Edition, H. F. Mark, N. M. Bikales, C. G. Overberger, G. Mendes, Eds., John Wiley and Sons, New York, Supplement volume, 1989.
31. R. Rautenbach and R. Albrecht, Membrane Processes, John Wiley and Sons, New York, 1989.
32. R. E. Kesting, Synthetic polymeric membranes, 2nd ed., Wiley, New York, 1985.
33. N. Toshima, Ed., Polymers for gas separation, VCH, Deerfield Beach, FL, 1992.
34. M. Mulder, Basic principles of membrane technology, Kluwer Academic, Dordrecht, 1991.
35. Y. Osada and T. Nakagawa, Eds., Membrane science and technology, Marcel Dekker, New York, 1992.

36. H. L. Frisch, Fundamentals of Membrane Transport, *Polymer Journal*, 23, 5, 445-456 (1991).
37. E. L. Cussler, Diffusion: mass transfer in fluid systems, Cambridge University Press, NY, 1984.
Also Second Edition, Cambridge University Press, NY, 1997.
38. H. Odani, T. Uyeda, Theories of sorption and transport in polymer membranes, *Polymer Journal*, 23, 5, 467 (1991).
39. Y. Maeda and D. R. Paul, Effect of AntiPlasticization on Gas Sorption and Transport. III. Free Volume Interpretation, *Journal of Polymer Science: Part B: Polymer Physics*, 25, 1005 (1987).
40. J. M. Mohr, D. R. Paul, G. L. Tullos, and P. E. Cassidy, Gas transport properties of a series of poly(ether ketone) polymers, *Polymer*, 32, 13, 2387-2394 (1991).
41. J. S. McHattie, W. J. Koros and D. R. Paul, Gas transport properties of polysulphones: 1. Role of symmetry of methyl group placement on bisphenol rings, *Polymer*, 32, 5, 840-850 (1991).
42. L. M. Costello and W. J. Koros, Temperature Dependence of Gas Sorption and Transport Properties in Polymers: Measurements and Applications, *Industrial Engineering Chemical Research*, 31, 2708 (1992).
43. A. Bos, I. G. M. Punt, M. Wessling, H. Strathmann, CO_2-induced plasticization phenomena in glassy polymers, *Journal of Membrane Science*, 155, 67-78 (1999).
44. J. S. Chiou, J. W. Barlow and D. R. Paul, Plasticization of Glassy Polymers by CO_2, *Journal of Applied Polymer Science*, 30, 2633 (1985).
45. R. G. Wissinger and M. E. Paulaitis, Glass Transitions in Polymer/CO_2 Mixtures at Elevated Pressures, *Journal of Polymer Science, Part B: Polymer Physics*, 29, 5, 631 (1991).
46. E. S. Sanders, Penetrant-induced plasticization and gas permeation in glassy polymers, *Journal of Membrane Science*, 37, 63-80 (1988).
47. M. Wessling, S. Schoeman, Th. Van den Boomgaard, C. A. Smolders, Plasticization of gas separation membranes, *Gas Sep. Purif.*, 5, 222-228 (1991).
48. Y. P. Handa, S. Lampron, M. L. O'Neill, On the plasticization of poly(2,6-dimethyl phenylene oxide) by CO_2, *J. Polym. Sci., Polym. Phys. Ed.*, 32, 2549-2553 (1994).
49. W.-C. Wang, E. J. Kramer, W. G. Sachse, Effects of high –pressure CO_2 on the glass transition temperature and mechanical properties of polystyrene, *J. Polym. Sci., Polym. Phys. Ed.*, 20, 1371-1384 (1982).
50. J. R. Fried, H.-C. Liu, C. Zhang, Effect of sorbed carbon dioxide on the dynamic mechanical properties of glassy polymers, *J. Polym. Sci., Polym. Part C*, 27, 385-392 (1989).
51. T. S. Chow, Molecular interpretation of the glass transition temperature of polymerdiluent systems, *Macromolecules*, 13, 362-364 (1980).
52. M. Wessling, Z. Borneman, Th. Van den Boomgaard, C. A. Smolders, Carbon dioxide foaming of glassy polymers, *J. Appl. Polym. Sci.*, 53, 1497-1512 (1994).
53. H. Hachisuka, T. Sato, T. Imai, Y. Tsujita, A. Takizawa, T. Kinoshita, Glass transition temperature of glassy polymers plasticized by CO_2 gas, *Polymer Journal*, 22, 1, 77 (1990).

54. J.-S. Wang, Y. Kamiya, Y. Naito, Effects of CO_2 conditioning on sorption, dilation, and transport properties of polysulfone, *Journal of Polymer Science: Part B: Polymer Physics*, 36, 1695 (1998).
55. K. Tanaka, M. Ito, H. Kita, K. Okamoto, Y. Ito, The effects of CO2-conditioning of polymers on positron annihilation and gas permeation properties, *Bull. Chem. Soc. Jpn.*, 68, 3011-3017 (1995).
56. G. K. Fleming and W. J. Koros, Dilation of Polymers by Sorption of Carbon Dioxide at Elevated Pressures. 1. Silicone Rubber and Unconditioned Polycarbonate, *Macromolecules*, 19, 2285 (1986).
57. G. K. Fleming and W. J. Koros, Carbon Dioxide Conditioning Effects on Sorption and Volume Dilation Behavior for bisphenol A - Polycarbonate, *Macromolecules*, 23, 1353 (1990).
58. A. G. Wonders and D. R. Paul, Effects of CO_2 Exposure History on Sorption and transport in Polycarbonate, *Journal of Membrane Science*, 5, 63 (1979).
59. S. M. Jordan, W. J. Koros, J. K. Beasley, Characterization of CO_2-induced conditioning of polycarbonate films using penetrants with different solubilities, *Journal of Membrane Science*, 43, 103-120 (1989).
60. D. S. Pope, G. K. Fleming, W. J. Koros, Effect of various exposure histories on sorption and dilation in a family of polycarbonates, *Macromolecules*, 23, 2988 (1990).
61. W. R. Vieth, L. H. Dao, and H. Pedersen, Non-equilibrium microstructural and transport characteristics of glassy poly(ethylene terephthalate), *Journal of Membrane Science*, 60, 41-62 (1991).
62. P. Gotthardt, A. Grűger, H. g. Brion, R. Plaetschke, and R. Kirchheim, Volume change of glassy polymers by sorption of small molecules and its relation to the intermolecular space, *Macromolecules*, 30, 8058-8065 (1997).
63. S.-H. Chen, S.-L. Huang, K.-C. Yu, J.-Y. Lai, M.-T. Liang, Effect of CO_2 treated polycarbonate membranes on gas transport and sorption properties, *Journal of Membrane Science*, 172, 105-112 (2000).
64. A. Bondi, Physical properties of molecular crystals, liquids, and glasses, Wiley, New York, 1968.
65. D. W. Van Krevelen, Properties of Polymers, Their correlation with chemical structure; their numerical estimation and prediction from additive group contributions, Third Ed, Elsevier, NY, 1990.
66. H. Fujita, *Fortschr. Hochpolym. Forsch.*, 3, 1 (1961).
67. J. Y. Park, D. R. Paul, Correlation and prediction of gas permeability in glassy polymer membrane materials via a modified free volume based group contribution method, *Journal of Membrane Science*, 125, 23-39 (1997).
68. Y. Yampolskii, S. Shishatskii, A. Alentiev, K. Loza, Correlations with and prediction of activation energies of gas permeation and diffusion in glassy polymers, *Journal of Membrane Science*, 148, 59-69 (1998).
69. W. M. Lee, Selection of barrier materials from molecular structure, *Polym. Eng. Sci.*, 20, 65-69 (1980).
70. J. S. McHattie, W. J. Koros and D. R. Paul, Effect of isopropylidene replacement on gas transport properties of polycarbonates, *Journal of Polymer Science: Part B: Polymer Physics*, 29, 731-746 (1991).

71. K. D. Dorkenoo, P. H. Pfromm. M. E. Rezac, Gas transport properties of a series of high T_g polynorbornenes with aliphatic pendant groups, *Journal of Polymer Science: Part B: Polymer Physics*, 36, 797-803 (1998).
72. K. Toi, H. Suzuki, I. Ikemoto, T. Ito, and T. Kasai, Permeation and sorption for oxygen and nitrogen into polyimide membranes, *Journal of Polymer Science: Part B: Polymer Physics*, 33, 777-784 (1995).
73. H.-J. Kim and S.-I. Hong, The transport properties of CO_2 and CH_4 for brominated polysulfone membrane, *Korean Journal of Chemical Engineering*, 16, 3, 343-350 (1999).
74. E. R. Hensema, A. P. Boom, Gas separation membranes from tailor-made polymers, 409-419 ( ).
75. A. Thran, G. Kroll, F. Faupel, Correlation between fractional free volume and diffusivity of gas molecules in glassy polymers, *Journal of Polymer Science: Part B: Polymer Physics*, 37, 3344-3358 (1999).
76. Y. C. Jean, J.-P. Yuan, J. Liu, Q. Deng, and H. Yang, Correlations between gas permeation and free-volume hole properties probed by positron annihilation spectroscopy, *Journal of Polymer Science: Part B: Polymer Physics*, 33, 2365-2371 (1995).
77. Y. Kobayashi, K. Haraya, S. Hattori, *Polymer*, 35, 925-928 (1994).
78. S. Trohalaki, L. C. DeBolt, J. E. Mark, H. L. Frisch, *Macromolecules*, 23, 813-816 (1990).
79. I. Kresse, A. Usenko, J. Springer, V. Privalko, Gas transport properties of soluble poly(amide imide)s, *Journal of Polymer Science: Part B: Polymer Physics*, 37, 2183-2193 (1999).
80. M. W. Hellums, W. J. Koros, G. R. Husk and D. R. Paul, Fluorinated polycarbonates for gas separation applications, *Journal of Membrane Science*, 46, 93 (1989).
81. Z. Wang, T. Chen, J. Xu, Novel poly(aryl ether ketone)s containing various pendant groups. II. Gas-transport properties, *Journal of Applied Polymer Science*, 1725-1732 (1997).
82. A. C. Savoca, A. D. Surnamer, and C.-F. Tien, Gas transport in poly(silylpropynes): The chemical structure point of view, *Macromolecules*, 26, 23, 6211-6216 (1993).
83. J. M. Mohr and D. R. Paul, Comparison of gas permeation in vinyl and vinylidene polymers, *Journal of Applied Polymer Science*, 42, 1711-1720 (1991).
84. L. M. Robeson, Correlation of Separation Factor versus Permeability for Polymeric Membranes, *Journal of Membrane Science*, 62, 165 (1991).
85. Z.-K. Xu, M. Böhning, J. Springer, F. P. Glatz, R. Mülhaupt, Gas transport properties of soluble poly(phenylene sulfone imide)s, *Journal of Polymer Science: Part B: Polymer Physics*, 35, 1855-1868 (1997).
86. W. J. Koros and D. R. Paul, Design considerations for Measurement for Gas Sorption in Polymers by Pressure Decay, *Journal of Polymer Science: Polymer Physics Edition*, 14, 1903 (1976).
87. W. J. Koros, D. R. Paul and A. A. Rocha, Carbon Dioxide Sorption and Transport in Polycarbonate, *Journal of Polymer Science, Polymer Physics Edition*, 14, 687 (1976).

88. J. L. Duda and J. M. Zielinski, Free-Volume Theory, *Plastics Engineering*, 32, 143 (1996).
89. J. M. Zielinski and j. L. Duda, Solvent Diffusion in Polymeric Systems, *Plastics Engineering*, 33, 35 (1996).
90. F. Doghieri and G. C. Sarti, Nonequilibrium lattice Fluids: A Predictive Model for the Solubility in Glassy Polymers, *Macromolecules*, 29, 24, 7885 (1996).
91. R. M. Conforti, T. A. Barbari, P. Vinalchand, and M. D. Donohue, A lattice-based activity coefficient model for gas sorption in glassy polymers, *Macromolecules*, 24, 3388-3394 (1991).
92. G. Glenn Lipscomb, Unified thermodynamics analysis of sorption in rubbery and glassy materials, *AIChE Journal*, 36, 10, 1505 (1990).
93. D. Boudouris, C. Panayiotou, On the solubility of gas molecules in glassy polymers and the nonequilibrium approach, *Macromolecules*, 31, 7915-7920 (1998).
94. W. R. Vieth, J. M. Howell and J. H. Hsieh, Dual Sorption Theory: Review Paper, *Journal of Membrane Science*, 1, 177-220 (1976).
95. E. J. Cain, W. Y. Wen, A. A. Jones, P. T. Inglefield, B. J. Cauley and J. T. Bendler, A Dual Mode Interpretation of Spin Relaxation for $^{13}CO_2$ Sorbed in Polycarbonate, *Journal of Polymer Science: Part B: Polymer Physics*, 29, 1009 (1991).
96. M. D. Sefcik and J. Schaefer, Solid-state carbon-13 NMR evidence for gas-polymer interactions in the carbon dioxide-polyvinyl chloride system, *Journal of Polymer Science: Polymer Physics Edition*, 21, 7, 1055-62 (1983).
97. A. Higuchi and T. Nakagawa, Infrared Spectroscopic studies of CO_2 Sorbed in Glassy and Rubbery Polymeric membranes, *Journal of Polymer Science: Part B: Polymer Physics*, 32, 1, 149 (1994).
98. K. Murata, S. Ogawa, E. Watanabe, Y. Hayashi, S. Yamashita, FT-IR measurements of some greenhouse gases in thin film of poly(methyl methacrylate), *Vibrational Spectroscopy*, 13, 235 (1997).
99. D. G. Pye, H. H. Hoehn and M. Panar, Measurement of Gas Permeability of Polymers. I. Permeabilities in Constant Volume / Variable Pressure Apparatus, *Journal of Applied Science*, 20, 1921 (1976).
100. R. D. Seigle and R. W. Coughlin, Errors in Diffusivity as Deduced from Permeation Experiments using Time Lag Technique, *Journal of Applied Polymer Science*, 14, 3145 (1970).
101. D. R. Paul and A. T. DiBenedetto, Diffusion in Amorphous Polymers, *Journal of Polymer Science: Part C*, 10, 17 (1965).
102. F. Vasak and Z. Broz, A method for determination of Gas Diffusion and Solubility coefficients in Poly(vinlytrimethylsilane) using a personal computer, *Journal of Membrane Science*, 83, 265 (1993).
103. J. B. Alexopoulos, J. A. Barrie and D. Machin, The Time Lag for the Diffusion of Gas Mixtures, *Polymer*, 10, 4, 265 (1969).
104. Christelle M. Laot, Understanding gas transport in physically aged, oriented and pressure densified amorphous glassy bisphenol-A polycarbonate, PhD preliminary examination thesis, Virginia Polytechnic Institute and State University, VA, USA, December 17, 1999.

Chapter 3

Literature review on physical aging and orientation, and their effects on the gas transport properties

3.1. Introduction

Backgrounds about physical aging and orientation are given in the first two sections of this chapter. Reviews of the pertinent literature concerning gas transport and physical aging, and gas transport and orientation, respectively, are then provided.

3.2. Physical aging

The excess free volume trapped in glassy polymers is at the origin of the non-equilibrium nature of the glassy state. The trapped volume can be visualized as dynamic microvoids or holes, with a distribution of sizes and shapes, dispersed inside the polymeric matrix. The size of the holes is on the order of Å. Glassy polymers tend to decrease their excess free volume with time by undergoing further chain packing. This phenomenon is referred to as physical aging or structural relaxation. Several reviews address this topic in the literature [1-12]. Obviously, the relaxation towards equilibrium is a self-retarding process, which takes an extremely long time since polymers below their glass transition temperature T_g do not have sufficient thermal energy to attain equilibrium

rapidly. The adjective "physical" is added to distinguish this particular aging phenomenon from other types of aging (chemical, biological, etc). Physical aging does not modify the structure of the polymers permanently; reversible changes in properties are always possible. The aging process is common to all glasses, and it can also be observed above T_g for semi-crystalline materials and polymers with fillers. Note though that no “true” physical aging should be possible above T_g if the glass transition peak (as seen in DMTA experiments for instance) is fully relaxed. Physical aging is generally monitored at constant temperature as a function of the logarithm of sub-T_g annealing time, although it could also be characterized by following changes with pressure or volume.

This section is dedicated to physical aging. Origin and typical aspects of physical aging are reviewed in the first subsection. Macrostructural and microstructural properties are discussed and compared in the second subsection. What one does know about physical aging and what remains to be solved is then mentioned. A short paragraph on the physical aging of polycarbonate is finally given.

3.2.1. Origin and typical aspects

3.2.1.1. Origin

Physical aging has been explained based on the same principles used to understand the glass transition temperature. The non-equilibrium nature of the glassy state has been attributed to the presence of free volume dispersed inside the polymeric matrix.

Physical aging can be understood by looking at

Figure **3.1**. The polymer in the liquid state is in equilibrium. However, as it is cooled down below T_g at a constant cooling rate, properties such as specific volume, enthalpy, and entropy deviate away from the equilibrium liquidus line. The polymer now possesses some excess thermodynamic quantities. The extent of the deviation from equilibrium depends on the rate of cooling. Indeed, T_g is not a true second order transition. It is a second order phase transition as defined by Ehrenfest [13] in the sense

that the first derivatives of the Gibbs free energy (the specific volume V, the enthalpy H, and the entropy S) are continuous at T_g, whereas the second derivatives (the heat capacity C_p, the isobaric coefficient of thermal expansion α, and the isothermal compressibility β) are discontinuous at T_g. However T_g is only a pseudo second order phase transition due to the fact that the glass is not a stable phase. T_g is a time-dependent quantity: the greater the cooling rate, the higher the value of T_g [14-22]. The T_g is actually defined as the temperature at which the free volume, or rather the mobility, is high enough to allow long-range cooperative motions of the molecules. The α-relaxation results from motions of the large segments of the polymer backbone. Actually, concerning the pseudo second order phase transition of the glass transition temperature, it is worth pointing out also that in volume relaxation measurements the T_g appears to be a second order transition in cooling but a first order transition in heating [20].

As the polymer is annealed at a temperature T_e below T_g, values of V, H, and S decrease gradually towards equilibrium and the property reaches a value X_g after some time t at T_e (see

Figure **3.1**). If enough time is allowed, the property may eventually reach the equilibrium liquid line. The rate towards equilibrium depends on the proximity of the sub-T_g annealing temperature T_e to T_g, as well as on chemical and structural factors. The greater the supercooling, the longer is the timescale of the relaxation process because of the reduced mobility. The lower the amount of free volume or configurational entropy, or the higher the coupling of the relaxation, the greater is the value of the relaxation time, and the slower the aging rate. Changes in the physical properties of the polymers have been found to depend on the value of T_e as well as on the aging time t_e.

When the aged polymer is heated back, it overshoots the equilibrium line at a temperature T_f referred to as the fictive temperature (see

Figure **3.1**). T_f may not be the same for all properties. Obviously, the longer the annealing time, the greater the difference between T_f and T_g. Initially, T_g and T_f are similar, and at equilibrium, T_f and T_e would be the same. The overshoot comes from the difference between the rates of cooling and heating. As a sample is quenched rapidly from above T_g and annealed for some time, the sample can be considered as slow cooled. Therefore,

when it is heated back there is a difference between slow cool and fast heat resulting in an overshoot.

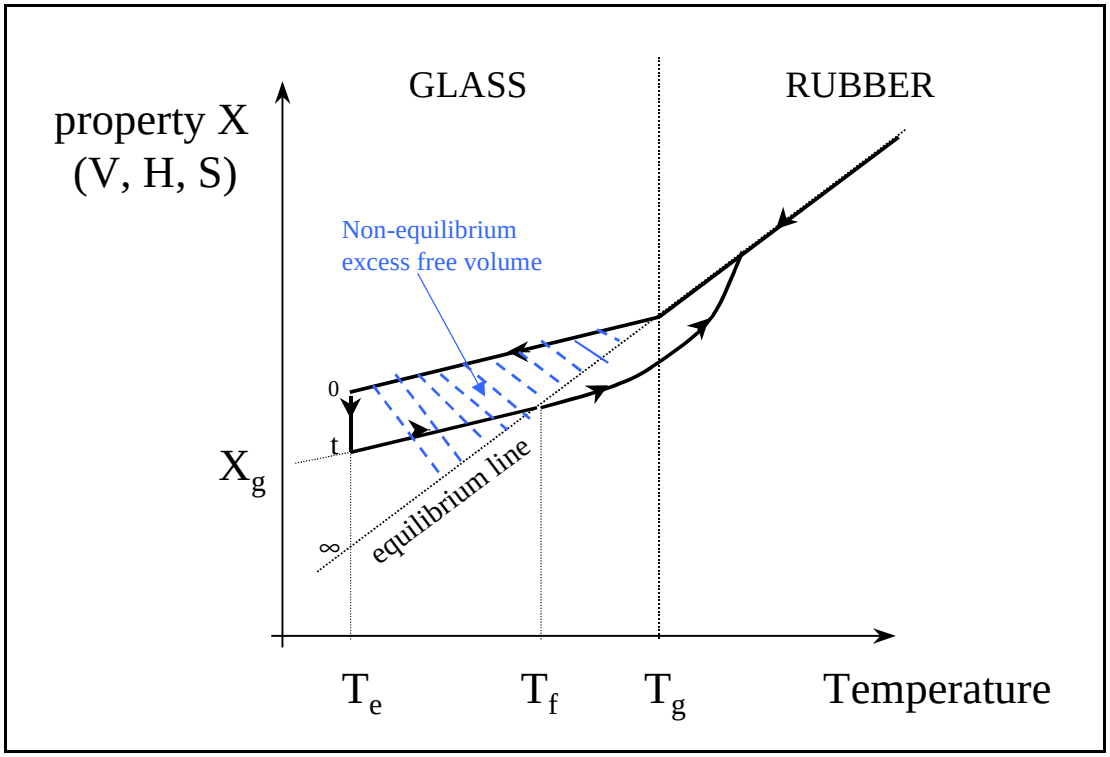

Figure 3.1: Schematic of property X (V, H, S) as a function of temperature showing the non-equilibrium excess free volume present in glassy polymers.

Physical aging is commonly studied at a given temperature and changes are monitored with time. The time-dependent structural changes affect any property that is a function of molecular mobility and especially the mechanical properties of the materials [1-11]. Yield stress, stiffness, deflection temperature, flexural and tensile strength, and elastic modulus are increased with sub-T_g annealing. Ductility, toughness, fracture energy, strain at break, and creep and stress relaxation rates are decreased. A transition from ductile behavior to brittle fracture is also observed with aging. The impact strength of amorphous polymers shows a discontinuity after some critical aging time. Aging has also a significant effect on the physical and thermal properties of polymers, such as density, refractive index, glass transition temperature, permeability, dielectric constant, specific volume, dimensions, etc. The enthalpy is also reduced since the endotherm area observed in DSC experiments is increased with aging.

Physical aging is generally explained based on the free volume concept outlined by Struik [1]. Below T_g the remaining free volume allows local motions and therefore conformational rearrangements. The molecules can oscillate between a limited number of conformations with minimum energy. With time, the free volume content contained in a glassy polymeric matrix decreases. The free volume concept is very useful in the sense that it gives a physical picture of the relaxation process. The concept originates from the work of Doolittle [23], who used it to describe the variation of the viscosity of liquids above T_g. Several theories, such as the one leading to the Williams, Landel, and Ferry (WLF) equation [24], have been based on the free volume idea. Although those theories should work strictly above the glass transition temperature T_g, they have been shown to be still useful in a range close to T_g. The glass transition temperature should not be explained based on the structure of the polymer since the same phenomenon is also observed in glassy metals, and low molecular weight or inorganic glassy materials.

Nevertheless, the definition of the free volume is not that precise, and actually different definitions can be found in the literature. The most common definition is that of fractional free volume, f, evaluated from the expression:

$$f = \frac{V - V_o}{V} = \frac{V_f}{V} \qquad \text{Eq (3.1)}$$

where V is the actual volume and V_o is the occupied volume. Thus V_f is the dynamic free volume or the excess space unoccupied by the molecules. It arises from the random arrangement of the molecules. The variation of the free volume with temperature has also been investigated. Above T_g, the following expression was suggested by Fox and Flory [25]:

$$f = 0.025 + \Delta\alpha\,(T - T_g) \qquad \text{Eq (3.2)}$$

where $\Delta\alpha$ is the difference between the thermal expansion coefficient above T_g and below T_g. Below T_g the fractional free volume is believed to remain constant and equal to 0.025.

However, the free volume concept remains fairly simple and is not enough to completely explain physical aging. Specimens of the same glassy polymer can have the same density, and therefore the same free volume, but still not the same thermal history,

and thus not necessarily the same properties. When a polymer that has been aged at a temperature T_e is heated to a higher temperature than T_e, but still below T_g, deaging effects are visible. In the early times, the polymer eliminates some of its thermal history, and then starts aging over again. That polymeric samples show memory effects has been studied extensively by Kovacs [26, 27]. The fact that the samples seem to remember their previous thermal histories is attributed to the existence of a distribution of relaxation times. Using a single relaxation time to model the aging phenomena is therefore completely inadequate. Furthermore, the relaxation is also characterized by a non-linearity, as discussed later in the subsection dealing with volume relaxation.

3.2.1.2. Typical aspects

The typical aspects of physical aging have been outlined by Struik [1]. They are summarized below.

- Aging in amorphous polymer glasses occurs between the highest secondary transition temperature (T_β) and T_g. For instance, the temperature range for polycarbonate is between -100°C and 150°C. Some researchers believe that the temperature range in which physical aging occurs is much smaller, however this may be due to the differences in the sensitivities of the techniques used to monitor aging.
- Aging is a reversible phenomenon. Indeed, previous histories can be erased by heating the sample above T_g or by rejuvenating it.
- Aging primarily affects relaxation times τ. τ increases with the aging time t_e.
- The aging time is the dominant aging parameter. Indeed, the retardation time τ is given as follows:

$$\tau = k\, t_e \left(T_g - T_e\right) \qquad \text{Eq (3.3)}$$

The difference between T_g and T_e cannot be that large, and therefore t_e happens to be the parameter to manipulate. The Arrhenius-type thermal activation used for instance for secondary relaxations does not apply to aging studies. Sometimes aging effects appear stronger at lower temperature than at higher temperature.

- The WLF superposition concepts apply to physical aging at constant temperature for a limited range below T_g. The WLF time-temperature superposition on unaged materials is carried out by following changes in the material at different temperatures. However here the rate of aging depends on the aging temperature T_e. When a polymer is aged at T_e, the shapes of the resulting curves are the same. Time-aging time superposition is achieved by shifting curves both horizontally and vertically with respect to a reference time. The shift rate μ is however defined only with respect to horizontal shifting. Consequently, we have:

$$\mu = \frac{\text{dloga}}{\text{dlogt}_e} \qquad \text{Eq (3.4)}$$

  where a is the WLF shift factor. The shift rate μ is generally very close to 1 just below T_g for amorphous polymers in the linear viscoelastic range. However the quantitative analysis is complicated by the fact that vertical shifts are generally performed. Furthermore, one has to be aware that this time-aging time superposition is based on the assumption that the relaxation strength remains constant and that the relaxation time distribution keeps the same shape on aging, which is not necessarily true. Actually, the data are sometimes impossible to superpose.
- Mechanical stresses have a strong effect on aging. Applying a stress before, during, and after aging leads to an acceleration of the aging, a retardation, and a deaging effect, respectively [5].

3.2.2. Macrostructural and microstructural properties

Physical aging can be observed macroscopically by studying volume or enthalpy relaxation, as well as microscopically by spectroscopic or scattering techniques. The methods used in both cases and the results relevant to physical aging are summarized in the following subsections.

3.2.2.1. Macrostructural relaxation

Changes in bulk properties have been investigated by several techniques, such as dilatometry, differential scanning calorimetry (DSC), creep, stress relaxation, dynamic mechanical analysis (DMA), tensile testing, and dielectric constant. Experimental results obtained by the first four methods can be extensively found in the literature.

3.2.2.1.1. Volume relaxation

Volume relaxation is assessed by dilatometry. Although dilatometers provide excellent data, the number of studies is rather limited because of the lack of commercial equipment. The specific volume is measured as a function of temperature at a constant heating rate. As a polymer is annealed at a temperature T_e, its volume decreases as well as the value of its glass transition temperature T_g. The specific volume is observed to decrease linearly with the logarithm of annealing time.

The relative departure from equilibrium is given by:

$$\delta_V = \frac{V - V_\infty}{V_\infty} \qquad \text{Eq (3.5)}$$

where V is the volume and V_∞ is the equilibrium volume at constant temperature. δ_V is usually plotted as a function of $\log(t-t_i)$ where t_i is the initial time.
The volume relaxation rate β_V is expressed as:

$$\beta_V = -\frac{d\delta_V}{d\log(t - t_i)} \approx -\frac{1}{V}\frac{dV}{d\log(t - t_i)} \qquad \text{Eq (3.6)}$$

The value of β_V has to be obtained at sufficient long aging times to ensure that the delay before the inflection slope has indeed been reached.

The essential features of the structural relaxation, i.e. the distribution of relaxation times and the non-linearity of the response are clearly observed by dilatometry. The distribution of relaxation times is reflected by the memory effects, as studied extensively by Kovacs [26, 27]. The non-linearity of the relaxation is observed while studying the kinetics of

isothermal recovery for a sample that is heated or cooled from a particular temperature. Although the magnitude of the temperature departure is the same for both expansion and contraction experiments (but of opposite signs), response curves are asymmetrical [27]. The equilibrium appears to be approached more rapidly by contraction ($\Delta T < 0$) than by expansion ($\Delta T > 0$). In addition, the relaxation is much slower than the exponential because of the two features of the relaxation, which are its distribution and its non-linearity.

The shape of the curves of the volume relaxation rates versus temperature are different for each polymer [22]. Usually the relaxation rate increases with temperature up to below T_g and then drops significantly. The maximum relaxation rate values obtained just below T_g differ also from one polymer to another. However in the case of PMMA two lower maxima are observed near the secondary transition temperatures [22].

The effective relaxation time is given by:

$$\frac{1}{\tau_{eff}} = -\frac{1}{\delta_V}\frac{d\delta_V}{dt} \qquad \text{Eq (3.7)}$$

A phenomenon referred to as the τ_{eff} paradox is sometimes mentioned in the literature. It is explained as follows. Indication of the temperature at which the relaxation time at equilibrium has been achieved is not sufficient; the path taken to equilibrium also affects the value of τ_{eff} at equilibrium. This paradox is a serious problem for the concepts outlined in the literature aimed at describing the glassy state. So far, only the coupling model [28] has been successful in describing the τ_{eff} paradox. The mathematical models will not be outlined in this literature review. The reader can refer to some excellent review if interested [4].

3.2.2.1.2. Enthalpy relaxation

Numerous differential scanning calorimetry (DSC) studies related to aging are available in the literature [29-42]. The experimental apparatus is simple to use and DSC equipment is easily found in research laboratories. A polymeric sample and a reference

material are heated at a constant rate, the difference in the electrical power needed for each is calculated, and the specific heat is given as a function of temperature. The enthalpy recovery (or enthalpy relaxation) is obtained by integrating the DSC scan. When a polymer has been aged at T_e well below T_g, its DSC scan shows an endothermal peak around T_g. This overshoot peak increases in magnitude with t_e and the position of the maximum T_{max} shifts to higher temperatures. Furthermore, the higher the annealing temperature, the higher is the value of T_{max} at the same annealing time. It has been demonstrated that T_{max} increases linearly with T_e and with log t_e. As expected from free volume concepts, the glass transition temperature increases with annealing time.

The distribution of relaxation times can be observed by the presence of an overshoot peak in the DSC scan, however enthalpy relaxation studies do not show the non-linearity aspect of the behavior, as do volume relaxation studies (see above).

The excess enthalpy δ_H is given by:

$$\delta_H = H_t - H_\infty \qquad \text{Eq (3.8)}$$

where H_t is the enthalpy at some time t and H_∞ is the equilibrium enthalpy. δ_H has been shown to be linearly dependent on log t_e. In order to get the value of H_∞, samples have to be scanned until no further change can be noticed in DSC traces. Obviously, the higher the annealing temperature, the faster the achievement of the equilibrium.

The enthalpy relaxation rate β_H is expressed as:

$$\beta_H = -\frac{d\delta_H}{dlogt} \qquad \text{Eq (3.9)}$$

The experimental error is quite large for δ_H, at least much larger than for δ_V. In order to eliminate errors due to sample-to-sample variation, instrumental baseline and calibration drift, and differences in location of the sample within the DSC cell, the following procedure has to be done. Aged samples which have been scanned and are therefore in the liquid state, and thus in equilibrium, have to be rapidly cooled and reheated one more time. The two scans are superimposed and the difference in the areas under the two curves can be evaluated.

Moreover, since DSC uses a heating scan mode, the history of the sample becomes quite complex, since additional aging is occurring during the measurement. Indeed, the thermal

cycle consists of three steps: cooling rate from the melt, annealing time at constant temperature, and heating rate. If the sample is prepared outside the DSC apparatus, the history is even more complex since some time at room temperature is also involved. Sub- and upper-T_g peaks are sometimes observed when specimens are reheated immediately after a quench [31]. DSC traces carry out contributions from both enthalpy and volume.

Modulated or oscillating DSC (referred to as MDSC) has been recently applied to study the aging process [43]. The advantage of this new technique is that the non-reversing and the reversing components can be separated. The former component indicates the enthalpy relaxation endotherm, whereas the latter gives the step change in C_p at T_g.

3.2.2.1.3. Mechanical and dielectric responses

The changes seen in the fundamental thermodynamic quantities are also reflected in the mechanical properties. Creep and stress relaxation tests are commonly carried out to study physical aging. Shift factors can easily be obtained from those two types of tests. Tensile testing also shows that the modulus and the yield point are increased with annealing [2, 44]. The yield stress and the drawing stress have been reported to increase linearly with log aging time [44]. Dielectric studies carried out on polycarbonate [45] showed that a new peak appeared at short aging time. The magnitude of the β-relaxation was found to decrease with aging [45, 46].

3.2.2.1.4. Conclusions

Structural relaxation occurring in the glassy state can be characterized by dilatometry, DSC, and mechanical and dielectric responses.

Physical aging is accompanied by decreases in volume and enthalpy. Although the responses given by dilatometry and DSC follow a similar trend, the physical aging rates are not identical in their magnitudes and vary also from one polymer to another. There is no simple correction factor that can account for the difference. The rate of the volume relaxation is generally considered to be greater than the one for enthalpy relaxation [4, 47]. Furthermore, the time scale for volume relaxation is shorter than that

for enthalpy relaxation. Equilibrium is indeed generally achieved faster in dilatometry than in DSC. In a careful study, Plazek and co-workers [48] have nevertheless concluded that for polystyrene the time for recovery of enthalpy and volume is the same, but the rate of recovery of the volume is faster. Molecular motions do not always contribute to a change in volume. Since the rates of volume and enthalpy relaxations are not equal, the thermodynamic description of the glassy state may require more than one additional parameter in addition to temperature and pressure. Mechanical measurements may be more correlated to one type of relaxation than another. Yield stress data for polycarbonate for instance follow enthalpy relaxation better than volume relaxation [33]. Mechanical response tends to reach equilibrium before the volume [49].

3.2.2.2. Microstructural aspects

Bulk properties are rather interesting in characterizing physical aging and distribution of relaxation times, however they do not give any insight about the nature of the processes taking place at the molecular level. However, the macroscopic properties can be interpreted only if the microscopic-scale phenomena are understood. Other techniques have to be used to probe mobility on a molecular scale and to investigate the molecular reorganizations taking place in the system with sub-T_g annealing. Those techniques are reviewed in the next section.

3.2.2.2.1. Electron spin resonance (ESR)

ESR measures the motion of nitroxide radicals. Both spin probes or spin labels (radical covalently bonded to the polymer) can be used. Radicals have been shown to be sensitive to their local environment as they diffuse into polymers. Aging is characterized by following the change in T_{50G}. T_{50G} refers to the temperature at which an abrupt change is observed for 50G. Although the results so far have been more qualitative than quantitative, ESR has the potential to reveal the existence of the distribution of free volume [50].

3.2.2.2.2. Fluorescence spectroscopy

Fluorescence spectroscopy seems to provide the most valuable results for aging studies, although the literature remains relatively sparse on the subject. While probing the structure of the polymer with fluorescent molecules, an increase in fluorescence intensity is attributed to a reduction in molecular mobility. Fluorescence spectroscopy has been able to examine a distribution of free volume as well as to observe memory effects [51]. However the most interesting feature of these fluorescence studies is that the relative departure from equilibrium δ_F is similar to that of enthalpy relaxation. As for volume and enthalpy relaxations, δ_F has also been shown to increase linearly with log t_e [52].

3.2.2.2.3. Positron annihilation

Positron annihilation lifetime spectroscopy (PALS) has been proven to be an effective tool in studying the free volume between different polymeric materials. It is at the moment the only technique believed to give an indication of the free volume directly. For a more comprehensive review of the subject, one can consult several reviews in the literature [16, 53-55]. Nevertheless a number of limitations are also associated with PALS. Briefly, PALS has been shown to measure both the free volume and the free volume distribution. Please note that this free volume is referred to as holes in the literature concerning PALS. PALS can probe spherical holes of about 0.5Å to 10Å, having a lifetime of at least 10^{-9}s. Three annihilation processes are possible for the positron (the antiparticle of the electron), each decay mode having its own characteristic lifetime (referred to as τ_1, τ_2, and τ_3). The area under each of the three decay curves provides information about three intensities called I_1, I_2, and I_3. The lifetime τ_3 is proportional to the average hole size, whereas the relative intensity I_3 provides a measure of the concentration or number of holes. Therefore, with the knowledge of those two quantities it is possible to calculate the hole size distribution. The fractional free volume for polycarbonate has been given as the product of τ_3, I_3, and a constant C (with C = $0.0018\%^{-1}ns^{-1}$ for polycarbonate [53, 55-58]). Changes in τ_3 and I_3 are however very

limited when studying aging compared to changes observed between various polymer structures.

PALS studies on physical aging have reached the following conclusions. It has been found that on aging at temperatures below the glass transition range, the free volume holes in polycarbonate do not decrease in size but rather in number [54, 59-63]. Indeed, τ_3 was reported to remain relatively constant with aging whereas I_3 was significantly reduced. Therefore, the free volume decreased with aging, although the average hole size remained unaffected by aging. It should be pointed out, however, that PALS results were specific to the polymer and cannot be generalized.

Nevertheless the PALS data are prone to problems while studying the physical aging phenomenon. Indeed, it has been shown that radiation effects from the source can also induce a reduction in intensity [4, 53, 63]. The longer the positron exposure time, the more is the reduction in intensity. Since PALS requires a minimum exposure time of 0.5h to get enough data to generate a smooth decay curve convertible to a mathematical expression, short aging time cannot be studied with the PALS technique because of the changes induced during the data collection. However, charging effects were determined not to be significant for polycarbonate when sensitive spectrometers were used [63, 64]. The results found in the literature are sometimes very misleading since they are plotted on a linear scale instead of a logarithmic one [54, 59, 61, 63, 65]. Anomalies in the PALS fitting procedure have also been pointed out [63].

PALS remains a static measure of the free volume. Although PALS gives the hole size directly, it cannot provide information on the mobility of this free volume.

In addition to PALS which measures the time of emission, two other techniques based on positron annihilation are also available. Those techniques are angular correlation of annihilation radiation (ACAR) and Doppler broadening spectroscopy (DBS). Energies of positron annihilation are obtained by the former technique, momenta by the latter one. ACAR can provide information about the geometry of the holes [66].

3.2.2.2.4. Photochromic probes and labels

UV-vis spectroscopy can detect the changes between the absorption spectra of reversible trans and cis-isomers of chromophores. Those changes appear in chromophores when there is sufficient molecular mobility. The free volume environment can thus be probed as a function of aging. It has been reported by photochromic probes that aging was due to a rapid reduction in the fraction of sites with large free volume [67-69]. The results were however incompatible with volume relaxation results by about one order of magnitude.

3.2.2.2.5. Infrared and Raman spectroscopies

Molecular motions can be characterized by infrared spectroscopy (IR). The effects of annealing and aging on the IR spectra of polycarbonate have been investigated. Conformational rearrangements were found to take place with annealing. The population of low energy trans-trans conformations increased while the trans-cis ones decreased [70]. In contrast, infrared data collected on amorphous PET showed a drive towards a more random structure. Annealing was accompanied by changes from a trans to a gauche conformation [71]. The structural rearrangements observed with annealing seemed therefore to depend on the polymer. One has to realize however that those conformational changes may not always induce a change in volume and thus a densification. Infrared studies by Heymans [70] have also shown that rejuvenation (or deaging of the glass) by cold-drawing induces an increase in the trans-cis conformation.

Raman difference spectroscopy has been used by Stolarski et al [72, 73] to demonstrate intermolecular cooperative motion in polycarbonate. Frequency shifts in aged samples due to conformational changes were observed to take place within the material with aging. Therefore, aging seemed to result from the drive towards a low energy conformation of the polymer chains.

3.2.2.2.6. Other methods

Several NMR studies using different techniques have shown that some low energy motions are present with aging [74-79].

The effects of physical aging on the gas transport properties will be reported in a separate subsection.

Small angle X-ray scattering (SAXS) measures density fluctuations inside polymers and thus the nonuniform distribution of local free volume. Unfortunately SAXS remains a static measure of the free volume. The local free volume distribution in polycarbonate is known to be quite broad. Quite surprisingly, changes occurring in the thermal density fluctuations of isotropic polycarbonate with aging appear only in a limited range around T_g (from 130 to 147^{o}C) [80]. This is observed independently of the aging time and the aging temperature. No changes could be detected at lower temperature where volume and enthalpy are considerably reduced. Unfortunately bulk properties yield information about an average free volume. Curro and Roe [80] suggested two possible explanations. The first one is that the timescale for changes in density fluctuations was much longer than that of volume or enthalpy relaxations. However this seems rather unlikely. The second explanation is that the average size of a free volume hole increased with aging while the free volume still decreased. The change in the density fluctuation is function of both the size of the holes and the free volume fraction and can be modeled. Based on the mathematical expression, if the density fluctuation remained constant, the size of the hole had to increase with aging.

3.2.2.3. Conclusions

Based on the previous discussions, it is rather clear that the phenomena observed macroscopically and the ones taking place at the molecular level are quite different. Changes in bulk properties are measured for all glassy polymers. The response is therefore universal. Nevertheless, the rates of the relaxations observed by dilatometry and DSC are not similar. No explanation has been found so far. The enthalpy may be more connected to the microscopic scale than one tends to believe. Changes observed at the

molecular level cannot be considered as universal anymore. They seem to depend on the chemical structure of the polymer of interest.

3.2.3. Physical aging: what is known and what remains to be known

3.2.3.1. What is known

The physical aging phenomenon results from a driving force towards equilibrium.

The free volume concept alone is not sufficient to explain physical aging. Indeed, two specimens of the same glassy polymer can have the same density and therefore the same free volume content, but still not the same thermal history and thus not necessarily the same properties. It has also been shown that an identical amount of aged volumetric departure from equilibrium cannot correspond to the same conformational structure because of the occurrence of crossing phenomena [81]. Properties may become controlled by the free volume content as the polymers approach the glass transition region [82].

The polymer chains have to reorganize themselves with time or to change their conformations in order to reach the equilibrium state.

Cooperativity concepts are likely to come into play in any physical aging picture. However those concepts may be needed only for longer-range motions, or at higher thermal energy levels. Localized motions and their dynamics seem to have an importance as well.

Any theory that intends to explain or model the aging process should be able to explain the time-dependent properties, the memory effects, the non-linearity, the asymmetry, and the τ_{eff} paradox.

3.2.3.2. What remains to be known

There remain several unanswered questions concerning physical aging.

The temperature range over which physical aging occurs is still a controversial subject. Struik [1] postulated that aging is taking place between T_β and T_g. However there is a body of evidence that showed that this should also occur at lower temperatures than T_β [22, 81].

The use of different techniques leads to different physical aging rates. There appears to be no simple correlation between the volume and the enthalpy relaxation rates of various polymers [4, 44]. The rate for volume relaxation is generally considered to be greater than the one for enthalpy relaxation [4, 47]. In a careful study, Plazek and co-workers [48] have concluded that for polystyrene the time for recovery of enthalpy and volume is the same, but the rate of recovery of the volume is faster. The shift factors of creep and enthalpy relaxations have also been found to differ [44]. The factors that influence the rates (and possibly the timescales) of physical aging remain to be found. Also, the correlations (if any) between on one side the volume and the enthalpy relaxations and on the other side mechanical properties such as creep and stress relaxations (that are believed to reflect the structural motions) should be investigated.

The nature and the dynamics of the microscopic molecular changes and their effects on the longer-range cooperative motions that lead to changes in the macroscopic properties are not fully understood.

The details of the molecular reorganizations need to be known.

The crossing phenomenon observed by dilatometry at temperatures below T_β or slightly above in atactic polystyrenes remains to be explained [81]. The kinetic theories that postulate the existence of an extrapolated equilibrium state and the convergence of the volumetric departure from equilibrium with time, hence the total free volume

dependence of the volume recovery, are unable to do so. The experimental results show that the volumetric relative departure from equilibrium does not converge with time. Instead, when the atactic polystyrene samples are quenched from various temperatures above T_g to the aging temperature, the response of the greater temperature crosses with time other curves obtained at lower temperatures of quenching.

Orientation has been shown to increase the density of polycarbonate [83-88] and hence reduce the free volume content. The value of the glass transition temperature T_g has also been found to increase with stretching [85, 87]. However when aging studies are conducted on uniaxially oriented amorphous glassy polymers, volume relaxation is enhanced by one order of magnitude in both cold and hot drawn samples despite the much higher density [83-86, 89-91]. Quite surprisingly, the creep aging rates were found to be reduced with orientation, in spite of the increase in the volume recovery [86]. Actually it should be pointed out that some researchers believed at the time of their publications that free volume was increased as a result of the cold-drawing process [83, 90, 92, 93].

Furthermore, enhanced physical aging has also been observed on pressure-densified amorphous polystyrene samples [94]. The samples were densified by applying a given pressure above T_g and by releasing it afterwards at room temperature.

Addition of low molecular weight additives in polycarbonate also resulted in a densification of the material and an acceleration of the volume recovery [95]. However in this particular case, the increased mobility was attributed to antiplasticization effects. The free volume theory cannot account for the plasticization of polar polymers by water either [96]. Although the density increases with water, the T_g decreases, in contradiction with the free volume theory. It has been postulated that water breaks intermolecular hydrogen bonds leading to a greater chain mobility.

The results outlined above suggest that the concept of free volume commonly used to provide a physical picture of physical aging may not be adequate. According to the free volume theory [1] a higher density should result in a lower mobility, and thus a lower aging rate. Instead, enhancement of physical aging has been observed in oriented and pressure densified polymers.

One could postulate that the nature of aging is different in the linear and the non-linear viscoelastic ranges. Nevertheless, a study by Costa et al [97] on completely amorphous 100% cis PTBA pointed out the importance of the microstructure. In this particular study, it was observed that packing was accelerated with aging in the higher density samples.

There must be another order parameter which could be used to determine the mechanical properties of glassy materials. The distribution of free volume, the degree of short-range structural order, or the shape of the free volume holes as well as polymer chain dynamics, may be also important in determining the mechanical and physical properties of glassy materials. It has been known for a long time that knowledge of the free volume alone does not allow prediction of the future behavior of the polymers. For instance, two polymers can have the same density, but completely different properties because of a difference in the free volume distribution. One sample could have been prepared under elevated pressures, while another oriented, yet another isothermally aged, etc. The memory effects studies by Kovacs [26] are also a manifestation of this fact. Based on evidence found in the literature, such as rejuvenation studies (aging was found not to be erased by deformation, in contradiction with the free volume theory) [98-100] or SAXS data on anisotropic samples [83, 90], local ordering is likely to be a very important parameter in determining the physical aging rate of oriented polymers, especially at temperatures below the glass transition region. The width of the free volume distribution of polycarbonate was observed by SAXS to increase with cold-drawing and to decrease with further annealing [83, 90]. Thermal density fluctuations of undrawn samples on the other hand have been shown to remain constant with aging, independently of the aging time and aging temperature [80, 90]. Cold-drawing was believed to generate cavities on the small-scale side of the distribution, which relaxed first with aging [83]. It was observed that density fluctuations in hot-drawn specimens were similar to those of isotropic samples [90]. A more random structure was observed by SAXS in pressure densified polymers [94]. Rejuvenation studies of McKenna and co-workers by torsional deformation [99], creep [100], and stress relaxation [98] have pointed out the invalidity of the free volume theory. For instance, it was observed that aging was not erased by deformation [100]. Struik [1] believes that some free volume is created whenever there is

a deformation, regardless of whether it is a tensile, a compressive, or a shear deformation. This would explain rejuvenation or deaging of the glass under high stresses. Struik [101] has attempted to justify the data of McKenna and co-workers (mentioned above) from his view point. However results obtained by Van Dilk [102] have not found an explanation so far by the defender of the free volume concepts. The volume was found by Van Dilk to decrease linearly in uniaxial compression. Furthermore, as suggested by Song and Roe [94], the T_g may not be an iso-free volume state, but a state of iso-relaxation time, depending not only on the amount of free volume, but also on the state of local packing of segments. In fact, the concept of an iso-free volume T_g has been shown to be inconsistent with isochoric results [103].

The cavity sizes affected by physical aging are not well-established. Contradictions can be found in the literature for polycarbonate for instance. The average hole size is said to decrease with time [104], to increase [80], or to remain unaffected by aging [54, 59-63, 105].

Finally, it is worth pointing out the results of a study by Wimberger-Friedl and de Bruin [95]. The researchers measured the density of isotropic polycarbonate at room temperature over a very long aging time period of as much as seven years. The resolution of the density gradient column was maintained at about 4×10^5 g/cm^3. Quite surprisingly, the change in specific volume was found to be accelerated after a period of about six months at room temperature. The slope increased by at least one order of magnitude. The results indicated that the mobility of the system could not be completely attributed to the free volume. It seems therefore impossible to predict long-term behavior from short-time tests. Furthermore, it also means that equilibrium could possibly be reached at some finite time. Note that the findings of Wimberger-Friedl and de Bruin [95] have been confirmed in a recent publication by Robertson and Wilkes using a dilatometer [106]. Polycarbonate did present a change in its volume relaxation rate after about six months at room temperature, whereas atactic polystyrene did not. The fact that polycarbonate is capable of crystallizing, whereas atactic polystyrene is not, was pointed out by the researchers. Nevertheless, no signs of crystallinity were found on the polycarbonate samples.

3.2.4. Physical aging of polycarbonate

Polycarbonate is often considered as a reference polymer. It should therefore behave like the other polymers. However, polycarbonate presents some particularities. For example, it is difficult to crystallize under normal conditions [107-109], no strain-induced crystallization occurs, aging accelerates at room temperature after a period of about six months [95], the entanglement molecular weight is rather low (about 4,800 g/mol [110]), the maximum shift rate is rather high (about 1.2 [1]), and the characteristic ratio C_∞ is very low (about 2.4).

At (T_g-15^{o}C) the volume relaxation rate of polycarbonate (PC) is given as about $8x10^{-4}$ per decade and that of the enthalpy relaxation rate as about 0.6 $J^{-1}g$ per decade [4]. The relaxation rates are therefore much higher than those of PMMA for instance measured at (T_g-15^{o}C) as well ($4x10^{-4}$and 0.4 $J^{-1}g$ per decade, respectively) [4]. Although PVC and PS showed similar volume relaxation rates than the volume relaxation rate of PC, they do possess higher enthalpy relaxation rates [4]. At (T_g-20^{o}C) the creep and the enthalpy relaxation shift rates of PC were found to differ (μ=0.87 and μ_H=0.49, respectively) [44]. This suggests that mechanical responses age faster than does the enthalpy (assuming that the theoretical models are correct). The relaxation time spectra may also be different in both cases.

Using photochromic probes it has been determined that all the cavity sizes in PC decreased equally with physical aging [105]. In contrast, a rapid reduction in the amount of large free volume sites in PS and PMMA has been observed by the same technique, therefore indicating a system-dependent relationship [67, 68, 111].

All typical polymers should behave similarly with aging at a macroscopic level. If there is any difference between two polymers, this has to occur at the microscopic level due to changes in the chemical structure.

3.3. Orientation

As a sample is stretched uniaxially, the chains orient themselves in the draw direction. The degree of orientation increases as the temperature decreases (at constant strain rate) and as the strain rate increases (at constant temperature) [112]. This degree is quantified in the literature by two quantities: the draw ratio λ and the Hermans' orientation function f.

The draw ratio λ is defined as follows:

$$\lambda = \left(\frac{l}{l_0} \right) \qquad \text{Eq (3.10)}$$

where l represents the length after the stretch and l_o the initial length before stretching. The draw ratio is related to the strain ε by the following relationship:

$$\lambda = 1 + \varepsilon \qquad \text{Eq (3.11)}$$

The Hermans' orientation function f is defined as follows:

$$f = \frac{3\left\langle \cos^2\theta \right\rangle - 1}{2} \qquad \text{Eq (3.12)}$$

The angle θ represents the angle between the reference axis and the polymer chain axis. The value of f varies from +1 to 0 to -0.5 for orientation that are respectively parallel, random and perpendicular to the uniaxial direction. A schematic is provided in Figure 3.2.

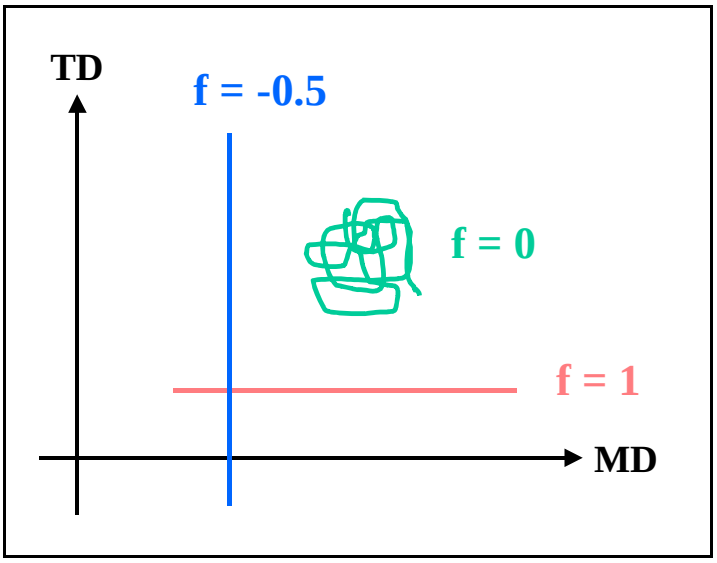

Figure 3.2: Schematic showing the various values of the Hermans' orientation function f. The value of f varies from 1 (parallel orientation to the uniaxial direction) to 0 (random) to –0.5 (perpendicular). MD and TD stand for the machine and the transverse directions, respectively. The lines at f = -0.5 and f = 1 correspond to fully oriented polymer chains.

Various techniques such as electron microscopy, sonic velocity, small-angle neutron scattering, birefringence, X-ray scattering and linear dichroism are capable of measuring the orientation of molecular chains and structures. The reader can refer to a review by Wilkes [113] for further insight on the use of various techniques in determining molecular orientation in polymers. Linear dichroism and birefringence are the most common techniques used to study orientation in polycarbonate [66, 84-87, 114-117]. A characteristic of infrared dichroism is that it gives information on the orientation of very localized parts of a molecular chain. The birefringence method provides only information about an average orientation of the molecules.

3.4. Physical aging and gas transport

The effects of physical aging on the gas transport properties of various polymers have been reported in the literature [118-126]. The gas transport parameters, namely the permeability coefficient P, the diffusion coefficient D, and the solubility coefficient S, were observed to decrease with aging time. Most of the data were analyzed in terms of the dual mode sorption model (DMS) presented in Chapter 2. C_H' has been shown to be

the only parameter dependent on aging [119]. C_H' has been reported to be directly related to the enthalpy of the material [119]. However the variations observed seem rather large to draw conclusions. Moreover, the limitations of the DMS model have been given in Chapter 2.

The vast majority of published data about physical aging and gas transport should be looked at very carefully. Most of the published data was obtained on conditioned samples, i.e. samples that had been exposed for some time to the highest pressure to be used in the experiment. The applied pressures were typically in the order of 20 to 30atm. The conditioning process enabled researchers to obtain reproducible data, unfortunately it may have induced irreversible structural changes inside the polymer as well [57, 127-132]. The penetrant could have induced some morphological changes by conformational rearrangements and consequently changed the free volume distribution. An hysteresis between sorption and desorption is typically observed for CO_2. Exposure of polycarbonate to high pressures of CO_2 was reported from positron annihilation lifetime spectroscopy (PALS) measurements to increase not only the hole content but the average hole size as well, indicating a broader hole size distribution [57]. After deaging, the samples could not recover the same characteristics they had before exposure. In addition, the conditioning time is not clearly reported in the literature, and therefore it seems difficult to compare data obtained by different research groups for the same polymer/gas system. The state of the sample should depend on the exposure time as well as on the resting time before characterizing the samples. Furthermore, exposure of a polymer to hydrostatic pressure may accelerate the rate of aging after releasing of the pressure [5]. Polymer films are also commonly used as as-received or cast from solution. The majority of published data from the membrane community has been obtained on as-received samples. Results may be complicated by the orientational state of the polymer since commercial films are very often oriented to some extent. The thermal history needs to be better controlled as this affects the properties tremendously. Solvents can also induce orientation [133] or even crystallize the polymers [134]. Carbon dioxide is generally used to study aging effects; however the fact that the gas induces plasticization [127-132, 135-151] may complicate the analysis. It has been shown that the T_g in bisphenol-A

polycarbonate for instance can drop by as much as 50°C for a CO_2 absorbed mass fraction of 0.05 [150]. Exposure to CO_2 has been observed to reverse the effect of sub-T_g annealing in polycarbonate [150, 151]. CO_2 in the gas state is even capable of inducing crystallization in some polymers [152]. Finally, the aging results reported in the literature were in general based on gas sorption rather than gas permeation experiments. Gas sorption experiments measure the amount of gas sorbed in a polymer as a function of pressure. Each data point is obtained at pseudo-equilibrium and this may take a few days to collect one data point. A sorption experiment can easily take more than a month to be completed [153], and therefore the polymer cannot be assumed to remain the same throughout the experiment because of aging effects.

Acceleration of aging has been reported to take place in thin membranes [154-156]. For films of sub-micron thickness, the lower the thickness, the greater is the loss in permeability with sub-T_g annealing, and the better is the selectivity between two gases. One may also point out that the fact that the membranes were cast from solution onto a glass plate may have induced some orientation. And this orientation may have accelerated aging (see above). Two mechanisms of free volume loss have been suggested by McCaig et al [157] for the sub-micron thickness films: a thickness dependent free volume diffusion to the film surface and a thickness independent lattice contraction. In addition, the glass transition of sub-micron thickness films has also been shown to depend nonlinearly on the thickness [158]. The lower the thickness, the lower is the T_g. This thickness dependent T_g has been used to predict the acceleration of aging in thin films [159]. The aging rate determined from gas transport measurements were also shown to be different at the surface and in the bulk [160]. The gas transport physical aging rate in sub-micron thickness films has been shown to be significantly reduced by crosslinking the polymer [161].

New gas transport studies free of the complications listed above should be conducted in order to confirm the trends reported in the literature.

3.5. Orientation and gas transport

The morphology of the polymer is expected to highly affect the gas transport properties. Nevertheless, little is known about the importance of molecular orientation on the gas transport properties of amorphous glasses. The few papers dealing with this subject are sometimes complicated by the presence of strain-induced crystallinity in the polymeric samples. The few studies dealing with orientation and gas transport are reviewed below.

The effect of uniaxial orientation on the gas transport properties of poly(vinyl chloride) (PVC) was investigated by El-Hibri and Paul [162]. This study remains the most complete in the field of gas transport and orientation. The permeability coefficient of He and Ar were found to decrease with orientation. Quite interestingly, when the permeability coefficient was plotted as a function of the drawing temperature, a strong change in slope was noticed at about (T_g + 15^{o}C), for a draw ratio of 3. In contrast, the curve corresponding to a draw ratio of 1, i.e. to the isotropic sample, decreased monotonically with the drawing temperature. Unfortunately the gas transport results were presented for a single draw ratio λ of 1 and 3. It would have been better to present those as a function of a particular Hermans' orientation function f since the relation between λ and f is not always linear [85]. Furthermore it is not clear whether the draw ratios of 3 obtained at various temperatures, both below and above T_g, correspond to the same Hermans' orientation function. Actually, the crosshead speed below T_g corresponded to 25% of the value of the speed above T_g. This change in crosshead speed is likely to change the value of f. The observed birefringence was reported as a function of the drawing temperature for the draw ratio of 3, although no change in slope was observed at T_g. Since the observed birefringence is not always equal to the orientational birefringence (especially below T_g where distortional birefringence cannot be neglected [84]), the correlations between observed birefringence and gas transport can yield erroneous results. At a stretching temperature of (T_g + 25^{o}C), the gas transport parameters were given as a function of the birefringence. The permeability coefficient was found to decrease almost linearly as a function of the birefringence for He, Ar, and N_2. A change

in slope was observed at a birefringence value of about 4×10^{-3} for both the diffusion and the solubility coefficients of Ar and N_2 (determination of those of He were impossible). The solubility coefficient decreased initially with birefringence and remained constant after this particular value of about 4×10^{-3} for the birefringence, whereas the decrease in the diffusion coefficient was accelerated after this particular value. Quite interestingly, the density was observed to remain constant throughout the whole birefringence range, indicating that the gas transport parameters may not be directly related to the amount of free volume. However mention of the presence of crystallinity in the commercial PVC samples raises some doubts about the conclusions of this publication. The researchers actually showed that annealing the PVC above T_g generated some secondary crystallization. The effect of crystallinity on gas transport properties is well-documented [163-167]. The crystals are impermeable to the gas molecules and therefore gas molecules have to travel around them. Relationships have been determined between the gas transport parameters and the crystallinity. The solubility coefficient S is reduced with crystallinity as follows:

$$S = S_a\, X_a = S_a\,(1 - X_c) \qquad \text{Eq (3.13)}$$

where X_c is the fraction of crystallinity, X_a the amorphous fraction, and S_a the solubility coefficient of the amorphous material. The diffusion coefficient does not decrease proportionally to the decrease of the amorphous fraction. The change in the diffusion coefficient D is given by:

$$D = \frac{D_a}{\tau} \qquad \text{Eq (3.14)}$$

where D_a is the diffusion coefficient in the amorphous polymer and τ is the tortuosity factor. τ depends on the degree of crystallinity, and on the size, shape, and distribution of the crystallites as well. El-Hibri and Paul [162] determined that the secondary crystallization rate of PVC was maximal at a drawing temperature of (T_g + 25°C). Similarly, the diffusion coefficient of isotropic PVC was observed to present a minimum at the same drawing temperature. The solubility coefficient presented a maximum at the same point. It seems, therefore, that their gas parameter results obtained for isotropic

samples at least (that were given the same thermal treatment as the anisotropic samples) were highly complicated by the presence of crystallinity.

Wang and Porter [163] investigated the CO_2 permeation of uniaxially hot-drawn atactic polystyrene (PS) samples. No crystallinity was apparently detected in the samples after drawing. The permeability and the diffusion coefficients were found to decrease with drawing, while the solubility coefficient remained constant. The decrease in the diffusion coefficient was attributed to the restriction in diffusion generated by orientation. However the fact that CO_2 plasticizes polymers [127-132, 135-151] complicates the results. The T_g and the density were nevertheless found to remain unaffected by drawing, in agreement with the solubility results. Therefore, the free volume in PS seems to remain constant with drawing.

Shelby and co-workers [168] investigated the room temperature oxygen permeability of hot-drawn polycarbonate films ($T_{stretch}$ = 160^{o}C). It was observed that the permeability first increased up to a draw ratio of about 1.25, and then decreased linearly with the draw ratio. Quite interestingly, the density was found to present a minimum at the same critical point. The maximum in the permeability was attributed to an increase in free volume initially with stretching.

Smith and Adam [169] studied the permeability coefficient of nitrogen through polycarbonate. The polymer was directly stretched inside the permeation apparatus and measurements were taken as a function of the strain. At 128^{o}C, i.e. about 22^{o}C below T_g, the permeability coefficient increased with stretching, but the response could be separated into two parts. At strain levels under 3%, the increase in the permeability coefficient was attributed to an increase in free volume, whereas above 3% (the upper experimental limit being 5%), the increase was assigned to crazing. The gas transport behavior of a cold-drawn polyimide film was studied as well by the same researchers. The behavior appeared as extremely complex since the response was completely different at 72^{o}C compared to 125^{o}C (both temperatures being much lower than the T_g of polyimide). The gas used in this study concerning polyimide was chosen as CO_2 and not N_2. The

permeability coefficient was found to increase with strain at 72^{o}C. However at 125^{o}C, it first increased, and at about 2% started to decrease almost linearly with the strain. A change in the microstructure of the polyimide was believed to be responsible for the changes. Since no physical tests were performed, it is rather difficult to explain the data.

Muzovskaya and Malkin [170] reported that the diffusion coefficient of oxygen in polycarbonate increased with uniaxial orientation, and decreased in compression. Unfortunately, no reference was given in the publication [170] and no trace of such data could be found in the literature.

Barker et al [171] observed a linear relationship between the logarithm of the preexponential factor for diffusion D_o and a well-established function involving the draw ratio taken from the rubber elasticity theory. The relationship was verified using various gases in a series of poly(alkyl methacrylates) stretched uniaxially above T_g and quenched immediately after drawing. It should be noted that the permeation experiments were performed at temperatures below T_g. The D_o value is likely to be different above T_g, though.

The various results discussed above suggest that the influence of orientation on the gas transport parameters is rather complex. Further studies need to be conducted. Especially, a polymer that does not show any signs of strain-induced crystallization has to be selected in order to isolate the effect of the amorphous orientation only. Moreover, gases that do not induce any plasticization effects have to be chosen, in order to isolate free volume changes due only to orientation.

3.6. References

1. L. C. E. Struik, Physical aging in amorphous polymers and other materials, Elsevier, New York, 1978.
2. M. R. Tant and G. L. Wilkes, An overview of the nonequilibrium behavior of polymer glasses, *Polymer Engineering and Science*, 21, 14, 874 (1981).
3. J. M. Hutchinson, Relaxation processes and physical aging, in The Physics of Glassy Polymers, edited by R. N. Haward and R. J. Young, Chapman & Hall, London, 1997.
4. J. M. Hutchinson, Physical aging of polymers, *Prog. Polym. Sci.* , 20, 703 (1995).
5. R. P. Chartoff, Thermoplastic polymers, in Thermal characterization of polymeric materials, E. A. Turi, edt, Academic Press, NY, 548-573 (1997).
6. L. C. E. Struik, Aging, Physical, *Encyclopedia of Polymer Science and Engineerin*g, vol 1, 595-611, Wiley, NY (1985).
7. J. M. O'Reilly, Review of structure and mobility in amorphous polymers, *CRC critical reviews in solid state and materials sciences*, 13, 3, 259-277 (1987).
8. J. Mijovic, L. Nicolais, A. D'Amore, J. M. Kenny, Principal features of structural relaxation in glassy polymers- A review, *Polymer Enginering and Science*, 34, 5, 381 (1994).
9. S, Matsuoka, Free volume, excess entropy and mechanical behavior of polymeric glasses, *Polymer Engineering and Science*, mid-october, 21, 14, 907-921 (1981).
10. J.-C. Bauwens, Physical aging: relation between free volume and plastic deformation, in Failure of plastics, W. Brostow and R. D. Corneliussen, edts, Hanser Publishers, Munich (1986).
11. L. C. E. Struik, Physical aging: influence on the deformation behavior of amorphous polymers, in Failure of plastics, W. Brostow and R. D. Corneliussen, edts, Hanser Publishers, Munich (1986).
12. R. A. Pethrick, Physical aging – an old problem revisited, *TRIP*, 1, 8, 226-227 (1993).
13. P. Ehrenfest, *Leiden Comm. Suppl.*, 756 (1933).
14. Dr. Hervé Marand, lecture notes.
15. B.–S. Hsu, S.-H. Kwan, Directional anisotropy of dielectric β-relaxation in oriented poly(ethylene terephthalate), *Journal of Polymer Science: Polymer Physics Edition*, 14, 1591 (1976).
16. D. M. Bigg, A review of positron annihilation lifetime spectroscopy as applied to the physical aging of polymers, *Polymer Enginering and Science*, 36, 6, 737 (1996).
17. W. J. Davis and R. A. Pethrick, Investigation of physical ageing in polymethylmethacrylate using positron annihilation, dielectric relaxation and dynamic mechanical thermal analysis, *Polymer*, 39, 2, 255 (1998).
18. A. J. Kovacs, J. J. Aklonis, J. M. Hutchinson, and A. R. Ramos, Isobaric volume and enthalpy recovery of glasses. II. A transparent multiparameter theory, *Journal of Polymer Science: Polymer Physics Edition*, 17, 1097-1162 (1979).
19. J. M. Hutchinson, J. J. Aklonis, and A. J. Kovacs, A new phenomenological approach to volume recovery in glasses, *Polymer preprints*, 16, 2, 94-99 (1975).

20. A. J. Kovacs, A multiparameter approach for structural recovery of glasses and its implication for their physical properties, in Structure and mobility in molecular and atomic glasses, edited by J. M. O'Reilly and M. Goldstein, *Annals of the New York Academy of Sciences*, 371, 38-66 (1981).
21. H. Hachisuka, H. Takizawa, Y. Tsujita, A. Takizawa, and T. Kinoshita, Gas transport properties in polycarbonate films with various unrelaxed volumes, *Polymer*, 32, 13, 2382-2386 (1991).
22. R. Greiner and F. R. Schwarzl, Thermal contraction and volume relaxation of amorphous polymers, *Rheologica Acta*, 23, 378-395 (1984).
23. A. K. Doolittle, Studies in Newtonian flow - II - The dependence of the viscosity of liquids on free-space, *Journal of Applied Physics*, 22, 12, 1471-1475 (1951).
24. M. L. Williams, R. F. Landel and J. D. Ferry, *J. Am. Chem. Soci.*, 77, 3701 (1955).
25. T. G. Fox and P. J. Flory, *J. Appl. Phys.*, 21, 581 (1950).
26. A. J. Kovacs, Transition vitreuse dans les polymères amorphes- Etude phénomenologique, *Fortschr. Hochpolym.- Forsch.*, 394-507 (1963).
27. J. J. Aklonis and A. J. Kovacs, A new look at the glass transition, 267- ( ).
28. R. W. Rendell, K. L. Ngai, G. R. Fung and J. J. Aklonis, *Macromolecules*, 20, 1070-1083 (1987).
29. I. M. Hodge, Enthalpy relaxation and recovery in amorphous materials, *Journal of non-crystalline solids*, 169, 211 (1994).
30. J. H. Wendorff, Enthalpy relaxation and thermal density fluctuations, *Journal of Polymer Science: Polymer Letters Edition*, 17, 765 (1979).
31. M. Ruddy and J. M. Hutchinson, Multiple peaks in differential scanning calorimetry of polymer glasses, *Polymer communications*, 29, 132 (1988).
32. C. Bauwens-Crowet and J.-C. Bauwens, Annealing of polycarbonate below the glass transition:quantitative interpretation of the effect on yield stress and differential scanning calorimetry measurements, *Polymer*, 23, 1599 (1982).
33. C. Bauwens-Crowet, J. C. Bauwens, Annealing of polycarbonate below the glass transition temperature up to equilibrium: a quantitative interpretation of enthalpy relaxation, *Polymer*, 27, 709 (1986).
34. R.-J. Roe, S. K. Lo and R. P. Chartoff, The enthalpy relaxation of poly(vinyl chloride) annealed below the glass transition temperature, *Polym. Prepr., Am. Chem. Soc., Div. Polym. Chem.*, 17(2), 167 (1976).
35. C. B. McGowan, D. Y. Kim and R. B. Blumstein, Kinetics of enthalpy relaxation upon physical aging in glassy main-chain nematic polymers, *Macromolecules*, 25, 4658-4664 (1992).
36. A. R. Berens, I. M. Hodge, Effects of annealing and prior history on enthalpy relaxation in glassy polymers -1- Experimental study on poly(vinyl chloride), *Macromolecules*, 15, 756-761 (1982).
37. I. M. Hodge and A. R. Berens, Effects of annealing and prior history on enthalpy relaxation in glassy polymers -2- Mathematical modeling, *Macromolecules*, 15, 762-770 (1982).
38. I. M. Hodge and G. S. Huvard, Effects of annealing and prior history on enthalpy relaxation in glassy polymers -3- Experimental and modeling studies of polystyrene, *Macromolecules*, 16, 371-375 (1983).

39. J. J. Tribone, J. M. O'Reilly, and J. Greener, Analysis of enthalpy relaxation in poly(methyl methacrylate): effects of tacticity, deuteration, and thermal history, *Macromolecules*, 19, 1732-1739 (1986).
40. J. M. O'Reilly and I. M. Hodge, Effects of heating rate on enthalpy recovery in polystyrene, *Journal of non-crystalline solids*, 131-133, 451-456 (1991).
41. A. Agrawal, Effect of temperature and molecular weight on enthalpy relaxation in polystyrene, *Journal of Polymer Science: Part B: Polymer Physics*, 27, 1449-1461 (1989).
42. I. M. Hodge, Effects of annealing and prior history on enthalpy relaxation in glassy polymers - 4 - Comparison of five polymers, *Macromolecules*, 16, 898-902 (1983).
43. K. Takahara, H. Saito, T. Inoue, Physical aging in poly(methyl methacrylate) glass: densification via density fluctuation, *Polymer*, 40, 3729-3733 (1999).
44. J. M. Hutchinson, S. Smith, B. Horne, and G. M. Gourlay, Physical aging of polycarbonate: enthalpy relaxation, creep response, and yielding behavior, *Macromolecules*, 32, 5046-5061 (1999).
45. L. Guerdoux, E. Marchal, Physical ageing of PMMA and polycarbonate in the region of secondary relaxation, *Polymer*, 22, 1199 (1981).
46. H. Higuchi, Z. Yu, A. M. Jamieson, R. Simha, and J. D. McGervey, Thermal history and temperature dependence of viscoelastic properties of polymer glasses: relation to free volume quantities, *Journal of Polymer Science: Part B: Polymer Physics*, 33, 2295-2305 (1995).
47. J. M. G. Cowie, S. Harris, and I. J. McEwen, Physical aging in poly(vinyl acetate) 2- Relative rates of volume and enthalpy relaxation, *Macromolecules*, 31, 2611-2615 (1998).
48. S. L. Simon, D. J. Plazek, B. J. Harper, and T. Holden, The rates of volume and enthalpy aging do not seem to be the same. Following on polystyrene, *PSME Preprints*, 76, 334 (1997).
49. G. B. McKenna, Y. Leterrier, C. R. Schultheisz, *Polym. Eng. Sci*., 35, 403 (1995).
50. G. G. Cameron, I. S. Miles, A. T. Bullock, *Br. Polym. J.*, 119, 129-134 (1987).
51. J. S. Royal, J. M. Torkelson, *Macromolecules*, 25, 1705-1710 (1992).
52. J. S. Royal, J. M. Torkelson, *Macromolecules*, 26, 5331-5335 (1993).
53. R. A. Pethrick, Positron annihilation – a probe for nanoscale voids and free volume? *Progress in Polymer Science*, 22, 1-47 (1997).
54. J. E. Kluin, H. Moaddel, M. Y. Ruan, Z. Yu, A. M. Jamieson, R. Simha, J. D. McGervey, Probe spectroscopy, free volume concepts, and physical aging of polymer glasses, in Structure-property relations in polymers: spectroscopy and performance, ACS, 236, 535-555 (1993).
55. G. P. Simon, The use of positron annihilation lifetime spectroscopy in probing free volume of multicomponent polymeric systems, *TRIP*, 5, 12, 394 (1997).
56. Y. C. Jean, J.-P. Yuan, J. Liu, Q. Deng, and H. Yang, Correlations between gas permeation and free-volume hole properties probed by positron annihilation spectroscopy, *Journal of Polymer Science: Part B: Polymer Physics*, 33, 2365-2371 (1995).
57. Y. C. Jean, X. Hong, J. Liu, C. M. Huang, H. Cao, C. Y. Chung, G. H. Dai, K. L. Cheng, H. Yang, High sensitivity of positron annihilation lifetime to time and

pressure effects in gas-exposed polymers, *Journal of Radioanalytical and Nuclear Chemistry, Articles*, 210, 2, 513-524 (1996).

58. X. Hong, Y. C. Jean, H. Yang, S. S. Jordan, W. J. Koros, Free-volume hole properties of gas-exposed polycarbonate studied by positron annihilation lifetime spectroscopy, *Macromolecules*, 29, 7859-7864 (1996).
59. A. J. Hill, I. M. Katz and P. L. Jones, Isothermal volume relaxation in aged polycarbonate measured by positron annihilation lifetime spectroscopy, *Polymer Enginering and Science*, 30, 13, 762 (1990).
60. T. C. Sandreczki, X. Hong, and Y. C. Jean, Sub-glass-transition-temperature annealing of polycarbonate studied by positron annihilation spectroscopy, *Macromolecules*, 29, 4015-4018 (1996).
61. A. J. Hill, C. M. Agrawal, Positron lifetime spectroscopy characterization of thermal history effects on polycarbonate, *Journal of Materials Science*, 25, 5036-5042 (1990).
62. T. C. Sandreczki, X. Homg, and Y. C. Jean, Sub-glass-transition temperature annealing of polycarbonate studied by positron annihilation spectroscopy, *Macromolecules*, 29, 4015-4018 (1996).
63. J. E. Kluin, Z. Yu, S. Vleeshouwers, J. D. McGervey, A. M. Jamieson, R. Simha, Temperature and time dependence of free volume in bisphenol A polycarbonate studied by positron lifetime spectroscopy, *Macromolecules*, 25, 19, 5089 (1992).
64. W. J. Davis and R. A. Pethrick, Positron annihilation studies of physical ageing in polycarbonate, *Eur. Polym. J.*, 34, 12, 1747-1754 (1998).
65. A. J. Hill, K. J. Heater, C. M. Agrawai, The effects of physical aging in polycarbonate, *Journal of Polymer Science: Part B: Polymer Physics*, 28, 387 (1990).
66. Y. C. Jean, Y. Rhee, Y. Lou, D. Shelby, G. L. Wilkes, Anisotropy of hole structures in oriented polycarbonate probed by two-dimensional angular correlation of annihilation radiation, *Journal of Polymer Science: Part B: Polymer Physics*, 34, 2979-2985 (1996).
67. J. G. Victor and J. M. Torkelson, *Macromolecules*, 20, 2241-2250 (1987).
68. J. G. Victor and J. M. Torkelson, *Macromolecules*, 21, 3490-3497 (1988).
69. J. S. Royal and J. M. Torkelson, *Macromolecules*, 25, 4792-4796 (1992).
70. N. Heymans, FTIR investigation of structural modification of polycarbonate during thermodynamical treatments, *Polymer*, 38, 14, 3435 (1997).
71. R. S. Moore, K. K. O'Loane and J. C. Shearer, Fourier transform infrared characterization of conformational changes in amorphous poly(ethylene terephthalate) during volume recovery, *Polymer Engineering and Science*, 21, 14, 903 (1981).
72. V. Stolarski, A. Letton, E. Nour, J. Laane, Conformational changes and physical aging in bisphenol-A polycarbonate; origins of mechanical properties, *ANTEC'94*, 2077 (1994).
73. V. Stolarski, A. Letton, S. N. Lee, J. Laane, Conformational changes and physical aging in bisphenol-A polycarbonate; origins of mechanical properties, *Polym. Mater. Sci. Eng.*, 71, 479-480 (1994).
74. J. Schaefer, E. O. Stejskal, R. A. McKay, W. T. Dixon, *Macromolecules*, 17, 1479 (1984).

75. M. P. Henrichs, M. Linder, et al., *Macromolecules*, 17, 2412 (1984).
76. M. P. Henrichs, V. A. Nicely, *Macromolecules*, 24, 2506 (1991).
77. J. Y. Iho, A. F. Yee, *Macromolecules*, 24, 1905 (1991).
78. M. P. Henrichs, V. A. Nicely, *Macromolecules*, 23, 3193 (1990).
79. M. P. Henrichs, H. R. Luss, R. P. Scaringe, *Macromolecules*, 22, 2731 (1989).
80. J. J. Curro and R.-J. Roe, Isothermal relaxation of specific volume and density fluctuation in poly(methyl methacrylate) and polycarbonate, *Polymer*, 25, 1424 (1984).
81. H. H. D. Lee and F. J. Mc Garry, Some previously unexpected phenomena of volume recovery, *J. Macromol. Sci. – Phys.*, B30, 3, 185-200 (1991).
82. H. Higuchi, A. M. Jamieson, and R. Simha, Free volume quantities and viscoelasticity of polymer glasses, *Journal of Polymer Science: Part B: Polymer Physics*, 34, 1423-1426 (1996).
83. J. Bartos, J. Muller, J. H. Wendorff, Physical ageing of isotropic and anisotropic polycarbonate, *Polymer*, 31, 1678 (1990).
84. M.-S. S. Wu, Intrinsic birefringence of amorphous poly(bisphenol-A carbonate), *Journal of Applied Polymer Science*, 32, 3263-3275 (1986).
85. M. D. Shelby and G. L. Wilkes, Thermodynamic characterization of the oriented state of bisphenol A polycarbonate as it pertains to enhanced physical aging, *Journal of Polymer Science: Part B: Polymer Physics*, 36, 2111 (1998).
86. M. D. Shelby and G. L. Wilkes, The effect of molecular orientation on the physical ageing of amorphous polymers - dilatometric and mechanical creep behaviour, *Polymer*, 39, 26, 6767-6779 (1998).
87. E. Ito, T. Hatakeyama, Studies of the amorphous region of polymers- II - Relationship between change of structure and glass-transition temperature in polycarbonate, *Journal of Polymer Science: Polymer Physics Edition*, 13, 2313-2320 (1975).
88. E. Ito, K. Sawamura and S. Saito, Effects of drawing on molecular motions in polycarbonate, *Colloid & Polymer Sci.*, 253, 480-484 (1975).
89. R. Pixa, B. Grisoni, T. Gay, and D. Froelich, Influence of deformation on physical aging of polycarbonate- 2 - Volume recovery near ambient temperature, *Polymer Bulletin*, 16, 381-387 (1986).
90. J. Muller, J. H. Wendorff, Thermal density- Fluctuations in rejuvenated and aged polycarbonate, *Journal of Polymer Science: Part C: Polymer Letters*, 26, 421 (1988).
91. J.-J. Pesce and G. B. McKenna, Prediction of the subyield extension and compression responses of glassy polycarbonate from torsional measurements, *J. Rheol.*, 41, 5, 929-942 (1997).
92. G. Yianakopoulos, J. Vanderschueren, and J. Niezette, Effect of mechanical deformations on thermally stimulated currents in polymers. 1. Uniaxially cold-drawn polycarboante, *Proceedings of the 6th International Symposium on electrets (ISE 6)*, Oxford, England, 131-136 (1988).
93. G. Yianakopoulos, J. Vanderschueren, and J. Niezette, Sub-Tg relaxation in cold-drawn polymers. Thermally-stimulated-current methods, *IEEE Transactions on electrical insulation*, 24, 3, 429-438 (1989).

94. H. H. Song and R.-J. Roe, Structural change accompanying volume change in amorphous polystyrene as studied by small and intermediate angle X-ray scattering, *Macromolecules*, 20, 2723-2732 (1987).
95. R. Wimberger-Friedl and J. G. de Bruin, The very long-term volume recovery of polycarbonate: is self-retardation finite? *Macromolecules*, 29, 4992-4997 (1996).
96. J. J. Aklonis, W. J. MacKnight, M. Shen, Introduction to polymer viscoelasticity, Wiley-Interscience, NY, 1972.
J. J. Aklonis and W. J. MacKnight, Introduction to polymer viscoelasticity, 2nd edition, John Wiley & Sons, NY, 1983.
97. G. Costa, S. Chikhaoui, A. Turturro, L. Carpaneto, Physical ageing phenomena in poly(tert-butylacetylene): influence of the microstructure, *Macromol. Chem. Phys.*, 198, 239-249 (1997).
98. D. M. Colucci, P. A. O'Connell, G. B. McKenna, Stress relaxation experiments in polycarbonate: a comparison of volume changes for two commercial grades, *Polymer Engineering and Science*, 37, 9, 1469 (1997).
99. M. M. Santore, R. S. Duran, G. B. McKenna, Volume recovery in epoxy glasses subjected to torsional deformations: the question of rejuvenation, *Polymer*, 32, 13, 2377 (1991).
100. A. Lee and G. B. McKenna, The physical ageing response of an epoxy glass subjected to large stresses, *Polymer*, 31, 423-430 (1990).
101. L. C. E. struik, On the rejuvenation of physically aged polymers by mechanical deformation, *Polymer*, 38, 16, 4053-4057 (1997).
102. D. J. Van Dijk, Thesis, Technical University, Delft, 1980.
103. D. M. Colucci, G. B. McKenna, J. J. Filliben, A. Lee, D. B. Curliss, K. B. Bowman, J. D. Russell, Isochoric and isobaric glass formation: similarities and differences, *Journal of Polymer Science: Physics Edition*, 1561-1573 (1997).
104. L. B. Liu, D. Gidley, A. F. Yee, Effect of cyclic stress on structural changes in polycarbonate as probed by positron annihilation lifetime spectroscopy , *Journal of Polymer Science: Part B: Polymer Physics*, 30, 231 (1992).
105. J. S. Royal and J. M. Torkelson, Photochromic and fluorescent probe studies in glassy polymer matrices. 5. Effects of physical aging on bisphenol-A polycarbonates and poly(vinyl acetate) as sensed by a size distribution of photochronic probes, *Macromolecules*, 25, 4792 (1992).
106. C. G. Robertson and G. L. Wilkes, Long-term volume relaxation of bisphenol A polycarbonate and atactic polystyrene, *Macromolecules*, 33, 3954-3955 (2000).
107. A. Siegmann and P. H. Geil, *J. Macromol. Sci. Phys.*, B4, 239 (1970).
108. A. Siegmann and P. H. Geil, *J. Macromol. Sci. Phys.*, B4, 273 (1970).
109. A. Alizadeh, S. Sohn, J. Quinn, H. Marand, L. C. Shank, H. Darrell Iler, Influence of structural and topological constraints on the crystallization and melting behavior of polymers: 3. Bisphenol A Polycarbonate, *Macromolecules*, 34, 4066-4078 (2001).
110. Richard P. Wool, *Polymer Interfaces- Structure and Strength*, Hanser Publishers, 1995.
111. H. L. Hampsch, J. Yang, G. K. Wong, and J. M. Torkelson, Dopant orientation dynamics in doped second-order nonlinear optical amorphous polymers. 2. Effects of physical aging on poled films, *Macromolecules*, 23, 3648-3654 (1990).

112. L. C. E. Struik, Internal stresses, dimensional instabilities and molecular orientations in plastics, John Wiley and Sons, New York, 1990.
113. G. L. Wilkes, Rheooptical properties, in Encyclopedia of Science and Engineering, 14 (1984).
114. E. Ito, K. Sawamura and S. Saito, Effects of drawing on molecular motions in polycarbonate, *Colloid & Polymer Sci.*, 253, 480-484 (1975).
115. R. Song, Q. Fan, Polycarbonate films in the state of high global chain orientation but nearly random segmental orientation, *European Polymer Journal*, 36, 1463-1470 (2000).
116. A. C. Lunn and I. V. Yannas, Chain-backbone motion in glassy polycarbonate studied by polarized infrared spectroscopy, *Journal of Polymer Science: Polymer Physics Edition*, 10, 2189-2208 (1972).
117. L. Lundberg and J.-F. Jansson, Anisotropic creep behaviour of oriented polycarbonate, *Polymer*, 35, 10, 2084-2089 (1994).
118. H. Hachisuka, H. Takizawa, T. Tsujita, A. Takizawa, T. Kinoshita, gas transport properties in polycarbonate films with various unrelaxed volumes, *Polymer*, 32, 13, 2383 (1991).
119. A. H. Chan and D. R. Paul, Effect of sub-Tg annealing on CO_2 sorption in polycarbonate, *Polymer Enginering and Science*, 20, 1, 87 (1980).
120. H. Hachisuka, Y. Tsujita, A. Takizawa, T. Kinoshita, Gas transport properties of annealed polyimide films, *Journal of Polymer Science: Part B: Polymer Physics*, 29, 11 (1991).
121. K. Toi, T. Ito, I. Ikemoto, Effect of aging and conditioning on the gas transport of poly(vinyl acetate), *Journal of Polymer Science: Polymer Letters Edition*, 23, 525-529 (1985).
122. K. Nagai, T. Nakagawa, Effects of aging on the gas permeability and solubility in poly(1-trimethylsilyl-1-propyne) membranes synthetized with various catalysts, *Journal of Membrane Science*, 105, 261-272 (1995).
123. Von K.-H. Illers, Einfluss der thermischen Vorgeschichte auf die Eigenschaften von Polyvinylchlorid, *Die Makromolekulare Chemie*, 127, 3032, 1-33 (1969).
124. T. Nakagawa, T. Watanabe, M. Mori, K. Nagai, Aging phenomena of gas permeability of poly[1-(tri-methylsilyl)-1-pripyne] and its blend polymer, Polym. Mater. Sci. Eng., 77, 249 (1997).
125. H. Hachisuka, K. Kito, Y. Tsujita, A. Takizawa, T. Kinoshita, O_2 and N_2 gas permselectivity of alternating copoly(vinylidene cyanide-vinyl acetate), *Journal of Applied Polymer Science*, 35, 1333 (1988).
126. T. L. Smith and R. E. Adam, Effect of tensile deformations on gas transport in glassy polymer films, *Polymer*, 22, 299-304 (1981).
127. S. M. Jordan, W. J. Koros, J. K. Beasley, Characterization of CO_2-induced conditioning of polycarbonate films using penetrants with different solubilities, *Journal of Membrane Science*, 43, 103-120 (1989).
128. D. S. Pope, G. K. Fleming, W. J. Koros, Effect of various exposure histories on sorption and dilation in a family of polycarbonates, *Macromolecules*, 23, 2988 (1990).

129. W. R. Vieth, L. H. Dao, and H. Pedersen, Non-equilibrium microstructural and transport characteristics of glassy poly(ethylene terephthalate), *Journal of Membrane Science*, 60, 41-62 (1991).
130. A. G. Wonders and D. R. Paul, Effects of CO_2 Exposure History on Sorption and transport in Polycarbonate, *Journal of Membrane Science*, 5, 63 (1979).
131. G. K. Fleming and W. J. Koros, Carbon Dioxide Conditioning Effects on Sorption and Volume Dilation Behavior for bisphenol A - Polycarbonate, *Macromolecules*, 23, 1353 (1990).
132. K. Tanaka, M. Ito, H. Kita, K. Okamoto, Y. Ito, The effects of CO2-conditioning of polymers on positron annihilation and gas permeation properties, *Bull. Chem. Soc. Jpn.*, 68, 3011-3017 (1995).
133. Dr. G. L. Wilkes, lecture notes.
134. J. Dybal, P. Schmidt, J. Baldrian and J. Kratochvil, Ordered structures in polycarbonate studied by infrared and raman spectroscopy, wide-angle X-ray scattering, and differential scanning calorimetry, *Macromolecules*, 31, 6611-6619 (1998).
135. A. Bos, I. G. M. Punt, M. Wessling, H. Strathmann, CO_2-induced plasticization phenomena in glassy polymers, *Journal of Membrane Science*, 155, 67-78 (1999).
136. J. S. Chiou, J. W. Barlow and D. R. Paul, Plasticization of Glassy Polymers by CO_2, *Journal of Applied Polymer Science*, 30, 2633 (1985).
137. R. G. Wissinger and M. E. Paulaitis, Glass Transitions in Polymer/CO_2 Mixtures at Elevated Pressures, *Journal of Polymer Science, Part B: Polymer Physics*, 29, 5, 631 (1991).
138. E. S. Sanders, Penetrant-induced plasticization and gas permeation in glassy polymers, *Journal of Membrane Science*, 37, 63-80 (1988).
139. M. Wessling, S. Schoeman, Th. Van den Boomgaard, C. A. Smolders, Plasticization of gas separation membranes, *Gas Sep. Purif.*, 5, 222-228 (1991).
140. Y. P. Handa, S. Lampron, M. L. O'Neill, On the plasticization of poly(2,6-dimethyl phenylene oxide) by CO_2, *J. Polym. Sci., Polym. Phys. Ed.*, 32, 2549-2553 (1994).
141. W.-C. Wang, E. J. Kramer, W. G. Sachse, Effects of high –pressure CO_2 on the glass transition temperature and mechanical properties of polystyrene, *J. Polym. Sci., Polym. Phys. Ed.*, 20, 1371-1384 (1982).
142. J. R. Fried, H.-C. Liu, C. Zhang, Effect of sorbed carbon dioxide on the dynamic mechanical properties of glassy polymers, *J. Polym. Sci., Polym. Part C*, 27, 385-392 (1989).
143. T. S. Chow, Molecular interpretation of the glass transition temperature of polymerdiluent systems, *Macromolecules*, 13, 362-364 (1980).
144. M. Wessling, Z. Borneman, Th. Van den Boomgaard, C. A. Smolders, Carbon dioxide foaming of glassy polymers, *J. Appl. Polym. Sci.*, 53, 1497-1512 (1994).
145. H. Hachisuka, T. Sato, T. Imai, Y. Tsujita, A. Takizawa, T. Kinoshita, Glass transition temperature of glassy polymers plasticized by CO_2 gas, *Polymer Journal*, 22, 1, 77 (1990).
146. J.-S. Wang, Y. Kamiya, Y. Naito, Effects of CO_2 conditioning on sorption, dilation, and transport properties of polysulfone, *Journal of Polymer Science: Part B: Polymer Physics*, 36, 1695 (1998).

147. G. K. Fleming and W. J. Koros, Dilation of Polymers by Sorption of Carbon Dioxide at Elevated Pressures. 1. Silicone Rubber and Unconditioned Polycarbonate, *Macromolecules*, 19, 2285 (1986).
148. P. Gotthardt, A. Grűger, H. g. Brion, R. Plaetschke, and R. Kirchheim, Volume change of glassy polymers by sorption of small molecules and its relation to the intermolecular space, *Macromolecules*, 30, 8058-8065 (1997).
149. S.-H. Chen, S.-L. Huang, K.-C. Yu, J.-Y. Lai, M.-T. Liang, Effect of CO_2 treated polycarbonate membranes on gas transport and sorption properties, *Journal of Membrane Science*, 172, 105-112 (2000).
150. B. G. Risch and G. L. Wilkes, Effects of physical aging and carbon dioxide absorption in bisphenol-A polycarbonate, *Journal of Applied Polymer Science*, 56, 1511 (1995).
151. A. H. Chan and D. R. Paul, Influence of history on the gas sorption, thermal, and mechanical properties of glassy polycarbonate, *Journal of Applied Polymer Science*, 24, 1539-1550 (1979).
152. J. S. Chiou, J. W. Barlow and D. R. Paul, Polymer Crystallization Induced by sorption of CO_2 Gas, *Journal of applied Polymer Science*, 30, 3911 (1985).
153. Christelle M. Laot, Understanding gas transport in physically aged, oriented and pressure densified amorphous glassy bisphenol-A polycarbonate, PhD preliminary examination thesis, Virginia Polytechnic Institute and State University, VA, USA, December 17, 1999.
154. P. H. Pfromm and W. J. Koros, Accelerated physical ageing of thin glassy polymer films evidence from gas transport measurements, *Polymer*, 36, 12, 2379 (1995).
155. P. H. Pfromm and W. J. Koros, Accelerated physical ageing of thin glassy polymer films, *Polym. Mater. Sci. Eng.*, 71, 401 (1994).
156. M. S. McCaig, D. R. Paul, Effect of film thickness on the changes in gas permeability of a glassy polyarylate due to physical aging. Part I. Experimental observations, *Polymer*, 41, 629-637 (2000).
157. M. S. McCaig, D. R. Paul, J. W. Barlow, Effect of film thickness on the changes in gas permeability of a glassy polyarylate due to physical aging. Part II. Mathematical model, *Polymer*, 41, 639-648 (2000).
158. J. L. Keddie, R.A.L. Jones, R. A. Cory, *Europhys. Lett.*, 27, 59 (1994).
159. K. D. Dorkenoo and P. H. Pfromm, Experimental evidence and theoretical analysis of physical aging in thin and thick amorphous glassy polymer films, *Journal of Polymer Science: Part B: Polymer Physics*, 37, 2239-2251 (1999).
160. K. Nagai, A. Higuchi, T. Nakagawa, Gas permeability and stability of poly(1-trimethylsilyl-1-propyne-co-1-phenyl-1-propyne) membranes, *Journal of Polymer Science: Part B: Polymer Physics*, 33, 289-298 (1995).
161. M. S. McCaig, D. R. Paul, Effect of UV crosslinking and physical aging on the gas permeability of thin glassy polyarylate films, *Polymer*, 40, 7209-7225 (1999).
162. M. J. El-Hibri and D. R. Paul, Effects of uniaxaial drawing and heat-treatment on gas sorption and transport in PVC, *Journal of Applied Polymer Science*, 30, 3649-3678 (1985).
163. L. H. Wang, R. S. Porter, On the CO2 permeation of uniaxially drawn polymers, *Journal of Polymer Science: Polymer Physics Edition*, 22, 1645-1653 (1984).

164. N. Kurosa, *Sen'i Gakkaishi*, 35, T-413 (1979).
165. W. J. Koros and D. R. Paul, *J. Polym. Sci.*, A-2, 16, 2171 (1978).
166. S. W. Lasoski, Jr., and W. H. Cobbs, *J. Polym. Sci.*, 36, 21 (1959).
167. N. E. Schlotter and P. Y. Furlan, A review of small molecule diffusion in polyolefins, *Polymer*, 33, 16, 3323 (1992).
168. M. D. Shelby, G. L. Wilkes, M. R. Tant, J. Zawada, T. J. Bastow and A. J. Hill, Amorphous orientation in glassy polycarbonate, *ACS, Polymeric Materials Science and Engineering, Conference Proceedings,* San Francisco, Spring 1997, 76, 485-6.
169. T. L. Smith and R. E. Adam, Effect of tensile deformations on gas transport in glassy polymer films, *Polymer*, 22, 299-304 (1981).
170. N. Yu. Muzovskaya and A. Ya. Malkin, Influence of orientation on the diffusion characteristics of polycarbonate, *Polymer Science USSR*, 27, 12, 2950-2954 (1985).
171. R. E. Barker, Jr., R. C. Tsai, R. A. Willency, Entropy correlation theory and diffusion measurements for oriented polymers, *Journal of Polymer Science: Polymer Symposium*, 63, 109-129 (1978).

Chapter 4

Experimental details

4.1. Introduction

This chapter provides a description of the materials and the instrumental methods used in this research. Details concerning the gas permeation data analysis are also provided. Calculations that need to be carried out to determine the gas transport parameters (P, D, and S) and the activation energies (E_P, E_D, and ΔH_s) are given.

4.2. The materials

As mentioned previously in Chapter 1, bisphenol-A polycarbonate was chosen in this research project due to its difficulty to crystallize under normal conditions and during stretching. This research does indeed focus on the amorphous solid state only. Furthermore, another feature of polycarbonate is that the main and secondary relaxations are well-separated in the dynamic thermal response, which makes aging easier to follow experimentally.

This particular section deals with the materials used in this research, their chemical characterization, and the film processing.

4.2.1. The polycarbonate

The chemical structure of bisphenol-A polycarbonate (PC) is given in Figure 4.1. A 3-d simulation of a portion of the polymer chain is also shown in Figure 4.2.

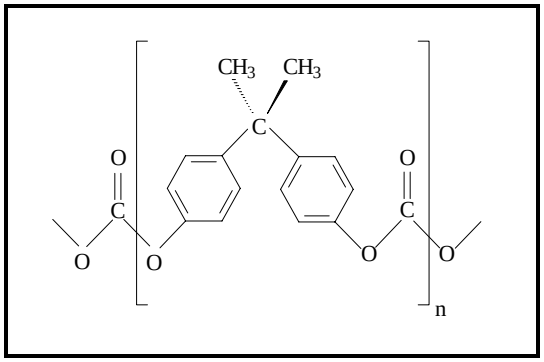

Figure 4.1: Chemical structure of bisphenol-A polycarbonate.

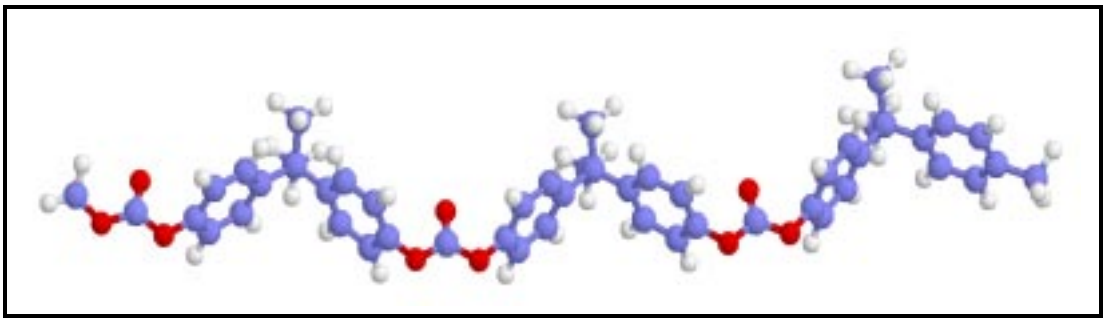

Figure 4.2: 3-dim simulation of a portion of the bisphenol-A polycarbonate chain. The simulation was obtained using the ChemWindow Spectroscopy software.

Bisphenol-A polycarbonate was ordered from two different suppliers. Polycarbonate pellets were purchased from Aldrich Chemical Company, Inc., Milwaukee, WI (catalog # 18,162-5, lot # 02409KN). The weight average molecular weight M_w was listed as 64,000 g/mol. Lexan 8010-112DC polycarbonate sheets were also obtained from General Electric GE Plastics. The molecular weight was unknown at the time of purchase. Two different thicknesses were ordered for the sheets, namely 7 mil and 30 mil. The sheets of a particular thickness were all coming from the same lot. However, a sheet of 7 mil from another lot was used in the first study of this research dealing with the effect of the free volume on the gas transport properties (Chapter 5). The

glass transition temperatures (T_g) of the Aldrich and the GE polycarbonates were given by the suppliers as 149^{o}C and 150^{o}C, respectively, as obtained by DSC from the second heating scan at a heating rate of 10^{o}C/min. The density was given as 1.2 g/cm^3 at 20^{o}C and the refractive index n_D^{20} as 1.585 in both cases.

The experimental data obtained in this research will mainly be based on the polymer purchased from Aldrich since this particular polymer is expected to contain less additives, if any, than the other polycarbonate.

4.2.2. Gel Permeation Chromatography (GPC)

Molecular weights, polydispersity indices, Mark-Houwink-Sakurada constants and radius of gyration of the polycarbonates used in this research were determined by Gel Permeation Chromatography (GPC). The data were obtained by Dr. Q. Ji and Dr. Y. Kim in the Chemistry Department of Virginia Tech.

A polycarbonate sample of about 30mg was dissolved in chloroform and a 100μL sample with a nominal concentration of about 3mg/mL was injected in the column having an elution solvent of chloroform with a flow rate of 1mL/min. The inlet pressure was maintained at 89.16kPa. The chromatograph was an Alliance Waters 2690 separations module equipped with HR 0.5+2+3+4 columns. The chromatograph possessed two types of detectors: an external refractometer and a Viscotek Model T60A viscometer. The molecular weights were determined based on those two detectors. At least two samples were run for each type of polycarbonate to ensure reproducibility in the measurements. The response in mV as a function of the retention volume in mL was obtained. The molecular weights were directly obtained by the instrument by comparing the data to adequate calibration curves. The reproducibility in M_w was found to be 5%.

The weight average molecular weight M_w, number average molecular weight M_n, polydispersity index PI (M_w/M_n), and radius of gyration $<Rg_n>$ of the various polymers used in this research are reported in Table 4.1. The Aldrich polycarbonate happens to have a much lower molecular weight than expected. As mentioned in the last subsection, M_w was listed in the Aldrich catalog as being about 64,000 g/mol. However, M_w was determined by GPC in this research to be about 34,000 g/mol. The experimental value

was confirmed by the company later on following our comment. The number average molecular weights M_n between the Aldrich and the GE polycarbonates differ by only 1.95%. The free volume is expected to relate to M_n more than to M_w, M_w being more appropriate to follow properties such as creep.

supplier	M_n	M_w	PI	$<Rg_n>$	comments
Aldrich	15,400 g/mol	34,000 g/mol	2,21	43.6 A	
GE	15,700 g/mol	37,800 g/mol	2,41	45.2 A	used in the free volume studies, 7 mil thickness
GE	20,900 g/mol	43,700 g/mol	2,09	52.0 A	7 mil thickness
GE	19,400 g/mol	43,700 g/mol	2,25	50.8 A	30 mil thickness

Table 4.1: GPC results of the various polycarbonates used in this study. The weight average molecular weight M_w, the number average molecular weight M_n, the polydispersity index PI ($=M_w / M_n$), and the radius of gyration $<Rg_n>$ are reported in the table.

4.2.3. Polycarbonate film preparation from pellets

Polycarbonate pellets were processed as described below in order to make a bubble free polymer film. A summary of the film processing is given in Figure 4.3. Films were compression molded in order to avoid the use of any solvent. Polycarbonate does not crystallize easily from the pure melt [1-3], but it does when exposed to solvent vapors or liquids [4-11] or nucleating agents [12, 13]. Furthermore, polymer films become oriented to some extent in the plane when cast from solution. The nature of the solvent has a critical influence on the final film orientation [14].

The pellets were first dried in a vacuum oven at 150^{o}C ($\approx T_g$) for 24h before processing. A Carver laboratory hot press was set at the maximum possible temperature, 270^{o}C (close to the melting point of polycarbonate, T_m, given as 267^{o}C). Nitrogen gas was provided in the box containing the hot press to avoid any degradation of the polymer by oxidation at the processing temperature. Dried polycarbonate pellets were put on Kapton® polyimide sheets, sandwiched between flat metal plates, and the resulting mold was placed in the hot press. The amount of polymeric material deposed on the Kapton® sheets was measured in order to obtain films of about the same thickness. Several steps were taken in order to produce the final polycarbonate film. The same processing conditions (temperature, time, pressure) were maintained throughout this research project

to ensure reproducibility in the sample preparation. The first step consisted of putting the two parts of the hot press in contact with the mold. Contact was ensured when the applied pressure increased slightly on the gauge. After contact, the pressure came back rapidly to zero because of the melting of the pellets. A waiting time of 1 min was allowed for the polymer to reach thermal equilibrium. The second step was critical to get rid of the air bubbles in the film. 3.5 metric tons were applied and released continuously for at least 1min 30s. The third step consisted of maintaining a pressure of 3.5 metric tons for 1 min. The final step was similar to the second step, except that it did last only 30s. The mold was removed from the hot press and quenched by blowing air. Results from DMTA experiments suggested that quenching the samples in ice-water (0^oC) or liquid nitrogen (-196^oC) induced some extra relaxations inside the polycarbonate matrix. An extra shoulder around 90^oC was easily distinguishable on the DMTA traces of the samples quenched in ice-water. It is actually well-known that the β-relaxation peak of polycarbonate (which occurs at about -100^oC) is highly sensitive to water as investigated by the dielectric method [15]. A relaxation was also noticed by DMTA experiments at about room temperature for the samples quenched in liquid nitrogen. This observation has actually been reported in the literature [16]. Based on the above observations, only air quenching was considered in this research.

The polymeric films made by compression molding were kept in a dessicator at all times to avoid any water moisture uptake.

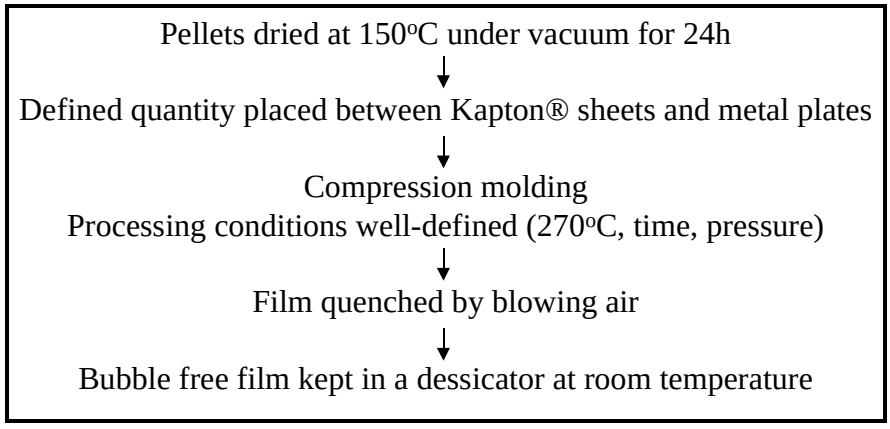

Figure 4.3: Summary of the film processing steps.

The thicknesses of the films were measured with a micrometer from Fowler, Japan (Model # 52-222-001) with a precision of 0.0001 inch. The thicknesses were typically varying from about 100 to about 200μm depending on the experiment.

Results of DMTA experiments suggested that the films processed by hot press had variable properties. This was attributed to the cooling rate from the melt. Indeed, the mold had to be taken to the air pipe in the laboratory for air quenching and obviously this time could not be exactly reproducible. It was therefore necessary to give the same thermal history to all the films. A schematic of the action taken to solve this problem is given in Figure 4.4. Prior to experiments, polymeric samples were put between Kapton® sheets of thickness 125μm and copper metal plates of thickness 0.11mm. The metal plates were suspended in the center of a gas chromatograph (GC) oven 8000 VEGA Series from Fisons Instruments S.p.A., Rodano, Italy (Serial # 260456). The GC oven was equipped with an internal fan and therefore heat transfer was assumed to be excellent on both sides of the metal plates sandwiching the polymer. The oven temperature could be controlled within 1^{o}C by the operator, although the overall accuracy was given by the manufacturer as 0.1^{o}C. The samples were heated in the GC oven from room temperature to 165^{o}C at a heating rate of 40^{o}C/min, kept at 165^{o}C for 15min to remove thermal history and eliminate possible orientation, and cooled within the oven at a programmed rate of typically 40^{o}C/min to room temperature. The room temperature was maintained at 30^{o}C. The cooling rate of the polymer may have been different from that of the oven. No thermocouple was available to directly measure the temperature of the polymer with time. However the procedure remained similar from one sample to another and thus reproducible. The films were then used immediately.

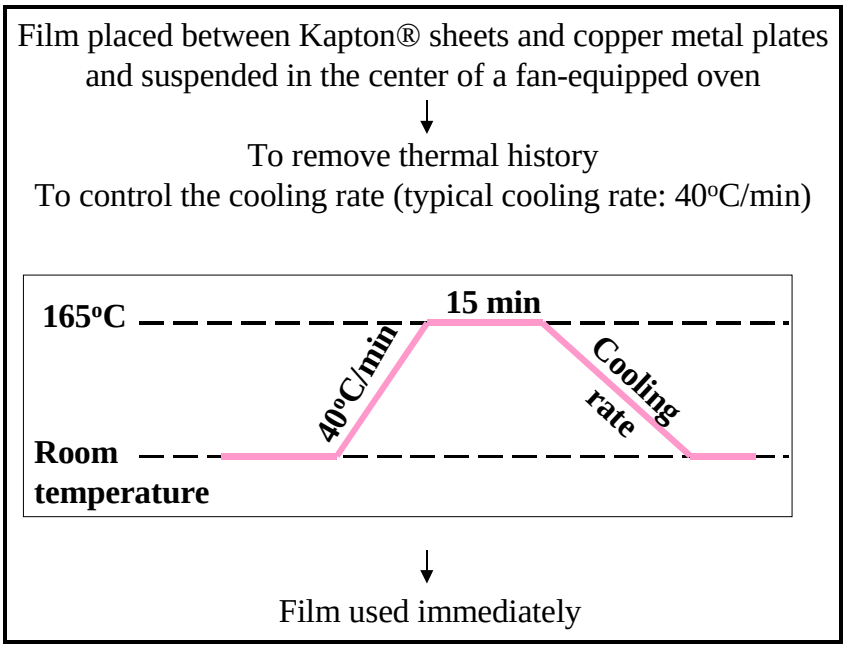

Figure 4.4: Schematic of the action taken to give the same thermal history to all the compression-molded polymeric films. The cooling rate was typically chosen as 40°C/min. The room temperature was maintained at 30°C. 15min were assumed to be sufficient to remove thermal history.

4.3. The instrumental methods

The following subsections describe the experimental techniques used in this research and the experimental conditions chosen to generate data.

The first subsection focuses on the permeation technique used to obtain gas transport measurements. The gas apparatus was built in the laboratory supervised by Dr. Eva Marand in the Chemical Engineering Department at Virginia Tech.

The remaining subsections present the techniques used to measure the physical properties of the polymers. The techniques involved in this research were dynamic mechanical thermal analysis (DMTA), density, birefringence, and Fourier transform infrared spectroscopy (FTIR).

4.3.1. Permeation

Permeation experiments were carried out using the permeation integral method [17, 18].

A schematic of the permeation process is given in Figure 4.5. Briefly, a membrane separates a closed volume from another volume, both volumes being initially degassed. At some time t=0, the pressure on the side not in contact with the closed volume increases from zero to a constant particular pressure p_f, p_f standing for feed pressure. The pressure of the feed or the upstream remains constant throughout the experiment. As the gas permeates through the membrane because of the concentration gradient [19], the pressure in the closed volume does rise with time. This pressure is referred to as p_p for permeation pressure. The pressure in the permeate or downstream side is being monitored with time by the computer until steady state conditions are achieved. The reader should have in mind that the steady state conditions do not correspond to equilibrium, as seen sometimes in the literature [20]. Steady state conditions do correspond to the time at which the slope of pressure versus time becomes linear. The curve of pressure versus time becomes linear at sufficient long times, and as long as the pressure in the closed volume remains negligible. This point will be proven later in this chapter. The slope is directly related to the permeability.

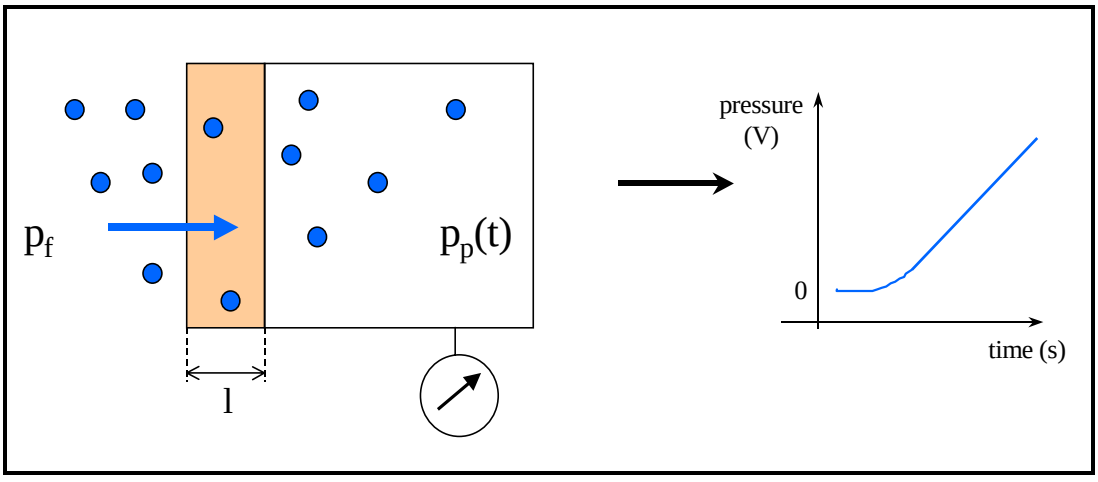

Figure 4.5: Schematic of the integral permeation method (left). p_f is the feed pressure, p_p the permeate pressure, and l the thickness of the membrane. The profile obtained while running permeation experiments is shown on the right side of the figure.

The closed volume permeation apparatus present in our laboratory has been described in an earlier publication [20]. This set-up has nevertheless been taken apart and completely rebuilt since then to allow a better computer control, to improve heat transfer, and to decrease the vacuum leaks significantly. An up-to-date schematic of the permeation set-up is given in Figure 4.6. The pressures of the gas cylinders were controlled by pressure regulators. Those pressure regulators remained untouched during this whole research project to ensure reproducibility in the feed pressure. The valves were solenoid or pneumatic block valves activated by air, at a pressure of at least 80 psia. Two pressure transducers were involved in the permeation apparatus to convert the pressure into electrical energy. The pressure transducer on the feed side was purchased from Senso-metrics, Inc., California (Model # SP974D). It was capable of measuring pressures ranging from 0 to 500 psia. This pressure transducer was calibrated to read 1V for 100 psia. The pressure transducer used to measure pressure on the permeate side of the membrane was a MKS Baratron pressure transducer from MKS Instruments, Andover, MA (Model # 121AA-00100B, Serial # 95139111A). The pressure range was 0 to 100 torr, the resolution being of 0.1% of full scale. This particular highly sensitive pressure transducer had to be calibrated by the manufactor each year. The output was ranging from 0 to 10 V, thus 1 V corresponded to 1 cmHg. While running experiments, the pressure transducer had to be protected from deadly over-range pressure. If the voltage became greater than 8V, such as what happened during membrane breakage, the computer protected the pressure transducer. The membrane cell that will be described below was placed in a programmable gas chromatograph oven 6000 VEGA Series from Carlo Erba Strumentazione, Milan, Italy (Serial # 258591) equipped with an internal fan. The oven temperature was controlled within 0.1^{o}C. The temperature inside the oven was monitored by two additional thermocouples. All the tubbings involved in the permeation apparatus were in stainless steel. A coil was made in the oven to make sure that the gas was at the correct temperature while entering the membrane cell. A vacuum as low as 1 mtorr could be achieved by a two stage vane vacuum pump from Alcatel Corp., France (Model # 1101006401). The oil was changed at least every three months. An external vacuum gauge from Televac, Pennsylvania (Model # B2A-1-REC-C) was added to the

set-up to monitor the vacuum process. The data acquisition cards for the valves, the thermocouples, the vacuum gauge and the pressure transducers were interfaced with a 486DX computer using a graphical interface programming software called Labtech from Laboratory Technologies Corporation, MA. The experimental data were therefore collected on-line.

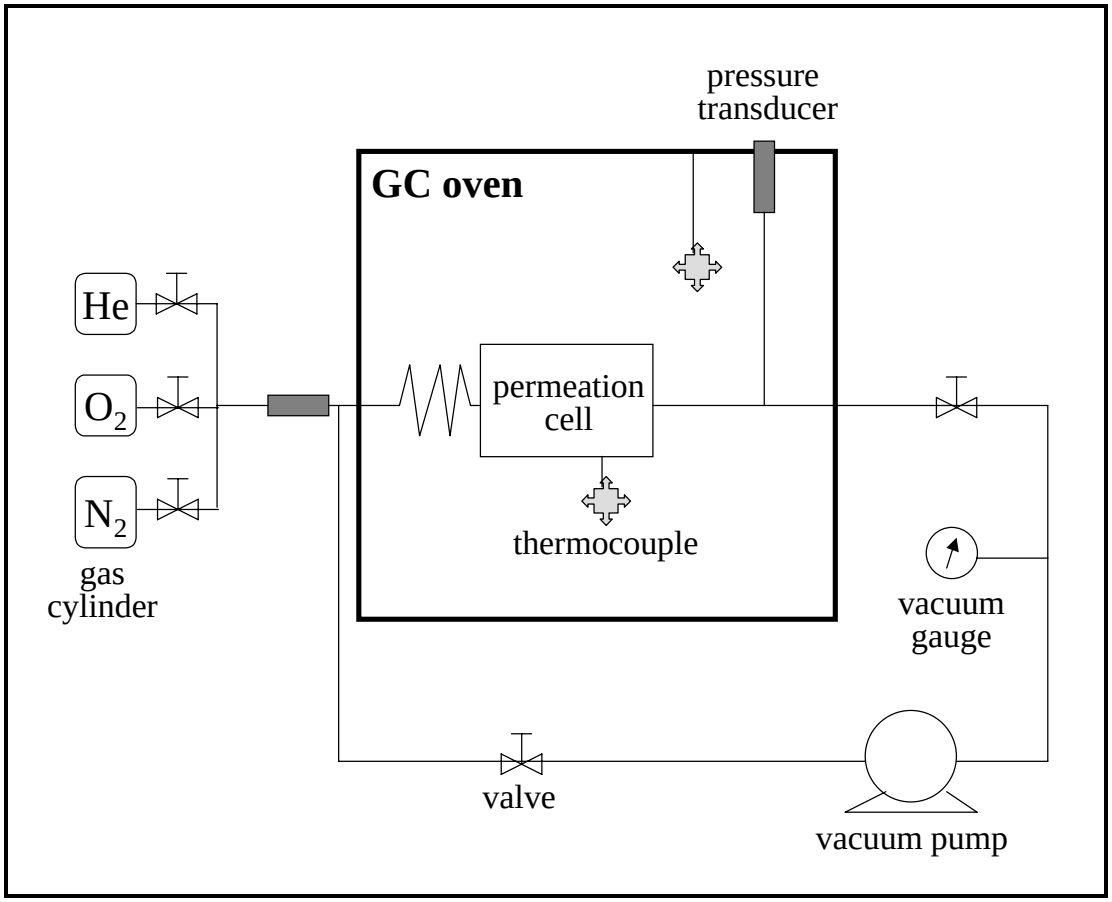

Figure 4.6: Schematic of the permeation apparatus.

Schematics of the permeation cell are provided in Figure 4.7 and Figure 4.8. This permeation cell made out of brass was based on a design provided by the Dow Chemical Company. The permeation cell consisted of two parts, an upper part and a lower part, as seen in Figure 4.7. The polymer was placed between those two parts. The cell was designed for films of about 125μm thickness. Two Viton® o-rings were used to seal the cell. No extra vacuum grease was needed. Stainless steel porous fritted discs were used to

support the membrane. The permeation area was estimated to be 13.36cm^2 based on the permeation cell dimensions. A polycarbonate film circle of diameter 4.8cm was cut and its thickness was measured with a micrometer from Fowler, Japan (Model # 52-222-001), with a precision of 0.0001 inch (with 1 inch = 2.54 cm). Values of the thickness were taken at five different area of the membrane, namely the center, top, bottom, left, and right. The polycarbonate membrane was placed inside the permeation cell and the cell was closed by tighting the four screws of Figure 4.7 in diagonal using a torque of 70 inch pounds on each screw.

The volume of the permeation closed volume was determined by using the ideal gas law applied to several separate volumes. Since the pressure was very low, no compressibility factor correction was needed. The permeate closed volume was found to be equal to 19.72 ± 0.25 cm^3. The closed volume corresponded to the volume of the cell and the tubbings on the permeation side of the membrane. The inherent leak rate of the permeation set-up on the permeate side was found to be 1 mtorr/hr, as measured over a period of 10 days [21]. Four days were nevertheless necessary to observe any leak rate, and therefore no correction was made to the experimental data to account for leaks. Since the cell and the tubbings were in stainless steel, adsorption of gas to the walls was assumed as negligible.

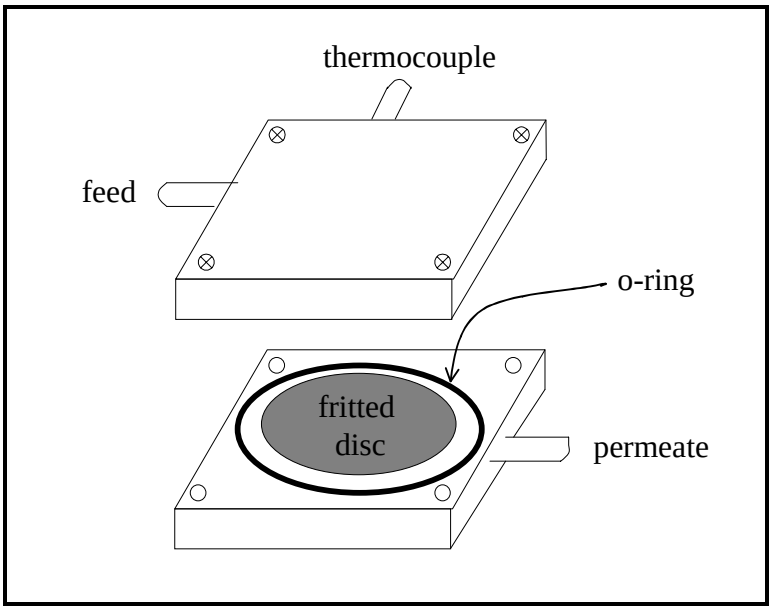

Figure 4.7: Schematic of the permeation cell.

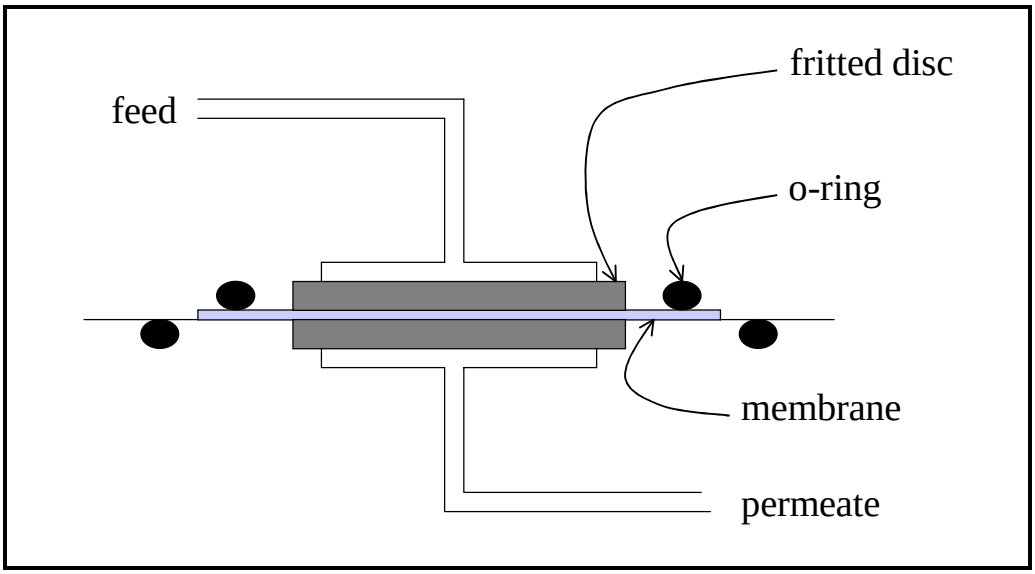

Figure 4.8: Cut view of the permeation cell.

Permeation experiments were carried out at 35°C using three different gases, namely He, O_2, and N_2, in that given sequence. Those gases were expected to interact only weakly with the polymer, through dispersive or Van der Waals-type interactions. Carbon dioxide CO_2 was not considered in this research in order to avoid any complications arising from plasticization effects [22-44]. The permeation behavior would be time and pressure dependent indeed. The kinetic diameters of helium He, oxygen O_2, and nitrogen N_2 are reported as 2.6Å, 3.46Å, and 3.64Å, respectively [45-48]. The kinetic diameter is defined as the smallest diameter zeolite window which allows the gas molecule to enter a zeolite cavity. It gives a good idea of the size of the small gas molecules for gas transport properties [49, 50]. The free volume present in glassy polymers can be probed by using gases of different kinetic diameters. The amount of free volume is assumed to remain constant during the timescale of the permeation experiments, as well as the overall free volume distribution. Freshly processed polymers in the glassy state (below T_g) have not reached their equilibrium conformations. Eventually they do gain adequate mobility by thermal motions to reduce their excess free volume with time. Obviously the timescale of the polymer relaxation process is very long compared to that of the permeation process. Some researchers refer to this as a

pseudoequilibrium phenomena [51]. Although the size and shape of individual microvoids may fluctuate during the permeation experiments due to the thermal motion of the polymer chains, the total amount and distribution of free volume is assumed to remain constant within the timescale of the permeation experiments. Because of the small kinetic diameters of the gas molecules and since the amount of gas sorbed by the polymer remains very low, the polymeric matrix is assumed not to be modified by the gas molecules. The purities of the gases used in this research were the following: 99% for He and N_2, and 99.996% for O_2. Each gas was passed through a molecular sieve prior to reaching the permeation apparatus itself in order to remove any water or oil. The applied pressures were fixed at about 2.5 atm for He, and 3.9 atm for O_2 and N_2. The applied pressures remained virtually constant during the whole duration of this research thanks to blocked pressure regulators. The applied pressures were low enough to assume that the structure of the polymer was not modified from the gas pressure. Any force convection (that would enhance the value of the diffusion coefficient by allowing cooperative movements to take place in the polymeric matrix) could be neglected in this work since the pressures remained in the pressure range where Henry's Law applies for polycarbonate. Indeed, Koros and co-workers [48] determined for instance that the curve of C (the equilibrium concentration of the gas in the polymer) versus pressure was linear up to 11atm for N_2 and at least up to 20atm for He in polycarbonate at 35^{o}C. The pressure of He was the most sensitive to a change in temperature in the laboratory. The applied pressure varied within 1%. The permeation experiments were programmed on the computer. The upper voltage limits were fixed as 0.3V for He, and 0.4V for both O_2 and N_2. Those limits were determined based on the permeation profile of polycarbonate. Steady state conditions were fully reached for the thicknesses and the applied pressures considered in this research project. Data points were collected as follows for He and O_2: every 0.1s for the first 60s, then every 1s for 600s, and finally every 10s. The program stopped by itself once the upper voltage limit was reached. Data points for N_2 were collected as follows: every 0.1s for 10s, then every 1s for 10s, and finally every 20s until the end. Three measurements were taken for each gas at each temperature to ensure reproducibility and to calculate the error involved in the permeation results. The membrane was initially degassed for 2h. The pressure typically reached under 5 mtorr

after that time. The degassing times between runs were usually 30min for He, 90min for O_2, and 90min for N_2, unless indicated in the experimental sections of each chapters. The membrane was degassed for 90min each time before changing the nature of the gas. The total cycle consisting of the permeation of the gases themselves and the degassing times took about 16h at 35°C. Since the same cycle was programmed each time on the computer, the data could easily be compared. Permeation experiments were also carried out on the same membrane at higher temperatures, right after the experiment at 35°C in order to determine the temperature dependent activation energies. Aging was found to be negligible at those temperatures within the timeframe of the experiments. Indeed, no significant change in density could be detected. In addition, the resulting data points did fit really well on the Arrhenius plots. The membrane cell remained untouched between temperature jumps. The membrane was degassed for about 4 hours before collecting data at a new temperature. About 1h 30min was needed for the gas permeation set-up to reach thermal equilibrium after a change in temperature. In order to verify that the results were repeatable, another polymer film was tested for isotropic fresh polycarbonates. It was verified that the data points did fit on the error bars previously measured.

4.3.2. Dynamic Mechanical Thermal Analysis (DMTA)

Dynamic mechanical thermal analysis (DMTA) was used to characterize the glass transition temperature T_g, the molecular motions, and the viscoelastic properties of the polycarbonates used in this research. In those experiments, a small-amplitude sinusoidal strain is applied to the material. A static force is applied in addition to the dynamic force. As the material is perturbed in a cyclic manner, a portion of the energy is stored and another is dissipated. The storage modulus E' measures the ability of the material to store energy elastically, whereas the loss modulus E" measures its ability to dissipate energy or loose heat. The ratio between each quantity is called the loss tangent tan δ, δ being the phase angle between the in-phase and the out-of-phase components. Therefore,

$$\tan\delta = \frac{E''}{E'} \qquad \text{Eq (4.1)}$$

The T_g corresponds to the temperature at which the polymer chains can move globally, in other words move together and possess intermolecular cooperative motions. The T_g was taken as the maximum of the loss modulus E" peak. Data reported in the literature are usually taken from the maximum of tan δ. The maximum of the E" peak was considered to be more appropriate than that of tan δ to estimate T_g since the maximum of E" corresponds to the softening point. Actually, it corresponds to the initial drop of the storage modulus from the glassy state into the glass transition region. In the glass transition region E' drops from about 10^9Pa to about 10^6Pa.

The dynamic mechanical experiments were carried out in the tensile mode under atmospheric air. GPC analysis suggested that samples were not degraded by oxidation during the timeframe of the experiments. The machine was a Rheometric Scientific DMTA IV from Rheometric Scientific, Piscataway, NJ. It was interfaced with a Pentium computer running a Rheometric Scientific software. The apparatus was monthly calibrated, and a daily check was performed to ensure accurate calibration.

Polycarbonate samples were cut in a rectangular shape using a perfectly rectangular home-made mold. The dimensions of the samples were typically 25*4mm. The dimensions were obtained with a micrometer from Mitutoyo Corp., Japan (Model # CD-6"CS, Serial # 0008517) with a precision of 0.01mm. The edges of the samples were polished with some sand paper if needed to ensure reproducibility between samples. A ratio of 3 between height and width was verified while doing DMTA experiments, as recommended by the manufactor to minimize sample edge effects. The gap between the grips of the tensile apparatus was set as 12mm. The thickness of the samples was assumed to be thin enough to avoid gradients of temperature in the samples while measuring dynamic properties. The position of the thermocouple remained unchanged between runs to ensure comparison between samples. A small variation in the position of the thermocouple could indeed affect the value of the maximum of the E" peak by as much as 5^oC. The thermocouple was forming a 45^o angle with the horizontal, and was about 5 mm from the sample. The temperature inside the DMTA apparatus was controlled within 0.1^oC.

The dynamic strain was chosen in the linear viscoelastic response range. As an amorphous glassy polymer is stretched, nonlinear viscoelasticity is gradually observed

for a strain above 0.2%, as seen in Figure 4.9. The dynamic strain was typically chosen as 0.025%.

Different types of tests were performed in this research. Those tests were: dynamic temperature ramp, dynamic frequency-temperature sweep, dynamic frequency/temperature sweep, dynamic frequency sweep, dynamic strain sweep, dynamic time sweep, and transient stress strain. The parameters chosen for the various DMTA experiments will be given in each chapter depending on the tests performed at that time.

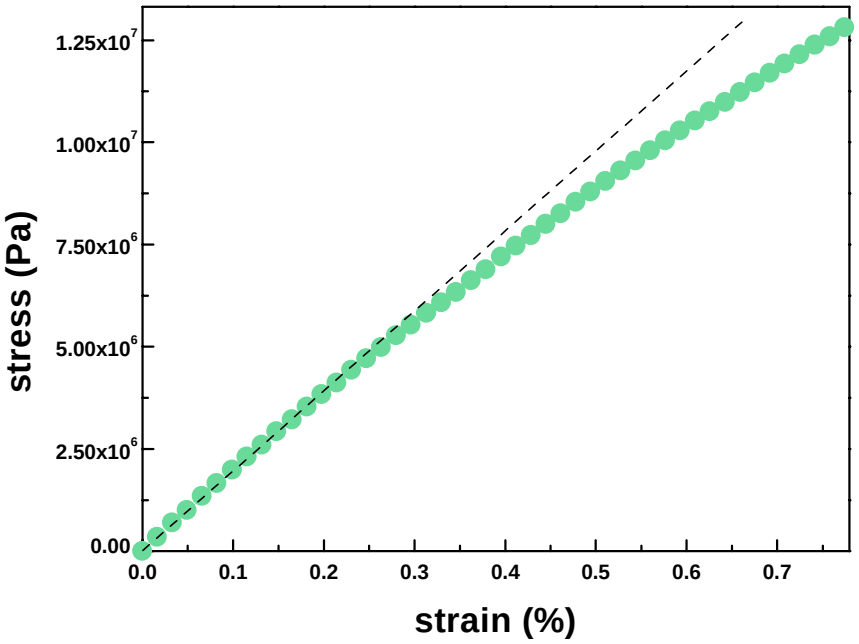

Figure 4.9: Limit of linear viscoelasticity in polycarbonate as measured by using the DMTA in the transient tensile mode at 27°C. The strain rate was chosen as 50 s^{-1}.

4.3.3. Density

The densities were measured at 18°C in a linear density gradient column made out of sodium bromide salt and distilled water.

A schematic of the density gradient column is given in Figure 4.10. A linear density gradient column can be prepared by mixing a heavy and a light solution, such as aqueous solutions of sodium bromide. The light solution is mixed to ensure homogeneity in the solution going to the column. Once the valves are opened, the liquid goes into the

column because of the hydrostatic pressure solely. The light solution goes into the column first. It goes up in the column tube once the liquid of higher density is introduced in the bottom of the column, and a density gradient is thereafter created with time, the solution at the bottom of the tube having a higher density than the one at the top. Care was taken to avoid touching the tube of the column as this would mix the solution and destroy the density gradient.

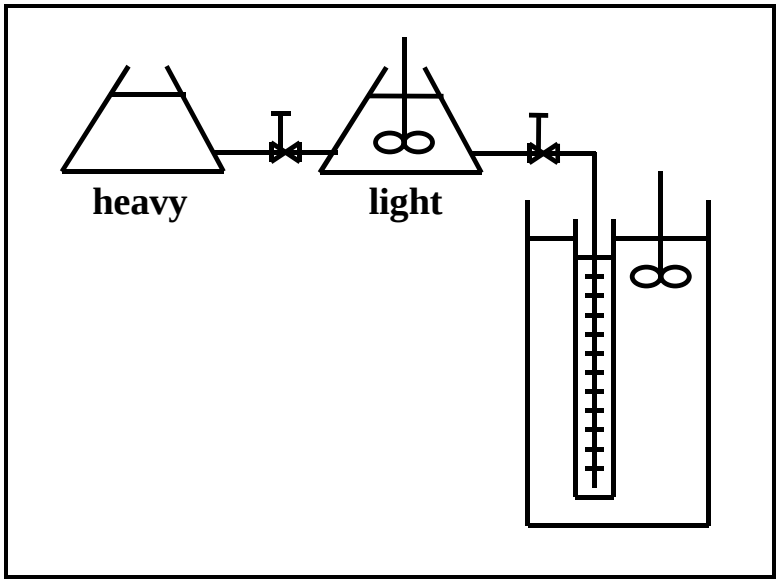

Figure 4.10: Schematic of the density gradient column. The heavy and light solutions were prepared by mixing sodium bromide salt and distilled water. The column itself was placed in a water bath maintained at 18^{o}C.

The volume of the column was about 1.6 liter and its height about 1m. The reading on the column ranged from 0 to 70, 0 being at the bottom of the column. The column was placed in a water bath to better control the temperature. The temperature was maintained at 18^{o}C. Direct exposure to the sun was avoided by closing the blinds in the laboratory since light could degrade the polymer. All the valves, tubbings, and containers were made out of glass. The connections between them were made by simply using vacuum grease. The glassware was thoroughfully cleaned and dried using acetone and compressed air prior to use.

The column was set-up for the various types of amorphous polycarbonate samples used in this research. Some of those samples were for instance physically aged or

oriented. Orientation was assumed to affect the densities the most, and therefore the density range of interest was based on oriented samples. According to the literature, the density for hot-drawn oriented amorphous polycarbonate ranges from 1.197 to 1.202 g/cm^3 [52-57]. Unfortunately, only three calibrated glass balls of well-known densities were available in the laboratory to cover this particular density range. It was decided to use at least five balls for accuracy reasons. Using five balls expanded the density range from 1.1808 to 1.2200 g/cm^3, and decreased the resolution of the column as well at the same time. The difference between the extreme densities Δd was equal to 0.0392 g/cm^3. A light and a heavy solutions of sodium bromide salt and distilled water were prepared. The sodium bromide NaBr salt was purchased from Aldrich Chemical Company, Inc., Milwaukee, WI (catalog # 22,034-5, lot # 00808TN). Its density was given as 3.203 g/cm^3. The salt was kept in a dessicator from the time of purchase until use to avoid water moisture uptake. The water was distilled water for high performance liquid chromatography grade (HPLC) with a density of 1 g/cm^3. The density of the light solution was determined by substracting $0.2\times\Delta d$ to 1.1808 g/cm^3, and that of the heavy solution by adding $0.3\times\Delta d$ to 1.2200 g/cm^3. Thus the densities of the desired light and the heavy solutions were calculated to be 1.1730 g/cm^3 and 1.2318 g/cm^3, respectively. The mass of NaBr salt per 1000 cm^3 of water was given by the following equation: (mass of NaBr / 1000cm^3 H_2O) = $-639.782 - 39.393\times\rho + 679.805\times\rho^2$, where ρ is the density of the solution [58]. The real density was lower than the calculated density because of the excess volume of mixing. One liter of each type of solution was prepared by stirring the salt with the water until complete dissolution. The mass of NaBr for the light solution was 249.31g, and that for the heavy one was 343.12g. The solutions remained untouched for one day to let any air bubbles rise to the surface. Big air bubbles could indeed threaten the construction of the density gradient column. The solutions were placed in the two containers shown in Figure 4.10. The two valves were opened and the liquid started going into the column. The flow rate could be controlled by turning the valve located between the light solution container and the column itself. The rate of filling was monitored with time. The optimum was calculated to be around 2min to go from one division to another [58], the distance between two divisions being equal to 0.2 on the reading. The rate of filling was initially determined to be around 1min 30sec / division; it was equal to 2min

30sec / division after 3h 30sec, and 4min 30sec / division after 11h 30min. Once the column was filled with the liquid, the glass tube placed inside the column for filling was slowly removed and glass balls of calibrated densities were dropped inside the column. The balls were wetted by the remaining of the heavy solution before dropping them in the column. The calibrated balls stopped at different levels or heights of the column depending on their respective densities. Out of the five balls, two of them were actually at the top and at the bottom of the column. However three balls were well dispersed inside the column. One day was allowed for equilibrium before reading. A calibration curve was built, as shown in Figure 4.11. A linear regression was performed on the experimental data points. From the knowledge of the height of a sample in the column, it was possible to determine the density from the calibration curve. The theoretical accuracy of the column was calculated to be 0.00005 g/cm^3. Polycarbonate samples were cut in different shapes in order to distinguish them. The surface areas were typically in the order of 0.12 cm^2. At least two specimens were prepared for each kind of samples to verify reproducibility. The specimens were wetted by the remaining of the heavy solution before dropping them in the column. At least 12h were waited before reading to ensure equilibrium. The calibration curve was rebuilt before reading data each time as the column may not be completely stable, especially because of the deterioration of the density gradient due to the introduction of samples. The variation in temperature was considered as negligible. The rate of evaporation was assumed as negligible as well. It was assumed that the liquid did not interact with the polycarbonate samples during the short period of time the samples were left inside the column. Swelling of the samples by water was assumed to be negligible.

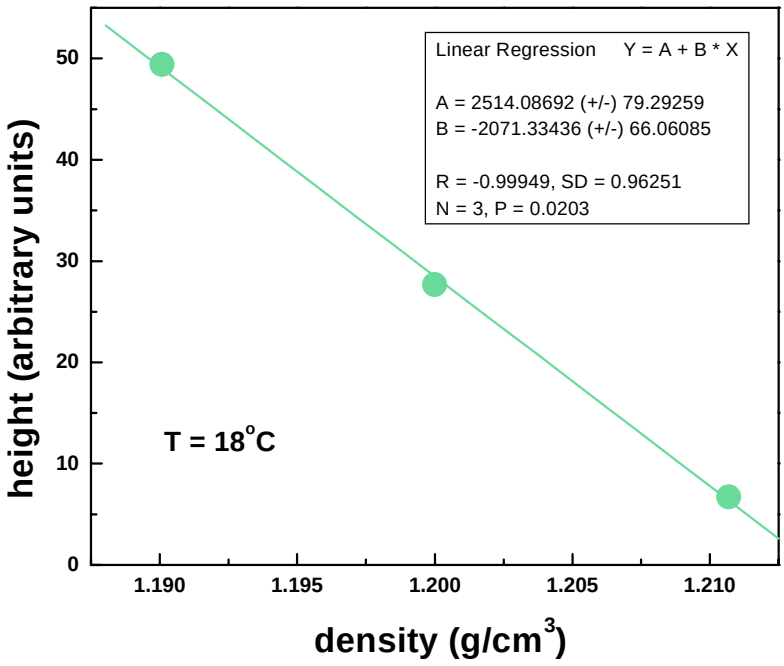

Figure 4.11: Calibration curve for the linear density gradient column at 18°C using three glass balls of well-known densities.

4.3.4. Birefringence

The average degree of orientation was determined from birefringence measurements. For oriented systems in principle the birefringence represents the difference in refractive index in the parallel and the perpendicular directions. The birefringence was measured on the transparent polycarbonate specimens by use of a Babinet compensator that consisted of two wedges in quartz perpendicular to each other. The light beam reached the compensator after transmission through the sample. A schematic of what is observed while doing birefringence experiments is drawn in Figure 4.12. Initially no sample was placed in the light beam and the reference line was put between the two marks appearing on the screen. The corresponding value was read on the scale for reference, which corresponded to a phase angle of zero. When an isotropic sample was placed in the light beam, no changes were observed and the birefringence was therefore equal to zero. The optically anisotropic sample was placed in the light beam. As seen in Figure 4.12, the reference line was not located between the two marks anymore, indicating a nonzero birefringence. The thickness of the calibrated quartz

material was adjusted to compensate the optical retardation induced by the orientated sample. By moving the wedges, it was possible to induce a negative phase shift to compensate for the phase shift created by the oriented sample. The lines were moved down to place the reference line between the two marks again and the corresponding value was read again.

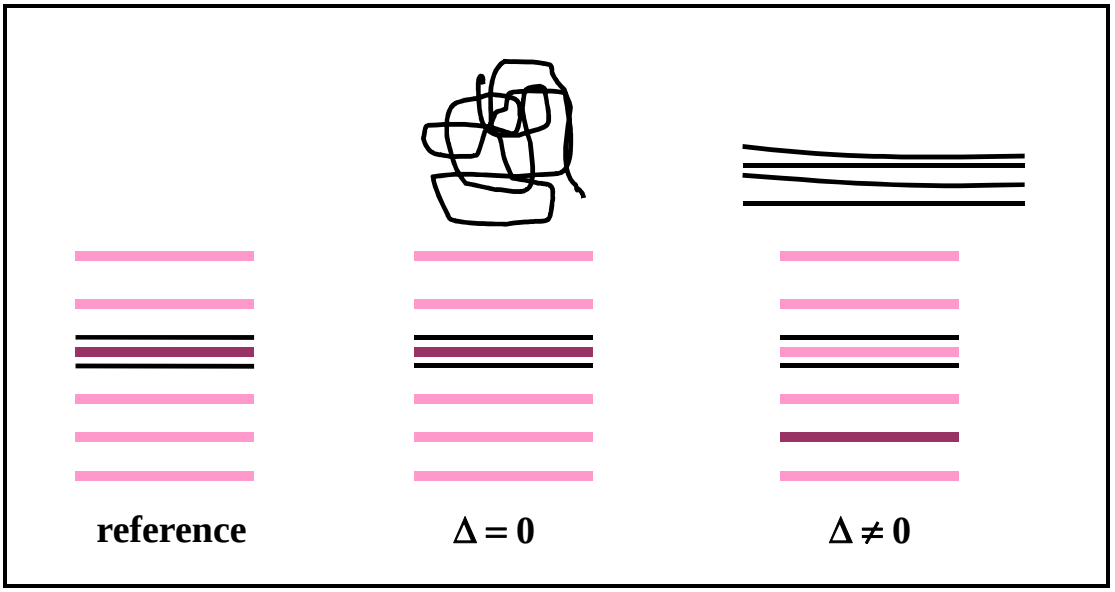

Figure 4.12: Schematic of what is observed while doing birefringence experiments. The schematics represent what is observed for a reference sample (left), an isotropic sample (middle), and an anisotropic sample (right). The aspect of the polymer chains is sketched at the top.

The error on the measurement was estimated to be 0.05 (the scale was ranging from about –11 to 37). The polycarbonate samples were always introduced in the beam path with the machine direction placed horizontally for consistency in the measurements. The membrane was taped to a support having a hole in the middle and placed in front of the compensator. The membrane was taped to the support in five different ways so that orientation could be determined in the center of the membrane, at the top, bottom, right, and left. Three measurements were taken and averaged for each position. The thickness was determined for those five areas as well using a micrometer from Fowler, Japan (Model # 52-222-001) with a precision of 0.0001 inch (with 1 inch = 2.54 cm). The experiments were carried out at room temperature (23^{o}C).

The birefringence Δ, which represents the difference in refractive index in the parallel and the perpendicular directions ($n_{//}$ - $n_{\perp}$), was calculated from the following relationship:

$$\Delta = \left[\frac{(\text{sample} - \text{reference}) * 4.103 \times 10^{-3}}{\text{thickness}} \right] \qquad \text{Eq (4.2)}$$

The difference between sample and reference corresponded to the phase shift induced by orientation. The thickness had to be taken in mil (1 mil = 1/1000 inch, with 1 inch = 2.54cm). The measured or total birefringence Δ corresponds to the sum of three distinct types of birefringence [59, 60]. We have:

$$\Delta = \Delta_f + \Delta_d + \Delta_{form} \qquad \text{Eq (4.3)}$$

where Δ_f is the orientation birefringence, Δ_d is the distortional birefringence, and Δ_{form} is the form birefringence. Since the samples contained a single phase, no correction was required for Δ_{form}. Δ_d was found to be negligible for fresh samples, and assumed to be negligible as well for hot-drawn samples because of the large-scale segmental motions above T_g.

4.3.5. Fourier Transform Infrared Spectroscopy (FTIR)

In order to verify the absence of strain-induced crystallization, FTIR spectra were collected on a BIO-RAD FTS-40A spectrometer purchased from Bio-Rad Laboratories, Inc. The spectrometer was equipped with a liquid nitrogen cooled mercury-cadmium-telluride or MCT detector. The compartment of the spectrometer was continuously gas purged in order to minimize the amount of water vapor and carbon dioxide within the compartment. The spectrometer was connected to a Pentium II computer running a Bio-Rad Laboratories software. The resolution was chosen as 4 cm^{-1} and the spectrum consisted of an average of 64 scans. No polarizer was used in this work.

Some absorption bands of the spectra collected in the transmission mode using KBr crystals saturated since polycarbonate absorbed strongly in the IR. Furthermore, the tight contact with KBr has also been shown to modify the molecular structure of polycarbonate [11]. Spectra were therefore collected in the ATR (attenuated total

reflectance) mode using a zinc selenide ZnSe hemisphere crystal from Harrick Scientific Corporation, Ossining, NY, with a refractive index of 2.42. A schematic of the apparatus is provided in Figure 4.13. A Seagull^{TM} ATR attachment from Harrick Scientific Corporation was used to sample one specific area of the polymer. The angle of incidence was chosen as 50^{o} based on the calculated critical angle of incidence of 40.92^{o}. Details of the ATR technique have already been reported in previous publications [61, 62]. Briefly, the ATR-FTIR technique provides information about the changes taking place at the surface of the material and not in the bulk. The limitation of the ATR technique is that a good contact is necessary between the crystal and the sample, especially right in the center in the case of a hemisphere apparatus. Using a rubber piece allowed, nevertheless, high enough absorbance. Furthermore, it was rather difficult to have a reproducible crystal/sample contact with the ATR technique. In the ATR experiment, the higher the wavenumber, the smaller is the value of the absorbance. This comes from the fact that, for a given angle of incidence, as the wavenumber increases, the penetration depth decreases, as illustrated in Figure 4.14. This characteristic makes it possible to study surfaces at different depths by simply changing the angle of incidence. However the penetration depth measured by the ATR technique still remains in the order of a few microns.

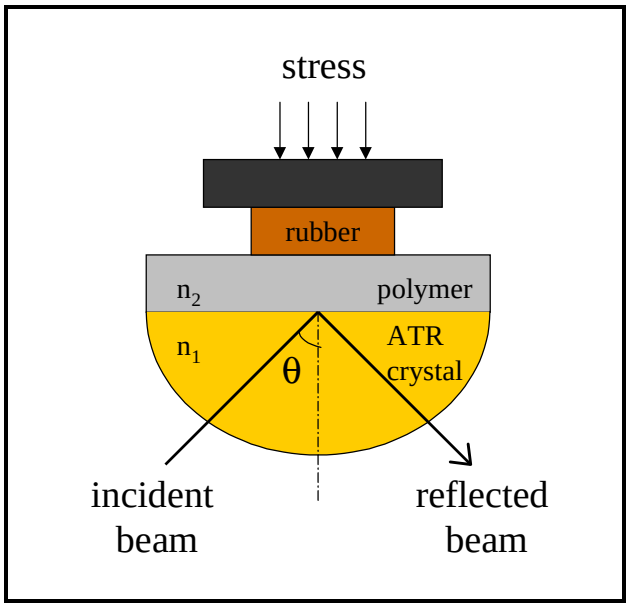

Figure 4.13: Schematic of the ATR apparatus. The polymer with a refractive index n_2 was placed on a ZnSe ATR crystal with a refractive index n_1. A piece of rubber was placed between the polymer and a hard metal plate. Some stress was applied on the metal plate to ensure good contact between the polymer and the ATR crystal. The incident beam entered the ATR crystal from one side and was totally reflected in the center of the crystal.

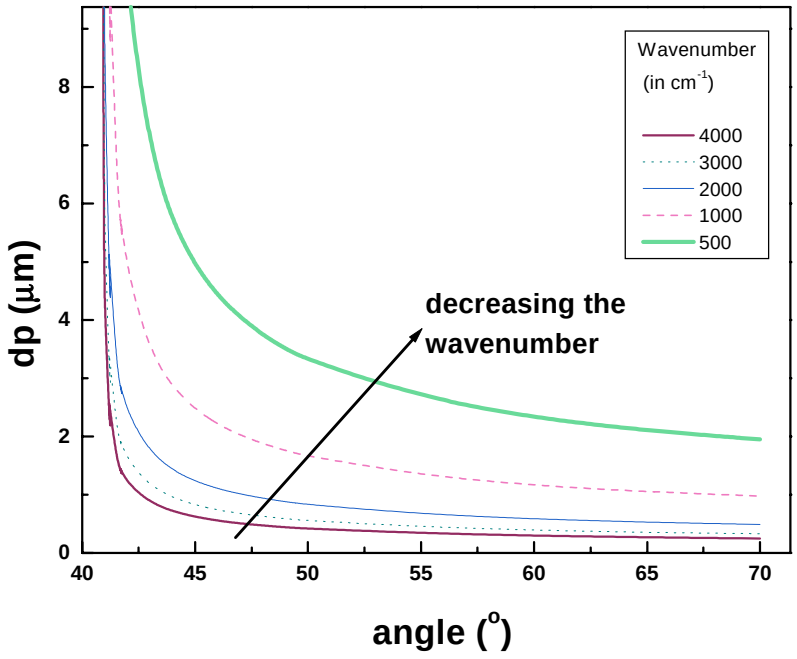

Figure 4.14: Penetration depth d_p of ATR as a function of the angle of incidence θ for different wavenumbers. The critical angle was calculated to be 40.92°. The refractive indices of the ZnSe ATR crystal and the polycarbonate were taken as 2.42 and 1.585, respectively.

4.4. Analysis of the gas permeation data

This subsection provides details about the gas permeation data analysis. Calculations that need to be carried out to determine the gas transport parameters (P, D, and S) and the activation energies (E_P, E_D, and ΔH_s) are given here.

4.4.1. The gas permeation data

Gas permeation data were typically reproducible within 1%. As shown in Figure 4.15, the larger the kinetic diameter, the lower the permeation for the same applied pressure. Only two measurements are shown on Figure 4.15 for each gas to ensure clarity in the figure, but three measurements were actually taken and averaged for analysis.

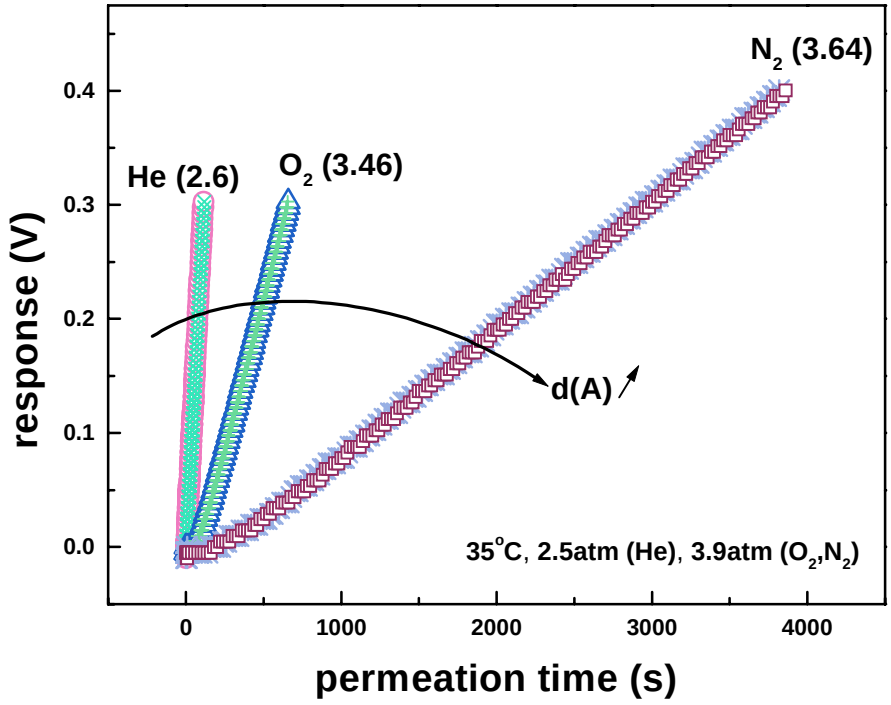

Figure 4.15: Permeation response at 35°C as a function of the permeation time for the Aldrich polymer cooled at 40°C/min. The kinetic diameters (in Å) of the gases of interest (He, O_2, and N_2) are given into brackets. Two measurements are plotted to show the reproducibility.

4.4.2. Determination of the gas transport coefficients (P, D, S)

The molecular diffusion of a gas through a membrane is given by the Fick's first law of diffusion [63]. Since the thickness of the membrane is very small compared to its surface area, the flux of the gas can be considered as unidirectional and perpendicular to the membrane plane surface. Assuming that the diffusion coefficient D is independent of concentration (because of noninteractive gases), we can employ Fick's second law of diffusion [63] to model the experiment:

$$\left(\frac{\partial C}{\partial t}\right) = D\left(\frac{\partial^2 C}{\partial x^2}\right) \qquad \text{Eq (4.4)}$$

where C is the concentration of the gas in the polymer in (cm^3@STP/cm^3), D is the mutual diffusion coefficient in cm^2/s, t is the time, and x is the distance in cm.

The initial and boundary conditions are given as follows:

$t < 0 \qquad 0 \le x \le l \qquad C = 0$ Eq (4.5)

$t \ge 0 \qquad x = 0 \qquad C = C_2 = \text{a constant}$ Eq (4.6)

$t \ge 0 \qquad x = l \qquad C = 0$ Eq (4.7)

When Eq (4.4) is solved, given Eq (4.5), Eq (4.6) and Eq (4.7), the solution is [63, 64]:

$$Q_t = C_2 l\left\{\left(\frac{Dt}{l^2}\right) + \frac{2}{\pi^2}\sum_{n=1}^{\infty}\frac{(-1)^n}{n^2}\left[1 - \exp\left(\frac{-Dn^2\pi^2 t}{l^2}\right)\right]\right\} \qquad \text{Eq (4.8)}$$

where Q_t is the volume of the gas that has permeated through the membrane in cm^3@STP.

At sufficient long time, Eq (4.8) reduces to:

$$Q_t = \frac{DC_2}{l}\left[t + \left(\frac{2}{\pi^2}\right)\left(\frac{l^2}{D}\right)\sum_{n=1}^{\infty}\frac{(-1)^n}{n^2}\right] \cong \frac{DC_2}{l}\left[t - \frac{l^2}{6D}\right] \qquad \text{Eq (4.9)}$$

The plot of Q_t versus t will thus be linear at sufficient long time as shown in Figure 4.16 and the time lag θ which is equal to (l^2/6D) can be calculated from the intercept of the slope with the time-axis. Please note that the plot will remain linear with time only as long as the concentration at x = l remains negligible. The boundary condition at x=l given in Eq (4.7) has been verified to be negligible in the present research. Computer simulations with a time-dependent concentration at x=l [65] did not show any significant

differences for the maximum pressure allowed on the permeate side of the membrane in the present research project. While doing experiments, Q_t was not exactly zero at t = 0. The experimental data were corrected to read zero for the vacuum at initial time. However the vacuum was excellent, and therefore the correction did not modify the results significantly.

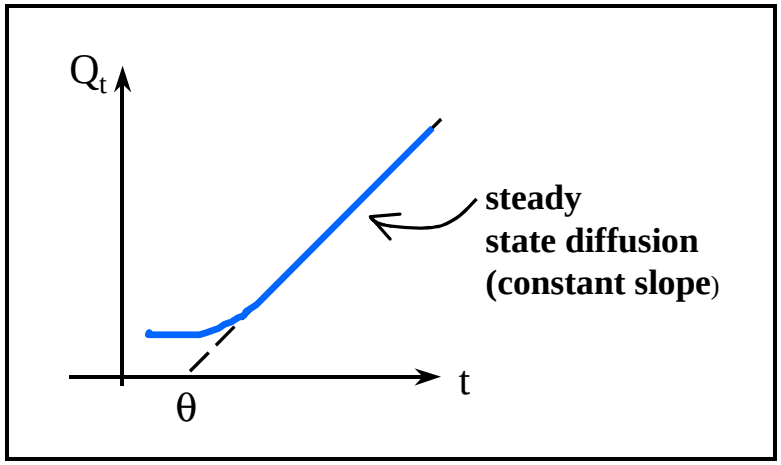

Figure 4.16: Plot of Qt versus t showing the steady state part and the time lag θ.

The diffusion coefficient D can be calculated easily provided that the thickness (in cm) is known. D in (cm^2/s) can be calculated from the value of the time-lag θ in s. We have:

$$D = \left(\frac{l^2}{6\theta} \right) \qquad \text{Eq (4.10)}$$

The time-lag method [63] is commonly used in the literature to determine the gas transport parameters, the permeability, diffusion, and solubility coefficients. The time-lag approach is based on the Henry's Law given by $C = k_D\, p$ where C is the equilibrium concentration, p is the pressure and k_D is the Henry's Law dissolution constant. Although the Henry's model is strictly obeyed for rubbery polymers only, estimation of the transport parameters can still be made for glassy polymers at low pressures. Assuming $P = k_D\, D$, and $C_2 = k_D\, p_f$ where p_f is the pressure of the feed, Eq (4.9) becomes:

$$Q_t = \frac{Pp_f}{l}\left(t - \frac{l^2}{6D}\right) \qquad \text{Eq (4.11)}$$

At sufficient long time, the slope is constant and equal to (Pp_f/l) or ($\partial Q_t/\partial t$). Finally,

$$P = \frac{l}{p_f}\left(\frac{\partial Q_t}{\partial t}\right) \qquad \text{Eq (4.12)}$$

In the present research, the permeability P in (cm^3STP.cm/cm^2.s.cmHg) was given by:

$$P = \left[\frac{(\text{slope})(l\ v\ V_d)}{p_f\ A\ R\ T}\right] \qquad \text{Eq (4.13)}$$

where the slope at steady state conditions was expressed in (cmHg/s), l was the thickness in cm, v was the molar volume of the gas at STP conditions (for an ideal gas, this is equal to 22414.1 cm^3@STP/mol), V_d was the permeate volume in cm^3 (19.72 cm^3), p_f was the applied pressure in cmHg (to multiply the pressure in psia by (76/14.696) to get it in cmHg; 1 atm = 14.696 psia = 76 cmHg), A was the permeation area in cm^2 (13.36 cm^2), R was the gas constant (6235.6 cmHg.cm^3/mol.K), and T was the temperature in K. The values of the molar volumes v in (cm^3@STP/mol) were calculated for the various gases of interest from thermodynamics relationships [66]. The compressibility factors were accounted for in the gas law. The values of v were estimated to be equal to 22434 cm^3@STP/mol for He, 22397 cm^3@STP/mol for O_2, and 22402 cm^3@STP/mol for N_2. The permeability coefficient is often expressed in barrers, with 1 barrer = 10^{-10} (cm^3@STP.cm /cm^2.s.cmHg).

The solubility coefficient S corresponds to the ratio of the permeability coefficient P divided by the diffusion coefficient D. We have:

$$S = \left(\frac{P}{D}\right) \qquad \text{Eq (4.14)}$$

The solubility coefficient S is expressed in (cm^3@STP/$cm^3_{polymer}$.cmHg). Therefore S can be obtained from permeation experiments, and does not require sorption experiments. As was explained into more details in Chapter 3, sorption experiments are complicated by several factors such as conditioning, plasticization, and aging. Permeation data may therefore be more reliable than sorption data.

The gas transport properties (P, D, S) can therefore be calculated from Eq (4.13), Eq (4.10), and Eq (4.14). Nevertheless, knowledge of the thickness was necessary. The films processed by hot press did not possess a complete uniform thickness. The average thickness was calculated as follows: (1/6) × ((2 × center) + left + right + top + bottom). The positions refer to the parts of the membrane where the thicknesses were measured.

A study by Shishatskii et al [67] has been published in the literature about the effects of the film thickness on the gas transport. The thicknesses were ranging from 5 to 150µm. It was found that the lower the film thickness, the higher the density, the lower the diffusion coefficient, and the higher the solubility coefficient. The permeability coefficient was found to remain unaffected by the film thickness. However, the data were obtained on PVTMS and PTMSNB films cast from hydrocarbon solutions on stretched cellophane films. Films prepared from solvents are well-known to be oriented to some extent [59], even though the solvent has almost been totally removed. Solvents are even capable of inducing crystallinity in polymers [4]. The absence of crystallinity was not verified by Shishatskii et al [67] in their work. Assuming that the samples were still amorphous, studies should have been conducted to determine the level of orientation of the samples. Orientation is expected to highly affect the gas transport parameters. A difference in orientation between the surface and the bulk could also be distinguished.

The effect of the film thickness was investigated in the present study. Gas transport parameters were determined on polycarbonate samples of 50µm and 200µm. Both films were processed in a similar way, the cooling rate chosen as 40^{o}C/min. The values of P, D, and S were found to be reproducible within 5%, and within the error bars. Therefore the gas transport properties do not seem to be affected by the thickness. Nevertheless, whenever a particular study was conducted, films of approximately the same thicknesses were used.

4.4.3. Determination of the gas transport activation energies (E_P, E_D, ΔH_S)

The permeation, diffusion, and solubility of non-interacting gas molecules in glassy polymers can be considered to be activated processes which can be described by Arrhenius-type equations [68-70].

Thus we have:
$$P = P_o \exp\left(\frac{-E_p}{RT}\right) \qquad \text{Eq (4.15)}$$

And from Eq(4.13):
$$\ln\left(\frac{slope}{T}\right) = \ln\left[\frac{P_o p_f AR}{lvV_d}\right] - \frac{E_p}{RT} \qquad \text{Eq (4.16)}$$

Where E_P is the activation energy for permeation and P_o the pre-exponential factor, both of them being independent of temperature in a given temperature range far from thermal transitions. E_p can be easily determined by plotting ln(slope/T) versus (1/RT), as shown in Figure 4.17 for He.

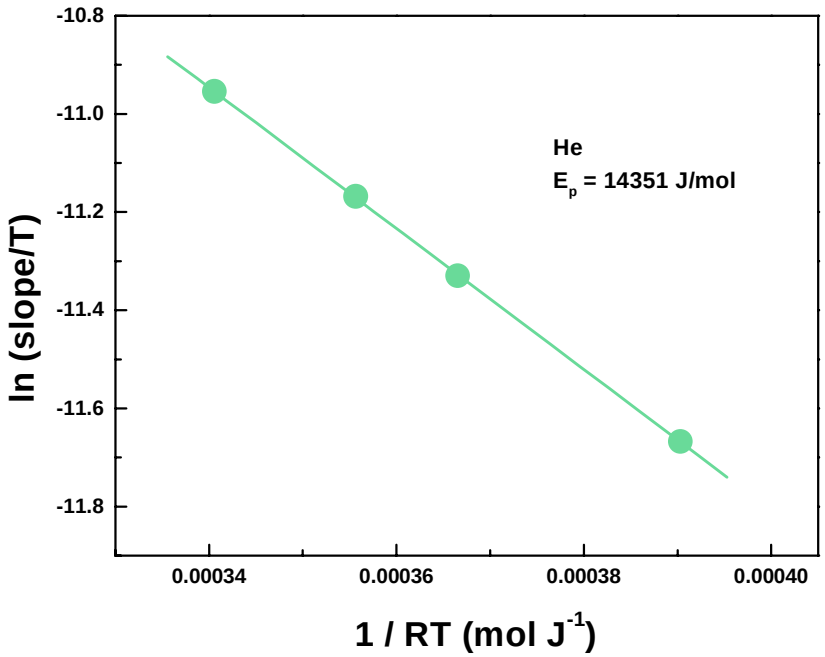

Figure 4.17: ln (slope/T) as a function of 1/RT for He. The slope corresponds to the activation energy for permeation and was determined in this case to be 14351 J/mol (R = -0.99997, SD = 0.00288). The Aldrich polymer was cooled at 40°C/min. The permeation temperatures were chosen as 35, 55, 65, and 80°C.

Similarly for the diffusion coefficient, $$D = D_o \exp\left(\frac{-E_D}{RT}\right)$$ Eq (4.17)

where E_D is the activation energy of diffusion.

Thus from Eq (4.10) and Eq (4.17) we get: $$-\ln(6\theta) = \ln\left(\frac{D_o}{l^2}\right) - \left(\frac{E_D}{RT}\right)$$ Eq (4.18)

The curve obtained for O_2 is shown in Figure 4.18. Obviously, the greater the kinetic diameter of the penetrant molecule, the greater the value of the activation energy for diffusion.

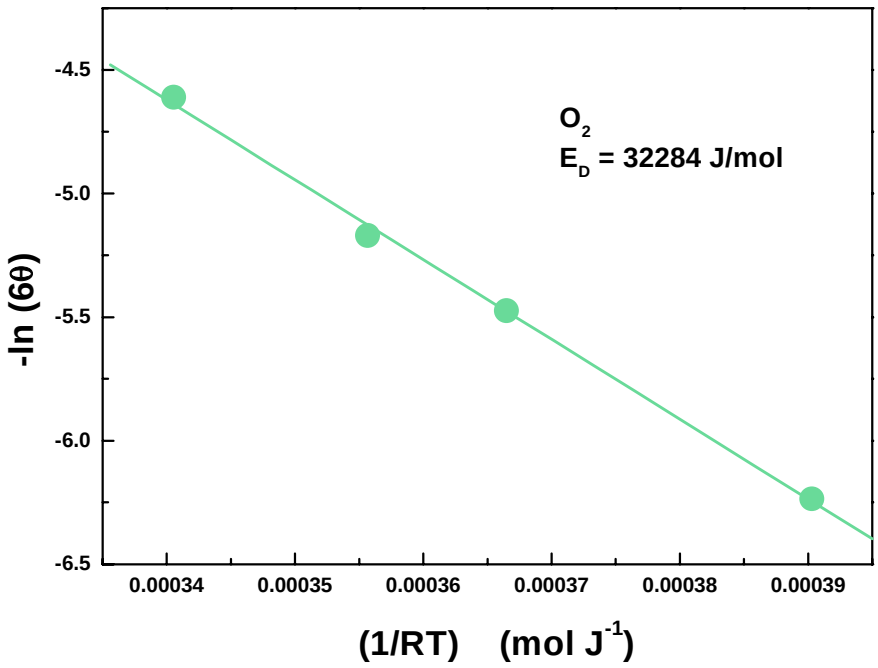

Figure 4.18: -ln(6θ) as a function of 1/RT for O_2. The slope corresponds to the activation energy for diffusion and was determined in this case to be 32284 J/mol (R = -0.99899, SD = 0.03715). The Aldrich polymer was cooled at 40°C/min.

As for the other two gas transport coefficients, the solubility coefficient S follows a Van't Hoff expression, ΔH_s being the enthalpy of sorption. Nevertheless, as the temperature increases, the solubility coefficient decreases since the penetrant becomes less condensable.

We have: $$S = \exp\left(\frac{-\Delta G_s}{RT}\right) = \exp\left(\frac{\Delta S_S}{R}\right)\exp\left(\frac{-\Delta H_S}{RT}\right)$$ Eq (4.19)

where ΔG_S is the Gibbs free energy for sorption.

And $$S = S_o \exp\left(\frac{-\Delta H_s}{RT}\right) \quad \text{Eq (4.20)}$$

Equating Eq (4.14) and Eq (4.20) we obtain:

$$\ln S = \ln P - \ln D = \ln S_o - \frac{\Delta H_s}{RT} \quad \text{Eq (4.21)}$$

From Eq (4.13), $$\ln\left(\frac{slope}{T}\right) + \ln\left(\frac{lvV_d}{p_f AR}\right) - \ln D = \ln S_o - \frac{\Delta H_s}{RT} \quad \text{Eq (4.22)}$$

Equivalent to $$\ln\left(\frac{slope}{T}\right) + \ln\left(\frac{lvV_d}{p_f AR}\right) - \ln\left(\frac{D}{l^2}\right) - \ln l^2 = \ln S_o - \frac{\Delta H_s}{RT} \quad \text{Eq (4.23)}$$

$$\ln\left(\frac{slope}{T}\right) + \ln\left(\frac{l^2}{D}\right) + \ln\left(\frac{lvV_d}{p_f ARl^2}\right) = \ln S_o - \frac{\Delta H_s}{RT} \quad \text{Eq (4.24)}$$

Finally: $$\ln\left[\left(\frac{slope}{T}\right)\times\left(\frac{l^2}{D}\right)\right] = \ln\left[\left(\frac{slope}{T}\right)\times(6\theta)\right] = \ln\left[\frac{S_o p_f ARl^2}{lvV_d}\right] - \frac{\Delta H_s}{RT} \quad \text{Eq (4.25)}$$

The product term on the left hand side corresponds to the expressions used to determine the previous activation energies E_P and E_D. The curve obtained for O_2 is shown in Figure 4.19.

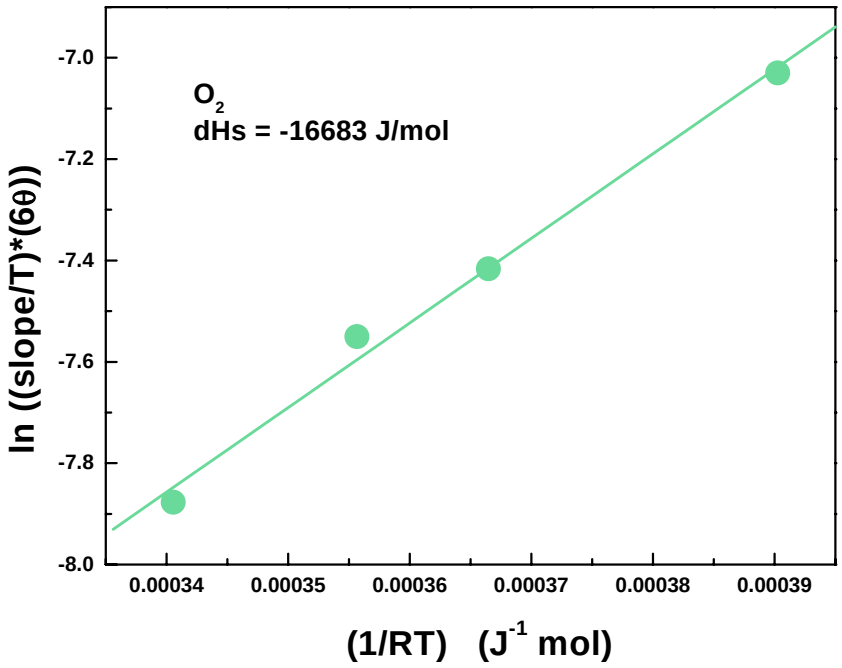

Figure 4.19: ln ((slope/T)*(6θ)) as a function of 1/RT for O_2. The slope corresponds to the enthalpy of sorption and was determined in this case to be equal to -16683 J/mol (R = 0.99584, SD = 0.03912). The Aldrich polymer was cooled at 40°C/min.

The activation energies E_P, E_D and ΔH_s could be determined without knowing the value of the membrane thickness, and therefore limit the errors in the analysis. Knowledge of only the permeation slope and the time lag were thus sufficient to obtain the activation energies. The activation energies were verified to be independent of the thickness experimentally as well. The activation energies listed above were determined by plotting the appropriate y-axis as a function of (1/RT). One should have ($\Delta Hs = E_P - E_D$) but slight differences may occur due to the errors induced by the linear regressions. The activation energy of diffusion and the enthalpy of sorption for O_2 and N_2 only were determined from the time lag method. The time lag could not be observed for He due to rapid permeation.

The preexponential factors P_o, D_o, and S_o were determined from the values of the intercepts in Eq (4.16), Eq (4.18), and Eq (4.25). Knowledge of the value of the thickness was necessary.

From Eq (4.16), $$\ln P_o = \text{intercept}_{\#1} - \ln\left(\frac{p_f AR}{lvV_d}\right) \quad \text{Eq (4.26)}$$

From Eq (4.18), $$\ln D_o = \text{intercept}_{\#2} + 2\ln(l) \quad \text{Eq (4.27)}$$

From Eq (4.25), $$\ln S_o = \text{intercept}_{\#3} - \ln\left(\frac{p_f ARl}{vV_d}\right) \quad \text{Eq (4.28)}$$

4.4.4. Others

The selectivity between two gases could be obtained by dividing the average slopes of the permeation responses of the two gases at steady state. Therefore the analysis did not involve any mathematical model for sorption, limiting errors. The greater the difference in kinetic diameters, the higher the selectivity between the gases. As seen in Figure 4.20, the selectivity for a given gas pair decreases with temperature since the polymeric matrix becomes more opened. By increasing the temperature, the polymer chains have more thermal motion, more free volume, or maybe a broader distribution of gap sizes, and thus a lower selectivity.

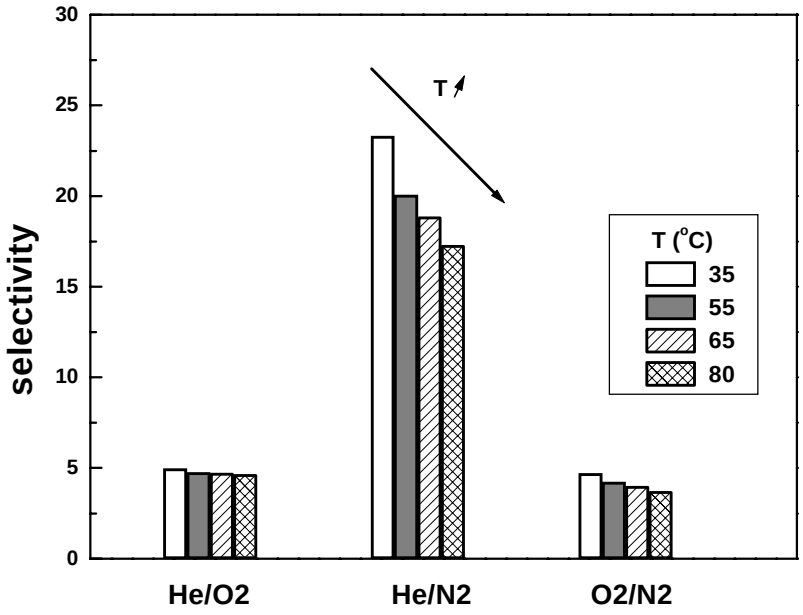

Figure 4.20: Selectivity as a function of temperature for the different gas pairs. The selectivity was calculated by dividing the average slopes of the permeation response of the two gases of interest at steady state. The temperatures were 35, 55, 65, and 80°C. The Aldrich polymer was cooled at 40°C/min.

As illustrated in Figure 4.21 using He as an example, the permeation slope itself presented an Arrhenius relationship with temperature. The fact that the data points fell on a straight line also confirmed the idea that aging was negligible at those temperatures. The slope corresponded to what is called an apparent activation energy $E_{Papparent}$. Therefore the logarithm of the selectivity between gas A and gas B should be linear as a function of 1/RT. The resulting slope was equal to the difference in apparent activation energies between gas B and gas A. An example is shown in Figure 4.22 for the He/N_2 gas pair. Obviously, as the kinetic diameter of the penetrant increased, the apparent activation energy increased, as shown in Figure 4.23.

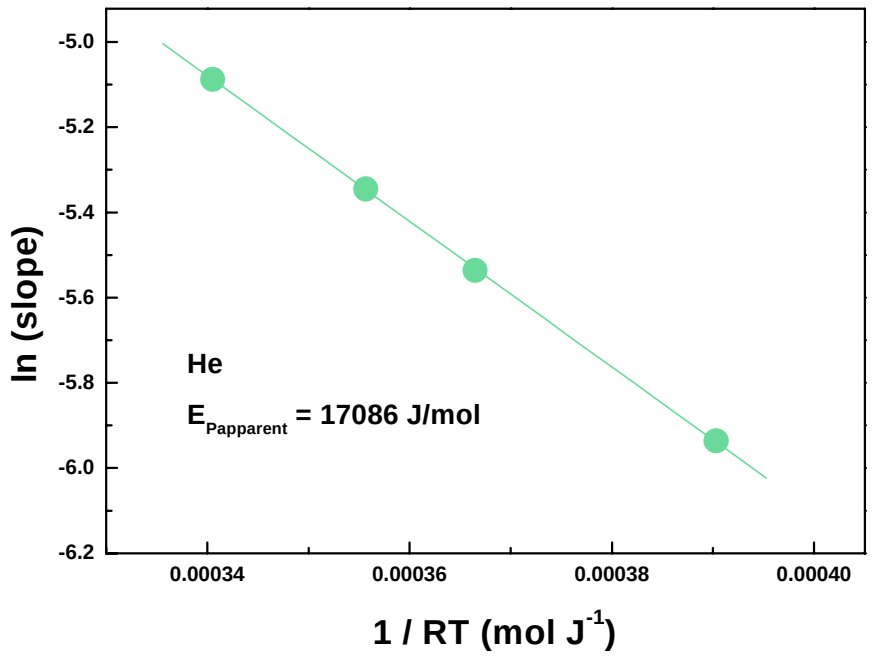

Figure 4.21: ln slope as a function of 1/RT for He. The slope corresponds to the apparent activation energy and was determined in this case to be 17086 J/mol (R = -0.99997, SD = 0.00355). The Aldrich polymer was cooled at 40°C/min.

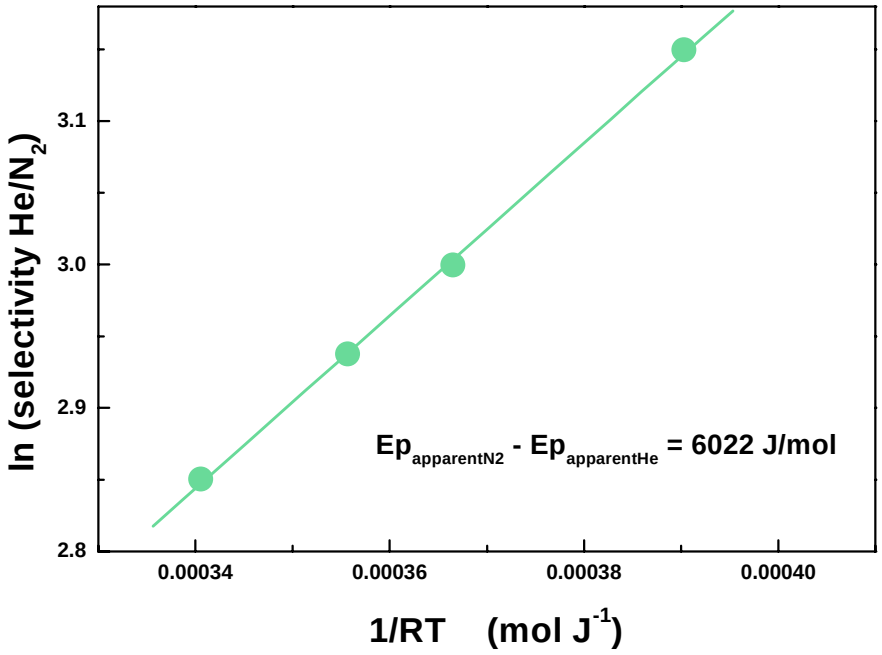

Figure 4.22: ln selectivity as a function of 1/RT for the He/N_2 gas pair. The selectivity was calculated by dividing the average slopes of the permeation response of the two gases at steady state. The slope corresponds to the difference in apparent activation energies between N_2 and He and was determined to be equal to 6022 J/mol (R = 0.99964, SD = 0.00415).

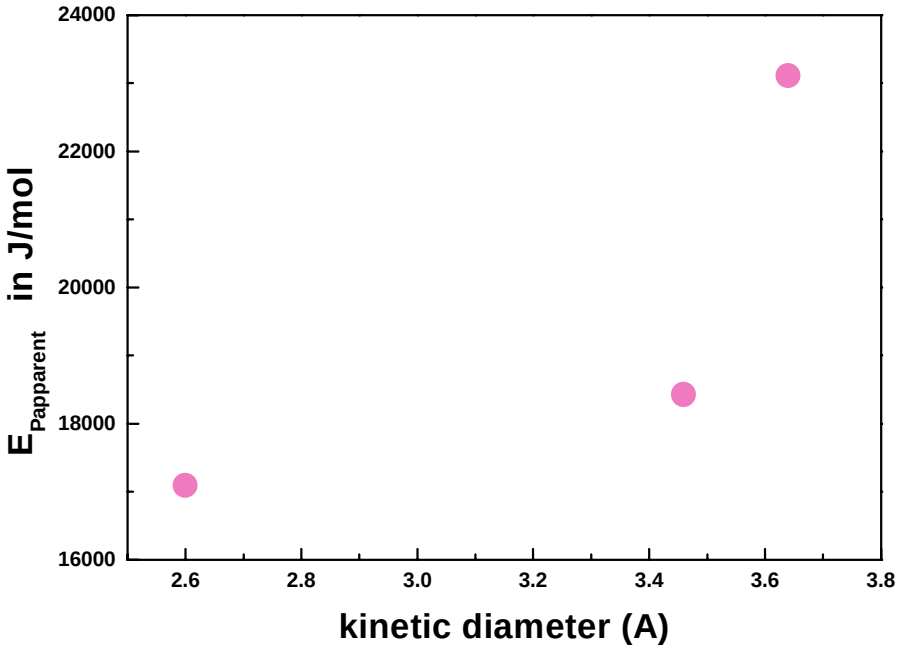

Figure 4.23: Apparent activation energy as a function of the kinetic diameter. The kinetic diameters of He, O_2, and N_2 are reported as 2.6, 3.46, and 3.64Å, respectively [45-48].

4.5. Conclusions

Bisphenol-A polycarbonate has been selected for this research due to the fact that crystallinity is unlikely to occur under normal conditions and on stretching. The suppliers, molecular weights, and preparation of the samples have been provided in this chapter. The experimental techniques involved in this research have also been presented. The technique used to measure gas transport, namely permeation experiment, was treated into details. The other techniques used to measure the physical properties of the polymers were also presented. Those techniques were dynamic mechanical thermal analysis (DMTA), density, birefringence, and FTIR spectroscopy. Finally, details have been provided concerning the gas permeation data analysis. Calculations needed to access the gas transport coefficients as well as the gas transport activation energies were given.

4.6. References

1. A. Siegmann and P. H. Geil, *J. Macromol. Sci. Phys.*, B4, 239 (1970).
2. A. Siegmann and P. H. Geil, *J. Macromol. Sci. Phys.*, B4, 273 (1970).
3. A. Alizadeh, S. Sohn, J. Quinn, H. Marand, L. C. Shank, H. Darrell Iler, Influence of structural and topological constraints on the crystallization and melting behavior of polymers: 3. Bisphenol A Polycarbonate, *Macromolecules*, 34, 4066-4078 (2001).
4. E. Laredo, M. Grimau, A. Muller, A. Bello and n. Suarez, Influence of aging and crystallinity on the molecular motions in bisphenol-a polycarbonate, *Journal of Polymer Science: Part B: Polymer Physics*, 34, 2863 (1996).
5. Polycarbonates, Ullmann's Encyclopedia of Industril Chemistry, vol A21, 207 (1992).
6. R. P. Kambour, F. E. Karasz, and J. H. Danne, *J. Polym. Sci., A-2*, 4, 327 (1966).
7. E. Turka and W. Benechi, *J. Appl. Polym. Sci.*, 23, 3489 (1979).
8. R. A. Ware, S. Tirtowidjojo, and C. Cohen, *J. Appl. Polym. Sci.*, 26, 2975 (1981).
9. J. P. Mercier, G. Groeninckx, and M. Lesne, *J. Polym. Sci.*, Part C, 16, 2059 (1967).
10. R. Legras and J. P. Mercier, *J. Polym. Sci., Polym. Phys. Ed.*, 15, 1283 (1977).
11. J. Dybal, P. Schmidt, J. Baldrian and J. Kratochvil, Ordered structures in polycarbonate studied by infrared and raman spectroscopy, wide-angle X-ray scattering, and differential scanning calorimetry, *Macromolecules*, 31, 6611-6619 (1998).
12. F. Gallez, R. Legras, and J. P. Mercier, *Polym. Eng. Sci.*, 16, 276 (1976).
13. R. Legras, J. P. Mercier, and E. Nield, *Nature*, 304, 432 (1983).
14. Dr. G. L. Wilkes, lecture notes.
15. E. Ito, K. Sawamura and S. Saito, Effects of drawing on molecular motions in polycarbonate, *Colloid & Polymer Sci.*, 253, 480-484 (1975).
16. C. Bauwens-Crowet, J.-C. Bauwens, The relationship between the effect of thermal pre-treatment and the viscoelastic behaviour of polycarbonate in the glassy state, *Journal of materials science*, 14, 1817-1826 (1979).
17. R. M. Felder, Estimation of Gas Transport Coefficients from Differential Permeation, Integral Permeation, and Sorption Rate Data, *Journal of Membrane Science*, 3, 15 (1978).
18. D. G. Pye, H. H. Hoehn and M. Panar, Measurement of Gas Permeability of Polymers. I. Permeabilities in Constant Volume / Variable Pressure Apparatus, *Journal of Applied Science*, 20, 1921 (1976).
19. T. Graham, *Philos. Mag.*, 32, 401 (1866).
20. S. S. Dhingra, Eva Marand, Mixed Gas Transport Study Through Polymeric Membranes, *Journal of Membrane Science*, 141, 45 (1998).
21. Christopher J. Cornelius, Physical and Gas Permeation Properties of a Series of Novel Hybrid Inorganic-Organic Composites Based on a Synthesized Fluorinated Polyimide, PhD Dissertation, Virginia Polytechnic Institute and State University, VA, USA, July 6, 2000.

22. A. Bos, I. G. M. Punt, M. Wessling, H. Strathmann, CO_2-induced plasticization phenomena in glassy polymers, *Journal of Membrane Science*, 155, 67-78 (1999).
23. J. S. Chiou, J. W. Barlow and D. R. Paul, Plasticization of Glassy Polymers by CO_2, *Journal of Applied Polymer Science*, 30, 2633 (1985).
24. R. G. Wissinger and M. E. Paulaitis, Glass Transitions in Polymer/CO_2 Mixtures at Elevated Pressures, *Journal of Polymer Science, Part B: Polymer Physics*, 29, 5, 631 (1991).
25. E. S. Sanders, Penetrant-induced plasticization and gas permeation in glassy polymers, *Journal of Membrane Science*, 37, 63-80 (1988).
26. M. Wessling, S. Schoeman, Th. Van den Boomgaard, C. A. Smolders, Plasticization of gas separation membranes, *Gas Sep. Purif.*, 5, 222-228 (1991).
27. Y. P. Handa, S. Lampron, M. L. O'Neill, On the plasticization of poly(2,6-dimethyl phenylene oxide) by CO_2, *J. Polym. Sci., Polym. Phys. Ed.*, 32, 2549-2553 (1994).
28. W.-C. Wang, E. J. Kramer, W. G. Sachse, Effects of high –pressure CO_2 on the glass transition temperature and mechanical properties of polystyrene, *J. Polym. Sci., Polym. Phys. Ed.*, 20, 1371-1384 (1982).
29. J. R. Fried, H.-C. Liu, C. Zhang, Effect of sorbed carbon dioxide on the dynamic mechanical properties of glassy polymers, *J. Polym. Sci., Polym. Part C*, 27, 385-392 (1989).
30. T. S. Chow, Molecular interpretation of the glass transition temperature of polymerdiluent systems, *Macromolecules*, 13, 362-364 (1980).
31. M. Wessling, Z. Borneman, Th. Van den Boomgaard, C. A. Smolders, Carbon dioxide foaming of glassy polymers, *J. Appl. Polym. Sci.*, 53, 1497-1512 (1994).
32. H. Hachisuka, T. Sato, T. Imai, Y. Tsujita, A. Takizawa, T. Kinoshita, Glass transition temperature of glassy polymers plasticized by CO_2 gas, *Polymer Journal*, 22, 1, 77 (1990).
33. J.-S. Wang, Y. Kamiya, Y. Naito, Effects of CO_2 conditioning on sorption, dilation, and transport properties of polysulfone, *Journal of Polymer Science: Part B: Polymer Physics*, 36, 1695 (1998).
34. K. Tanaka, M. Ito, H. Kita, K. Okamoto, Y. Ito, The effects of CO2-conditioning of polymers on positron annihilation and gas permeation properties, *Bull. Chem. Soc. Jpn.*, 68, 3011-3017 (1995).
35. G. K. Fleming and W. J. Koros, Dilation of Polymers by Sorption of Carbon Dioxide at Elevated Pressures. 1. Silicone Rubber and Unconditioned Polycarbonate, *Macromolecules*, 19, 2285 (1986).
36. G. K. Fleming and W. J. Koros, Carbon Dioxide Conditioning Effects on Sorption and Volume Dilation Behavior for bisphenol A - Polycarbonate, *Macromolecules*, 23, 1353 (1990).
37. A. G. Wonders and D. R. Paul, Effects of CO_2 Exposure History on Sorption and transport in Polycarbonate, *Journal of Membrane Science*, 5, 63 (1979).
38. S. M. Jordan, W. J. Koros, J. K. Beasley, Characterization of CO_2-induced conditioning of polycarbonate films using penetrants with different solubilities, *Journal of Membrane Science*, 43, 103-120 (1989).

39. D. S. Pope, G. K. Fleming, W. J. Koros, Effect of various exposure histories on sorption and dilation in a family of polycarbonates, *Macromolecules*, 23, 2988 (1990).
40. W. R. Vieth, L. H. Dao, and H. Pedersen, Non-equilibrium microstructural and transport characteristics of glassy poly(ethylene terephthalate), *Journal of Membrane Science*, 60, 41-62 (1991).
41. P. Gotthardt, A. Grűger, H. g. Brion, R. Plaetschke, and R. Kirchheim, Volume change of glassy polymers by sorption of small molecules and its relation to the intermolecular space, *Macromolecules*, 30, 8058-8065 (1997).
42. S.-H. Chen, S.-L. Huang, K.-C. Yu, J.-Y. Lai, M.-T. Liang, Effect of CO_2 treated polycarbonate membranes on gas transport and sorption properties, *Journal of Membrane Science*, 172, 105-112 (2000).
43. B. G. Risch and G. L. Wilkes, Effects of physical aging and carbon dioxide absorption in bisphenol-A polycarbonate, *Journal of Applied Polymer Science*, 56, 1511 (1995).
44. A. H. Chan and D. R. Paul, Influence of history on the gas sorption, thermal, and mechanical properties of glassy polycarbonate, *Journal of Applied Polymer Science*, 24, 1539-1550 (1979).
45. W. J. Koros and G. K. Fleming, Membrane-based Gas Separation, *Journal of Membrane Science*, 83, 1-80, (1993).
46. W. J. Koros and M. W. Hellums, Transport Properties, Encyclopedia of Polymer Science and Engineering, 2nd Edition, H. F. Mark, N. M. Bikales, C. G. Overberger, G. Mendes, Eds., John Wiley and Sons, New York, Supplement volume, 1989.
47. D. W. Breck, Zeolite molecular sieves, John Wiley & Sons, Inc., New York, 1974.
48. W. J. Koros, A. H. Chan and D. R. Paul, Sorption and Transport of Various Gases in Polycarbonate, *Journal of Membrane Science*, 2, 165 (1977).
49. D. W. Van Krevelen, Properties of Polymers, Their correlation with chemical structure; their numerical estimation and prediction from additive group contributions, Third Ed, Elsevier, NY, 1990.
50. D. R. Paul, Yuri P. Yampol'skii, editors, *Polymeric gas separation membranes*, CRC Press, Boca Raton, 1994.
51. F. Doghieri and G. C. Sarti, Nonequilibrium lattice Fluids: A Predictive Model for the Solubility in Glassy Polymers, *Macromolecules*, 29, 24, 7885 (1996).
52. M. D. Shelby and G. L. Wilkes, The effect of molecular orientation on the physical ageing of amorphous polymers - dilatometric and mechanical creep behaviour, *Polymer*, 39, 26, 6767-6779 (1998).
53. M. D. Shelby and G. L. Wilkes, Thermodynamic characterization of the oriented state of bisphenol A polycarbonate as it pertains to enhanced physical aging, *Journal of Polymer Science: Part B: Polymer Physics*, 36, 2111 (1998).
54. E. Ito, K. Sawamura and S. Saito, Effects of drawing on molecular motions in polycarbonate, *Colloid & Polymer Sci.*, 253, 480-484 (1975).
55. Y. C. Jean, Y. Rhee, Y. Lou, D. Shelby, G. L. Wilkes, Anisotropy of hole structures in oriented polycarbonate probed by two-dimensional angular

correlation of annihilation radiation, *Journal of Polymer Science: Part B: Polymer Physics*, 34, 2979-2985 (1996).

56. M. D. Shelby, G. L. Wilkes, M. R. Tant, J. Zawada, T. J. Bastow and A. J. Hill, Amorphous orientation in glassy polycarbonate, *ACS, Polymeric Materials Science and Engineering, Conference Proceedings,* San Francisco, Spring 1997, 76, 485-6.
57. M.-S. S. Wu, Intrinsic birefringence of amorphous poly(bisphenol-A carbonate), *Journal of Applied Polymer Science*, 32, 3263-3275 (1986).
58. Dr. Azar Alizadeh, personal communication.
59. G. L. Wilkes, Rheooptical properties, in Encyclopedia of Science and Engineering, 14 (1984).
60. I. M. Ward, Structure and Properties of Oriented Polymers, Wiley, New York, 1975.
61. Christelle M. Laot, Eva Marand and Hideko T. Oyama, Spectroscopic Characterization of Molecular Interdiffusion at a Poly(vinyl pyrrolidone)/Vinyl ester Interface, *Polymer*, 40, 1095-1108 (1999).
62. Christelle M. Laot, Spectroscopic Characterization of Molecular Interdiffusion at a Poly(vinyl pyrrolidone)/Vinyl ester Interface, Master of Science Thesis, Virginia Polytechnic Institute and State University, VA, USA, August 25, 1997 (thesis available on-line at http://scholar.lib.vt.edu/theses/available/etd-73197-10251/).
63. J. Crank, *The Mathematics of Diffusion*, second edition, Oxford Science Publications, 1975.
64. R. D. Seigle and R. W. Coughlin, Errors in Diffusivity as Deduced from Permeation Experiments using Time Lag Technique, *Journal of Applied Polymer Science*, 14, 3145 (1970).
65. Christelle M. Laot, Understanding gas transport in physically aged, oriented and pressure densified amorphous glassy bisphenol-A polycarbonate, PhD preliminary examination thesis, Virginia Polytechnic Institute and State University, VA, USA, December 17, 1999.
66. J. M. Prausnitz, R. N. Lichtenthaler, E. G. de Azevedo, Molecular thermodynamics of fluid-phase equilibria, 2nd Edition, PTR Prentice Hall, Englewood Cliffs, New Jersey, 1985.
67. A. M. Shishatskii, Y. P. Yampol'skii and K. V. Peinemann, Effects of Film Thickness on Density and Gas Permeation Parameters of Glassy Polymers, *Journal of Membrane Science*, 112, 275 (1996).
68. R. M. Barrer, *Trans. Faraday Soc.*, 35, 644 (1939).
69. V. T. Stannett, Simple gases, Diffusion in Polymers, Wiley, New York, 1971.
70. G. J. Van Amerongen, Diffusion in elastomers, *Rubber. Chem. Technol.*, 37, 5, 1065 (1964).

Chapter 5

Is the transport of gas molecules through polymers directly related to the amount of free volume?

5.1. Introduction

One would expect that the greater the amount of free volume in a freshly processed polymer, the more permeable the material, and the lower the activation energy for permeation. Nevertheless, although this trend has been observed for the transport of gas molecules through various polymer structures [1, 2], the literature is relatively sparse on the role of the free volume in gas transport through a particular amorphous glassy polymer as a function of processing conditions. It should however be pointed out that in studies dealing with various polymer structures, the free volume amount was calculated from group contribution methods [3, 4], and never measured. The relationship between the polymer free volume and/or polymer chain dynamics and the gas transport properties needs to be understood for any given polymer. Knowledge of this relationship is necessary to further fundamental research as well as to optimize polymers in industrial applications.

Two different amorphous glassy bisphenol-A polycarbonates with different free volume contents will be compared. The amount of free volume will be characterized from

time-temperature superposition concepts. The influence of the free volume on the gas transport properties will be examined.

5.2. Experimental details

The following subsections briefly review the materials and the instrumental methods. The complete experimental details have been provided in Chapter 4.

5.2.1. The materials

Bisphenol-A polycarbonate was ordered from two different suppliers. Polycarbonate pellets were ordered from Aldrich. The weight average molecular weight M_W was determined by GPC to be about 34,000 g/mol, and the polydispersity index about 2.2. Lexan 8010 polycarbonate sheets were ordered from General Electric (GE). Lexan was chosen in this research because of the number of studies in the literature based on this particular polymer grade. The weight average molecular weight was determined by GPC to be 38,000 g/mol and the polydispersity 2.4. The density was given by the suppliers as 1.2 g/cm^3 at 20^{o}C in both cases.

Polymeric films of the Aldrich polymer were prepared as outlined in Chapter 4. The sheets provided by GE and referred to as Lexan were dried at room temperature for one day in a vacuum oven. The polymeric films were kept in a dessicator at all time to avoid any water moisture uptake.

The films were put between Kapton® sheets and copper metal plates. The metal plates were suspended in the center of an internal fan gas chromatograph oven 8000 VEGA Series to improve heat transfer on both sides. The samples were heated in the GC oven from room temperature to 165^{o}C at a heating rate of 40^{o}C/min, kept at 165^{o}C for 15min to remove thermal history, and cooled within the oven at a programmed rate of 40^{o}C/min to room temperature. The room temperature was about 30^{o}C. The polymer films were then used immediately.

The thicknesses of the sheets were about 190μm.

5.2.2. The instrumental methods

Density measurements, dynamic mechanical thermal analysis (DMTA) experiments, and gas permeation experiments were carried out in this study.

The densities were measured at 18^{o}C in a density gradient column made out of sodium bromide salt and distilled water. The theoretical accuracy of the column was about 5×10^{-5} g/cm^3. At least three samples of each type of polycarbonate were dropped in the column to verify reproducibility.

The dynamic mechanical experiments were carried out in the tensile mode. Different types of tests were selected for this study. The conditions are given below.

The dynamic frequency-temperature sweep mode was chosen to generate data to build the master curves. A torque of 15cNm was used on each clamp. Optimization of the dynamic experimental conditions was performed initially to ensure reproducibility of the results [5]. The soak time was found to be the most critical parameter. The soak time corresponds to the time the sample is left at a particular temperature before recording data points. Enough time (at least 5min at 50^{o}C [6], less at higher temperatures) has to be allowed for temperature equilibrium, but the time should not be too long because of possible aging. The dependence of the data on the soak time was found to depend on the temperature increments as well. Dynamic mechanical measurements were collected as a function of temperature using eight different frequencies, namely 0.5, 0.75, 1, 3, 5, 10, 14, and 18Hz. The initial temperature was chosen as 140^{o}C; the final temperature corresponded to the temperature at which measurements were not possible because the sample softened. A waiting time of about 5min at 140^{o}C was chosen prior to starting the dynamic experiments themselves to ensure thermal equilibrium. Although the heat conductivity of polymers is rather low, it has nevertheless been established in the literature [6] that for an amorphous plastic sample of 200μm thick, 5 min at 50^{o}C in air are sufficient for a flat sheet to reach thermal equilibrium. The strain level was

determined by dynamic strain sweep. The strain level was chosen within the range of linear viscoelasticity and for a corresponding force of about 10g. In our experiments, the strain was set at 0.0125%. The optimized conditions were the following: the temperature steps were chosen as 2°C and the soak time as 240s. The static force was determined at 155°C by dynamic frequency sweep test (strain control). The static force corresponding to the thickness of the samples was set as 2g.

Dynamic temperature ramp experiments were carried out with the following conditions. A torque of 10cNm was used on each clamp nut. The frequency was chosen as 1Hz, the heating rate as 2°C/min, the initial temperature as 25°C, the strain as 0.025%, and the static force as 22g.

Dynamic frequency/temperature sweep tests were carried out with the following conditions. A torque of 10cNm was used on each clamp. The frequencies were chosen as 0.5, 3, and 10Hz. The heating rate was 1°C/min, the initial temperature 25°C, the final temperature 175°C, the strain 0.025%, and the static force 40g.

Permeation experiments were carried out using the permeation integral method described in Chapter 4. The experiments were performed at 35°C using three different inert gases, namely He, O_2, and N_2, in that given sequence. The applied pressures were fixed at about 2.5 atm for He, and 3.9 atm for O_2 and N_2. Three measurements were taken for each gas to ensure reproducibility and to calculate the error involved in the permeation results. Permeation experiments were also carried out on the same membrane at 55, 65, and 80°C, right after the experiment at 35°C in order to determine the temperature dependent activation energies. Aging was found to be negligible at those temperatures within the timeframe of the experiments.

5.3. Results and discussion

Density, DMTA, and gas permeation results are presented and discussed in the following subsections.

5.3.1. Density results

The densities of the two polymers are shown in Figure 5.1. Although the density of the Aldrich polymer seems lower, the error bars nevertheless suggest that the densities are quite similar. The errors on those measurements came from the fact that some samples could have possibly been stuck to other samples or could have been attracted to the walls of the density column.

The fractional free volume (FFV) was calculated from Bondi's method [3, 4]. The details of the group contribution calculations will be detailed in Chapter 6. Please note that in this case FFV is allowed to vary below T_g, in contrast with the free volume defined in viscoelastic theories which is fixed below T_g (see later in this chapter). Although the Aldrich polymer appears to possess more free volume than the polymer purchased from GE, the differences are within experimental errors (see Figure 5.2).

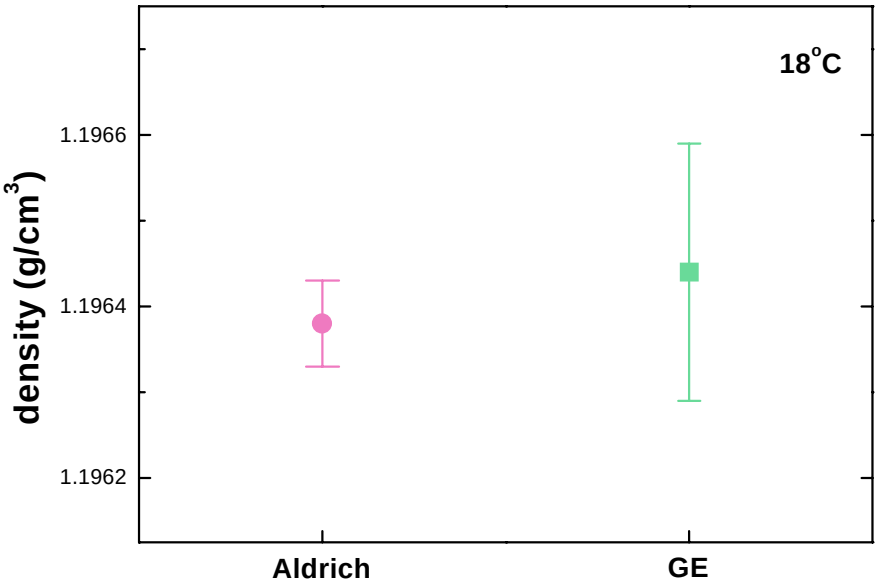

Figure 5.1: Densities of the two polymers selected in this study. The densities were measured at 18°C using a density gradient column.

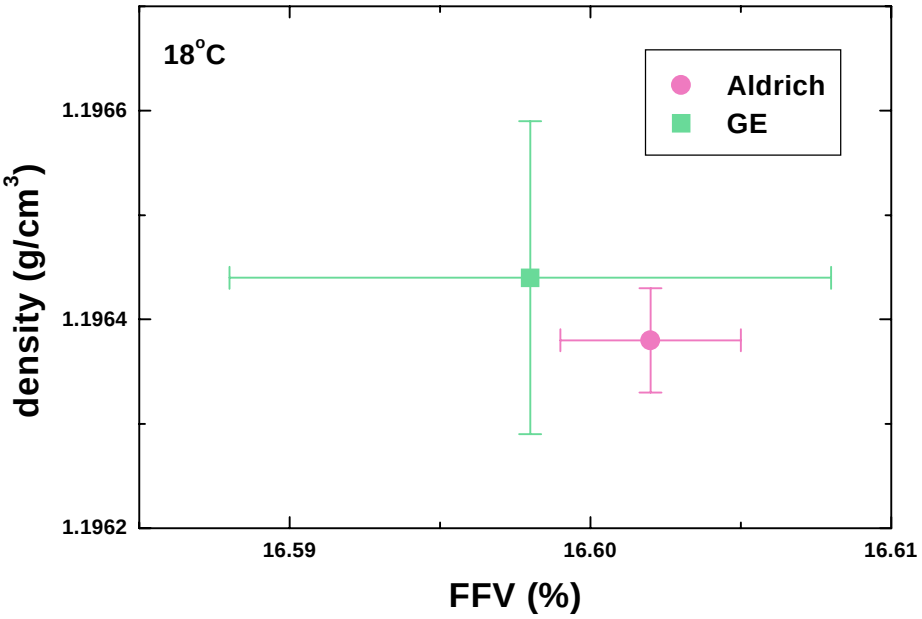

Figure 5.2: Densities of the two polymers selected in this study as a function of the fractional free volume calculated from Bondi's method. The densities were measured at 18°C using a density gradient column.

5.3.2. DMTA results

Dynamic mechanical thermal analysis (DMTA) experiments gave information on the glass transition temperature T_g and the frequency activation energy. The amount of free volume contained in the polymers at T_g could be estimated from time-temperature superposition concepts. Finally, the most probable number of molecular segments which must relax simultaneously for relaxation to occur could also be calculated from fragility concepts.

5.3.2.1. T_g

The glass transition temperature T_g was taken as the maximum of the loss modulus E" peak, as illustrated in Figure 5.3. The T_g's of the Aldrich and the GE polycarbonates were estimated to be 153.3°C and 154.6°C, respectively. As one can see from Figure 5.3, the DMTA measurements were quite reproducible for each polycarbonate. Please note that no extra-relaxations could be distinguished on the DMTA

traces at temperatures between the room temperature and the glass transition region. The T_g of the Lexan as received (used without any treatment once received from the supplier) was lower than that of the Lexan prepared as given in the experimental section of this chapter, probably because of the presence of moisture inside the polymeric matrix that may have plasticized the polymer.

The fact that the T_g of the Aldrich polymer is lower than that of the GE polymer should imply that the Aldrich polymer contained a greater amount of free volume. Since the T_g corresponds to the temperature at which the polymer chains can move globally, a greater free volume amount should imply a lower T_g [7, 8], as the polymer is heated from the glassy state to the rubbery state. Since the critical entanglement molecular weight M_e of polycarbonate is given as 4,800 g/mol [9], and since the molecular weights are high enough to be in the asymptotic part of the curve of T_g versus molecular weight, the difference in T_g between both types of polycarbonate is not believed to originate from the difference in the molecular weights of the materials. It is well established that [10, 11]:

$$T_g = T_{g\infty} - \frac{C}{M_n} \qquad \text{Eq (5.1)}$$

where C is a constant and $T_{g\infty}$ corresponds to the T_g at an infinite molecular weight. If the value of M_n is high enough though, the value of the T_g should barely be affected by an increase in M_n. Also, the weight average molecular weights of the Aldrich and the GE polymers were determined to be 34,000g/mol and 38,000g/mol, respectively, thus corresponding to a number of repeat units in excess of 130. Note that for monodisperse samples of polycarbonate the T_g has actually been found to be directly correlated with M_w rather than with $(M_n)^{-1}$, M_w ranging from about 4,000g/mol to 55,000g/mol [12]. The difference in the values of the glass transition temperatures between the Aldrich and the GE polymers (about 1.3^{o}C) may be due to the presence of additives inside the polymeric matrices, or to the slight differences in the polydispersity indices.

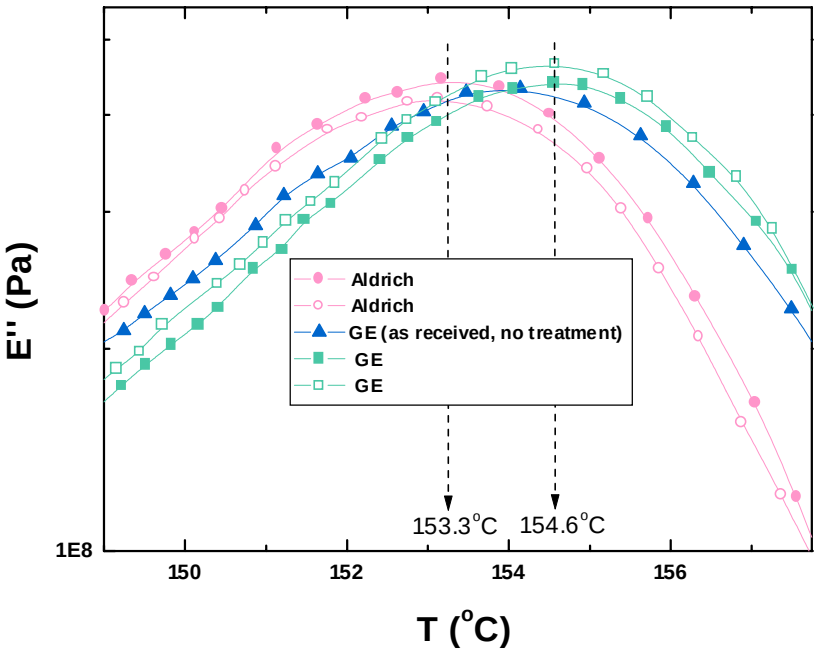

Figure 5.3: Loss modulus as a function of temperature for the polymers studied in this research. Both polymers were heated at 165°C for 15min and cooled at 40°C/min prior to DMTA experiments, unless indicated. The DMTA conditions were the following: frequency = 1Hz, strain = 0.025%, initial temperature = 25°C, heating rate = 2°C/min, static force = 22g. The maximum of the loss modulus was taken as the glass transition temperature.

5.3.2.2. Frequency activation energy

The activation energy for frequency was also determined for both polymers. We have:

$$\gamma = \gamma_o \exp\left(\frac{-\Delta Ha}{RT}\right) \qquad \text{Eq (5.2)}$$

where γ is the frequency and ΔHa is the activation enthalpy.

DMTA traces were collected as a function of temperature for three different frequencies, as shown in Figure 5.4. T^* (equal to T_g in this case since T_g was taken by us as the maximum of E") was obtained from the maximum of E", and the natural logarithm of the frequency was plotted as a function of $(1/RT^*)$. In a limited temperature range, the data points fit on a straight line for the α-relaxation, as shown in Figure 5.5 (Note that this line is strictly linear for the β-relaxation only [13]). The slope corresponded to $-\Delta Ha$. No real difference could be distinguished between the two polymers studied in this

chapter. The activation energy ΔHa was determined to be 1.06×10^6 J/mol for the Aldrich polycarbonate, and 1.02×10^6 J/mol for the GE polymer.

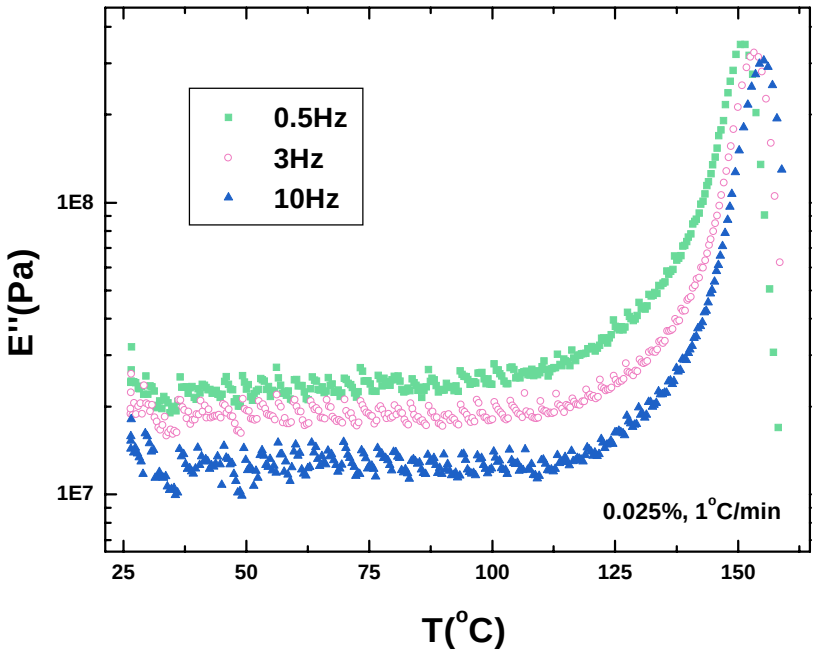

Figure 5.4: Loss modulus of the Aldrich polycarbonate as a function of temperature for different frequencies (0.5, 3, and 10Hz). The DMTA conditions were the following: strain = 0.025%, heating rate = 1°C/min, static force = 40g, clamp force = 10cNm, initial temperature = 25°C.

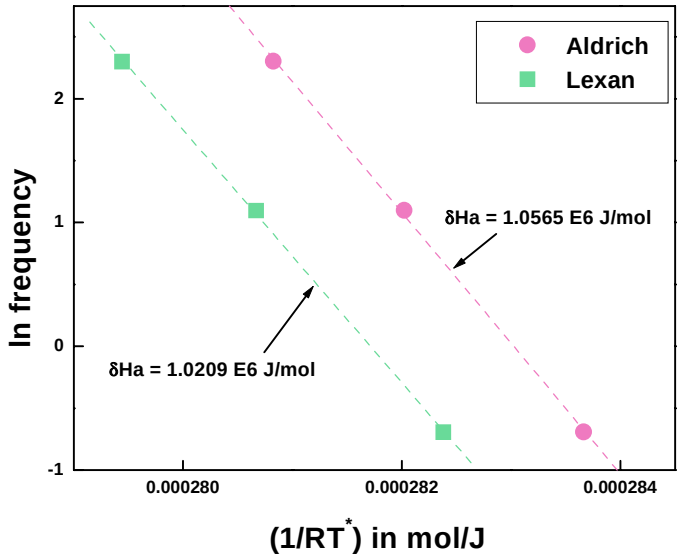

Figure 5.5: ln frequency versus ($1/RT^*$) (see Figure 5.4 for experimental details). T^* was determined from the maximum of the E" peak. The slope corresponded to -ΔHa, ΔHa being the frequency activation energy.

5.3.2.3. WLF parameters and fragility concepts

5.3.2.3.1. WLF parameters

The amount of free volume present in a polymer can be determined using the time-temperature superposition concepts developed by Williams, Landel, and Ferry (referred to as WLF) [14]. Although the viscoelastic parameters are usually obtained from creep or stress relaxation experiments [13, 15, 16], they can also be assessed using dynamic frequency temperature sweep.

The WLF equation [14] that supposes that the glass transition temperature T_g is an iso-free volume state and that the system possesses a single relaxation mechanism (same activation energy shared by all the relaxation modes represented in the relaxation time spectrum) is given by:

$$\log a_T = \frac{-C_1(T - T_g)}{C_2 + (T - T_g)} \qquad \text{Eq (5.3)}$$

$$\text{with} \quad a_T = \frac{\eta(T)}{\eta(T_g)} = \frac{t}{t_g} \qquad \text{Eq (5.4)}$$

$$C_1 = \left(\frac{B}{2.303 \ f_g} \right) \qquad \text{Eq (5.5)}$$

$$C_2 = \left(\frac{f_g}{\alpha_f} \right) \qquad \text{Eq (5.6)}$$

The viscoelastic constants or WLF parameters C_1 and C_2 are not universal but depend on the polymer. Originally, C_1 and C_2 were believed to be constant, and equal to 17.4 and 51.6K, respectively. However the non-universality of those constants has been demonstrated later on [11]. C_1 is nevertheless rather constant for all systems, but C_2 can vary widely. For example, while considering seven various polymers C_1 ranges from 8.6 to 19.8 whereas C_2 ranges from 14.2 to 200.4 [17]. The value of the glass transition temperature is usually taken from volumetric, or calorimetric measurements obtained at a heating rate of 10^oC/min [18]. In this research the T_g was determined from DMTA temperature ramp measurements. Please note that the WLF equation Eq (5.3) assumes

that $T \geq T_g$. Nevertheless this equation is sometimes still valid up to 50°C below T_g [11]. a_T is the WLF shift factor which is equal to the viscosity at a temperature T divided by the viscosity at T_g (assuming that the viscosity is directly proportional to the product of the density and the time). The Doolittle parameter B is assumed to be about 1 and the fractional free volume at the glass transition temperature f_g is believed to be about 0.025 for all systems. However f_g has actually been reported to vary between 1% and 7% [11]. The fractional free volume corresponds to the ratio of the free volume available to the system divided by the total volume of the system. The thermal expansion coefficient of the fractional free volume α_f varies from one polymer to another. α_f is generally taken as:

$$\alpha_f = \alpha_r - \alpha_g \qquad \text{Eq (5.7)}$$

where α_r and α_g correspond to the thermal expansion coefficients in the rubbery and the glassy state, respectively. However there is no method a priori to determine α_f.

If a reference temperature T_{ref} is taken instead of the glass transition temperature T_g (with $T_{ref} > T_g$) the WLF equation Eq (5.3) becomes:

$$\log a_T = \frac{-C_1^{\,o}(T - T_{ref})}{C_2^{\,o} + (T - T_{ref})} \qquad \text{Eq (5.8)}$$

$$\text{with} \quad C_1^{\,o} = \left(\frac{B}{2.303 \; f_{ref}} \right) \qquad \text{Eq (5.9)}$$

$$\text{and} \quad C_2^{\,o} = \left(\frac{f_{ref}}{\alpha_f} \right) \qquad \text{Eq (5.10)}$$

The fractional free volume above T_g at T_{ref}, f_{ref}, is assumed to be given as follows:

$$f_{ref} = f_g + \alpha_f (T_{ref} - T_g) \qquad \text{Eq (5.11)}$$

Therefore f_{ref} increases with temperature, which allows an enhancement of the molecular motions with temperature. The fractional free volume below T_g is believed to be frozen and thus remains constant and equal to f_g. This is however not strictly true since physical aging leads to a slight decrease in the free volume content.

Thus $$C_1^{\,o} = \frac{C_1 C_2}{C_2 + (T_{ref} - T_g)} \quad \text{or} \quad C_1 = \frac{C_1^{\,o} C_2^{\,o}}{C_2} \qquad \text{Eq (5.12)}$$

And $$C_2^{\,o} = C_2 + (T_{ref} - T_g) \quad \text{or} \quad C_2 = C_2^{\,o} + T_g - T_{ref} \qquad \text{Eq (5.13)}$$

In order to generate a master curve, data were collected as a function of temperature using eight different frequencies with just one sample. Using only one sample reduced the error involved in the measurements since the geometry and the thermal history remained exactly the same. As an example, the storage modulus data E' for the Aldrich polymer are displayed in Figure 5.6. The DMTA traces were plotted back as a function of the logarithm of the frequency for different temperatures, as shown in Figure 5.7 for the storage modulus E'. The master curves illustrated in Figure 5.8 for a reference temperature T_{ref} of 154^{o}C were generated by moving the curves horizontally around the curve obtained at T_{ref}. The reference temperature T_{ref} was calculated by taking the middle of the experimental temperature range. The curves adjacent to T_{ref} were moved first by common computer softwares, and then the other curves were moved until the data points met. The tan δ data points were manipulated initially. Further manipulations were made simultaneously on the storage modulus E', the loss modulus E" and the compliance modulus D". Manipulating the three moduli simultaneously was necessary to generate consistent results. The viscoelastic parameters obtained with either one of the curves should be identical. Additional vertical shifting did not generate a smoother master curve than simple horizontal shifting and therefore vertical shifting was not performed in this study.

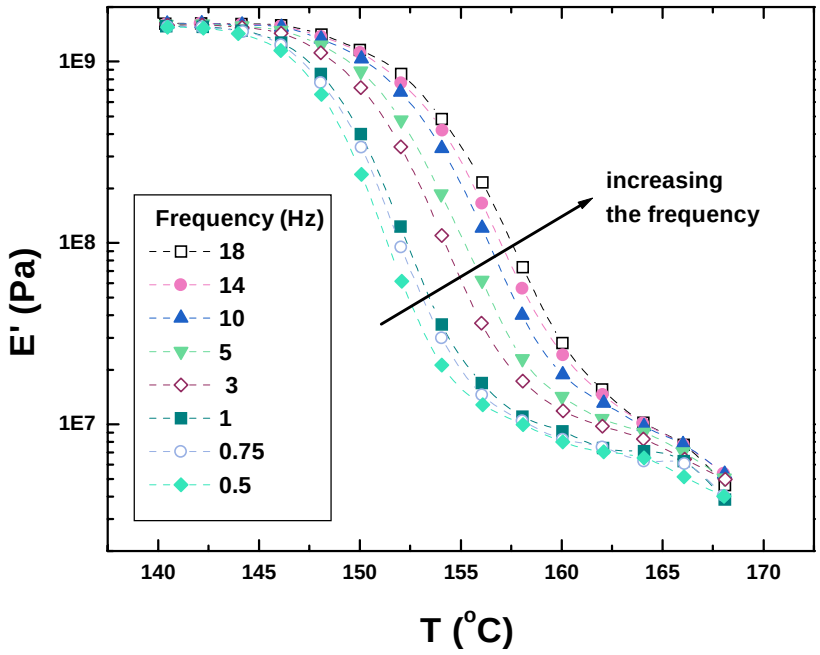

Figure 5.6: Storage modulus E' of the Aldrich polycarbonate as a function of temperature for eight different frequencies (namely 0.5, 0.75, 1, 3, 5, 10, 14, and 18Hz). The DMTA conditions were the followings: strain = 0.0125%, soak time = 240s, data collected every 1°C, initial temperature = 140°C, static force = 2g.

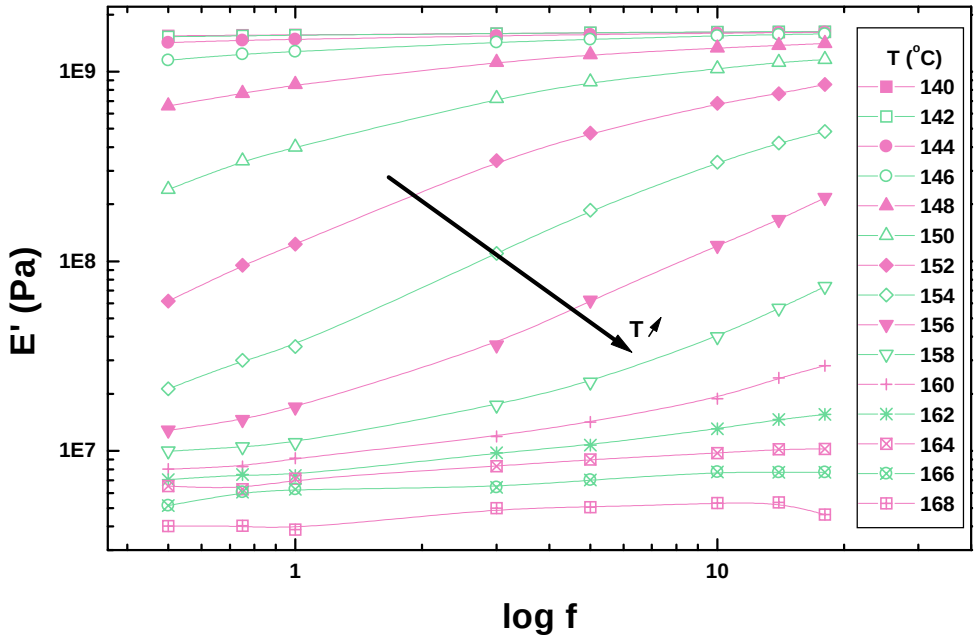

Figure 5.7: Storage modulus E' of the Aldrich polycarbonate as a function of frequency for different temperatures (see Figure 5.6 for experimental details).

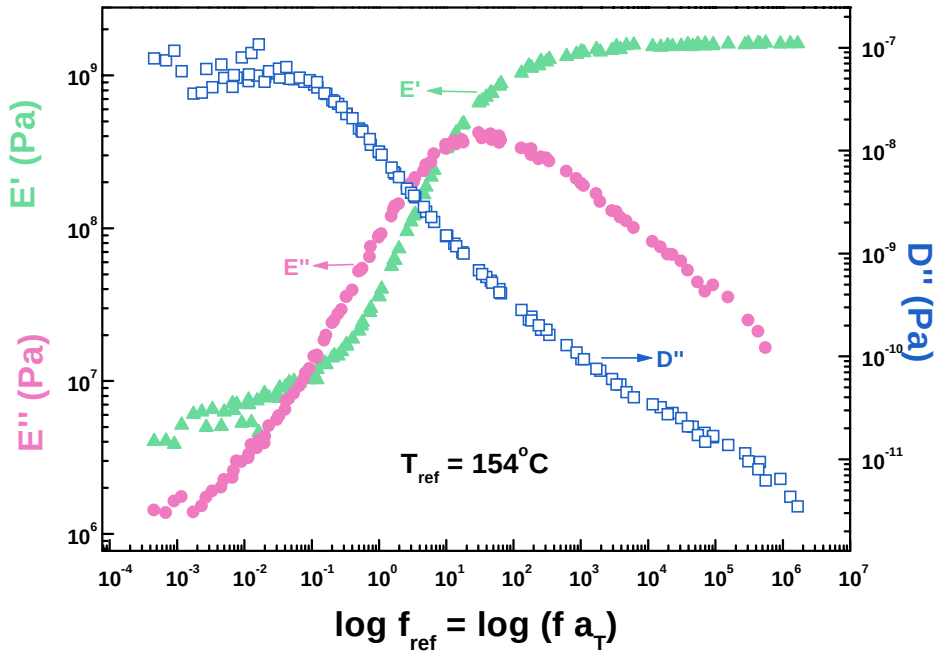

Figure 5.8: Master curves of the Aldrich polymer based on E', E", and D". The reference temperature was chosen as 154°C.

The shift factor a_T was calculated based on the reference temperature of 154°C. The shift factor basically indicated by how much each curve has to be multiplied at a given temperature to reach the curve at T_{ref}. For a frequency f we have:

$$\log a_T = (\log f_{ref} - \log f) \qquad \text{Eq (5.14)}$$

$\log f_{ref}$ is the new value of log f at T_{ref} (after the horizontal shift of all the curves). log f is the initial value (now observed only at T_{ref}). $\log a_T$ was calculated for each temperature. At T_{ref}, $a_T = 1$ and $\log a_T = 0$. Below T_{ref} $\log a_T$ is positive, and above T_{ref} $\log a_T$ is negative.

Data obtained at temperatures much lower than the glass transition temperature T_g are not always considered in the literature for further analysis because of the curvature observed at those temperatures (see Figure 5.8). The free volume concepts on which the WLF equation is based are valid only in the glass transition range and above. This has been confirmed by experiments on polycarbonate [19, 20]. Therefore all the data points obtained in the glassy state should not be considered for analysis. Moreover, the building of the master curve assumes no undergoing changes such as physical aging.

The WLF equation Eq (5.8) can be rearranged to give:

$$\frac{1}{\log a_T} = \frac{-C_2^{\,o}}{C_1^{\,o}(T - T_{ref})} - \frac{1}{C_1^{\,o}} \qquad \text{Eq (5.15)}$$

Thus a plot of $(1 / \log a_T)$ versus $(1 / (T\text{-}T_{ref}))$ has a slope of $(-C_2^{\,o} / C_1^{\,o})$ and an intercept with the y-axis at $(-1/C_1^{\,o})$. The linear regression obtained with the experimental data points collected in this study for the Aldrich polymer is shown in Figure 5.9. The values obtained for $C_1^{\,o}$ and $C_2^{\,o}$ are equal to 12.32 ± 1.00 and 48.04 ± 0.33 K, respectively.

However doing a non-linear curvefit led to "better" results. The results obtained with the Levenberg-Marquardt algorithm are displayed in Figure 5.10. The initial fitting values were taken as the "universal" constants, namely 17.4 and 51.6K. The curvefit was typically successfully progressed in four rounds. The values obtained for $C_1^{\,o}$ and $C_2^{\,o}$ were given as 11.74 ± 0.50 and 43.55 ± 1.58 K, respectively. C_1 and C_2 were calculated from Eq (5.12) and Eq (5.13) to be 11.93 and 42.85K, respectively. The value of the T_g was taken from the DMTA measurements. Using Eq (5.5) and Eq (5.6), the value of f_g was calculated as 0.036 and that of α_f as $8.5*10^{-4}\ ^oC^{-1}$.

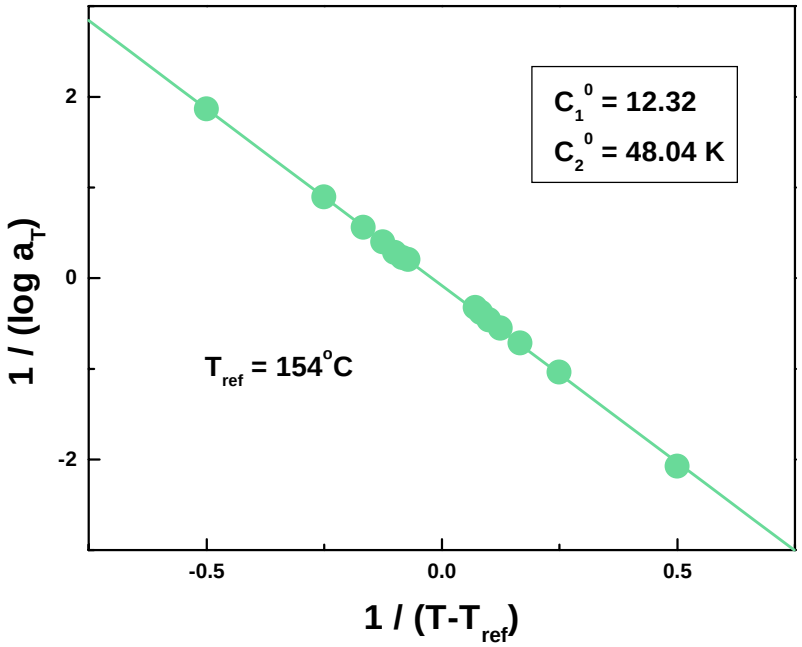

Figure 5.9: $(1/(\log a_T))$ versus $(1/(T\text{-}T_{ref}))$ for the Aldrich polycarbonate. The reference temperature was chosen as 154°C. Linear regression analysis led to values of 12.32 and 48.04 for $C_1^{\,o}$ and $C_2^{\,o}$, respectively (R = -0.99973, SD = 0.02281).

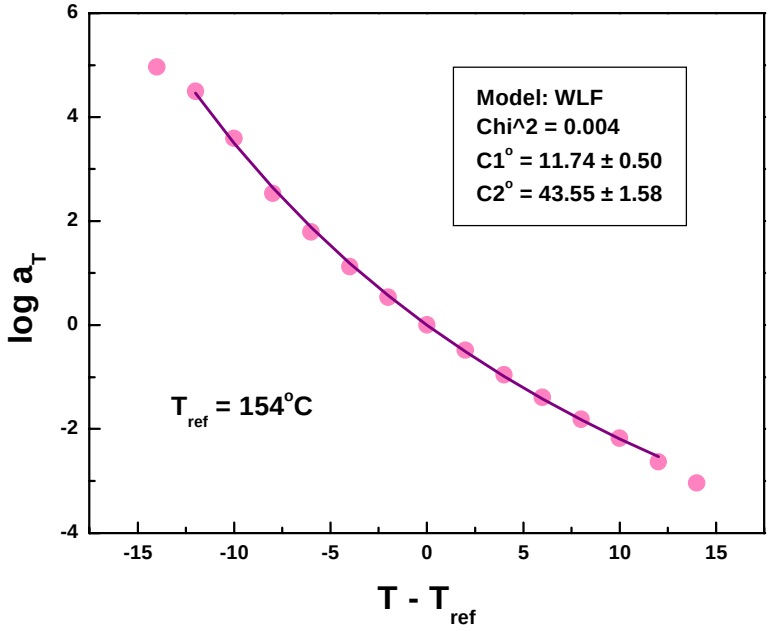

Figure 5.10: Non-linear regression for the Aldrich polymer using the Levenberg-Marquardt algorithm. The initial fitting values were taken as the "universal" constants, namely 17.4 and 51.6K. The curvefit was typically successfully progressed in four rounds. The values obtained for C_1^o and C_2^o were given as 11.74 and 43.55, respectively (χ^2 = 0.00422). The reference temperature was chosen as 154°C.

Similar analysis was performed on the polymer purchased from GE. In this particular case the reference temperature was set at 158°C. The final non-linear regression is shown in Figure 5.11. The values obtained for C_1^o and C_2^o were given as 15.86 ± 1.06 and 76.15 ± 4.44 K, respectively. C_1 and C_2 were equal to 16.60 and 72.75K, respectively. The value of f_g was equal to 0.026 and that of α_f to $3.6*10^{-4}$ $^oC^{-1}$.

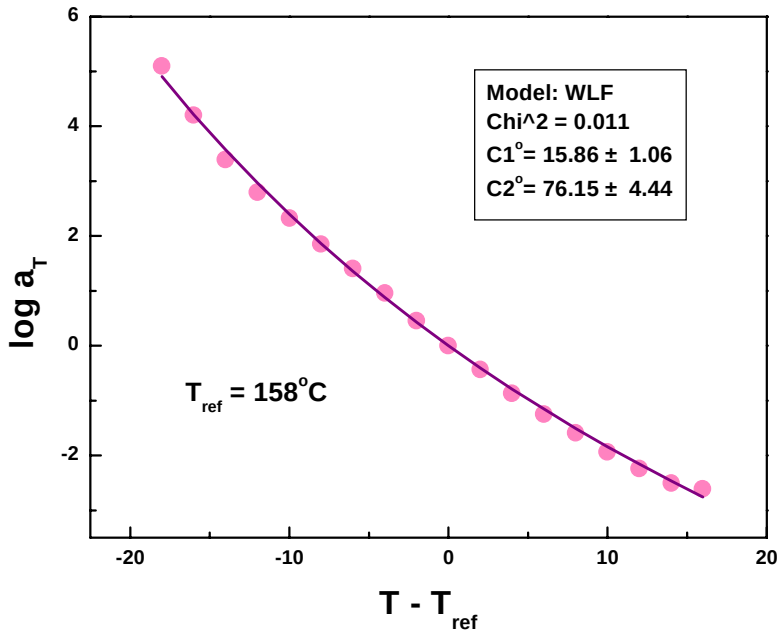

Figure 5.11: Non-linear regression for the GE polymer using the Levenberg-Marquardt algorithm. The initial fitting values were taken as the "universal" constants, namely 17.4 and 51.6K. The curvefit was typically successfully progressed in four rounds. The values obtained for C_1^o and C_2^o were given as 15.86 and 76.15, respectively (χ^2 = 0.01056). The reference temperature was chosen as 158°C.

5.3.2.3.2. Fragility concepts

The most probable number of molecular segments which must relax simultaneously or cooperatively for relaxation to occur can be calculated from the fragility concepts developed by Angell [21-23]. A correlation may exist between the measure of cooperativity, z, and the gas transport properties.

The apparent activation energy for viscoelastic relaxation E_a can be calculated at each temperature by taking the tangent of the slope of ln a_T versus 1/T, as illustrated in Figure 5.12 on the experimental data. The slope ($d(\ln a_T)/d(1/T)$) corresponds to E_a/R.

$$\frac{d \ln a_T}{d\left(\frac{1}{T}\right)} = \frac{E_a}{R} \qquad \text{Eq (5.16)}$$

E_a can also be calculated from the differentiation of the WLF equation Eq (5.3). Calculations leads to:

$$E_a = \frac{RT^2 C_1 C_2 \ln 10}{\left(C_2 + T - T_g\right)^2} = \frac{2.303 C_1^{\,o} C_2^{\,o} RT^2}{\left(C_2^{\,o} + T - T_{ref}\right)^2} = 2.303 R C_1 C_2 \left[\frac{1}{\left(1 - \frac{T_o}{T}\right)^2}\right] \qquad \text{Eq (5.17)}$$

where T_o ($=T_g - C_2$) is the Vogel temperature, which corresponds to the true thermodynamic second order transition temperature, if it exists. T_o is also equal to T_2, the Gibbs-DiMarzio transition temperature [24]. Please note that T should be greater than T_g since this assumption was part of the WLF derivation.

At the glass transition temperature T_g we have:

$$E_a\big|_{at\ Tg} = \frac{2.303 R C_1 T_g^{\,2}}{C_2} \qquad \text{Eq (5.18)}$$

E_a at T_g was calculated for both polymers. The value came out as 9.69×10^5 J/mol for the Aldrich polymer, and 7.99×10^5 J/mol for the GE polymer.

Please note that:

$$E_a = R\frac{d \ln a_T}{d\left(\frac{1}{T}\right)} = R\,(\ln 10)\frac{d \log a_T}{d\left(\frac{1}{T}\right)} = 2.303\,R\,T_g\,\frac{d \log a_T}{d\left(\frac{T_g}{T}\right)} \qquad \text{Eq (5.19)}$$

Comparing Eq (5.19) for $T=T_g$ and Eq (5.18) leads to:

$$\left.\frac{d \log a_T}{d\left(\frac{T_g}{T}\right)}\right|_{at\ Tg} = \frac{C_1\,T_g}{C_2} \qquad \text{Eq (5.20)}$$

The left hand side term of Eq (5.20) provides a measure of the fragility of the polymer m, m being a dimensionless parameter.

Thus we have:

$$m = \left.\frac{d \log a_T}{d\left(\frac{T_g}{T}\right)}\right|_{at\ Tg} = \frac{E_a\big|_{at\ Tg}}{2.303\,R\,T_g} \qquad \text{Eq (5.21)}$$

The fragility concept developed by Angell [21-23] gives a measure of the increase in the most probable segmental relaxation time with a decrease in temperature in the vicinity of T_g. The larger the m value, and thus the greater the fragility, the steeper is the slope of log a_T versus (T_g/T), the greater is the temperature sensitivity, the greater is the rate at which the degree of cooperativity varies with a decrease in temperature, and the greater is the degree of intermolecular coupling. The glassy state is well-known to possess indeed a high degree of intermolecular cooperativity [25]. The fragility values m were calculated for the Aldrich and the GE polymers. m were found to be equal to 118.7 and 97.6, respectively. The fragility results suggest that the Aldrich polymer has a more cooperative behavior and does possess a broader relaxation time distribution. Note that the fragility values have been reported in the literature to be dependent on the experimental technique. In a study involving twenty-three various polymers, Huang and McKenna [17] showed that the dynamic fragility m and the thermodynamic fragility (C_p^l/C_p^g) (ratio of the heat capacities in the liquid and in the glassy states) tend to be inversely correlated.

At high temperatures (for $T>>T_o$ in Eq (5.17)), the Vogel energy is:

$$E = 2.303\ R\ C_1\ C_2 \qquad \text{Eq (5.22)}$$

E corresponds to the activation energy of noncooperative intramolecular bond rotation, also referred to as $\Delta\mu^*$ by Matsuoka [26].

The ratio of E_a divided by $\Delta\mu^*$ corresponds to z, the most probable number of molecular segments or "beads" which must relax simultaneously or move cooperatively for relaxation to occur. Cooperative interactions are possible only within a group, the system being divided into several groups of particles.

$$z = \frac{E_a}{\Delta\mu^*} = \frac{E_a}{E} = \frac{1}{\left(1 - \frac{T_o}{T}\right)^2} \qquad \text{Eq (5.23)}$$

And at T_g

$$z_g = \left(\frac{T_g}{C_2}\right)^2 \qquad \text{Eq (5.24)}$$

From Eq (5.24), one can see that z decreases with an increase in temperature (T being greater than T_g). In this study, z_g was found to be greater for the Aldrich polymer than for the GE polymer (99.04 versus 34.57, respectively).

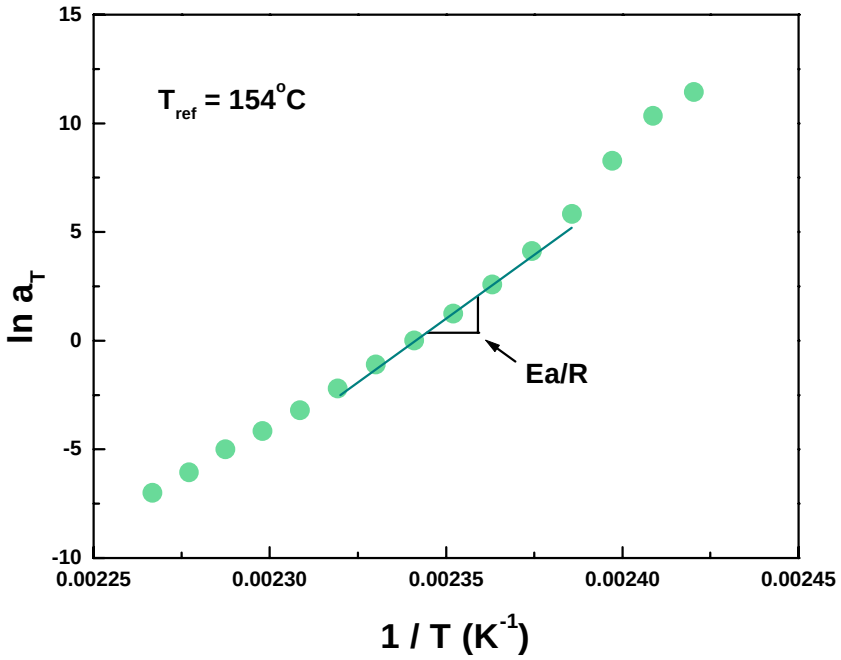

Figure 5.12: ln a_T versus 1/T for the Aldrich polymer. The apparent activation energy for viscoelastic relaxation can be calculated at each temperature by taking the tangent of the slope at that particular temperature, and by dividing it by the gas constant R. The reference temperature was chosen as 154°C.

5.3.2.3.3. Summary

The viscoelastic results obtained for both polymers are summarized in Table 5.1.

The values of C_1 and C_2 are the same order of magnitude as the values reported in the literature. For instance, the values of C_1 and C_2 for polycarbonate have been determined, respectively, to be 17.9 and 52.3K [27], 13.8 and 89.4K [28], 12.2 and 52.0K [17], 13.4 and 47.3K [29], 10.2 and 73.3K [30], and 9.9 and 91.0K [31]. Ideally the C_1 values should be the same for the two types of polycarbonate since C_1 should be a material parameter [10]. The reference temperature at which both C_1 values are the same should be readjusted for in this work. Nevertheless, C_2 has been shown to depend highly on the technique used to measure the WLF parameters. For instance, C_1 and C_2 were determined by torsional relaxation response to be 49.7 and 174.6K for polycarbonate

aged until equilibrium [32]. In addition, a transition from a WLF to an Arrhenius-type behavior has been observed as the glass transition of polycarbonate is being approached [32].

As expected from the free volume theory [7, 8], the polymer with the highest glass transition temperature T_g was found to contain a lower free volume amount. The amounts of free volume between the two polymers studied in this research differed by as much as 27%. The fractional free volume at T_g (f_g) was determined to be 2.6% for the GE polymer, in excellent agreement with the theoretical value of 2.5% predicted by Fox and Flory [11]. f_g was found to be 3.6% for the Aldrich polymer. Because f_g has been reported to vary between 1 and 7% [11], the results are in a probable range. The difference in the amounts of free volume between the two polycarbonates of interest in this research is unlikely to originate from the differences in molecular weight which are very slight. As a reminder, the number average molecular weights M_n of the Aldrich and the GE polymers were determined by GPC to be 15,400 g/mol and 15,700 g/mol, respectively. As stated earlier, the difference may be due to the presence of additives in the polymers, or to the slight differences in the polydispersity indices.

The value of the thermal expansion coefficient of the fractional free volume α_f for the GE polymer is in excellent agreement with the literature. For instance, the α_f value for polycarbonate has been reported to have the following values: $3.9\times10^{-4}\ ^oC^{-1}$ [33], $2.8\times10^{-4}\ ^oC^{-1}$ [33], $4.2\times10^{-4}\ ^oC^{-1}$ [27], or $3.7\times10^{-4}\ ^oC^{-1}$ [34]. Although the value of α_f for the Aldrich polymer seems a bit high compared to published values, it is the right order of magnitude.

The values of m and z_g are not too far from the ones published in the literature. While investigating a series of six polymers, Bartos and Kristiak determined that m varied between 46 and 137 [35]. The value of m was shown to range between 23 and 214 while considering twenty-three various polymers [17]. Especially, for polycarbonate m has been reported to be 120 [36], or 132 [17]. A value of 80 [36] has been given for z_g for polycarbonate. Nevertheless it seems rather strange that the polycarbonate with the lower T_g possesses a higher z_g. Indeed, one would expect that as the size of the cooperative domain increases, the material is less mobile, hence it becomes more difficult for the polymer chains to undergo large-scale motions, and the T_g should therefore be observed

at a higher temperature. The problem may originate from the fact that the T_g in this study was taken from the T_g value determined by the DMTA experiment in the heating mode. It would have been better to obtain the T_g while cooling the material from the melt, however such a procedure is not possible in the DMTA apparatus. The respective T_g values may have been inversed; this would affect in turn the values of C_2 and z_g. Although the difference in the T_g values we measured by DMTA was evaluated to be about 1°C, the difference may actually be greater; the breadth of the T_g peak may also vary. The difference in the polydispersity indices between both materials estimated to be about 9% is actually very significant. This should influence the T_g values, especially if the T_g scales with the inverse of the weight average molecular weight M_W, and not with the number average molecular weight M_n, as recently suggested in the literature [12]. The C_2 value may be influenced by the presence of additives in the polymeric matrix, or may even be highly sensitive to the curvefitting procedure. The difference in the z_g values could also be explained by an incorrect choice of the reference temperature used to calculate C_2, and therefore z_g.

	Aldrich	GE
T_{ref}	154°C	158°C
C_1^o	11.74	15.86
error on C_1^o	0.50	1.06
C_2^o	43.55 K	76.15 K
error on C_2^o	1.58 K	4.44 K
$T_{g\ (DMTA)}$	153.3°C	154.6°C
C_1	11.9	16.6
C_2	42.8 K	72.7 K
f_g	0.036	0.026
α_f	8.5×10^{-4} °C^{-1}	3.6×10^{-4} °C^{-1}
E_a (T_g)	9.7×10^5 J/mol	8.0×10^5 J/mol
m	119	98
z_g	99	35

Table 5.1: Summary of the free volume results. C_1^o and C_2^o were obtained from the Levenberg-Marquardt algorithm. The values of the viscoelastic parameters C_1 and C_2 were calculated from the T_g value determined from DMTA measurements. The errors were given in the text.

5.3.3. Permeation results

The gas transport coefficients, namely the permeability coefficient P, the diffusion coefficient D, and the solubility coefficient S were evaluated for the two polymers investigated in this chapter. Corresponding activation energies were also determined. The results are compared and discussed in this subsection.

5.3.3.1. Determination of the gas transport coefficients (P,D,S)

The gas transport results determined at 35^{o}C are shown in Figure 5.13, Figure 5.14 and Figure 5.15. The permeability coefficients tend to be the same for both polymers, within experimental errors. The nitrogen (N_2) diffusion coefficient appears to be lower in the Aldrich polymer, in contrast to the N_2 solubility coefficient S, which is greater in the Aldrich polymer. The difference in the experimental results is believed to be significant. The oxygen (O_2) diffusion and solubility coefficients appear to be the same in both types of polymers.

The previous DMTA results suggest that the Aldrich polymer does possess a greater amount of free volume. The similar permeability results between the Aldrich and the GE polymers suggest that P is not directly related to the free volume amount, in contrast to the literature concerning gas transport through various polymer families or classes [1, 2]. However one has to keep in mind that P corresponds to the product of S and D. It seems reasonable that S should be greater for the Aldrich polymer since S is related to the amount of free volume and this amount of free volume is greater for the Aldrich polycarbonate (see above). On the other hand, the diffusion coefficient is related to the mobility of the polymer chains. The fact that an increase in the free volume content does not result in an increase in the diffusion coefficient is in contradiction with free volume theories applied to gas diffusion [37-41].

As seen previously, the Aldrich polymer has been found to have the higher fragility or the higher probable number of segments which must move cooperatively for relaxation to occur, making it possibly more difficult for activated diffusion to take place.

The Aldrich polymer maybe more stiff locally than the GE polymer, despite of the greater overall free volume content. Nevertheless the diffusion phenomenon may not be a cooperative phenomenon as the diffusion process is likely to involve only a few segments at a time, and explanations based on fragility concepts may not be totally correct.

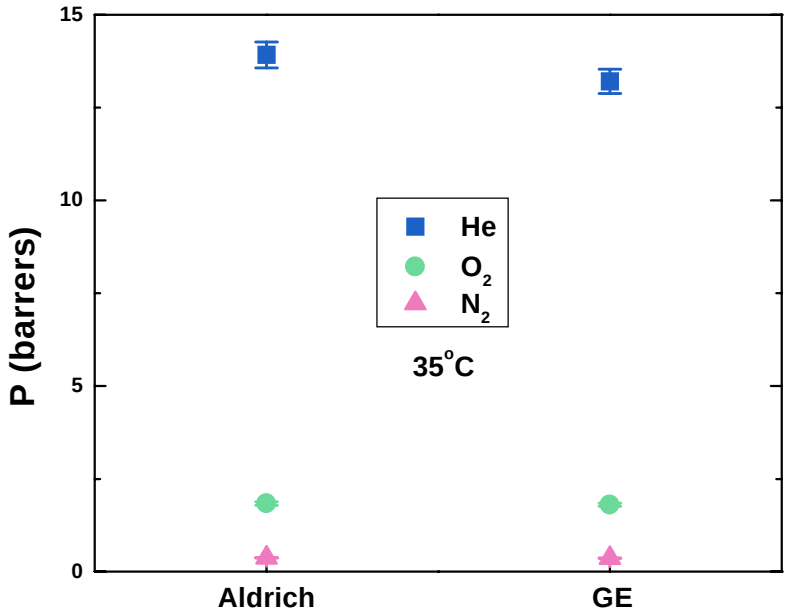

Figure 5.13: Permeability coefficients of the Aldrich and the GE polymers. The permeation experiments were performed at 35°C. The applied pressures were maintained at 2.5atm for He, and 3.9atm for O_2 and N_2.

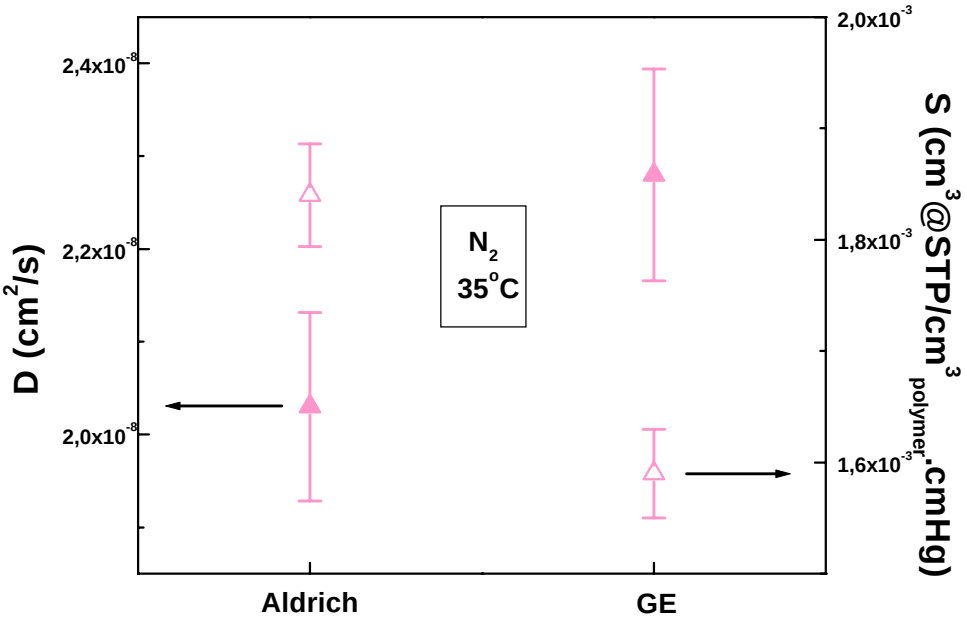

Figure 5.14: Diffusion and solubility coefficients of N_2 for the Aldrich and the GE polymers. The permeation experiments were performed at 35°C. The applied pressure was maintained at 3.9atm.

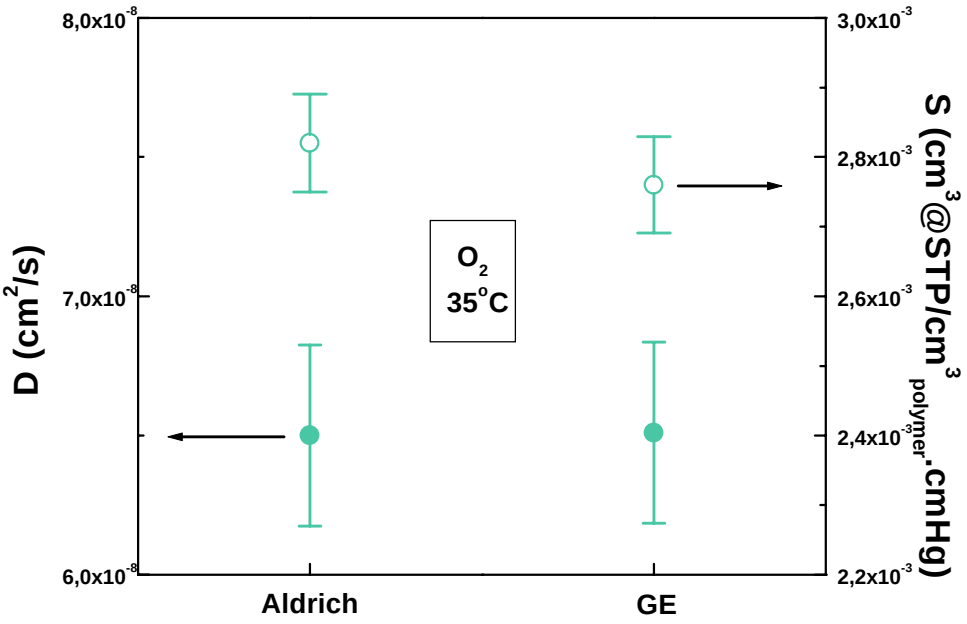

Figure 5.15:. Diffusion and solubility coefficients of O_2 for the Aldrich and the GE polymers. The permeation experiments were performed at 35°C. The applied pressure was maintained at 3.9atm.

5.3.3.2. Determination of the gas transport activation energies (E_P, E_D, ΔH_S)

The gas transport activation energies were determined for both polymers in order to investigate how the amount of free volume affects those quantities. Activation energy results obtained for both polymers are shown from Figure 5.16 to Figure 5.18. The activation energy of permeation E_P seems rather constant for both polymers, except for He for which the GE polycarbonate has a slightly higher activation energy. The activation energy of diffusion E_D and the enthalpy of sorption ΔH_S seem higher for the Aldrich polymer. The trends are believed to be significant for N_2.

One would expect that activation energies would be lower for the Aldrich polymer since it has been found to possess a higher free volume content. This trend commonly found in the literature has actually been verified by Yampolskii and co-workers [2] using a database involving various amorphous glassy polymers. However, the data presented here show an opposite trend.

One may think that activation energies may be related to the number of segments which must move cooperatively for relaxation to occur. This number is referred to as z_g at T_g. Cooperativity is necessary for relaxation to take place. Since the Aldrich polymer was characterized by a greater fragility m and a greater z_g value (z_g was determined to be about 99 for the Aldrich polymer versus to about 35 for the GE polymer), it may take more energy to relax the chains and unable diffusion to occur, despite of the greater free volume content. As shown in Figure 5.19, the greater the value of z_g, the greater is the activation energy of diffusion. However the z_g values are estimated at T_g whereas gas transport measurements are taken about 115^{o}C below T_g. It seems therefore unlikely that activation energies can be fully explained from fragility concepts, although some degree of cooperativity is necessary to permit diffusion even at room temperature.

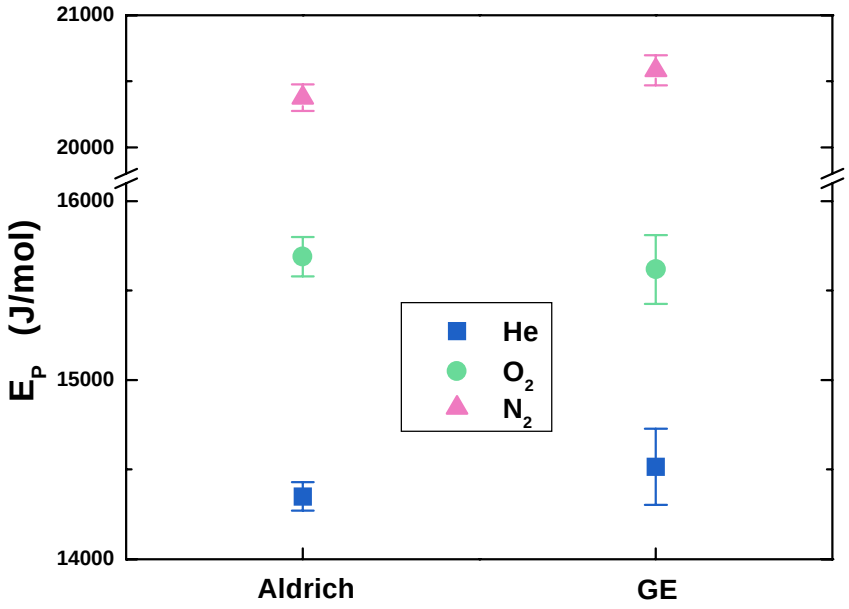

Figure 5.16: E_P of the two polymers of interest for He, O_2, and N_2. The permeation experiments were successively performed at 35, 55, 65, and 80°C. The applied pressures were maintained at 2.5atm for He, and 3.9atm for O_2 and N_2.

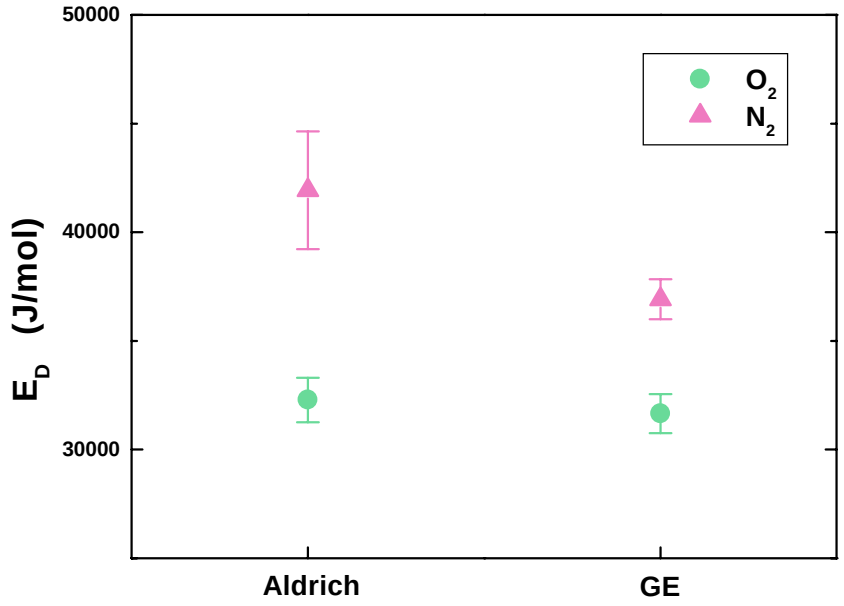

Figure 5.17: E_D of the two polymers of interest for O_2 and N_2. The permeation experiments were successively performed at 35, 55, 65, and 80°C. The applied pressure was maintained at 3.9atm for O_2 and N_2.

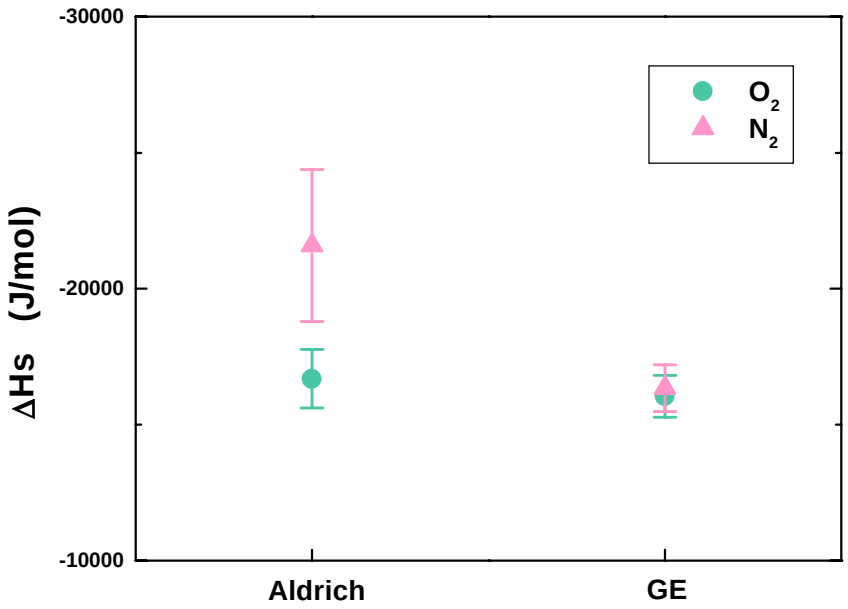

Figure 5.18: ΔHs of the two polymers of interest for O_2 and N_2. The permeation experiments were performed at 35, 55, 65, and 80°C. The applied pressure was maintained at 3.9atm for O_2 and N_2.

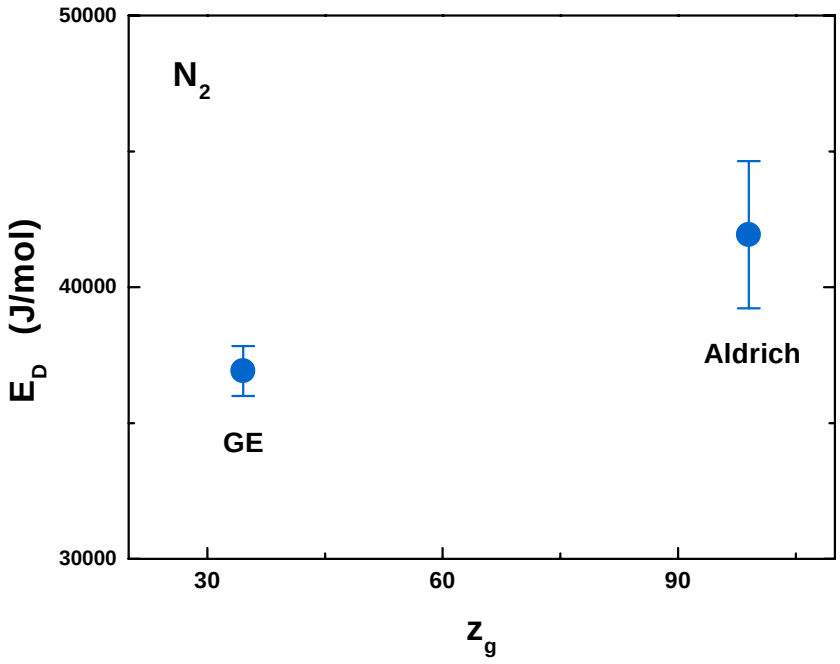

Figure 5.19: E_D versus z_g for the two polymers selected in this study and for N_2.

5.4. Conclusions

The results obtained in this study dealing with the relationship between the amount of free volume and the gas transport properties are summarized in Table 5.2 and Table 5.3. Two different polycarbonates of about the same molecular weights were ordered from two different suppliers: Aldrich and General Electric (GE). The Aldrich polycarbonate was characterized by a greater free volume content as determined from density and T_g values, as well as from time-temperature superposition concepts. Despite of this higher free volume content, the Aldrich polymer was found to have permeability coefficients similar to those of the GE polymer. The solubility coefficient was higher in the Aldrich polymer and the diffusion coefficient was found to be lower for the Aldrich polycarbonate. Gas transport activation energies were determined for both polymers. The activation energy of diffusion was found to be greater for the polymer containing the greatest amount of free volume. An explanation based on cooperativity concepts, or on a higher number of segments which have to move cooperatively for relaxation to occur, seems to work in interpreting the diffusion coefficients and the activation energies of diffusion, even though at room temperature the process most likely involves localized segments of the polymer chains.

	Aldrich	**GE**
ρ	1.19638 g/cm^3	1.19644 g/cm^3
$T_{g\ (DMTA)}$	153.3^{o}C	154.6^{o}C
M_n	15,400 g/mol	15,700 g/mol
PI	2.2	2.4
ΔH_a	1.06×10^6 J/mol	1.02×10^6 J/mol
f_g	0.036	0.026
E_a (at T_g)	9.7×10^5 J/mol	8.0×10^5 J/mol
m	119	98
z_g	99	35

Table 5.2: Summary of the physical properties obtained in this study.

P_{He}	Aldrich	=	GE
P_{O2}	Aldrich	=	GE
P_{N2}	Aldrich	=	GE
D_{O2}	Aldrich	=	GE
D_{N2}	Aldrich	<	GE
S_{O2}	Aldrich	=	GE
S_{N2}	Aldrich	>	GE
E_{PHe}	Aldrich	<	GE
E_{PO2}	Aldrich	=	GE
E_{PN2}	Aldrich	=	GE
E_{DO2}	Aldrich	=	GE
E_{DN2}	Aldrich	>	GE
dHs_{O2}	Aldrich	=	GE
dHs_{N2}	Aldrich	>	GE

Table 5.3: Summary of the gas transport results obtained in this study.

However, the most important conclusion of this study suggests that the transport of gas molecules through polymers may not be directly related to the amount of free volume. The free volume concept has been extremely popular in the literature to explain gas transport through polymers [1, 2, 37-43]. The same concept was also used to explain gas transport activation energies [2]. It was reported that the greater the free volume content in polymer families or classes, the greater the values of the gas transport coefficients and the lower the gas transport activation energies. This study shows that the solubility coefficient may be the only parameter directly linked with the amount of free volume contained in the polymer. The diffusion coefficient and the activation energies for diffusion do not appear to be directly related to this free volume content, in contrast to theories found in the literature [2, 37-41], but rather to the local stiffness of the polymer segments. P was not found to be enhanced in the greater free volume content material, in contrast to the literature [1, 2].

The fact that gas transport and free volume may not be directly related has actually been recently suggested by Pekarski and co-workers [44], who has demonstrated

that the diffusion coefficient of carbon dioxide (CO_2) in polycarbonate was lower in a conditioned sample (thus possessing a greater amount of free volume) than in an aged one. Similarly, the activation energy of diffusion was found to be lower in the aged sample. The results were attributed to a difference in the free volume distribution.

Nevertheless, the gas transport results presented in this study are complicated by the fact that additives may be present in the polycarbonates. Chemicals are indeed commonly added to polymers to improve the flow viscosity and processing behavior, to enhance some target properties, to increase softness and flexibility, or to decrease the final cost of the product. Additives can be of different types: plasticizers, fillers, carbon fibers, lubricants, fame retardants, antioxidants, antistatics, UV stabilizers, etc. Plasticizers for instance do decrease the T_g value and allow the polymer to absorb more energy. Plasticizers also modify the interactions between the gas and the polymer [45], thus eventually influencing the solubility coefficient. In a study involving stress relaxation experiments, Colucci and co-workers [46] reported dramatically different behaviors between two grades of bisphenol-A polycarbonates obtained from different suppliers. The volume change measurements performed in both uniaxial tension and compression showed that the mechanical responses of the two polymers were extremely different. This observation suggests that some polycarbonates may have more molecular mobility than others. The nature and quantity of the additives are likely to differ from one supplier to another. The additives contained in the polycarbonates may act at low temperature, or also broaden the relaxation time distribution. End groups may also be different. Moreover, although the number average molecular weights M_n of the polymers selected in this research were about the same (the difference was only about 2%), the difference in polydispersity indices PI (of about 9%) may affect the free volume distribution, and thereafter the gas transport properties. Actually, an increase of the value of the T_g with a narrowness of the molecular weight distribution has been reported in the literature [47, 48]. In the present research, we did observe a greater T_g value for the higher polydispersity index material.

In order to carefully evaluate the effect of the free volume on the gas transport properties, it is therefore necessary to use exactly the same polymer throughout the study.

The amount of free volume present in a particular glassy polymer can be modified by changing the cooling rate from the melt for instance. This will be done in the next chapter dealing with the effect of the cooling rate on the gas transport properties of polycarbonate.

5.5. References

1. J. Y. Park, D. R. Paul, Correlation and prediction of gas permeability in glassy polymer membrane materials via a modified free volume based group contribution method, *Journal of Membrane Science*, 125, 23-39 (1997).
2. Y. Yampolskii, S. Shishatskii, A. Alentiev, K. Loza, Correlations with and prediction of activation energies of gas permeation and diffusion in glassy polymers, *Journal of Membrane Science*, 148, 59-69 (1998).
3. A. Bondi, Physical properties of molecular crystals, liquids, and glasses, Wiley, New York, 1968.
4. D. W. Van Krevelen, Properties of Polymers, Their correlation with chemical structure; their numerical estimation and prediction from additive group contributions, Third Ed, Elsevier, NY, 1990.
5. Christelle M. Laot, Understanding gas transport in physically aged, oriented and pressure densified amorphous glassy bisphenol-A polycarbonate, PhD preliminary examination thesis, Virginia Polytechnic Institute and State University, VA, USA, December 17, 1999.
6. S. Hawley, Conditioning, in R. Brown, editor, Handbook of polymer testing – Physical methods, Marcel Dekker, Inc., New York, 141-156, 1999.
7. T. G. Fox and P. J. Flory, *J. Am. Chem. Soc.*, 70, 2384 (1948).
8. T. G. Fox and P. J. Flory, *J. Appl. Phys.*, 21, 581 (1950).
9. Richard P. Wool, *Polymer Interfaces- Structure and Strength*, Hanser Publishers, 1995.
10. Dr. Hervé Marand, lecture notes.
11. L. H. Sperling, *Introduction to physical polymer science*, Second edition, John Wiley and Sons, 1992.
12. Seungman Sohn, Crystallization behavior of bisphenol-A polycarbonate: effects of crystallization time, temperature, and molar mass, PhD Dissertation, Virginia Polytechnic Institute and State University, VA, USA, April, 2000.
13. J. J. Aklonis, W. J. MacKnight, M. Shen, Introduction to polymer viscoelasticity, Wiley-Interscience, NY, 1972.
    J. J. Aklonis and W. J. MacKnight, Introduction to polymer viscoelasticity, 2nd edition, John Wiley & Sons, NY, 1983.
14. M. L. Williams, R. F. Landel and J. D. Ferry, *J. Am. Chem. Soci.*, 77, 3701 (1955).
15. I. M. Ward, Mechanical properties of solid polymers, Wiley-Interscience, NY, 1971. 2nd Edition, 1983.

16. J. D. Ferry, Viscoelastic properties of polymers, 3rd edition, John Wiley & Sons, Inc., New York, 1980.
17. D. Huang and G. B. McKenna, New insights into the fragility dilemna in liquids, *Journal of Chemical Physics*, 114, 13, 5621-5630 (2001).
18. M. Connolly, F. Karasz, M. Trimmer, Viscoelastic and dielectric relaxation behavior of substituted poly(p-phenylenes), *Macromolecules*, 28, 1872-1881 (1995).
19. H. Higuchi, Z. Yu, A. M. Jamieson, R. Simha, J. D. McGervey, Thermal history and temperature dependence of viscoelastic properties of polymer glasses: relation to free volume quantities, *Journal of Polymer Science: Part B: Polymer Physics*, 33, 2295-2305 (1995).
20. H. Higuchi, A. M. Jamieson and R. Simha, Free volume quantities and viscoelasticity of polymer glasses, *Journal of Polymer Science: Part B: Polymer Physics*, 34, 1423-1426 (1996).
21. C. A. Angell, *Science*, 267, 1924 (1995).
22. C. A. Angell, *Journal of Non-Crystalline Solids*, 131-133, 13 (1991).
23. C. A. Angell, *J. Res. Natl. Inst. Stand. Technol.*, 102, 2, 171 (1997).
24. J. H. Gibbs and E. A. DiMarzio, *J. Chem. Phys.*, 28, 3, 373 (1958).
25. J. Greener, Relaxation phenomena in polymers: a snapshot, PMSE News, Summer'93, 26-27.
26. S. Matsuoka, Relaxation phenomena in polymers, Hanser Publishers, NY, 1992.
27. R. O. E. Greiner, J. Kaschta, Prediction and calculation of the shear creep behavior of amorphous polymers under progressive physical aging in multiphase reactor and polymerization system hydrodynamics, Houston, Tex.: Gulf Pub., p 683-709 (1996).
28. M. Mours and H. H. Winter, Viscoelasticity of polymers during heating/cooling sweeps, *Ind. Eng. Chem. Res.*, 34, 3217-3222 (1995).
29. J. P. Mercier, G. Groenincks, *Rheol. Acta*, 8, 516 (1969).
30. C. D. Han, K. Y. Lee, and N. C. Wheeler, Plasticating single-crew extrusion of amorphous polymers: development of a mathematical model and comparison with experiment, *Polymer Engineering and Science*, 36, 10, 1360-1376 (1996).
31. P. J. Mercier, J. J. Aklonis, M. Litt, A. V. Tobolsky, Viscoelastic behavior of the polycarbonate of bisphenol-A, *J. Appl. Polym. Sci.*, 9, 447-459 (1965)
32. P. A. O'Connell and G. B. McKenna, Arrhenius-type temperature dependence of the segmental relaxation below Tg, *Journal of Chemical Physics*, 110, 22, 11054-11060 (1999).
33. T. L. Smith and R. E. Adam, Effect of tensile deformations on gas transport in glassy polymer films, *Polymer*, 22, 299-304 (1981).
34. D. M. Colucci, G. B. McKenna, in *Structure and Dynamics of Glasses and Glass Formers, C. A. Angell editor, J. Res. Natl. Inst. Stand. Technol.*, 102, 2, 171 (1997).
35. J. Bartos and J. Kristiak, Free volume aspects of the strong-fragile classification of polymer liquids, *Journal of non-crystalline solids*, 235-237, 293-295 (1998).
36. D. J. Plazek and K. L. Ngai, *Macromolecules*, 24, 1222 (1991).
37. J. L. Duda and J. M. Zielinski, Free-Volume Theory, *Plastics Engineering*, 32, 143 (1996).

38. M. H. Cohen and D. Turnbull, *J. Chem. Phys.*, 31, 1164 (1959).
39. J. S. Vrentas and J. L. Duda, *J. Polym. Sci.*, 15, 403 (1977).
40. J. S. Vrentas and J. L. Duda, *J. Polym. Sci.*, 15, 417 (1977).
41. H. Fujita, *Fortschr. Hochpolym. Forsch.*, 3, 1 (1961).
42. W. M. Lee, Selection of barrier materials from molecular structure, *Polym. Eng. Sci.*, 20, 65-69 (1980).
43. E. R. Hensema, M. H. V. Mulder and C. A. Smolders, On the Mechanism of Gas Transport in Rigid Polymer Membranes, *Journal of Applied Polymer Science*, 49, 2081 (1993).
44. P. Pekarski, J. Hampe, I Böhm, H.-G. Brion, and R. Kirchheim, Effect of aging and conditioning on diffusion and sorption of small molecules in polymer glasses, *Macromolecules*, 33, 2192-2199 (2000).
45. W. R. Vieth, L. H. Dao, and H. Pedersen, Non-equilibrium microstructural and transport characteristics of glassy poly(ethylene terephthalate), *Journal of Membrane Science*, 60, 41-62 (1991).
46. D. M. Colucci, P. A. O'Connell, G. B. McKenna, Stress relaxation experiments in polycarbonate: a comparison of volume changes for two commercial grades, *Polymer Engineering and Science*, 37, 9, 1469 (1997).
47. J. J. Curro and R.-J. Roe, Isothermal relaxation of specific volume and density fluctuation in poly(methyl methacrylate) and polycarbonate, *Polymer*, 25, 1424 (1984).
48. R.-J. Roe and J. J. Curro, Small-angle X-ray scattering study of density fluctuation in polystyrene annealed below the glass transition temperature, *Macromolecules*, 16, 428 (1983).

Chapter 6

Effect of the cooling rate on the gas transport properties of polycarbonate

6.1. Introduction

Only a few studies have dealt with the influence of the cooling rate on the gas transport properties of amorphous glassy polymers [1, 2]. In a study concerning polycarbonate and the influence of quenching [1], it was observed that the solubility was enhanced in a quenched film compared to a slowly cooled film. Nevertheless, some polycarbonate samples were quenched in ice-water. Polycarbonate is very sensitive to water [3] and the properties may have been greatly affected by the presence of water. Furthermore, these studies relied on gas sorption experiments using carbon dioxide CO_2 as the penetrant. However such types of sorption experiments do possess several limitations. CO_2 is indeed well-known to plasticize glassy polymers by decreasing the value of the glass transition temperature T_g and by dilating the polymer chains [4-26]. The permeability coefficient P first decreases with the applied pressure, however above the plasticization pressure (the minimum of the curve of P versus pressure), P starts to increase. The permeation rate is accelerated and the selectivity reduced. CO_2 in the gas state is even capable of inducing crystallization in some polymers [27]. Furthermore, samples used in sorption experiments are very often conditioned initially prior to experiments. This conditioning, which consists of exposing the samples to the highest

pressure that will be used in the sorption experiments, may modify the polymers in an irreversible manner [16, 18-22]. It should be noted at this point that the majority of studies published by the membrane community have actually been carried out on as-received or conditioned polymers. The preparation of the samples should be better controlled. Moreover, a period of sometimes two months for CO_2 is necessary to obtain a sorption curve [28]. This comes from the fact that sorption data have to be taken at equilibrium. Therefore, the material has time to age during the sorption experiment, and its properties may be greatly affected by physical aging and change from the beginning of the experiment to the end. The applied pressures are also rather high in sorption experiments (up to about 20 to 30atm). Because of all the reasons cited above, permeation experiments seem more accurate to generate gas transport data.

The cooling rate from the rubbery state to the glassy state should be regarded as an important processing parameter since it is expected to affect the amount of free volume present in the polymeric materials and its size and shape distribution. The reason for this is that the glassy state corresponds to a non-equilibrium state. Physical aging, that has been explained in Chapter 3, is its most obvious manifestation. The greater the cooling rate from a particular temperature above T_g, the greater is the amount of free volume trapped inside the polymeric matrix as the polymer undergoes a transition from the rubbery to the glassy state with cooling.

The transport of gas molecules through amorphous glassy polymers is generally believed to relate to the amount of free volume present in the polymeric material [29-33]. In light of the results reported in Chapter 5, knowledge of the free volume content alone may not be sufficient to predict the gas transport properties. Not only the free volume content but also its distribution may be an important parameter in describing the gas transport phenomenon. A recent study by Nagel et al [34] suggested that the permeation is determined not only by the amount of free volume, but also by the distribution of free volume. Yet again, the study involved different types of glassy and rubbery polymers instead of a particular polymer. Similarly, in a study involving a family of substituted polycarbonates, Banerjee and Lipscomb [35] pointed out that the free volume distribution may be extremely important in sorption and permeation. The variations in the heats of

sorption of CO_2 in the various polymers were believed to give an indication about the weighted average of the free volume distribution since they did not correlate with the free volume content.

Knowledge of the relationship between the permeability and the cooling rate is of fundamental importance to various industrial applications. By selecting the cooling rate of the polymer, it could maybe be possible to control the performance of the polymeric materials.

6.2. Experimental details

The following subsections mention briefly the materials and the instrumental methods. The complete experimental details have been provided in Chapter 4. The reader should refer to this particular chapter for deeper understanding of the materials and the instrumental methods used in this research.

6.2.1. The materials

Bisphenol-A polycarbonate (BPA-PC) pellets with a weight average molecular weight of 34,000g/mol were purchased from Aldrich, Milwaukee, WI. The pellets were processed as detailed in Chapter 4. The thicknesses of the resulting polycarbonate films were about 130μm. The films were kept in a dessicator at all times to avoid any water moisture uptake.

Prior to experiments, the polymeric films were put between Kapton® sheets and copper metal plates. The metal plates were suspended in the center of the internal fan GC oven described in Chapter 4. The samples were heated in the GC oven from room temperature (30°C) to 165°C at a heating rate of 40°C/min, kept at 165°C for 15min to remove thermal history, and cooled within the GC oven at several controlled rates to room temperature (30°C). A schematic of the temperature program is provided in Figure 6.1. It was determined that 15min were sufficient to remove thermal history. Room temperature was assumed to be low enough (T_g–120°C) to freeze-in the material during

the timeframe of the experiments. It has actually been reported in the literature that quenching polycarbonate from a given temperature above T_g to either 0°C or –94°C did not affect properties such as solubility, density, or volume relaxation [1].

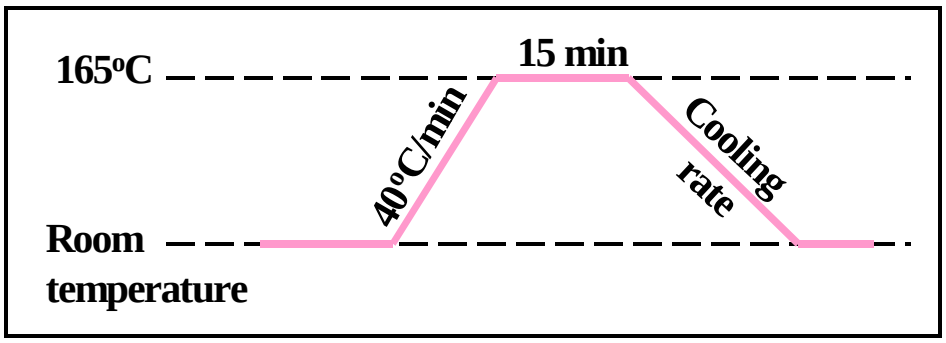

Figure 6.1: Schematic of the temperature program. The polycarbonate films were heated from room temperature (30°C) to 165°C at a heating rate of 40°C/min, kept at 165°C for 15min to remove thermal history, and cooled with the internal fan oven at several controlled rates to room temperature.

The cooling rates possible with the GC oven ranged from 0.5°C/min to 40°C/min. The programmed cooling rates were therefore chosen as 0.5°C/min, 10°C/min, and 40°C/min. It was observed that the GC oven did not always cool linearly with time. The responses observed for the various chosen cooling rates are given from Figure 6.2 to Figure 6.4. The rate of cooling was linear with time for a cooling rate of 10°C/min and below only. At a cooling rate of 40°C/min, the temperature profile decayed exponentially with time. Although the cooling rates did not always decrease linearly with time as programmed, the experimental data were reproducible for a given cooling rate. The cooling rate of the polymer may have been different from that of the oven, especially at high cooling rates. No thermocouple was available to directly measure the temperature of the polymer itself.

The system consisting of the polymer sandwiched between the Kapton® sheets and the metal plates was also cooled by opening the door of the GC oven and by blowing air immediately inside the oven with an external fan. The power of the fan, which was controlled by a variable autotransformer, was set at the maximum power. The polymer was believed to cool faster than when cooled by the internal fan located inside the GC oven. The cooling rate was in excess of 40°C/min. Although precautions were taken to

have reproducibility between samples, it is obvious that samples cooled by the fan cannot be as reproducible as samples cooled inside the oven.

The polymer films were used immediately once taken out of the GC oven.

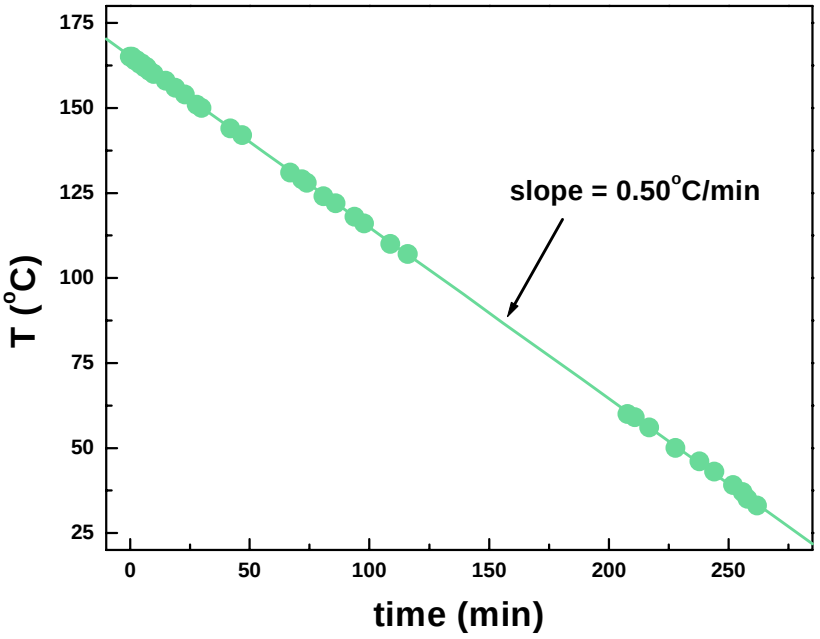

Figure 6.2: Temperature measured inside the oven for a programmed cooling rate of 0.5°C/min. The samples were heated at 165°C for 15min and cooling was monitored with time. The cooling rate was found to be a linear function of time.

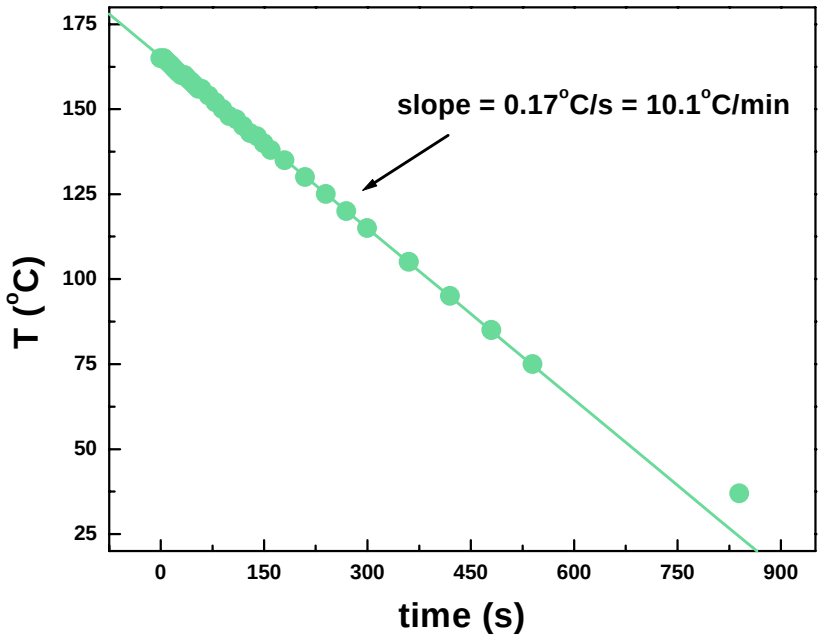

Figure 6.3: Temperature measured inside the oven for a programmed cooling rate of 10°C/min. The samples were heated at 165°C for 15min and cooling was monitored with time. The cooling rate was found to be a linear function of time.

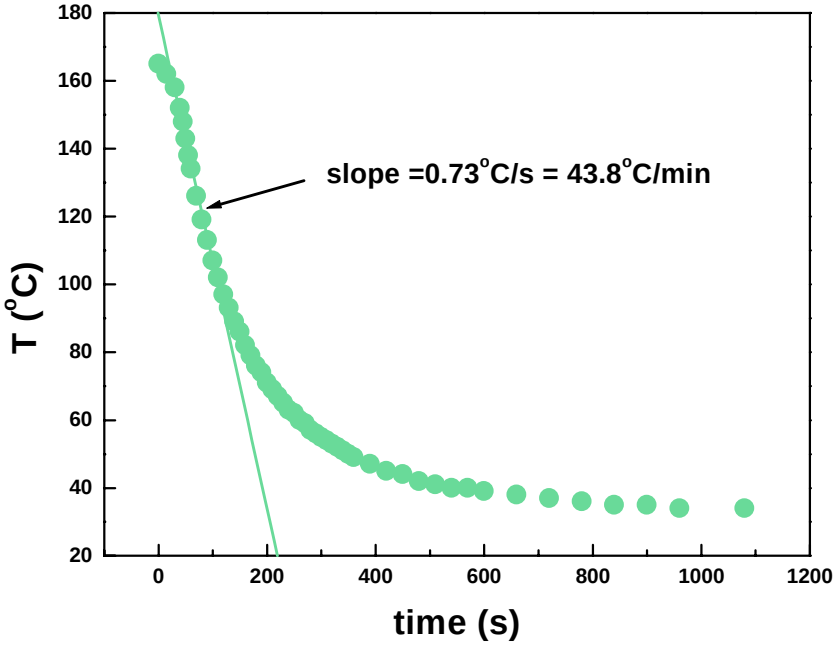

Figure 6.4: Temperature measured inside the oven for a programmed cooling rate of 40°C/min. The samples were heated at 165°C for 15min and cooling was monitored with time. The cooling rate was found to decay exponentially with time. The initial drop indicated by the line was determined to be 43.8°C/min, instead of the 40°C/min expected for the chosen cooling rate. The error on the reading was 1°C.

6.2.2. The instrumental methods

The density was obtained at 18°C using a linear density gradient column made of an aqueous solution of sodium bromide as described in Chapter 4. The theoretical resolution of the column was about 5×10^{-5} g/cm^3. At least three samples for each cooling rate were dropped in the column to verify reproducibility.

The dynamic mechanical experiments were carried out in the tensile mode as described in Chapter 4. Dynamic temperature ramp experiments were carried out with the following conditions. A torque of 10cNm was used on each clamp. The frequency was chosen as 1Hz, the heating rate as 2°C/min, the initial temperature as 25°C, the strain as 0.025%, and the static force as 33g. The static force was optimized by running dynamic frequency sweep test (strain control) at room temperature. Forgetting to enter this static force in the DMTA parameters engenders some extra relaxations in the DMTA traces. The tensile test may compress instead of pulling. For each cooling rate treatment, at least two samples were run in the DMTA to verify reproducibility. The test stopped by itself at about 7°C above T_g.

Permeation experiments were carried out using the permeation integral method described in Chapter 4. The experiments were performed using three different gases, namely He, O_2, and N_2, in that given sequence. The applied pressures were fixed at about 2.5 atm for He, and 3.9 atm for O_2 and N_2. Three measurements were taken for each gas to ensure reproducibility and to calculate the error involved in the permeation results. Please note that the degassing time between consecutive nitrogen runs were chosen as 120 min, and not 90min as given in Chapter 4. Permeation experiments were consecutively performed on the same membrane at 35, 55, 65, and 80°C in order to determine the activation energies for gas transport. Aging was found to be negligible at those temperatures within the timeframe of the experiments. Indeed, no significant change in density or in the DMTA traces could be observed. In order to verify that the results were repeatable, another polymer film was also tested. It was verified that the data points did fit on the error bar previously measured.

6.3. Results and discussion

Density, DMTA, and gas permeation results are presented and discussed in the following subsections.

6.3.1. Density results

The densities of the polycarbonate samples cooled with different cooling rates were obtained at 18^{o}C using a linear density gradient column. The experimental results are given in Figure 6.5. As expected, the greater is the cooling rate, thus the greater is the amount of free volume trapped inside the polymeric matrix as the polymer undergoes a transition from the rubbery to the glassy state, the lower is the density. The fact that the density of quenched samples is lower than that of as-received samples is well-documented in the literature for various polymers [36].

The density values of Figure 6.5 also indicate that no crystallization took place inside the material since the density values are too low for this to have happened [37].

Since the thicknesses of the polycarbonate films were rather small (about 130μm), we do not expect the occurrence of a density distribution between the skin and the core of the material. The presence of such a density distribution in thicker samples has been shown to be caused by cooling stresses [38].

The difference in the density values with the cooling rate are in agreement with the literature. Wimberger-Friedl and de Bruin [39] studied the specific volume of polycarbonate at different cooling rates. The experimental results were obtained in a density gradient column filled with a K_2CO_3 water solution at 23^{o}C. Since specific volume and density are inversely related, one can easily calculate the density at the different cooling rates obtained in the cited study. The densities ranged from about 1.1902 g/cm^3 for a polycarbonate sample cooled at 0.1^{o}C/min to about 1.1887 g/cm^3 for a sample cooled at 80^{o}C/min. Therefore the density difference between the two cooling rates was about 0.0015 g/cm^3. However if one considers the cooling rates at 1^{o}C/min and

10°C/min, the difference becomes around 0.00057 g/cm^3. With the cooling rates selected in the present research, the difference is about 0.00065 g/cm^3 between the cooling rate of 0.5°C/min and that obtained by cooling with the fan, therefore in reasonable agreement with the work cited above. In another study, Wimberger-Friedl and co-workers [38] determined a linear relationship between the density of polycarbonate and the logarithmic cooling rate. The slope showing a decrease in density with an increase in the cooling rate was evaluated to be 3.4x10^{-4} (g.cm^{-3}/°C.min^{-1}). It is not possible to evaluate the density as a function of the cooling rate in this study since it has been observed that at a cooling rate of 40°C/min for instance the cooling rate was not constant with time.

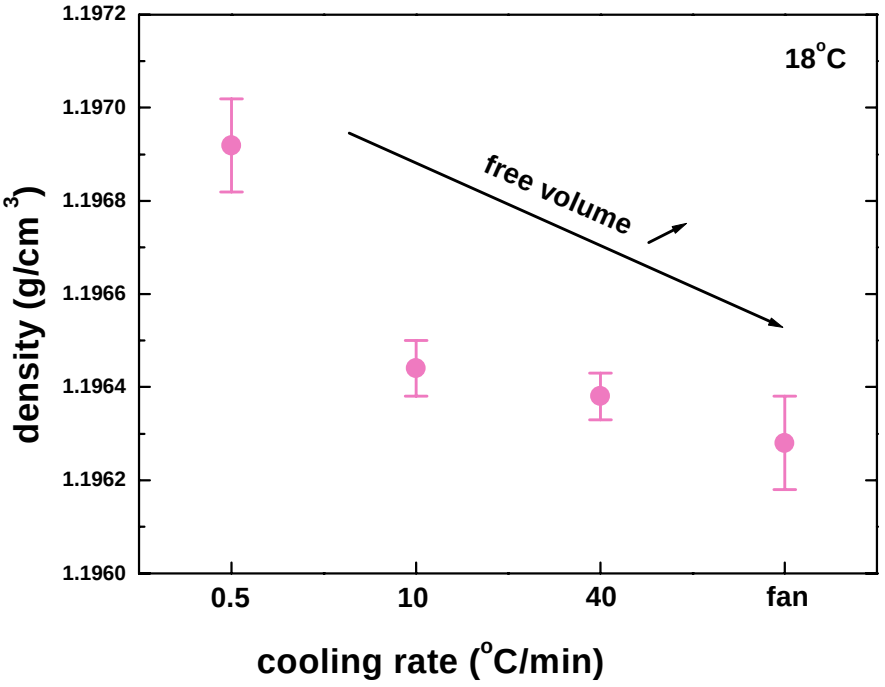

Figure 6.5: Density as a function of the cooling rate (note that the x-axis is not a continuous axis). The densities were measured at 18°C using a linear density gradient column.

6.3.2. DMTA results

The glass transition temperature T_g was determined from dynamic temperature ramp measurements. The DMTA traces are shown in Figure 6.6. Because the glassy state is not a stable phase, the T_g is not a true second order phase transition. The glass

transition temperature is a rate dependent phenomenon, and its value should be a function of the cooling rate. As seen in Figure 6.7, the slower the cooling rate, the higher is the value of the glass transition temperature T_g. The T_g corresponds to the temperature at which the polymer chains can move globally. It gives an idea of the chain flexibility. As the cooling rate decreases, the amount of free volume available for the polymer chains to move decreases, and therefore the T_g is observed at higher temperature when heated from room temperature to above T_g. A good definition of T_g has been given by Bicerano [40]. It reads as follows: "We can define T_g as the temperature at which the forces holding the distinct components of an amorphous solid together are overcome, so that these components become able to undergo large-scale viscous flow, limited mainly by the inherent resistance of each component to such flow" [40]. Cooperativity concepts may also be used to explain the glass transition temperature values. As a sample has been cooled slowly, the amount of free volume may not be sufficient to allow rearrangements easily and the number of conformers needed for relaxation to occur may be increased. Those conformers should move together simultaneously for cooperative relaxation to take place. Matsuoka and Hale have indeed shown that the T_g scales with the logarithm of the average molecular weight of the conformers [41].

The value of the T_g was not found to be a linear function of the cooling rate. The results were complicated by the fact that the experimental oven cooling rate may not have been exactly equal to the cooling rate of the polymer, as mentioned previously. Furthermore, the experimental oven cooling rate was not always a linear function of time (see above). Kovacs [42, 43] determined that the T_g and the cooling rate q are linked as follows:

$$\left.\frac{\Delta T_g(q)}{\Delta \ln|q|}\right|_{T_o >> T_g(q)} = \theta^{-1} \qquad \text{Eq (6.1)}$$

where T_o is the starting temperature and θ is a material constant. However in this case the T_g was determined from cooling the polymer from the rubbery to the glassy state, and not by heating the glassy samples. This point will be addressed later on.

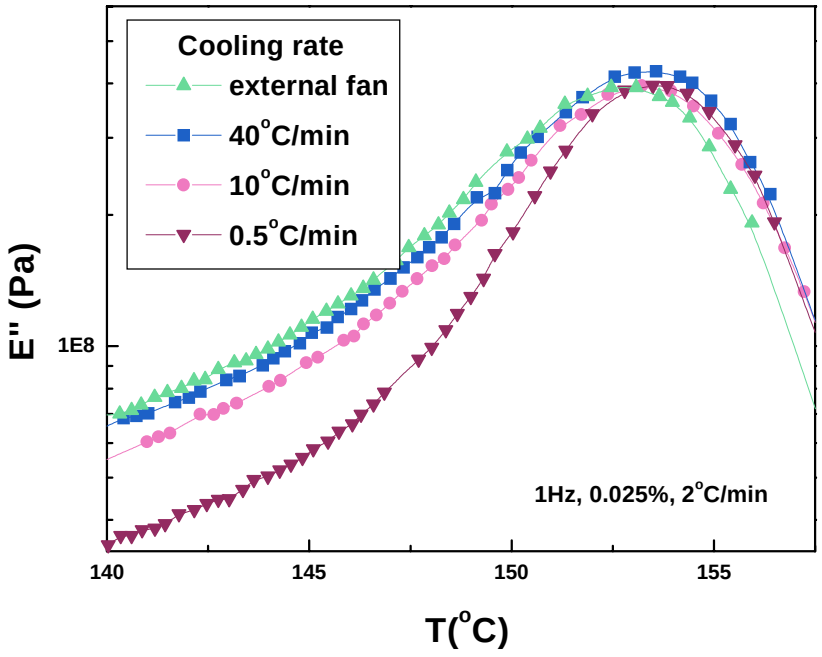

Figure 6.6: Loss modulus E" as a function of temperature for the samples cooled at different cooling rates. The DMTA conditions were the following: frequency = 1Hz, strain = 0.025%, heating rate = 2°C/min, static force = 33g, clamp force = 10cNm, initial temperature = 25°C.

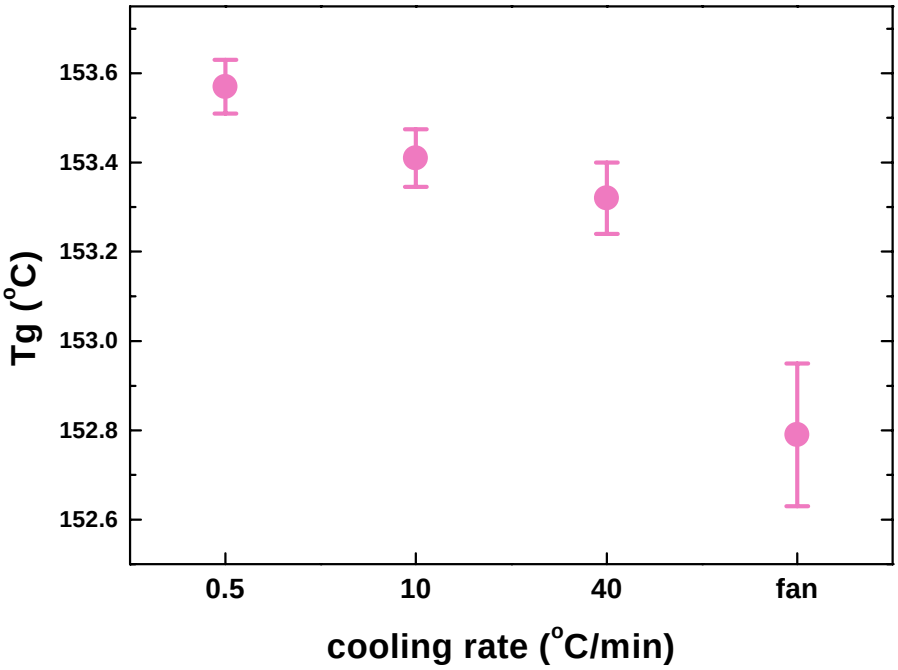

Figure 6.7: Glass transition temperature T_g (°C) versus rate of cooling (°C/min) (note that the x-axis is not a continuous axis). The T_g was determined from the maximum of the loss modulus E" peak. The DMTA conditions were the following: frequency = 1Hz, strain = 0.025%, heating rate = 2°C/min, static force = 33g, clamp force = 10cNm, initial temperature = 25°C.

The literature reports that when a polymer is cooled from the rubbery state to the glassy state, the T_g is lower for the lower cooling rate, as sketched in Figure 6.8 [42, 44-50]. The position of the T_β peak has also been shown to be affected by the cooling rate [50]. As the cooling rate is varied by a factor of 10 the T_g is shifted by about 3°C and the T_β by about 6 to 7°C [50].

Gibbs and DiMarzio [51] postulate the existence of a true second order thermodynamic transition below which the entropy remains zero. At equilibrium, the value of the true T_g, referred to as T_2, is given by:

$$T_2 = T_g - C_2 \qquad \text{Eq (6.2)}$$

At T_2, only the lowest conformational energy state is allowed. C_2 is the WLF parameter defined in Chapter 5. C_2 should be constant for a given polymer since the parameters should be determined above T_g, thus in the equilibrium state. Since C_2 is positive, it is clear from Eq (6.2) that T_2 is lower than the observed T_g and thus that T_g should decrease with a decrease in free volume.

The fact that in the present study the T_g possesses the highest value for the lowest cooling rate, hence for the sample closer to the equilibrium state, seems to be in contradiction with the thermodynamic theory of the glass transition temperature mentioned above. While heating a polymer from the glass (hence rather than by cooling it from the liquid state), it seems nevertheless reasonable that the T_g should be higher for the lower cooling rate, as seen in this study (see Figure 6.7), and reported also in the literature [52]. The polymer had more time to cool down from the liquid state and thus to decrease the amount of free volume trapped inside the polymeric matrix. Since the T_g corresponds to the temperature at which the polymer chains can move globally, a lower free volume content should imply a higher T_g, as predicted from the free volume theory. Fox and Flory [53, 54] postulate that T_g corresponds to a critical free volume below which not enough room is available for molecular conformational changes. Although this model has been shown not to be verified under isochoric conditions, it is still valid under isobaric conditions [55]. Similarly, it is well-established for instance that when a polymer is cooled under pressure, the higher the applied pressure, the higher is the density, thus the lower is the amount of free volume in the material, and the higher is the T_g [55, 56-58]. Finally, if one has some doubts about the free volume theory of the glass transition

temperature, the results obtained by heating the polymer may also suggest that the polymer cooled slower aged faster. Indeed since the glassy state is a non-equilibrium state, aging takes place during the DMTA measurement. This point will be commented further in Chapter 7.

It is well-established that the behavior of samples is different in heating and in cooling. An hysteresis is observed in volume relaxation measurements for instance [59]. The discrepancies between T_g values obtained by heating and by cooling the polymer has several consequences. In the frame of this research, one of them is that results showing some trends between the T_g and gas transport should be looked at with scrutiny since the T_g is usually determined by heating the polymer. In publications based on literature databases this is even more critical since some researchers may determine the T_g on heating, and others on cooling.

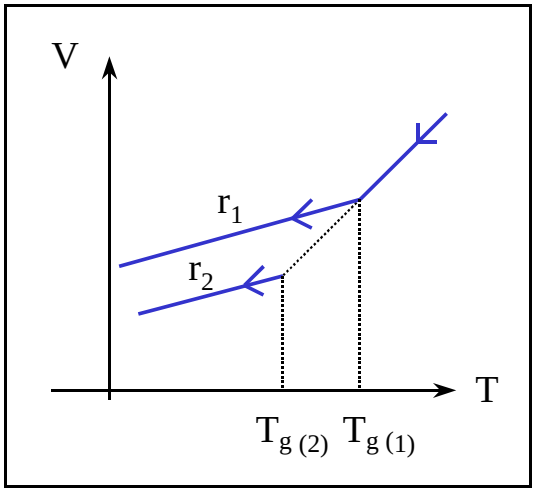

Figure 6.8: Typical schematic showing the influence of the rate of cooling r on the value of the T_g ($r_1>r_2$). The results are obtained by cooling the polymer from the rubbery to the glassy state. The T_g appears to be lower for the lower cooling rate.

The loss modulus E" traces were normalized to read unity at T_g, as illustrated in Figure 6.9. The traces were normalized in order to correct for the geometry factor. In addition, if a particular polymer sample is run at three different frequencies in the DMTA apparatus, as what as been done for instance in Chapter 5 to determine the activation energy for frequency, the magnitude of the E" peak is modified for each frequency. The higher the frequency, the greater is the shift to higher temperatures, and the lower is the

magnitude of E" (see Chapter 5). Nevertheless, the density remains constant from one DMTA trace to another since only one sample is tested to generate those data. If one normalizes the three E" traces to read unity at T_g, the same breadth is observed in the glass transition range for a chosen value of E". This breadth can be characteristic of a given free volume amount and distribution.

The breadth of the normalized loss modulus peak was determined for several values of the loss modulus, and for the different cooling rates selected in this research. The results are given in Figure 6.10. As obvious from the figure, as the cooling rate decreased, the breadth of the loss modulus decreased. This observation is in agreement with the literature [60]. As suggested by Matsuoka [61], a decrease in the breadth of the loss modulus peak may be attributed to a narrowing of the distribution of relaxation times. This decrease corresponds to a lower degree of intermolecular cooperative motion, or to a lower coupling. A large loss modulus peak breadth may correspond to a broader distribution of free volume sizes. A study by Takahara, Saito, and Inoue [62] pointed out a relationship between the width of the glass transition temperature and the degree of density fluctuations. The value of T_g was determined by oscillating-DSC and the density fluctuations by light scattering. Although the study focused on PMMA and physical aging, it was reported that the width of the T_g increased when the density fluctuations increased. The width of the T_g in DSC experiments is likely to correspond to the breadth of the T_g peak in DMTA traces. Therefore, the greater the cooling rate, the greater is the breadth of the E" peak, and possibly the greater is the size distribution of free volume.

Similarly, the value of the normalized E" was determined at different temperatures, and for the different cooling rates. As seen in Figure 6.11, the value of the normalized loss modulus decreased with temperature, and the decrease occurred faster for the lower cooling rate. Results obtained right below and right above the glass transition temperature were not identical, as shown in Figure 6.12. This came from the fact that the loss modulus peak was not symmetrical. The value of E" decreased faster above than below T_g. Moreover, the difference between the cooling rate curves seemed to disappear above T_g, probably due to the fact that the polymer had reached conformational equilibrium.

The DMTA curves were too noisy at about room temperature to distinguish any forms of local motions at that particular temperature. The β-transition (at about –100°C) was not characterized either.

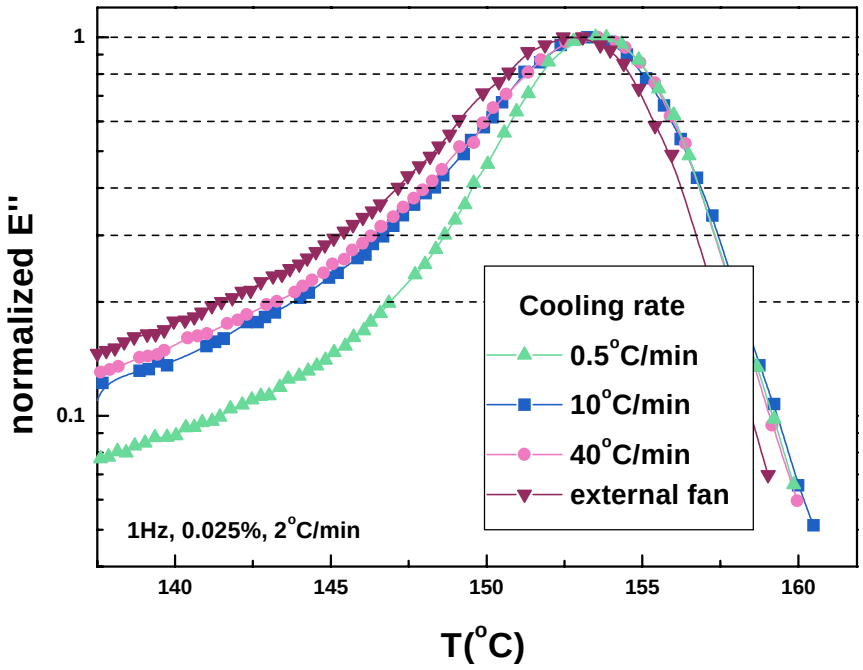

Figure 6.9: Normalized loss modulus E" traces. The traces of Figure 6.6 were normalized to read unity at T_g (see Figure 6.6 for experimental details). The dotted lines correspond to various values of the loss modulus.

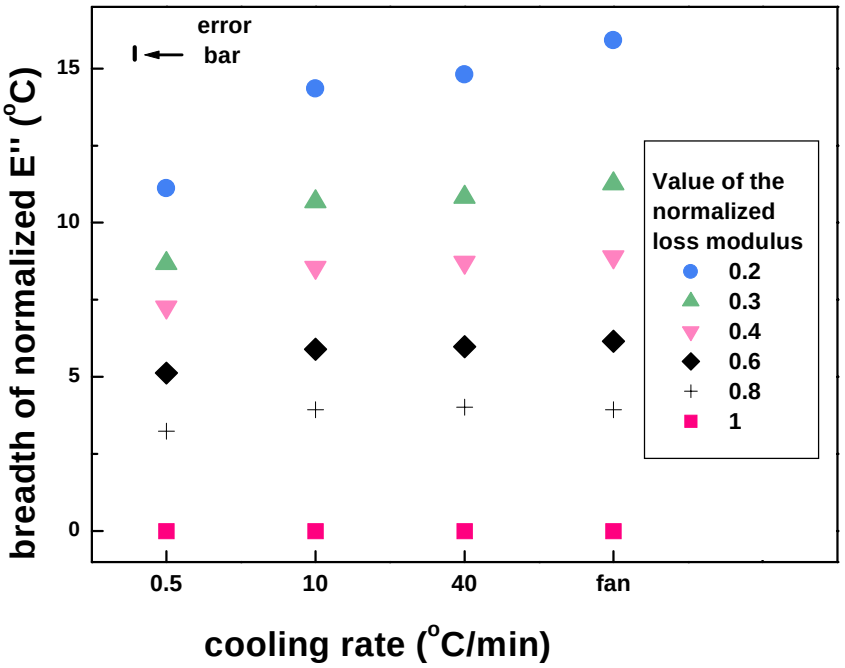

Figure 6.10: Breadth of the normalized loss modulus peak in °C as a function of the cooling rate for different values of E" (note that the x-axis is not a continuous axis). See Figure 6.6 for experimental details.

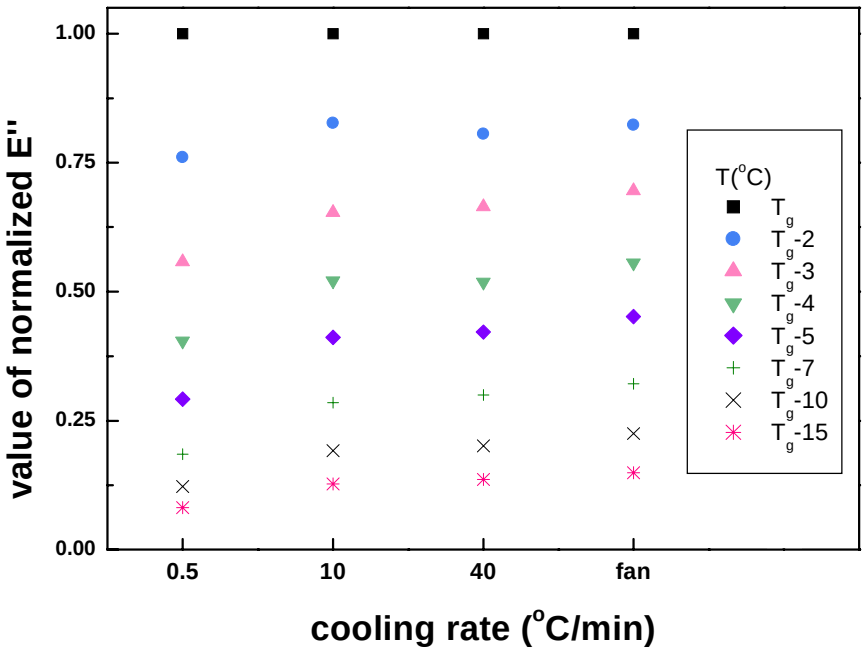

Figure 6.11: Value of the normalized loss modulus as a function of the cooling rate for different temperatures at or below T_g (note that the x-axis is not a continuous axis). The error on the reading was negligible. The T_g's of the samples cooled at 0.5°C/min, 10°C/min, 40°C/min, and by the external fan were taken as 153.57°C, 153.41°C, 153.32°C, and 152.79°C, respectively.

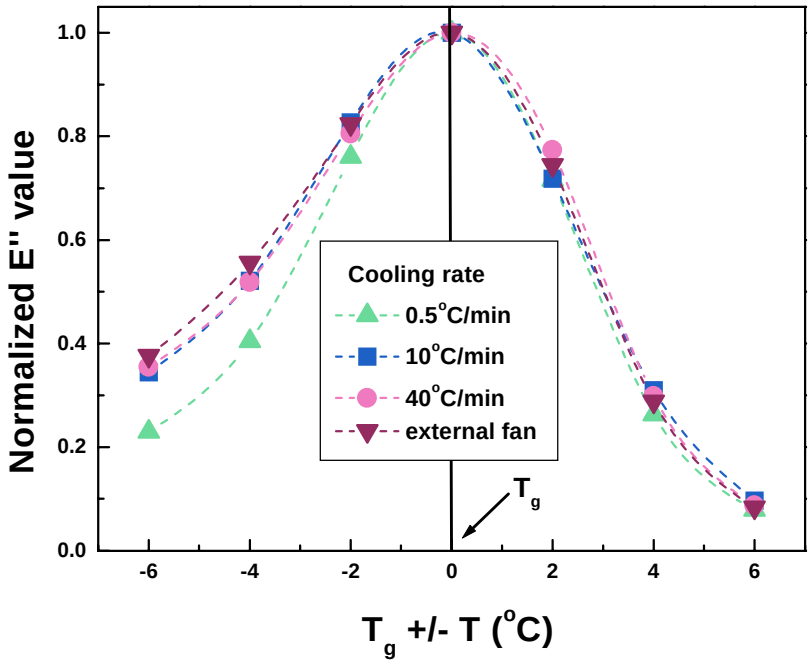

Figure 6.12: Normalized E" as a function of $T_g \pm T$ (°C) for different cooling rates showing the asymmetry of the loss modulus peak (see Figure 6.6 for experimental details).

6.3.3. Density / DMTA results

The T_g obtained on heating the polymer from the glassy to the rubbery state was plotted as a function of the density to determine whether or not there was a linear relationship between those two properties. Recall, the value of the T_g may be explained from free volume concepts (see above). As seen in Figure 6.13, the T_g and the density are not linearly related. Since the density is expected to be related to the amount of free volume contained in the polymeric matrix, the value of the T_g should be explained differently. Inconsistencies in the behaviors of the T_g and the density have been reported in the literature for oriented samples [63, 64]. More details will be given in Chapter 8.

The T_g value may take into account the distribution of free volume as well, as suggested by Song and Roe [65]. Actually, the idea of an iso-free volume T_g has been shown to be inconsistent with isochoric results [55]. The behavior of polycarbonate under both isobaric (constant pressure) and isochoric (constant volume) conditions was examined by Colucci, McKenna, and co-workers [55]. Please note that measurements were taken from the rubbery state to the glassy state, and that the rate of cooling was the

same in both types of experiments. A glass transition temperature was shown to exist under both sets of conditions. Indeed, a change in the slope of either the volume or the pressure versus temperature was observed, this change in slope being more pronounced in the isobaric case. After appropriate adjustment, it was shown that the T_g values were the same in both the isobaric and isochoric conditions, as well as the rubbery responses, but the glassy responses were different. The Fox and Flory theory [53, 54] postulating the existence of an iso-free volume T_g was finally investigated by the researchers. An iso-free volume T_g means that the amount of free volume is constant at T_g, independently of the pressure (for isobaric conditions) or the volume (for isochoric conditions). T_g corresponds to a critical free volume below which not enough room is available for molecular conformational changes. The free volume V_f was observed to be constant as a function of temperature below T_g and then to increase with temperature in both cases. Nevertheless, in the case of isobaric experiments, V_f was not found to have the same values below T_g for each volumes, thus contradicting the idea of an iso-free volume T_g. The Prigogine Defay ratio has also been observed to differ from unity in several cases [55, 65].

The definition of the glass transition temperature T_g remains still ambiguous nowadays. Three major theories can be found in the literature to define this T_g : the free volume theory, the thermodynamic theory, and the kinetic theories [66]. However none of them really stands apart and a full understanding of the T_g remains still an area of active research.

Reporting a single value for T_g may not be sufficient. Indeed, the T_g may be better defined by a range (from xx^{o}C to xx^{o}C). This range should however be different while using different techniques. The transition zone is sometimes only 30^{o}C by DSC, and about 100^{o}C by DMTA [67]. The transition range is usually wider for DMTA. Values obtained for T_g by DSC and DMTA are also different since the principles on which the techniques are based are different. DSC measures the change in heat capacity whereas DMTA measures the transition associated with cooperative chain motion. Similarly, T_g values obtained by the dielectric and the DMTA methods differ since those methods do probe a different length scale, although they both measure the relaxation mechanism (dielectric: monomer unit, DMTA: 5 to 10 repeat units) [68].

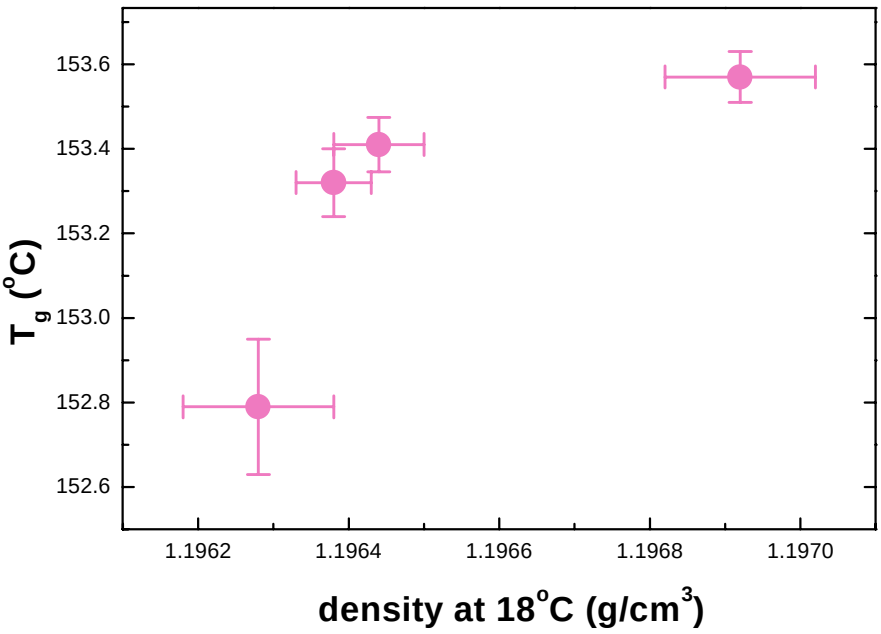

Figure 6.13: Glass transition temperature T_g versus density. The T_g was obtained from DMTA measurements. The density was determined at 18°C using a linear density gradient column.

Published data seem to suggest that the breadth of the DMTA peak may be related to the distribution of free volume [62]. Instead, it has been found in this study that the breadth of the loss modulus E" DMTA peak is directly correlated with the density, as seen in Figure 6.14. Only one linear regression is shown in Figure 6.14 for clarity, but the same behavior was observed for all the E" values. Obviously, since the density and the T_g are not linearly correlated, neither are the E" breadth and the T_g (see Figure 6.15). Therefore it appears from this study that the breadth of the E" peak is directly correlated with the density, and thus with the amount of free volume.

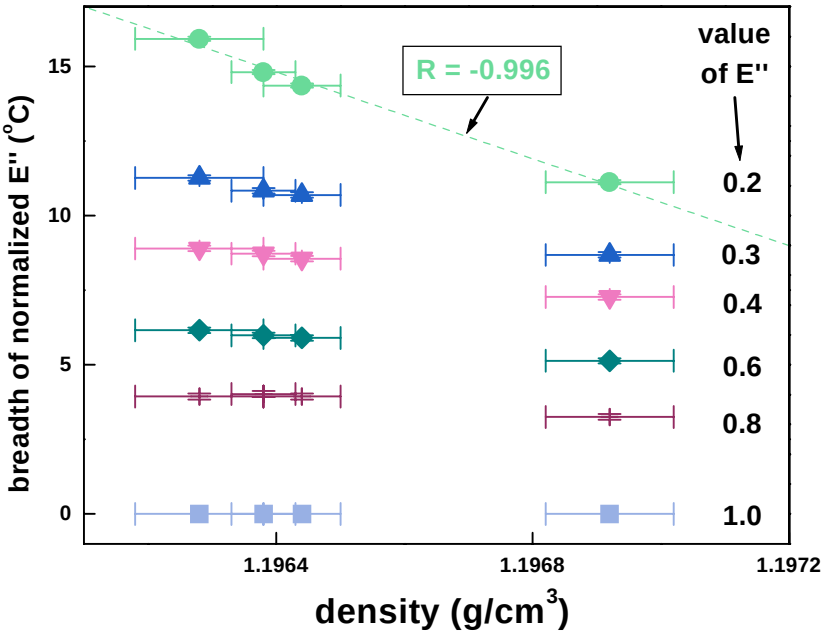

Figure 6.14: Breadth of the E" peak as a function of density for various E" values. The DMTA traces were normalized to read unity at T_g (see previous figures for details). The densities were measured at 18°C using a linear density gradient column. The breadth was observed to be directly related to the density. Only one linear regression is shown on the figure for clarity, but the same behaviors were observed for all the E" values.

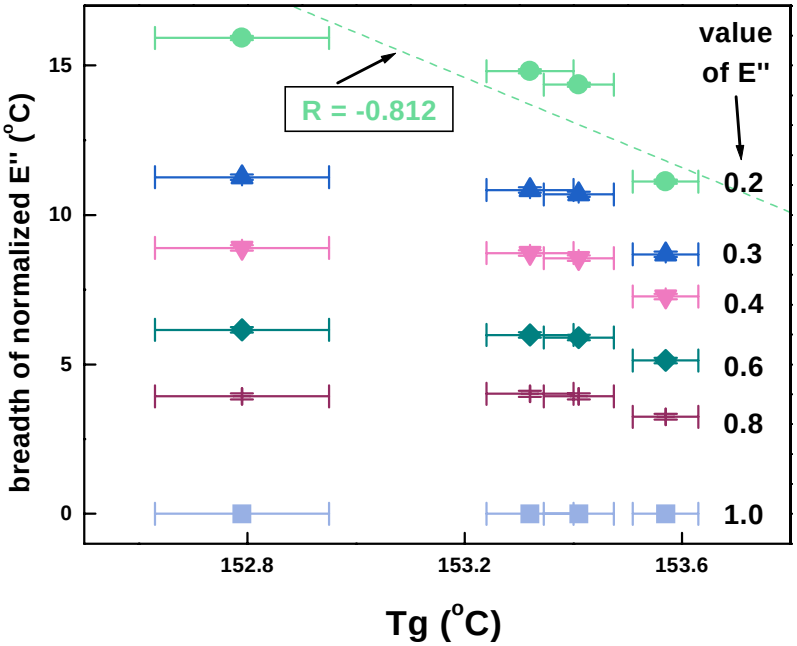

Figure 6.15: Breadth of the E" peak as a function of T_g for various E" values. The DMTA traces were normalized to read unity at T_g (see previous figures for details). The T_g was determined from the maximum of the loss modulus E".

6.3.4. Permeation results

The gas transport parameter and activation energy results are presented in this subsection. The influence of the cooling rate is examined. Applicability of the free volume theory is also investigated based on the experimental data obtained in this study. Finally, the gas transport data are used to estimate the average distances between polymer chains.

6.3.4.1. Determination of the gas transport coefficients (P,D,S)

The gas transport coefficients were determined as a function of the cooling rate. One would expect that if the free volume amount in the material increases, the permeability P will also increase [69, 70]. However, as seen in Figure 6.16, this is not the case for polycarbonate. P remains relatively constant with the cooling rate. The free volume present in polymers is commonly believed to allow molecular motions, to enhance the diffusional jumps, and to increase the permeability [69]. This study points out that the permeability coefficient should not be directly related to the T_g or the overall free volume content, as what is commonly done in the literature [69, 70]. On the other hand, the lower the kinetic diameter of the penetrant gas molecule, the greater is the permeability. The kinetic diameters of He, O_2, and N_2 are reported as 2.6 Å, 3.46 Å, and 3.64 Å, respectively [71-74].

The selectivity α_{AB} (as defined by Eq (6.3)) between two gases A and B remains therefore constant with the cooling rate. Please note that in this research the applied pressure was lower for He compared to O_2 and N_2 because of the rapidity of the He permeation. However studies in the literature have demonstrated that P in polycarbonate is independent of pressure, at least up to 10 atm [75]. Therefore the selectivity is not expected to change much at a lower He applied pressure.

$$\alpha_{AB} = \left(\frac{P_A}{P_B} \right) \qquad \text{Eq (6.3)}$$

The main objective of the membrane community is to create new materials having a high permselectivity. Unfortunately, an increase in permeability is generally accompanied by a decrease in selectivity. This ultimate property is expected to be reached by creating materials with a narrow free volume distribution. The average free volume size should be lower than the size of the undesirable gas molecule [76]. Regions of high free volume are believed to decrease the selectivity. The experimental data obtained in this study suggest that the amount of free volume may not be a critical parameter to look at in order to achieve a high permselectivity. The free volume distribution may instead be the parameter to control.

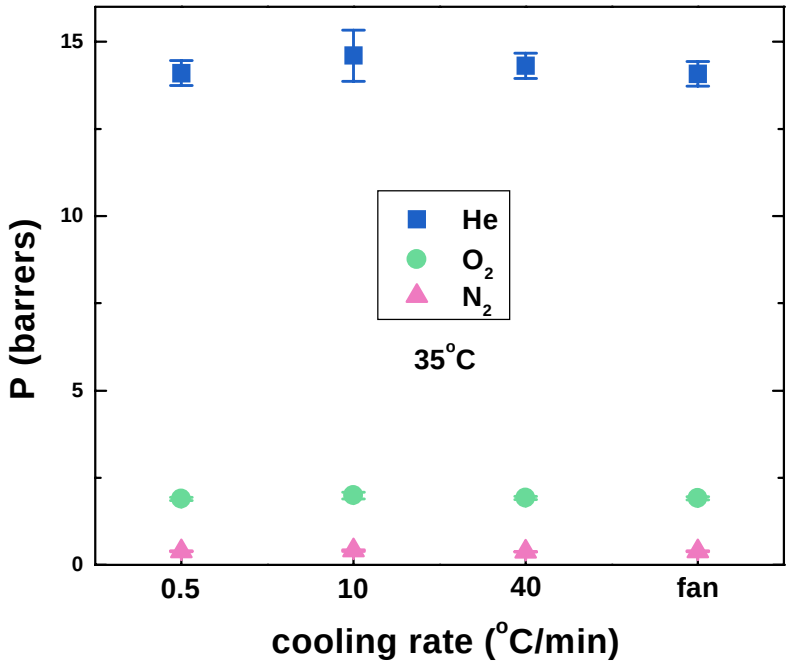

Figure 6.16: Permeability coefficient P for He, O_2, and N_2 as a function of the cooling rate (note that the x-axis is not a continuous axis). The permeation experiments were performed at 35°C. The applied pressures were fixed at about 2.5atm for He, and 3.9atm for O_2 and N_2.

The effects of the cooling rate on D and S were evaluated. The analysis was not possible for helium due to the short time lag (and thus large error) observed for that particular gas. The experimental results are shown in Figure 6.17 and Figure 6.18.

Although P remained unchanged with an increase in the cooling rate (see Figure 6.16), D and S appear to be significantly affected by the cooling rate, especially for the greater kinetic diameter gas molecule (see Figure 6.18). However the trends seen for D and S are inversely related. The greater the cooling rate, the greater is the solubility coefficient S, and the lower is the diffusion coefficient D. The error bars for each gas reflect the accuracy between three successive gas transport measurements on the same membrane, and another measurement on another membrane in addition. They are therefore not underestimated. The changes seen for N_2 were reproducible and significant.

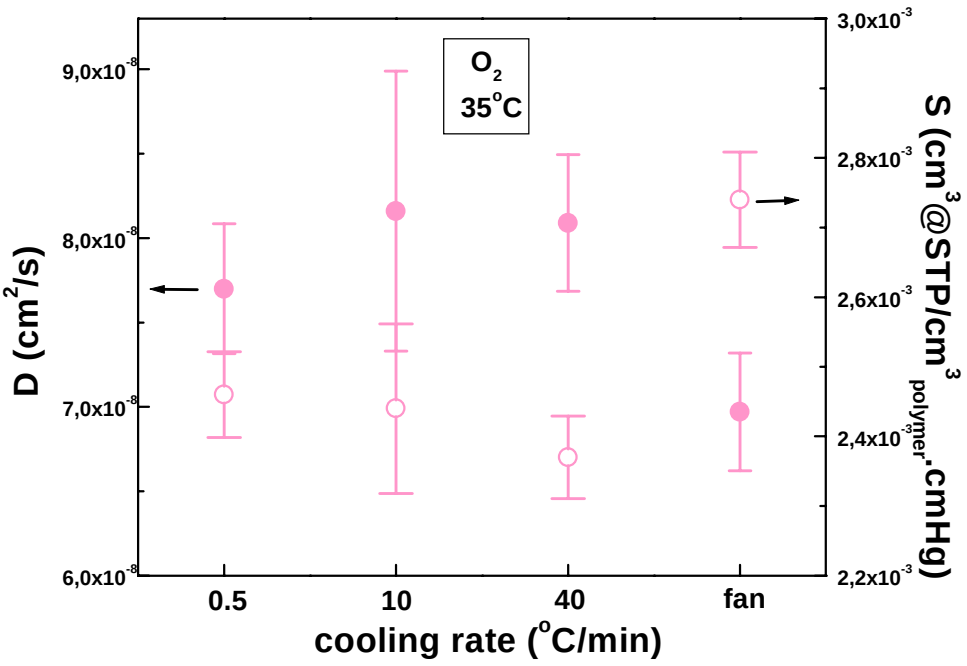

Figure 6.17: Diffusion coefficient D and solubility coefficient S for O_2 as a function of the cooling rate (note that the x-axis is not a continuous axis). The permeation experiments were performed at 35°C. The applied pressure was fixed at about 3.9atm for O_2.

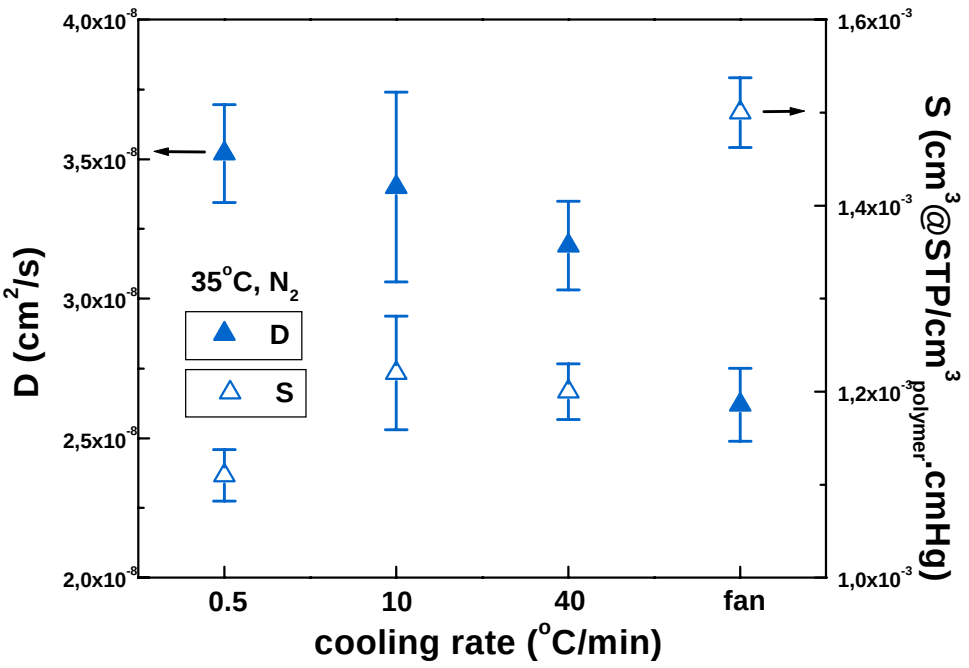

Figure 6.18: Diffusion coefficient D and solubility coefficient S for N_2 as a function of the cooling rate (note that the x-axis is not a continuous axis). The permeation experiments were performed at 35°C. The applied pressure was fixed at about 3.9atm for N_2.

On one hand, the solubility coefficient S relates to the amount of free volume present in the material. If a particular polymeric material increases its overall free volume content, S should show a greater value for a given penetrant since the material can sorb more gas molecules. This fact is observed in Figure 6.18. The faster the cooling rate, and thus the greater the amount of free volume trapped inside the polymeric matrix, the greater is the solubility.

In this study, S appears to be greater for O_2 than for N_2. The free volume contained in the polymeric matrix and accessible for sorption decreases with the kinetic diameter of the gas molecule [77]. However the degree to which the penetrant interacts with the polymeric matrix plays also an important role for sorption. The greater the interactions between the gas and the polymer, the more soluble the gas into the polymer. In addition, usually S increases with the permeant size because of the increase in boiling points. Nevertheless, the solubility coefficient of O_2 in polycarbonate is greater than that of N_2 despite of the lower kinetic diameter. Our results are in agreement with the literature [75].

On the other hand, D surprisingly decreases with the cooling rate. As expected though, the smaller the kinetic diameter of the gas molecule, the greater is the value of D since a small molecule should be able to go through a polymer more rapidly. The decrease in D with an increase in the free volume content cannot be justified employing free volume arguments.

It is first of all important to understand how small molecule diffusion eventually occurs in polymer glasses. Gases diffuse from one polymer cavity to an adjacent one by activated jumps (see Figure 6.19). Since polymer chains move constantly due to thermal motions, a temporary channel can open for a short period of time (of about a few hundred picoseconds [78]) and allow a gas molecule to go to a nearby cavity through this large enough transient gap. In this new cavity, the gas molecule will have to wait for another opportunity to jump to the next cavity, etc. Some researchers visualize this as cages formed by four polymer chains [30]. Obviously, at low permeation temperatures the gas molecule stays longer in a cavity since the polymer does not have enough thermal energy for rapid molecular motions and thus to create large enough gaps in the polymeric matrix rapidly. The diffusional process of small molecules through glassy polymers should involve only a few local polymeric segments, or a low level of cooperativity. The total amount of free volume present in the polymeric matrix may not be a critical parameter. Diffusive jumps should be dependent on the nature and/or composition of the polymer, its molecular weight and molecular weight distribution, its topology and morphology, the penetrant size, and the interactions between the polymer and the penetrant. Moreover, the distribution, possibly the shape of the free volume, as well as the dynamics of the polymer chains may also affect the diffusional jumps.

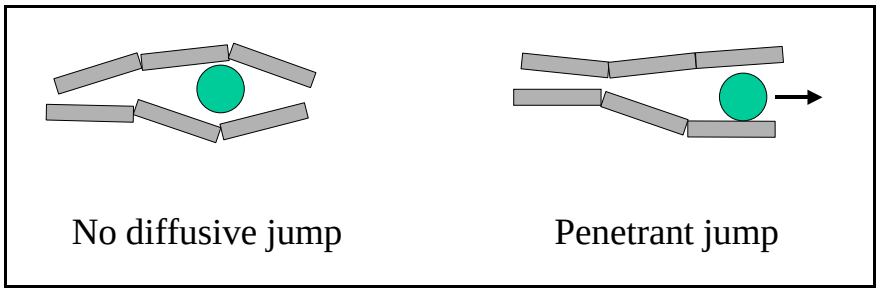

Figure 6.19: Schematic of the diffusion activated jumps.

Motions can be classified into several types depending on their scale: they can either be local motions, segmental motions, or even reptation. The mobility depends also obviously on temperature. The greater the temperature, the greater the length of the movable portion of the polymer chain. Because of those molecular motions the conformation of the polymer chain is capable of changing with time. And all types of motions should contribute to the relaxation process.

Kovacs and co-workers [42] and Tool [79] have shown that a distribution of relaxation times must exist in polymers, and that each particular relaxation time actually constitutes a unique parameter for the glass transition phenomena. Since the polymer chains are characterized by many modes of molecular motions, a distribution of relaxation times is necessary. If a polymeric sample is cooled slowly, the fast processes with short relaxation times are fully relaxed. The relaxation time distribution spectrum is truncated [42, 43], as shown in Figure 6.20.

A paper by Araki et al [60] reported the dynamic mechanical behavior of polycarbonate samples with different thermal histories. It was shown that a sample cooled slowly from 260^{o}C to room temperature at a cooling rate of 0.7^{o}C/min presented a different loss modulus E" curve than a sample directly quenched to room temperature. Indeed, the values of E" and tan δ were much higher for the sample quenched while measured as a function of temperature. The curves of the quenched and the slowly cooled samples merged at around T_g though. This suggested to Araki and co-workers that the sample that has been quenched possessed a larger amount of unrelaxed segments. Those segments subsequently relaxed during the DMTA measurement. Please note that the samples were less than 0.1mm thick and hence a skin-core distribution can be assumed as negligible. The above conclusions tend to confirm the fact that local or segmental parts are more relaxed in a slowly cooled sample.

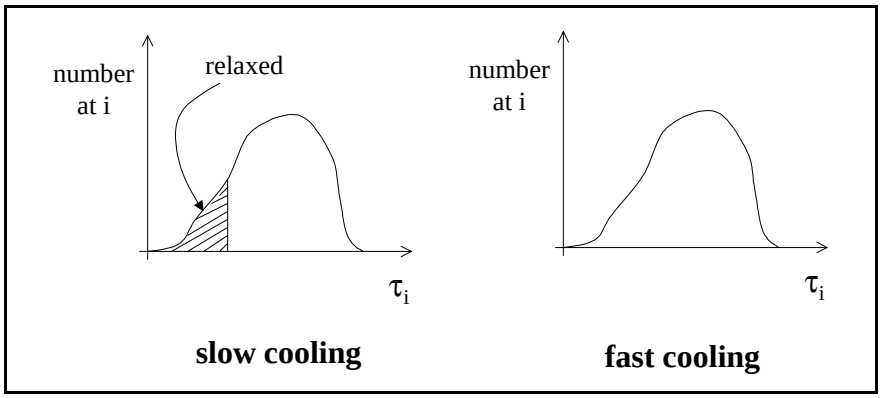

Figure 6.20: Schematic of the relaxation time distribution.

Now the question is, how can those relaxed short relaxation times affect gas transport at room temperature? Recall, the diffusion coefficient has been found to be greater in the sample cooled slowly despite of the lower free volume amount. This suggests that the mobility at the local level is greater for the sample cooled slowly. This remark is obviously in disagreement with the free volume theory [80].

Each relaxation time corresponds to a particular mode of molecular motion. It has also been suggested in the literature that short relaxation times are associated with a small amount of excess free volume [48]. The short relaxation times or fast processes should be the factors controlling the diffusion of gases through polymers since the dynamics should affect only a few segments of the polymer chain and not the whole chain. Cooperative conformational changes are not believed to play a major role in the gas transport process since cooperativity affects a larger scale than that involved in gas transport. Localized molecular motions are assumed to have much shorter relaxation times than the larger scale slower motions. Fast processes may involve only a local portion of the chain whereas slow processes may take into account the whole chain.

As explained above the spectrum of relaxation times is affected by the cooling rate, and so are the internal degrees of freedom. Each macromolecule is characterized by numerous internal degrees of freedom (actually equal to three times the number of atoms). The degrees of freedom can be of two kinds [81]. On one side those that allow limited movements through changes in valence angles and bond lengths (molecular vibrations in the infrared region). And on the other side those that allow rotations of the bonds and are capable of going through the different conformational states. This last type

is the only one of concern here. As a polymer is cooled slowly from the liquid state, the segments may be able to reach their equilibrium conformation, and therefore loose some degrees of freedom. In this case the equilibrium conformation would be the trans-trans conformation. It is well-established for instance that on slow cooling certain polymers (isotactic mainly) can form crystals. The chains adopt a trans-trans conformation.

In amorphous polycarbonate one can find two main conformations: the trans-trans and the trans-cis conformations. The molecule should be in either one of those conformational states most of the time, and vibrate around the energy minimum. Of course, intermediate conformations can also be found in polycarbonate. It has been shown for instance that with sub-T_g annealing (the annealing temperature being in the vicinity of T_g) the population of trans-trans conformers increases whereas that of trans-cis conformers decreases [82, 83]. Nevertheless, aging at room temperature does not show such conformational rearrangements but rather a narrowing of the distribution of conformations around the trans-cis and the trans-trans conformations, hence by extremely local rearrangements around the local minima [83]. Closer local packing of the polymer chains occurs in the trans-trans conformation. Some local parallel alignment of neighboring chain segments may also take place, although this idea is still controversial. The trans-trans conformation is also known to be more stable. As the temperature increases however the trans-cis conformations become favored [82, 84].

If the above remarks are applied to our experimental results, this would mean that the sample that has been cooled slowly may contain more trans-trans conformations, as the polymer has more time to reach the low energy conformation. However, how can this closer local packing enhance the diffusion process?

Not only the static but also the dynamics of the polymer chains is an important factor in the gas transport process. The dynamics may actually be important in explaining even the glass transition, as suggested by Angell [85]. Nevertheless, some caution about this have been given elsewhere [86]. Segmental motions are necessary in order to allow the gas molecules to jump from cavities to cavities. The amount of cavities as well as the ease with which a gas molecule jumps from one cavity to another is an important factor. The vibrations or fluctuations allow a local rearrangement of the conformations, which may facilitate the gas transport phenomenon. The thermal energy is dissipated with time

as the molecules change their conformations. Computer simulations provide information on the evolution of the molecular conformations with time on a length scale of a few bonds [87]. The lifetime of the channels facilitating the jumping process from one cavity to another has been shown from computer simulation studies to have an effect on the value of the diffusion coefficient [88]. The longer the channel lifetime, the greater is the tendency of the molecule to go back to the previous cavity through this channel instead of jumping to the next cavity separated by a higher energy barrier, hence slowing down the diffusion process. Less activated energy is believed to be necessary for a molecule to move along the chain [89]. Nevertheless the molecules have to jump across chains as well due to entanglements.

Our experimental results suggest that a gas molecule goes faster through a polymer possessing a greater amount of trans-trans conformations. The fluctuations or redistributions of the polymer glass caused by thermal motions may be greater in that case. The polymer chains may be capable of fluctuating more around the lowest energy state position, the trans-trans conformation, despite of the lower overall free volume, hence facilitating the gas diffusion process. We postulate therefore that the dynamics of the polymer chains are more rapid in the trans-trans conformation.

A recent publication reporting molecular modeling in polypropylene has shown the influence of the dynamic conformation [90]. When the polymer torsional degrees of freedom are allowed to exist during the event, this affects significantly the energy barriers. On one hand the energy selectivity of O_2 and N_2 is reduced by four orders of magnitude as the polymer is allowed to have different degrees of freedom, or to change its conformations during the timescale of the calculations. On the other hand the entropic selectivity remains rather unchanged. The ratio of the diffusion coefficients of A and B (A and B being the components of a gas mixture) can be calculated from transition state theory to correspond to:

$$\frac{D_A}{D_B} = \exp\left(\frac{\Delta S_{A,B}}{k}\right) \exp\left(\frac{-\Delta U_{A,B}}{kT}\right) \qquad \text{Eq (6.4)}$$

where k is the Boltzmann constant and $\Delta S_{A,B}$ and $\Delta U_{A,B}$ are the differences in entropy and energy barriers, respectively. The first term corresponds to the entropic selectivity and the second term to the energetic selectivity.

As a gas molecule goes through a polymer, the polymer chains have to rearrange themselves because of the presence of the gas molecule in their surroundings. This implies that the structure should go through various conformations, or more precisely that the polymer will have different degrees of freedom, which will affect the diffusion process in return. Our diffusion data suggest that the polycarbonate sample cooled slowly possesses more segmental mobility. This should be reflected by a lower activation energy for diffusion.

As a conclusion, we can only make hypothesis about the explanation of the diffusion data. Gas transport through glassy polycarbonate may be controlled by several parameters which are:

- the free volume content
- the distribution of free volume
- the dynamics of the free volume
- the interactions between the gas and the polymer
- the conformations of the chains
- the chemical structure
- the intra- and the intermolecular distances.

To our knowledge no paradox between the cooling rate and the free volume content has been reported for isotropic samples by mechanical measurements such as creep and stress relaxation. For instance, the average stress relaxation of polycarbonate has been determined to increase with decreasing the cooling rate at 135^{o}C [91]. The effect of the cooling rate was therefore similar to that of the aging time, and the cooling rate was considered to be an aging process with continuous changes in temperature. Mechanical tests are believed to be more related to the segmental motions of the materials and therefore could be possibly linked with gas transport measurements. However the interaction of a stress and a strain with the aging process may also affect the data. It has been determined that the required free volume size for stress relaxation in polycarbonate is larger than that required for gas diffusion [92]. Such a scale difference may explain why more mobility appears to take place in slowly cooled samples despite of

the lower free volume content by gas transport measurements and not in mechanical tests. Cavities of given sizes may be needed for stress relaxation to take place.

The change in percent of the gas transport coefficients has been plotted as a function of the cooling rate for a specific gas. The plots are shown from Figure 6.21 to Figure 6.23. The trends are clearly significant for N_2. The permeability coefficient appears to remain constant within the experimental errors, whereas the diffusion coefficient decreases and the solubility coefficient increases with the cooling rate.

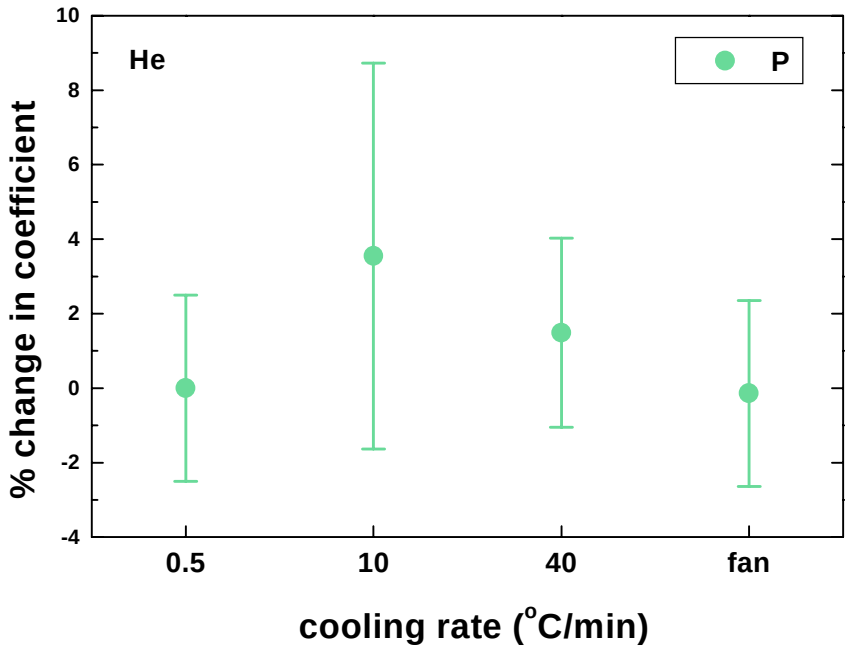

Figure 6.21: % change in permeability coefficient for He (note that the x-axis is not a continuous axis). The data obtained for a cooling rate of 0.5°C/min were taken for reference. A positive percent change corresponds to an increase in the coefficient, a negative one to a decrease.

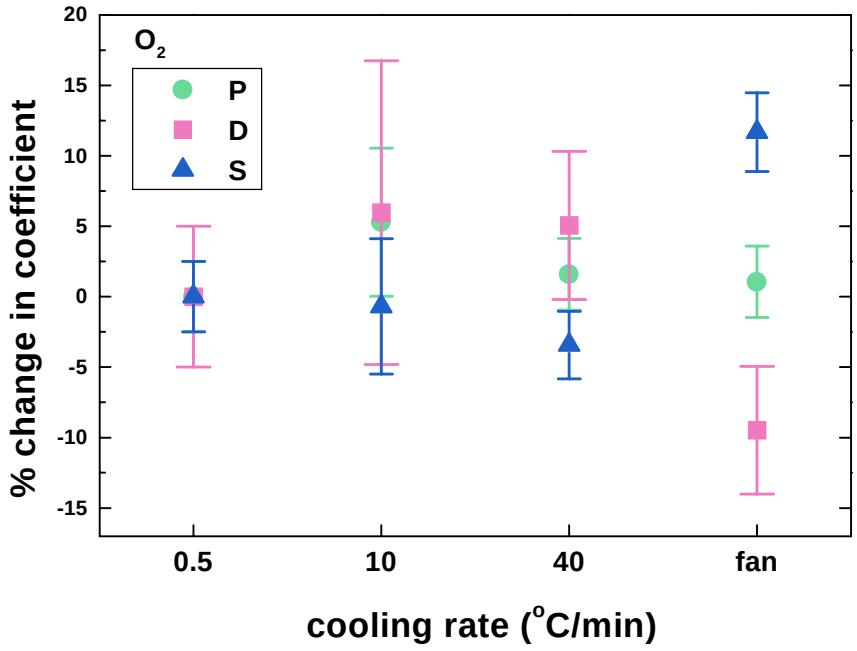

Figure 6.22: % change in permeability, diffusion, and solubility coefficients for O_2 (note that the x-axis is not a continuous axis). The data obtained for a cooling rate of 0.5°C/min were taken for reference. A positive percent change corresponds to an increase in the coefficient, a negative one to a decrease.

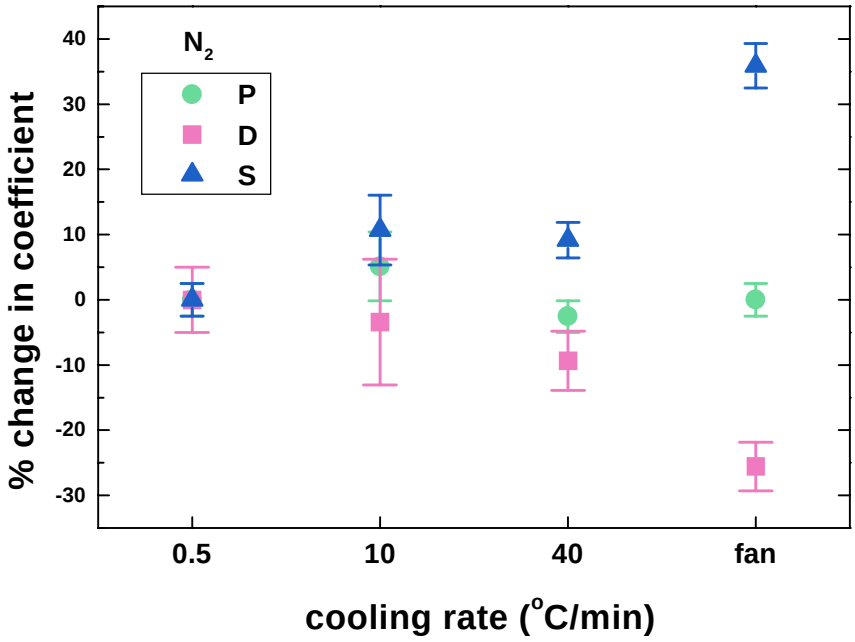

Figure 6.23: % change in permeability, diffusion, and solubility coefficients for N_2 (note that the x-axis is not a continuous axis). The data obtained for a cooling rate of 0.5°C/min were taken for reference. A positive percent change corresponds to an increase in the coefficient, a negative one to a decrease.

The complete permeation data are recapitulated in Table 6.1 through Table 6.3 . The permselectivities appear to remain constant with a change in the cooling rate, as mentioned previously. The diffusion selectivity between O_2 and N_2 increases with the cooling rate. In contrast, the solubility selectivity decreases with the cooling rate. As a polymer is cooled faster, it possesses a greater overall free volume amount, as well as probably bigger cavities. Therefore it becomes more difficult to separate gas molecules based on their sizes, at least based on sorption effects. The fact that the diffusion selectivity is higher in the high content free volume material may be a result of the differences in the local chain dynamics.

The value of the permeability coefficient P in polycarbonate is in agreement with the literature, as seen in Table 6.4. The value of the applied pressure in this work is not always the same as in the literature, however Costello and Koros [75] observed that P in polycarbonate was almost independent of the applied pressure, at least up to 10 atm. Again, the values of S and D are consistent with the literature for polycarbonate, as seen in Table 6.5.

cooling rate	P_{He} (barrer)	P_{O2} (barrer)	P_{N2} (barrer)	P_{He} / P_{O2}	P_{He} / P_{N2}	P_{O2} / P_{N2}
0.5°C/min	14.1 (+/-) 0.35	1.89 (+/-) 0.05	0.39 (+/-) 0.01	7.5	36.2	4.8
10°C/min	14.6 (+/-) 0.73	1.99 (+/-) 0.10	0.41 (+/-) 0.02	7.3	35.6	4.9
40°C/min	14.31 (+/-) 0.36	1.92 (+/-) 0.05	0.38 (+/-) 0.01	7.5	37.7	5.1
fan	14.08 (+/-) 0.35	1.91 (+/-) 0.05	0.39 (+/-) 0.01	7.4	36.1	4.9

Table 6.1: Permeability coefficients at 35°C. The applied pressures were 2.5atm for He, and 3.9atm for O_2 and N_2.

cooling rate	D_{O2} (cm^2/s)	D_{N2} (cm^2/s)	D_{O2} / D_{N2}
0.5°C/min	7.70E-08 (+/-) 3.85E-09	3.52E-08 (+/-) 1.76E-09	2.2
10°C/min	8.16E-08 (+/-) 8.30E-09	3.40E-08 (+/-) 3.40E-09	2.4
40°C/min	8.09E-08 (+/-) 4.05E-09	3.19E-08 (+/-) 1.60E-09	2.5
fan	6.97E-08 (+/-) 3.49E-09	2.62E-08 (+/-) 1.31E-09	2.7

Table 6.2: Diffusion coefficients at 35°C. The applied pressures were 2.5atm for He, and 3.9atm for O_2 and N_2.

cooling rate	S_{O2} (cm^3@STP/cm^3.cmHg)			S_{N2} (cm^3@STP/cm^3.cmHg)			S_{O2} / S_{N2}
0.5°C/min	2.9E-03	(+/-)	7.3E-05	1.3E-03	(+/-)	3.3E-05	2.2
10°C/min	2.9E-03	(+/-)	1.4E-04	1.5E-03	(+/-)	7.0E-05	2.0
40°C/min	2.8E-03	(+/-)	7.0E-05	1.4E-03	(+/-)	3.6E-05	2.0
fan	3.3E-03	(+/-)	8.1E-05	1.8E-03	(+/-)	4.5E-05	1.8

Table 6.3: Solubility coefficients at 35°C. The applied pressures were 2.5atm for He, and 3.9atm for O_2 and N_2.

P_{He}	P_{O2}	P_{N2}	reference	conditions
14.31	1.92	0.38	this work	35°C, 2.5atm for He, 3.9atm for O_2 and N_2
11	2	0.3	75	35°C, 5atm
13	1.6	0.36	95	35°C, 2atm
15	1.48	0.29	124	35°C
14.5		0.28	74	35°C, 2atm

Table 6.4: Comparison of the results of the present work with those reported in the literature. The results obtained at a cooling rate of 40°C/min in this work are reported in the table. Permeability coefficients are given in barrer.

D_{O2}	D_{N2}	S_{O2}	S_{N2}	reference	conditions
8.09E-08	3.19E-08	2.8E-03	1.4E-03	this work	35°C, 2.5atm for He, 3.9atm for O_2 and N_2
		2.60E-03	1.60E-03	75	35°C
5.80E-08		2.80E-08		71	
7.90E-08		2.80E-03		95	35°C, 2atm
4.11E-08	1.59E-08			105	data listed in a database
5.10E-08	1.64E-08			125	35°C, 1atm

Table 6.5: Comparison of the results of the present work with those reported in the literature. The results obtained at a cooling rate of 40°C/min in this work are reported in the table. Diffusion coefficients are given in (cm^2/s), solubility coefficients in (cm^3@STP/cm^3.cmHg). Please note that solubility coefficients given in the literature were determined from sorption experiments.

6.3.4.2. Fractional free volume (FFV) calculations

The vast majority of the models developed by researchers to explain gas transport in glassy polymers is based on the concept of free volume [29-33]. The fractional free volume (FFV) is defined as follows:

$$FFV = \left(\frac{V_f}{V} \right) = \left(\frac{V - V_o}{V} \right) = 1 - \left(\frac{V_o}{V} \right) = 1 - V_o \, \rho \qquad \text{Eq (6.5)}$$

where V is the polymer specific volume (=1/ρ, where ρ stands for density), V_f is the average hole free volume (=(V-V_o)), and V_o is the specific volume occupied by the polymer molecules. The fractional free volume FFV can thus be estimated from the knowledge of the experimental density and that of the occupied volume.

The most common approach used by the gas transport community to determine the occupied volume V_o is based on Bondi's group contribution method [93]. The polymer repeat unit is separated into chemical groups, and each chemical group i is attributed a given value for the Van der Waals volume V_W. The values of V_{Ws} have been estimated by Bondi for specific chemical groups [93], and reported by Van Krevelen [94]. Multiplying the sum of those V_{Ws} by a universal empirical factor of 1.3 gives an estimate of V_o. The empirical factor has been estimated by Bondi based on the packing densities of molecular crystals at 0K, and the value of 1.3 is assumed to apply to all types of chemical groups. Therefore we have:

$$V_o = 1.3 \sum_{i=1}^{n} (V_W)_i \qquad \text{Eq (6.6)}$$

And from Eq (6.5) we get: $$FFV = 1 - 1.3 \, \rho \left(\sum_{i=1}^{n} (V_W)_i \right) = 1 - 1.3 \rho \, V_W \qquad \text{Eq (6.7)}$$

Please note that the fractional free volume given above is different from the one estimated from viscoelastic measurements in Chapter 5 since the definitions are different in both cases. In Chapter 5, the fractional free volume was determined at T_g, hence the name f_g. The WLF theory (see Chapter 5) assumes that the fractional free volume keeps a constant value below T_g, and is therefore fixed as f_g. Nevertheless, in the equations given above, FFV is allowed to change below T_g since it is based on the density value. The definitions and evaluations of the fractional free volume are indeed the major limitation of free volume theories.

A new evaluation method for glassy polymers with rigid backbones suggested by Park and Paul [69] appears to improve considerably the estimation of the occupied volume. This method is still based on a group contribution method, but now a different

occupied volume is calculated for each penetrant gas. The researchers think that each type of gas molecule may not probe the same occupied volume and therefore a gas-dependent factor may be needed in the calculation of V_o. Using different occupied volumes for each gas means that the free volume a gas can probe will be different for each gas. This fact seems physically acceptable since the same amount of free volume may not be accessible to all the gases [77]. Indeed, a small kinetic diameter molecule should be able to access more cavities in the polymer. However, we believe that the free volume quantity should be characteristic of a polymer only. In the method of Park and Paul the occupied volume is defined as follows:

$$\left(V_o\right)_j = \sum_{i=1}^{n} \gamma_{ij} \left(V_W\right)_i \qquad \text{Eq (6.8)}$$

where i refers to the chemical group and j to the gas of interest. γ_{ij} have been determined by Park and Paul from a database of experimental data and tabulated [69]. The FFV can be calculated for each gas j of interest. We have:

$$FFV = \left(\frac{V - \left(V_o\right)_j}{V} \right) \qquad \text{Eq (6.9)}$$

The two methods outlined above will be applied in this research to determine the fractional free volumes present in the various glassy polycarbonate samples.

The polycarbonate repeat unit was divided into specific chemical groups as shown in Figure 6.24. Four chemical groups were distinguished, one of them being repeated twice. The empirical factors needed to estimate the occupied volume V_o are reported in Table 6.6. It appears from Table 6.6 that the values of γ_{ij} do not differ that much from 1.3 (the universal value of Bondi) for polycarbonate. However they do change greatly for other chemical groups [69]. The occupied volumes V_o (in cm^3/mol_{RU} where the subscript RU stands for repeat unit) were calculated from Eq (6.6) and Eq (6.8). From the knowledge of the molecular weight and the number of repeat units it was possible to obtain V_o in (cm^3/g). We have:

$$V_o(cm^3/g) = V_o(cm^3/mol_{RU}) \times \left(\frac{\text{number of repeat units}}{\text{molecular weight of PC in g/mol}} \right) \qquad \text{Eq (6.10)}$$

The molecular weight of the polycarbonate used in this research was evaluated to be 34,000 g/mol. Since the molecular weight of a polycarbonate repeat unit ($C_{16}H_{14}O_3$) is 254 g/mol, the number of repeat units is about 134 repeat units. Eq (6.10) is actually equivalent to:

$$V_o(cm^3/g) = V_o(cm^3/mol_{RU}) \times \left(\frac{1}{\text{molecular weight of repeat unit in g/mol}} \right) \qquad \text{Eq (6.11)}$$

The above equation is better in the sense that it does not require knowledge of the molecular weight.

The occupied volume results are given in Table 6.7. The value of V_o predicted from Bondi's method was equal to 0.697 cm^3/g. Assuming a density of 1.2 g/cm^3 for polycarbonate, Eq (6.5) leads to a fractional free volume FFV of 16.4%. This value is in excellent agreement with the one calculated by Koros and co-workers [21, 95] for polycarbonate (ρ = 1.2 g/cm^3, FFV = 0.164). Shelby and co-workers [96] calculated FFV to be about 16.84% for polycarbonate (ρ = 1.1982 g/cm^3, T = 23°C). Unfortunately, the intermediate group contribution calculations in these two papers were not reported; only the final result was given. One would expect that the theoretical calculations based on the same theory should predict the same answers. According to our calculations, the value of FFV in the paper of Shelby and co-workers [96] for instance should be equal to 16.49%. A recent paper by Bos et al [4] does report intermediate calculations. For example, V_o (in cm^3/mol) was listed as 177.1, exactly the same as the value determined in the present study (see Table 6.7). A density of 1.209 g/cm^3 corresponded to a FFV of 15.8%, in agreement with our calculations. The molecular weight of the repeat unit was taken as 254.3 g/mol. Pope et al [21] did report the values of the Van der Waals volume and the occupied volume for polycarbonate as well. Their results are consistent with ours. A study by Colucci, McKenna, and co-workers [55] reported an experimental value of the occupied volume of polycarbonate V_o at 0K. V_o was obtained from extrapolating the rubbery PVT surface to the absolute zero. V_o was determined to be 0.6506 ± 0.02 cm^3/g, therefore about 7% lower than the one calculated from the Bondi's method.

But the value of 16.4% for FFV calculated in this research for $\rho = 1.2$ g/cm^3 is not in agreement with the one determined by Jean et al [97] using positron annihilation lifetime spectroscopy (PALS). The researchers mentioned as well that their FFV value (6.23%) was 2.1 smaller than the one calculated by Hellums et al [95] from group contribution methods. The fractional free volume was determined from PALS measurements, given a model treating the holes of the free volume as perfect spheres. The validity of the assumption of spherical holes for bisphenol-A polycarbonate has been shown elsewhere [98]. Jean et al [97] attributed the rather large difference in FFV compared to the work of Hellums et al [95] to the various definitions and assumptions behind the free volume concept. In another paper by Jean et al [99], FFV was estimated from PALS measurements to be around 4.2% for polycarbonate, i.e. more than 30% lower than their other published data for polycarbonate. It seems therefore that FFV determined from PALS is not that reproducible. However what is important to note for our purposes is that there is not a complete equivalence between the FFV calculated from the Bondi's group contribution method and the measurements from PALS. Since the PALS measure can probe a smaller scale than gas molecules (see above), it would be reasonable to expect that FFV would be greater for PALS. However, this is not the case.

The fractional free volume FFV was determined from the two methods detailed previously using Eq (6.7) and Eq (6.9), and by using the experimental densities recorded at 18^{o}C. The results are shown in Figure 6.25 as a function of the cooling rate. The results for each particular method are plotted in Figure 6.26 through Figure 6.29. The fractional free volume increases lightly with the cooling rate, which makes sense, as explained previously. FFV calculated from Bondi's method is greater than the one calculated from the method of Park & Paul. Nevertheless, the method of Park & Paul seems rather suspicious. Indeed, FFV is greater for the gas possessing the greater kinetic diameter. One would think that the free volume accessible to a small size gas molecule should be greater than the one accessible to a big gas molecule [77, 100]. In addition, one has to keep in mind that the evaluation method of Park and Paul was based on a database containing 102 different polymers. The researchers modified the parameters given by Bondi in order to observe better linear regressions between the gas transport parameters and FFV, hence calculating a gas-dependent FFV. We believe however that FFV should

be a fixed quantity characteristic of a given polymer. As a consequence, only the Bondi's method will be kept for further calculations requiring the value of FFV.

Equations have also been provided by research groups to predict the density from group contribution methods. Van Krevelen [94] suggested that:

$$V = \beta \sum_{i=1}^{n} (V_W)_i \qquad \text{Eq (6.12)}$$

with β = 1.55 at 25°C for glassy polymers. Park and Paul [69] proposed that the β parameter (a packing factor) depends on the chemical group.

$$V = \sum_{i=1}^{n} \beta_i (V_W)_i \qquad \text{Eq (6.13)}$$

The β parameter appeared to differ greatly from 1.55 for several chemical groups. Its value is listed in Table 6.6 for the groups of interest in this research work. The calculated and experimental densities were reported to agree really well for the 102 different polymers contained in the database of Park & Paul [69].

The density of polycarbonate was predicted using Eq (6.12) and Eq (6.13), and results are provided in Table 6.7. The density came out as 1.203 g/cm^3 and 1.221 g/cm^3 for the first and second methods, respectively. Therefore, Eq (6.12) seems to predict the density more accurately than Eq (6.13) (the density of polycarbonate is about 1.2 g/cm^3). Although the density prediction method of Park & Paul [69] seems rather accurate for polymer families, the error in the case of polycarbonate is nevertheless equal to 2.1×10^{-2} g/cm^3, assuming a real density of 1.2 g/cm^3. However both equations have serious limitations, especially when a particular polymer is selected. Indeed, the prediction methods are based on the chemical structure of the polymer only. The methods do not take into account the position of the chemical structures in the polymer. Please note that the group contribution methods apply only to polymers for which additivity rules are verified. This means that each group contributes to the same extent to the final property. This is not verified in the case of hydrogen bonding for instance. Moreover, the prediction methods cannot predict changes in density for a same polymer. However, a polymer does change its density with time for instance (this observation will be reported in Chapter 7 dealing with physical aging). As we saw at the beginning of this chapter, the

density is even affected by the cooling rate. The density should be affected by the molecular weight as well, as long as the molecular weight remains at low values. Furthermore, no dependence of the temperature or the pressure on the density is taken into account by the models.

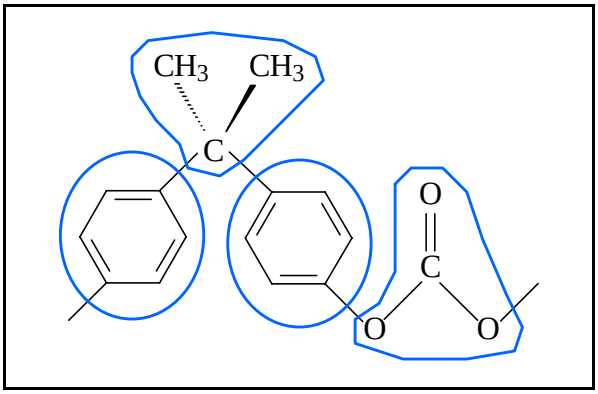

Figure 6.24: Chemical structure of polycarbonate divided into chemical groups.

number in polycarbonate	Group	V_W (cm^3/mol_{RU})	β	γ(He)	γ(O_2)	γ(N_2)
1	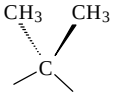	30.7	1.54	1.25	1.30	1.32
2	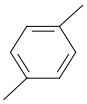	43.3	1.58	1.36	1.28	1.28
1	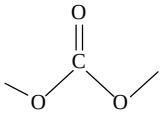	18.9	1.27	1.29	1.52	1.40

Table 6.6: Empirical factors as given by Park and Paul [69]. The Van der Waals volumes V_w were reported from Van Krevelen [94].

	METHOD	
	Bondi	Park & Paul
sum(V_W) (cm^3/mol_{RU})	136.20	
V_o (cm^3/mol_{RU})	177.06	
V_o(He) (cm^3/mol_{RU})		180.53
$V_o(O_2)$ (cm^3/mol_{RU})		179.49
$V_o(N_2)$ (cm^3/mol_{RU})		177.83
V_o (cm^3/g)	0.697	
V_o(He) (cm^3/g)		0.711
$V_o(O_2)$ (cm^3/g)		0.707
$V_o(N_2)$ (cm^3/g)		0.700
$V_{predicted}$ (cm^3/mol_{RU})	211.11	208.11
$\rho_{predicted}$ (g/cm^3)	1.203	1.221

Table 6.7: Group contribution calculations obtained from the two methods selected in this study.

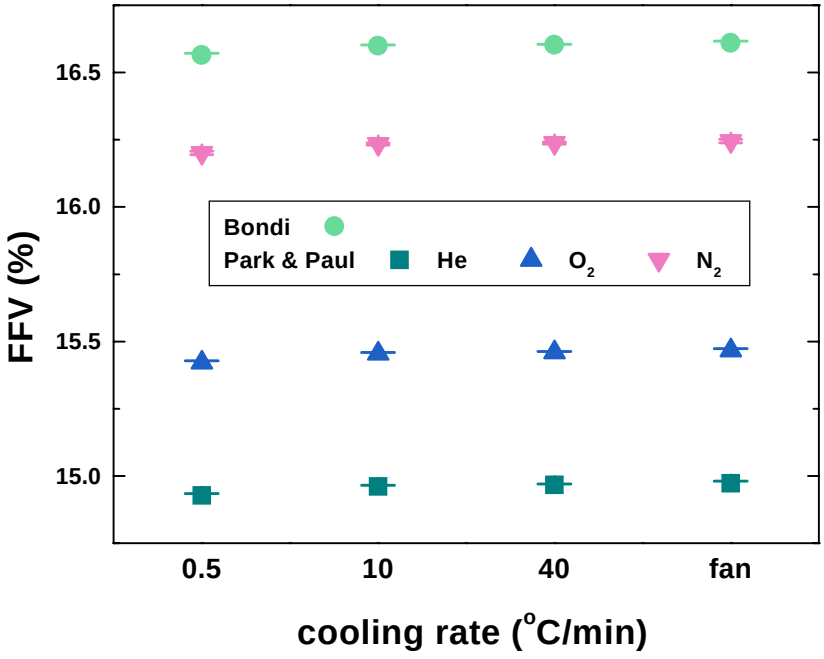

Figure 6.25: FFV at 18°C as a function of the cooling rate (note that the x-axis is not a continuous axis). The FFV was calculated from both the Bondi and the Park & Paul methods.

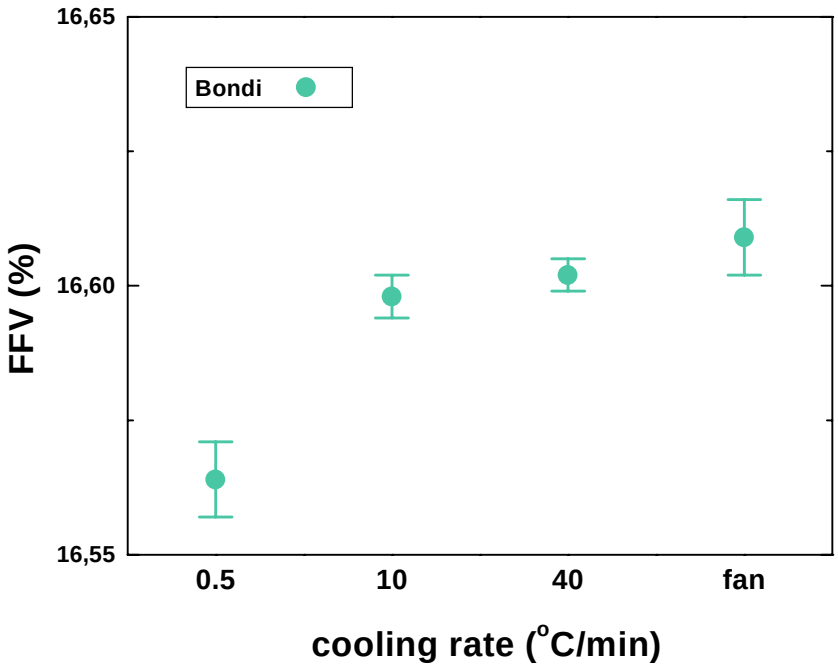

Figure 6.26: FFV at 18°C as a function of the cooling rate (note that the x-axis is not a continuous axis). The FFV was calculated from Bondi's method.

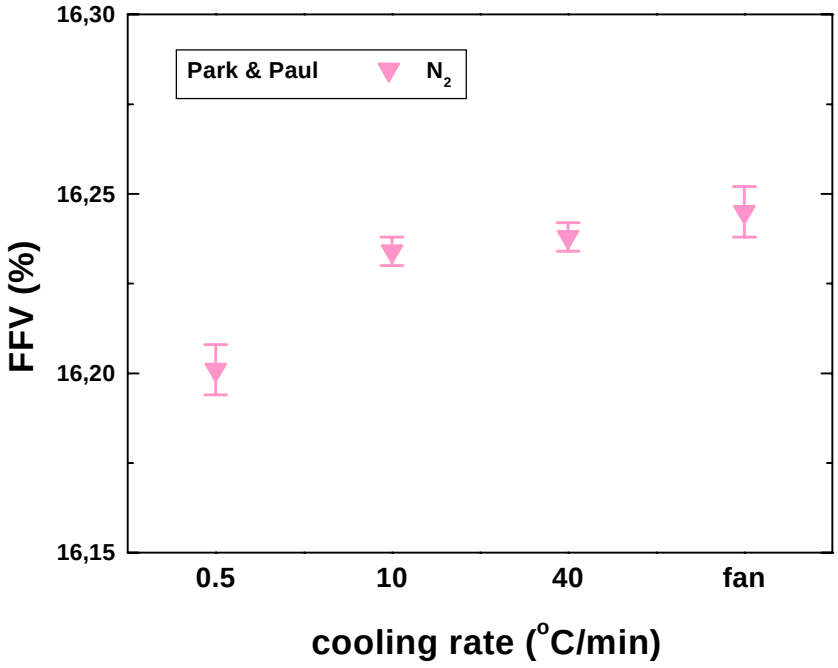

Figure 6.27: FFV at 18°C as a function of the cooling rate (note that the x-axis is not a continuous axis). The FFV was calculated from the Park & Paul method for N_2.

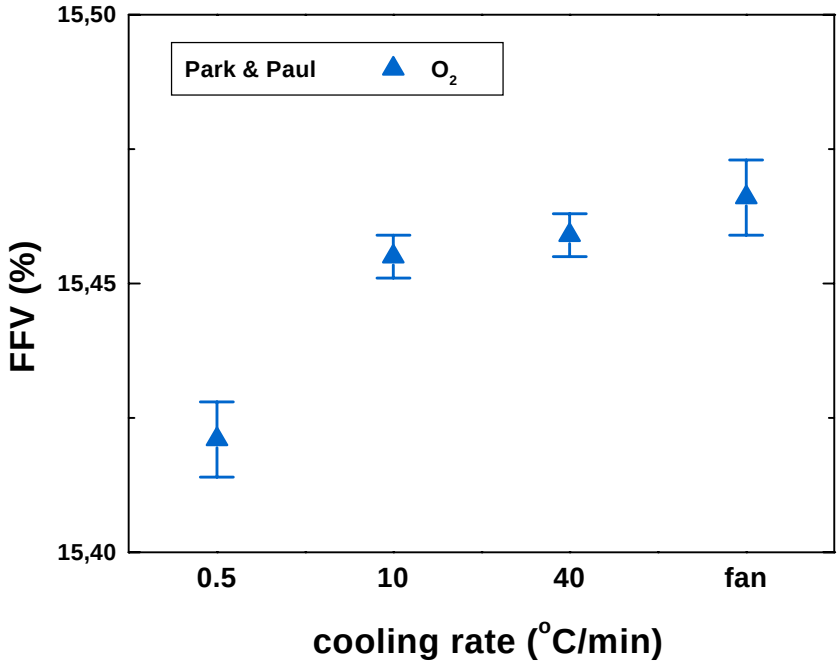

Figure 6.28: FFV at 18°C as a function of the cooling rate (note that the x-axis is not a continuous axis). The FFV was calculated from the Park & Paul method for O_2.

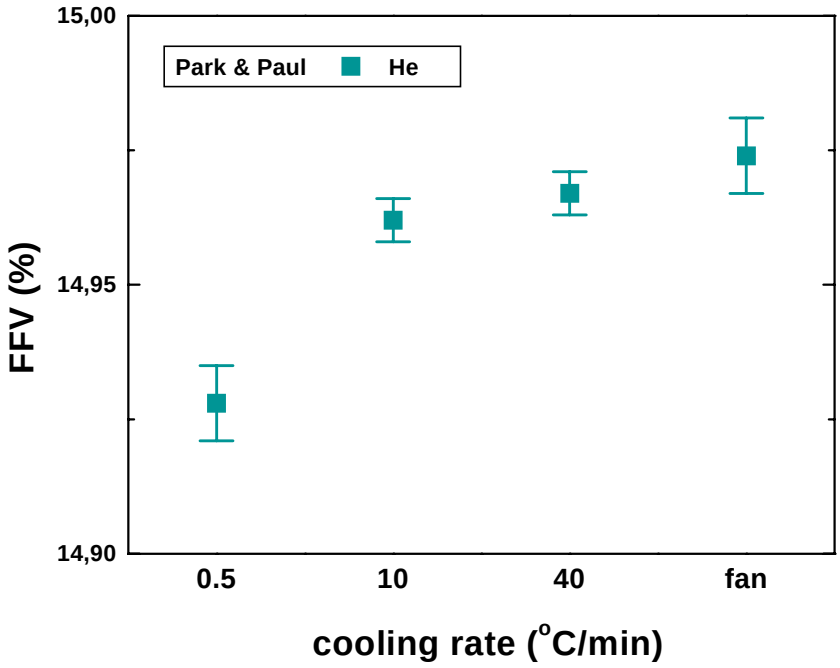

Figure 6.29: FFV at 18°C as a function of the cooling rate (note that the x-axis is not a continuous axis). The FFV was calculated from the Park & Paul method for He.

6.3.4.3. Analysis of the permeation data in terms of the predicted FFV

The diffusion coefficient D was plotted as a function of the fractional free volume FFV. The resulting plot is shown in Figure 6.30. D and FFV appear not to be directly correlated. The fact that the diffusion of a small gas molecule is lower in the material possessing the higher amount of free volume is in contradiction with the free volume theory for diffusion originally proposed by Cohen and Turnbull [30]. This theory assumes that the diffusion is determined by the amount of microvoids since the penetrant mobility occurs by diffusion jumps inside those microvoids. One has to keep in mind that free volume theories are usually developed for temperatures close to or above the glass transition temperature. The free volume theories may not be applicable in the glassy state. The free volume theory in the glassy state may become valid only for bigger size penetrant molecules where more polymeric units are involved in the diffusion process, the diffusion being more cooperative.

The free volume has been nevertheless shown to affect greatly the diffusion coefficients of glassy polymers [69, 101-104]. A paper by Thran et al [105] investigated the relationship between the diffusion coefficient of gases and the fractional free volume determined from Bondi's method. The study was based only on experimental results available in the literature, and this for various amorphous glassy polymers. The diffusion coefficient was reported to increase with an increase in fractional free volume. However the data appear to be quite scattered to really draw solid accurate conclusions. The difference in the preparation of the samples from one study to another complicates obviously the results. Furthermore, the estimation of the fractional free volume from the group contribution method of Van Krevelen [94] may not have always been calculated the same way. Dividing the polymer into chemical groups is indeed rather subjective.

In a study by Jean et al [97], the fractional free volume was determined from PALS measurements. The study involved four polycarbonate-based materials, namely bisphenol-A polycarbonate (PC), tetramethyl bisphenol-A polycarbonate (TMPC), hexafluorobisphenol-A polycarbonate (6FPC), and tetramethylhexafluorobisphenol-A polycarbonate (TM6FPC). Again, it was found that the diffusion coefficient increased with the fractional free volume. Nevertheless, D and not ln D was plotted as a function of

the fractional free volume (FFV). It is therefore impossible to say if whether or not a linear relationship was observed between ln D and (1/FFV), as predicted from the free volume theory applied to the diffusion of gases in polymers [33]. In addition, the results should be looked at with scrutiny. Indeed, the authors of the study did not measure gas transport themselves. They just used values found in the literature for the same polymers. One knows that the preparation of the samples is extremely important and therefore it is not clear if whether or not the samples used in PALS experiments were prepared in exactly the same way as those reported in the literature for gas transport measurements. Furthermore, the temperature at which the gas and density measurements were performed is not reported in the paper. Gas transport properties are commonly reported at 35°C, whereas density data are obtained around 20°C. No mention of a correction factor is given. The temperature at which the PALS experiments were performed is not even given. It was found by Jean et al [97] that the fractional free volume determined from PALS was directly proportional to the fractional free volume estimated from group contribution methods, the former being smaller by a factor of 2.1, as already mentioned previously. The results based on additive group contributions were taken from the work of Koros et al [95, 106-107]. Since Jean et al [97] found a linear relationship between the fractional free volume determined by PALS and the one calculated by Koros et al for the four same various polymers, it means that the proportionality factor is independent of the nature of the polymer. The proportionality factor could maybe be due to the differences in scales or timeframes while probing the free volume. If PALS does indeed probe the polymer free volume, and assuming that the assumptions and calculations behind the PALS technique are correct, the group contribution method seems a reasonable method to evaluate the amount of free volume, or rather to determine the changes in free volume from one polymer sample to another. Moreover, Jean et al [97] noticed that the densities of the four polymers did not correlate with the fractional free volume. As mentioned above, the difference may be due to the preparation of the samples, or to the fact that the densities (taken from the literature) were not determined at the same temperature. However we can observe also that the specific volumes of PC and TMPC were probably inverted. Indeed, the specific volume of polycarbonate PC was reported as 0.923 cm^3/g, which corresponds to a density of 1.08 g/cm^3 for PC! The diffusion coefficient was found

to increase with the fractional free volume, with the mean free volume hole radius, and with the broadening of the free volume distribution. This result is in contradiction with the present research project. The free volume theory may grossly apply to different polymer structures, but may not discern the subtle differences of a given polymer at different thermal histories.

A contradiction between the free volume content and the gas transport properties has also been reported by Kim et al [108]. Miscible blends and random copolymers of bisphenol-A and tetramethyl bisphenol-A polycarbonates of the same chemical composition were compared. Although the copolymers were characterized by a greater free volume content they showed reduced gas transport properties. The results were explained in terms of the local chain motions. It was suggested that the slight difference in the free volume contents between both types of polymers could be of secondary importance compared to the local chain dynamics.

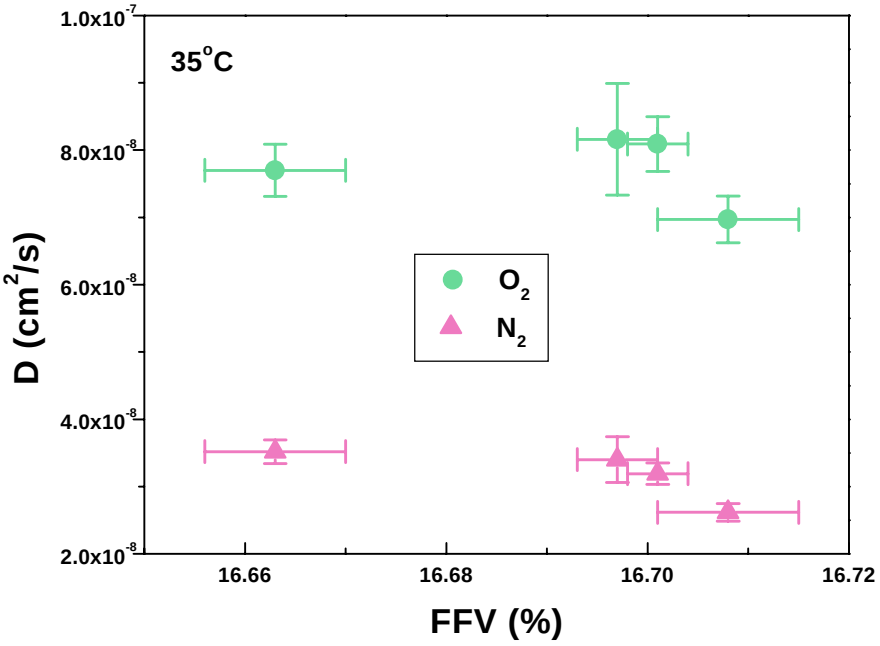

Figure 6.30: Diffusion coefficient D (cm^2/s) as a function of the fractional free volume FFV (%). Diffusion results were obtained at 35°C. The density values were corrected to obtain FFV at 35°C as well.

The simplified free volume theory applied to gas transport (similar to the Doolittle equation for the treatment of the viscosity of polymers above T_g mentioned in Chapter 5)

expresses the diffusion coefficient D as a function of the fractional free volume FFV as follows [33]:

$$D = A \exp\left(\frac{-B}{FFV}\right) \qquad \text{Eq (6.14)}$$

where A and B are constant for a particular gas. A is a function of the size and shape of the gas molecule; B relates to the critical polymer cavity size needed to do a diffusive jump. If the free volume theory is verified, a plot of ln D versus (1/FFV) should be linear, with a slope of (-B) and an intercept of ln A.

In the literature it is not quite clear if whether or not diffusion coefficients and densities are taken at the same temperature. However we believe that the diffusion coefficient and the density have to be taken at the same temperature. Since our diffusion values have been obtained at 35°C, and our density data at 18°C, we need to evaluate the density at 35°C. From the conservation of mass, we have:

$$\rho_{35^\circ C} = \left(\frac{\rho_{18^\circ C} V_{18^\circ C}}{V_{35^\circ C}}\right) \qquad \text{Eq (6.15)}$$

where ρ_i is the density and V_i the volume of the material.

But $$V_{35^\circ C} = V_{18^\circ C} + dV_{(35\text{-}18)^\circ C} \qquad \text{Eq (6.16)}$$

The volumetric coefficient of expansion α (in K^{-1}) is given by the following expression:

$$\alpha = \frac{1}{V}\left(\frac{\partial V}{\partial T}\right)_P \qquad \text{Eq (6.17)}$$

Therefore $$V_{35^\circ C} = V_{18^\circ C} + \alpha_G (35-18) V_{18^\circ C} = V_{18^\circ C}(1+17\,\alpha_G) \qquad \text{Eq (6.18)}$$

where α_G stands for the thermal expansion coefficient in the glassy state.

Finally $$\rho_{35^\circ C} = \left(\frac{\rho_{18^\circ C}}{1+17\,\alpha_G}\right) \qquad \text{Eq (6.19)}$$

From the literature, it was found that $\alpha_G = 70\times10^{-6}$ K^{-1} for polycarbonate for temperatures ranging between 28 and 80°C [109]. The experimental density values were determined at 18°C using a density gradient column. Obviously, the density decreases with an increase in temperature. As the temperature increases, the polymeric system is dilated, the amount of free volume increases, and thus the density decreases. Please note that α_f determined in Chapter 5 (with $\alpha_f = 8.5\times10^{-4}$ K^{-1} for a cooling rate of 40°C/min) does not correspond

to α_G. Indeed, $\alpha_f \approx (\alpha_R - \alpha_G)$ represents the difference between the thermal expansion coefficients in the rubbery and the glassy states, respectively, assuming that α_G remains constant.

Plots of ln D versus (1/FFV) for O_2 and N_2 are shown in Figure 6.31. The fractional free volume FFV was calculated at 35°C using Bondi's method only since the method of Park & Paul does not seem to always make physical sense (see above). As seen in Figure 6.31, the data points do not fall on a straight line. Therefore, the free volume theory does not apply to our system. Whenever the free volume theory applied to gas transport is verified in the literature, various gases in various glassy polymers are considered. The theory may be applicable to polymer families (or to polymers with various chemical structures) but not to a particular polymer at various processing conditions. Moreover, FFV calculated from group contribution methods is based on the bulk density, which is a macroscopic quantity. The calculations do not take into account the distribution and topology of the free volume. Nevertheless one can always wonder whether or not the method selected to calculate FFV is correct. Furthermore, the total amount of free volume may not be accessible to gas transport. Researchers use the concept of interstitial free volume to refer to this inaccessible free volume [29]. In a study involving average stress relaxation times and free volume, it was also determined that the Doolittle equation was not applicable to glassy polycarbonate [110]. The Doolittle equation was found to become valid for polycarbonate only above 135°C, thus in the transition region where properties are governed by the free volume content.

Similarly, the free volume theory was applied to the solubility and the permeability coefficients. While considering the permeation data of various gases in various typical polymers, Park & Paul [69] determined for instance the values of the constants A and B applied to permeation. Lee [111] observed that ln P was proportional to $(V_f)^{-1}$ for various polymers. Polymers with fluorinated groups should not be however considered in the analysis since their permeability has been shown not to correlate with the density [95]. Plots were generated based on the experimental results obtained in this research and again the logarithms of the coefficients did not appear to be linear with the inverse of the fractional free volume. As mentioned previously, FFV for polycarbonate determined from group contribution methods has been found to correspond (by a

proportionality factor) to the free volume determined from PALS measurements [97]. Since there is no linear relationship between ln P and $(FFV)^{-1}$, it means that ln P would not correlated with measurements from PALS either for a particular polymer.

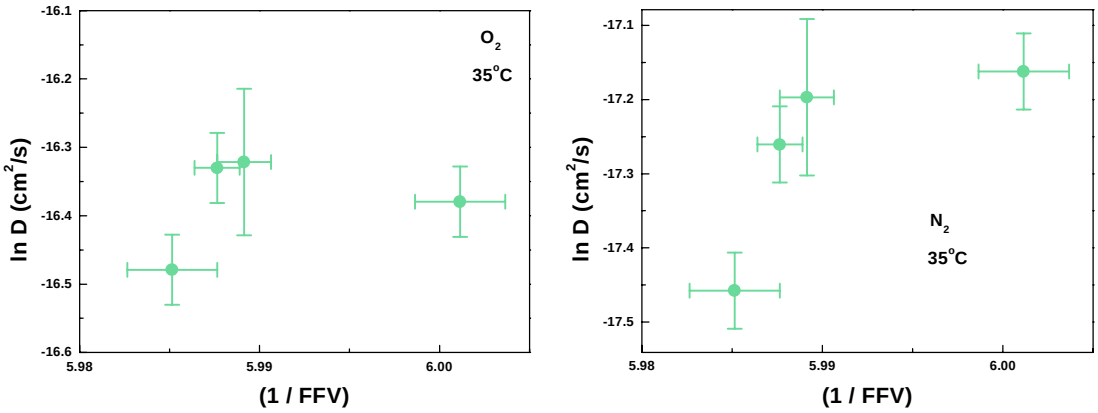

Figure 6.31: Plots of ln D versus (1/FFV) for O_2 (left) and N_2 (right). Data were taken at 35°C.

Although the free volume theory applied to gas transport is given by Eq (6.14), one can always remark that the Doolittle equation [112, 113] is given as follows:

$$\eta = A \exp\left[B\left(\frac{1}{FFV} - 1\right)\right] \qquad \text{Eq (6.20)}$$

where η is the viscosity , and A and B are constant (but different from the constants given in Eq (6.14)). FFV is still defined as (V_f / V) where V is the total volume of the system and V_f the free volume available to the system.

Therefore the following modified equation could also be investigated to relate the diffusion coefficient D to FFV:

$$D = A \exp\left[B\left(\frac{1}{FFV} - 1\right)\right] \qquad \text{Eq (6.21)}$$

But again, a linear relationship should be observed between ln D and $(1/FFV)^{-1}$, which is not the case.

6.3.4.4. Determination of the gas transport activation energies (E_P, E_D, ΔH_s) and the preexponential factors (P_o, D_o, S_o)

The gas transport activation energies and the corresponding preexponential factors were determined for the polymers cooled at different cooling rates by running successive permeation experiments at 35, 55, 65, and 80°C. Obviously, the higher the temperature, the higher the permeability, but the lower the selectivity between two gases.

6.3.4.4.1. The gas transport activation energies (E_P, E_D, ΔH_s)

The activation energies of permeation E_P, diffusion E_D, and the enthalpy of sorption ΔH_s results are shown from Figure 6.32 to Figure 6.34. These results were obtained without entering the value of the thickness in the calculations. The calculation details have been provided in Chapter 4. Since the estimation of the thickness is not needed to determine the various activation energies, errors are extremely small and based mainly on the linear regressions performed on four data points. The coefficient of correlation R reported for the linear regressions was generally found to be greater than 0.999. In the worst case, R was found to be about 0.95.

As expected, the greater the kinetic diameter of the gas molecule, the greater the activation energies. Larger cavities are indeed necessary for the diffusion of larger gas molecules and hence the activation energies will be larger to create channels for the diffusion of bigger molecules. It was impossible to calculate E_D and ΔH_s for helium due to the small time lag value. Even though the difference between the kinetic diameters of O_2 and N_2 is rather small (about 0.18Å), the two diatomic gas molecules differ by other factors. For instance, the nitrogen gas molecule is longer and needs to rotate much more around itself to go through a molecular channel [114]. This should result in a lower diffusion coefficient for N_2. The polarizabilities of the gases (which indicate how easily the molecule electrons can be displaced by an electric field) differ also between the gases of interest in this research work. The polarizability of He is given as $0.20\times10^{-24}cm^3$, that of O_2 as $1.58\times10^{-24}cm^3$, and that of N_2 as $1.74\times10^{-24}cm^3$ [115].

Higher free volume inside the polymeric material should dictate lower activation energies. This trend has actually been verified by Yampolskii et al [70] using a data base

involving various amorphous glassy polymers. The changes in the polymer structures were responsible for the changes in free volume. However the change of free volume for a given polymer as a function of thermal history for instance was not reported. Quite surprisingly, the activation energies and cooling rate show an opposite correlation in the present study involving polycarbonate. Indeed, as seen from Figure 6.32 to Figure 6.34, the activation energies are greater for the samples cooled by the fan (high free volume) than for the sample cooled extremely slowly (low free volume). The greater the cooling rate, the greater is the activation energy for nitrogen. The oxygen molecule is too small to be sensitive to the cooling rates. The activation energy changes in percent as a function of the cooling rate for a specific gas are shown from Figure 6.35 to Figure 6.37. The great influence of N_2 on the activation energies appears clearly in Figure 6.37.

It is possible that the activation energies may be more related to the level of conformational energy than to the overall free volume content. If a polymer has more time to cool down to room temperature from above T_g, the chains pack more closely and have more time to relax. The polymer chains may attain the most stable chain conformation, and a lower energy conformation, or a lower Gibbs free energy for the system. If the temperature increases for instance, it takes less energy to respond, expand or dilate the polymer chains surrounding the gas molecule, and therefore enable the gas molecule to jump into another cavity. The activation energy of diffusion corresponds indeed to the energy necessary to open a diffusion path.

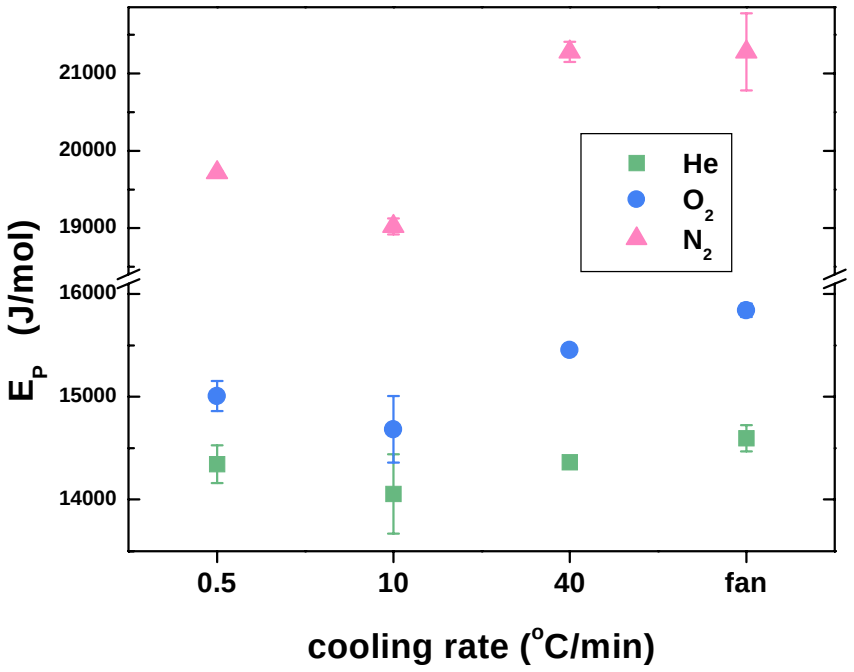

Figure 6.32: E_P as a function of the cooling rate for He, O_2, and N_2 (note that the x-axis is not a continuous axis). The applied pressures were fixed at about 2.5atm for He, and 3.9atm for both O_2 and N_2. Permeation experiments were consecutively performed on the same membranes at 35, 55, 65, and 80^{o}C. Aging was found to be negligible at those temperatures within the timeframe of the experiments.

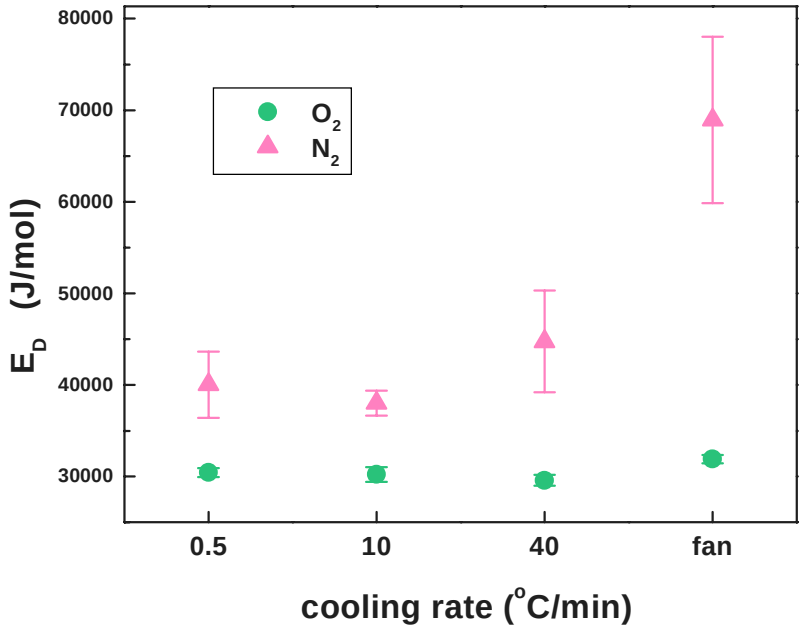

Figure 6.33: E_D as a function of the cooling rate for O_2 and N_2 (note that the x-axis is not a continuous axis). The applied pressure was fixed at about 3.9atm for both O_2 and N_2. Permeation experiments were consecutively performed on the same membranes at 35, 55, 65, and 80^{o}C. Aging was found to be negligible at those temperatures within the timeframe of the experiments.

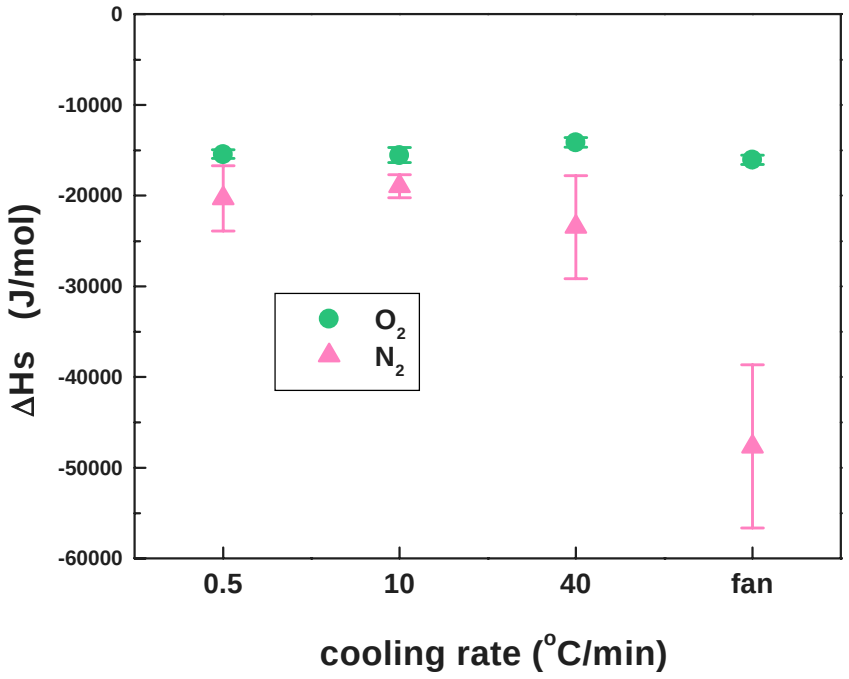

Figure 6.34: ΔH_s as a function of the cooling rate for O_2 and N_2 (note that the x-axis is not a continuous axis). The applied pressure was fixed at about 3.9atm for both O_2 and N_2. Permeation experiments were consecutively performed on the same membranes at 35, 55, 65, and 80°C. Aging was found to be negligible at those temperatures within the timeframe of the experiments.

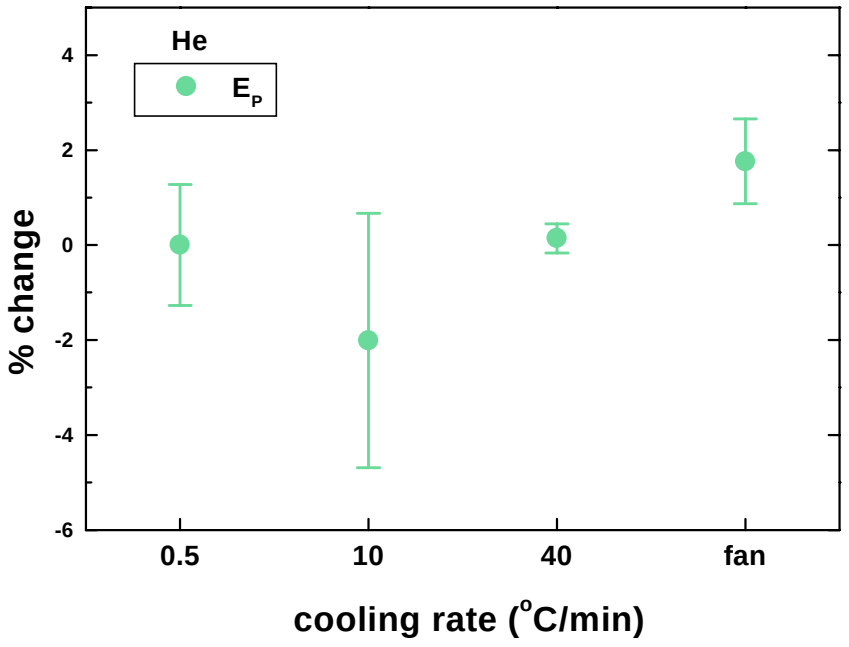

Figure 6.35: % change in E_P for He (note that the x-axis is not a continuous axis). The data obtained for a cooling rate of 0.5°C/min were taken for reference.

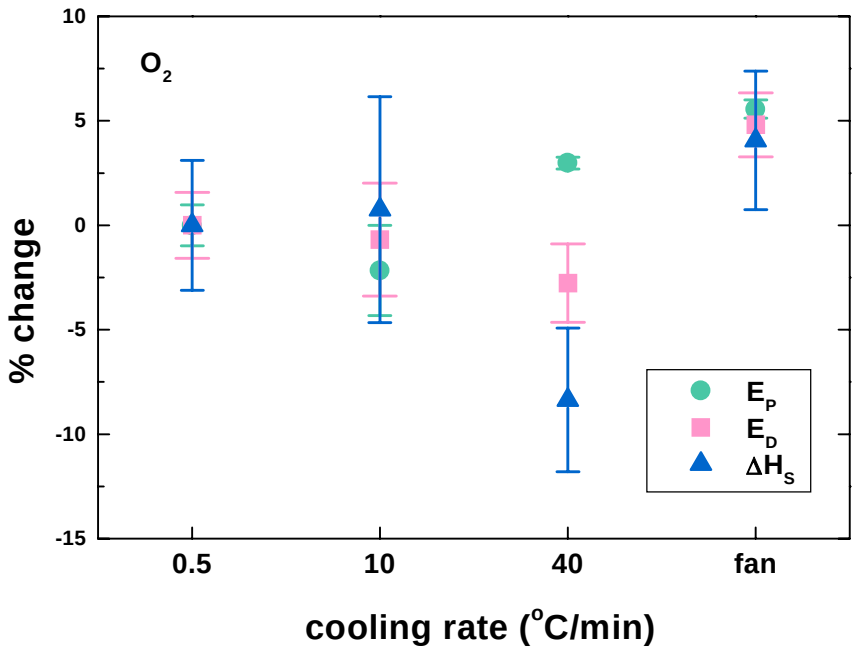

Figure 6.36**:** % change in E_P, E_D, and ΔH_s for O_2 (note that the x-axis is not a continuous axis). The data obtained for a cooling rate of 0.5°C/min were taken for reference.

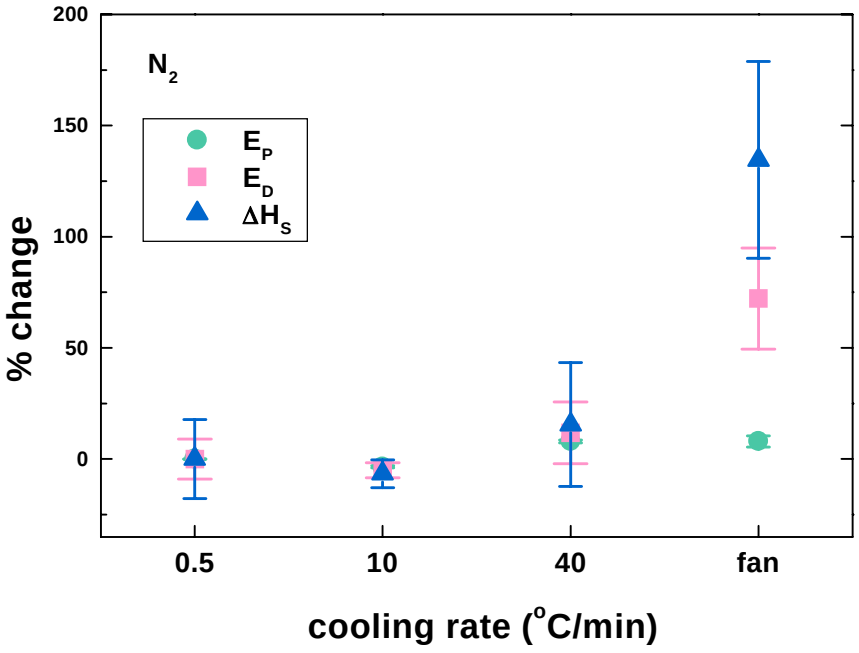

Figure 6.37: % change in E_P, E_D, and ΔH_s for N_2 (note that the x-axis is not a continuous axis). The data obtained for a cooling rate of 0.5°C/min were taken for reference.

6.3.4.4.2. The preexponential factors (P_o, D_o, S_o)

The preexponential factors P_o, D_o, and S_o were determined as explained in Chapter 4. As stated at that time, the constants were not determined from both the values of (P, D, S) at a given temperature and from the values of the activation energies, but rather from appropriate intercepts. The reader should refer to Chapter 4 for further understanding. Unlike the procedure used for obtaining the values of the activation energies, knowledge of the thickness and the feed pressure was necessary.

The results are shown from Figure 6.38 to Figure 6.41. As seen in Figure 6.39, the error on D_o was extremely big for N_2. This was caused by the linear regression performed on the sample cooled with the fan. An absolute correlation factor of only 0.98 was obtained. Therefore Figure 6.40 shows the dependence of D_o on the cooling rate for O_2 only. Trends cannot be easily distinguished as a function of the cooling rate for the preexponential factors.

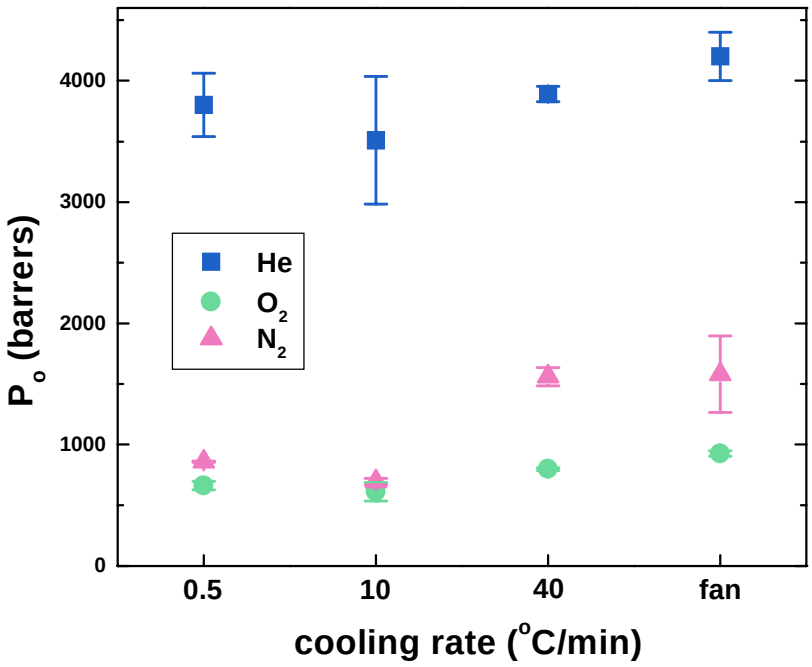

Figure 6.38: Preexponential factor P_o as a function of the cooling rate (note that the x-axis is not a continuous axis).

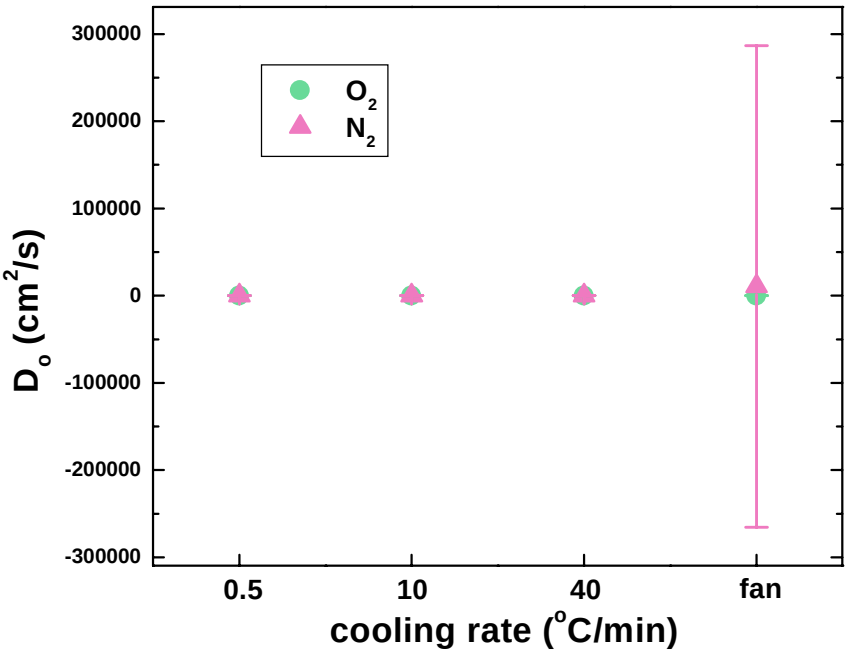

Figure 6.39: Preexponential factor D_o as a function of the cooling rate (note that the x-axis is not a continuous axis).

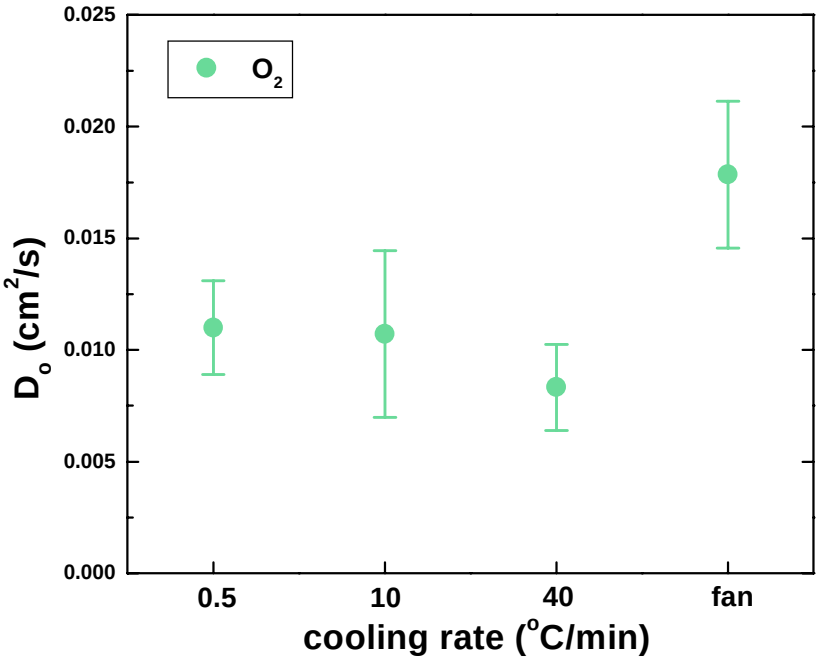

Figure 6.40: Preexponential factor D_o as a function of the cooling rate (note that the x-axis is not a continuous axis).

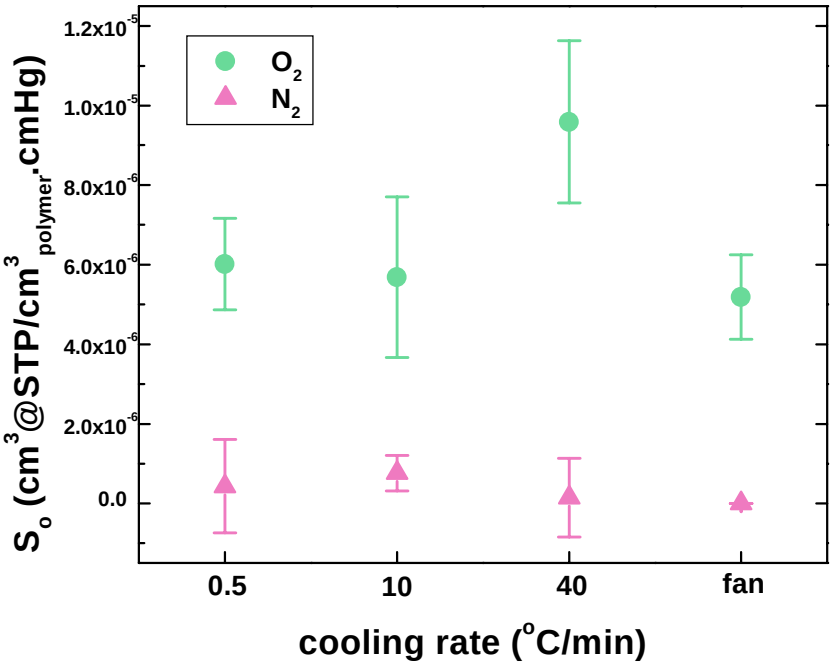

Figure 6.41: Preexponential factor S_o as a function of the cooling rate (note that the x-axis is not a continuous axis).

6.3.4.4.3. Summary of the permeation results

Activation energies and preexponential factors found in this research work are recapitulated in Table 6.8 through Table 6.10. Table 6.11 reports the values obtained by Costello and Koros for amorphous glassy bisphenol-A polycarbonate [75]. The literature values have been modified in order to have the same units as the ones used in this research. The orders of magnitude of the activation energies obtained by the researchers are in good agreement with this work. Obviously, the preexponential factors are more difficult to compare. The S and P results of Costello and Koros were obtained from sorption and permeation experiments, respectively, and the D results were calculated from the P=DS equation. It would have been interesting to estimate S as well from permeation experiments (as what has been done in this research work), to evaluate the activation energy, and to compare with the direct sorption data. The polycarbonate selected by Costello and Koros was purchased from General Electric. The Lexan sheets were used as-received. Such commercial extruded sheets may be highly oriented. Moreover, moisture may have complicated the results. In a later publication [116],

Costello and Koros did mention however that birefringence measurements on the as-received films showed no evidence of orientation.

cooling rate	penetrant	E_P (kJ/mol)	error (+/-)	P_o (barrer)	error (+/-)
0.5°C/min	He	14.3	0.2	3.8E+03	2.6E+02
	O_2	15.0	0.1	6.6E+02	3.6E+01
	N_2	19.7	0.0	8.6E+02	6.2E+00
10°C/min	He	14.1	0.4	3.5E+03	5.3E+02
	O_2	14.7	0.3	6.1E+02	7.6E+01
	N_2	19.0	0.1	6.9E+02	2.6E+01
40°C/min	He	14.4	0.0	3.9E+03	6.4E+01
	O_2	15.5	0.0	8.0E+02	1.2E+01
	N_2	21.3	0.1	1.6E+03	7.6E+01
fan	He	14.6	0.1	4.2E+03	2.0E+02
	O_2	15.8	0.1	9.3E+02	2.2E+01
	N_2	21.3	0.5	1.6E+03	3.2E+02

Table 6.8: E_P and P_o values obtained in this work.

cooling rate	penetrant	E_D (kJ/mol)	error (+/-)	D_o (cm^2/s)	error (+/-)
0.5°C/min	O_2	30.4	0.5	1.1E-02	2.1E-03
	N_2	40.0	3.6		
10°C/min	O_2	30.2	0.8	1.1E-02	3.7E-03
	N_2	38.0	1.4		
40°C/min	O_2	29.6	0.6	8.3E-03	1.9E-03
	N_2	44.7	5.6		
fan	O_2	31.9	0.5	1.8E-02	3.3E-03
	N_2	68.9	9.1		

Table 6.9: E_D and D_o values obtained in this work.

cooling rate	penetrant	ΔH_s (kJ/mol)	error (+/-)	S_o (cm^3@STP/cm^3.cmHg)	error (+/-)
0.5°C/min	O_2	-15,4	0,5	6,0E-06	1,2E-06
	N_2	-20,3	3,6	4,3E-07	1,2E-06
10°C/min	O_2	-15,5	0,8	5,7E-06	2,0E-06
	N_2	-19,0	1,3	7,6E-07	4,5E-07
40°C/min	O_2	-14,1	0,5	9,6E-06	2,0E-06
	N_2	-23,5	5,7	1,4E-07	9,9E-07
fan	O_2	-16,1	0,5	5,2E-06	1,1E-06
	N_2	-47,7	9,0	1,5E-11	3,8E-10

Table 6.10: ΔHs and S_o values obtained in this work.

penetrant	E_P (kJ/mol)	P_o (barrer)	E_D (kJ/mol)	D_o (cm^2/s)	ΔH_s (kJ/mol)	S_o (cm^3@STP/cm^3.cmHg)
He	17.6 +/- 0.4	1,1E+04	28.4 +/- 3.3	0,14	-10.5 +/- 2.9	7,8E-06
O_2	19.6 +/- 0.8	3,4E+03	30.5 +/- 1.7	0,0096	-10.9 +/- 0.8	3,6E-05
N_2	25.1 +/- 0.8	5,3E+03	40.5 +/- 2.1	0,13	-15.5 +/- 1.3	4,2E-06

Table 6.11: From [75].

6.3.4.5. Verification of the relationship between E_D and D_o

The Zener's theory [117] was also considered in the evaluation of our data. This theory, originally developed for metals, stipulates that there is a linear relationship between the logarithm of the preexponential factor for diffusion D_o and the activation energy of diffusion E_D. The Zener's theory was derived assuming that the free enthalpy of diffusion was mainly controlled by the additional elastic distortion arising from a movement of the particle from its equilibrium position into the saddle point configuration, which corresponds to a strained polymeric matrix. We have:

$$\ln D_o = a E_D + b \qquad \text{Eq (6.22)}$$

If such a relationship is verified for our experimental data, this would further confirm that our values of D_o and E_D are correct.

To our knowledge, this theory has been verified in the literature for the diffusion of various gases in a given polymer only [118, 119]. In the present research, data for only one gas (O_2) are available, but the polymer is prepared in four different ways, the parameter being the cooling rate. $\ln D_o$ was plotted as a function of E_D for O_2 only since the error in D_o for N_2 was too big, as mentioned previously. The data points of Figure 6.42 fall onto a straight line, thus verifying Eq (6.22). The slope was found to be equal to 3.28×10^{-4} mol/J. Van Krevelen [94] reported the value of the slope determined using diffusion data of several gas molecules in several glassy polymers. The slope came out as 1.2×10^{-4} mol/kJ. Nevertheless, the slope was obtained from a plot having a y-axis of log D_o (m^2/s). Therefore the slope has to be multiplied by (ln 10) to compare it with ours. This gives a slope of 2.76×10^{-4} mol/kJ, or 2.76×10^{-7} mol/J. The slope value given by Van Krevelen was found to be independent of the type of the polymer [94]. However this value is not verified here, when different thermal histories are considered instead of different gases.

Quite interestingly, it was also observed that $\ln P_o$ linearly correlated with E_P for the three gases selected in this research. The slopes were determined to be 3.56×10^{-4} mol/J, 3.83×10^{-4} mol/J, and 3.61×10^{-4} mol/J, for He, O_2, and N_2, respectively. Similarly, a linear relationship was found between $\ln S_o$ and dH_s for O_2 and N_2. The resulting slopes were found to be 3.27×10^{-4} mol/J and 3.77×10^{-4} mol/J for O_2 and N_2, respectively. The fact that a Zener-type relationship applies to the permeability and the solubility results may indicate that the error bars on the experimental data points are too big to draw confident conclusions.

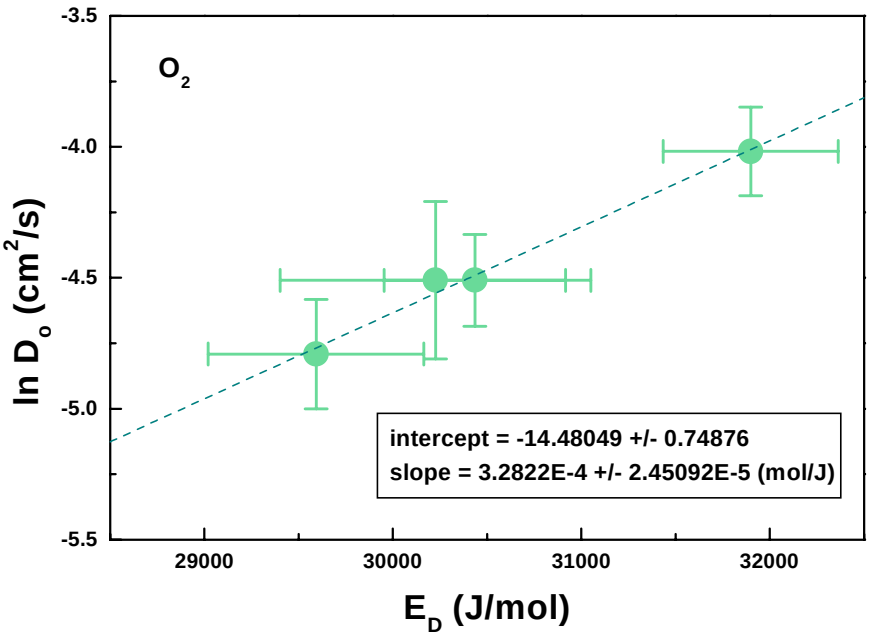

Figure 6.42: $\ln D_o$ versus E_D for O_2. The data points have been obtained at different cooling rates.

Assuming that the free volume theory is valid, combining Eq (6.16) and Eq (6.14) leads to:

$$\ln D_o = \frac{E_D}{RT} + \ln A - \left(\frac{B}{FFV}\right) \qquad \text{Eq (6.23)}$$

Since we saw above that there is a linear relationship between $\ln D_o$ and E_D, the intercept (lnA–(B/FFV)) has to be constant. This is however impossible since density and thus (FFV) depends on thermal history. Moreover, how can we choose a temperature for the slope since D_o and E_D are fixed in a given temperature range? The free volume theory

does not seem to be consistent with the experimental data for D_o and E_D. Eq (6.23) could apply to the diffusion of various gases in a given polymer at a particular temperature. However FFV could be dependent on the nature of the gas [77]. Therefore this point still does not validate the free volume theory.

6.3.4.6. Determination of the average distances between polymer chains

In order to validate the values of the activation energy of diffusion E_D (as a reminder, E_D was found to be greater for a high free volume material, in contradiction with expectations written in the literature), the average distance between chains was calculated for each cooling rate. The Brandt's Model [120] was used to relate the activation energy of diffusion E_D to the average interchain separation.

E_D is well-known to be directly proportional to the kinetic diameter squared d^2 of the penetrant [94, 119, 121, 122]. Meares [121] suggested that E_D was proportional to the cohesive energy density (CED) of the polymer.

$$E_D = \left(\frac{1}{4}\right)\pi d^2 N_o \lambda (CED) \qquad \text{Eq (6.24)}$$

where d is the collision diameter of a diffusant molecule (which can be taken as the kinetic diameter of the gas), λ is the penetrant jump length, N_o is the Avogadro's number, and CED is equal to (ρ E_{coh}), where E_{coh} is the molar cohesion energy. This equation predicts that E_D increases with the kinetic diameter of the gas, as verified experimentally.

The Brandt's model [120] assumes the existence of a finite average distance between chains in the equilibrium state. We have:

$$E_{Di} = \text{intercept} + (\text{slope}) d_i^2 \qquad \text{Eq (6.25)}$$

where i stands for a gas i. The average distance between chains can be calculated by taking the square root of (-intercept/slope) [120].

As shown in Figure 6.43, E_D was plotted versus the square of the kinetic diameter of the gas, and a linear regression was performed. Since E_D was obtained only for O_2 and N_2, the linear regression was based on two data points only for each cooling rate.

Obviously, the errors were far from being negligible. Nevertheless, a trend can still be distinguished. As seen in Table 6.12, the greater the cooling rate, the greater the average distance between chains. As expected, chains are further apart for the sample cooled really fast. The average interchain separations given in Table 6.12 happen to be on the same order of magnitude than the kinetic diameters of the gas molecules. Recall, the kinetic diameters of He, O_2, and N_2 are reported as 2.6 Å, 3.46 Å, and 3.64 Å, respectively [71-74]. This result is expected since the diffusion is restricted and believed to be controlled by the thermal motions of the polymer chains (activated jump motion).

The fact that the average distance between chains increases with the cooling rate may induce a decrease in the Van der Waals forces. Such a decrease could explain why the T_g is lower for the highest cooling rate since the forces that need to be overcome for the material to become rubbery are lower.

The wide-angle X-ray diffraction (WAXD) d-spacing has been determined to be about 5.1 or 5.2Å for polycarbonate [23, 95], about 2Å more than the average distance between chains given in Table 6.12. The d-spacing of amorphous polymers is believed to indicate the intersegmental distance between polymer chains. Note that the term "correlation length" should be used instead since the word "d-spacing" refers to crystalline materials. The fractional free volume determined from group contribution methods and the average distance between chains as calculated above may give a better estimate of the openness of the polymeric matrix than the correlation length. While studying polymers with bulky ring substituents, it has for instance been shown that the correlation lengths, that indicate the distance between chain centers, overestimate the amount of free volume [95]. However there is no evidence that the correlation length corresponds to the space necessary for gas molecules to go through the polymer. A recent study concerning 6FDA-based polyimide [123] suggests indeed that gas permeability in glassy polymers may not be related to the correlation lengths.

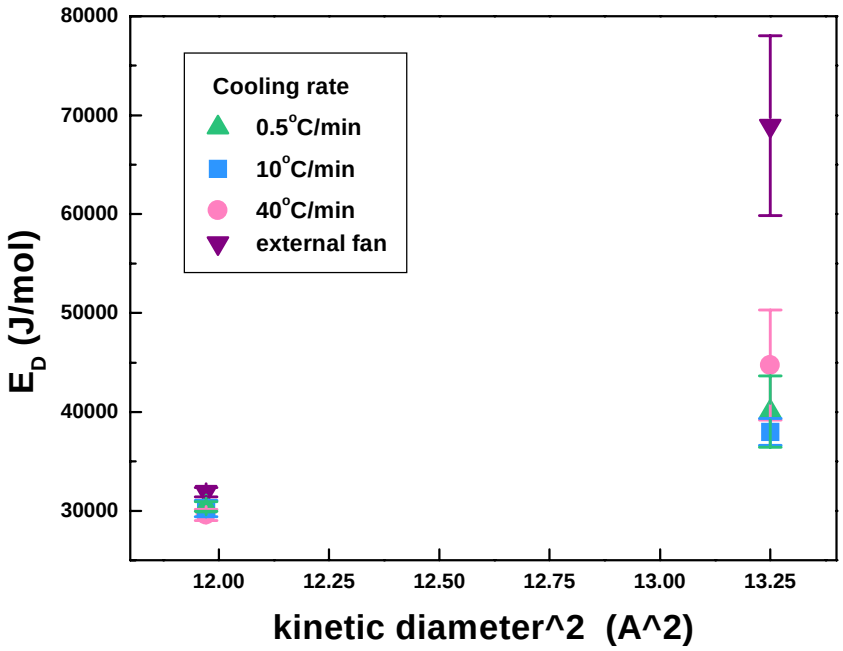

Figure 6.43: E_D as a function of the square of the kinetic diameter of the gas penetrant. Knowledge of the slope and the intercept provides a rough estimation of the average distance between chains. The average distance between chains was calculated by taking the square root of (-intercept/slope). The values of the slopes were (7513.3, 6077.5, 11859.2, and 28985.9 J/(mol.Å^2)) and the values of the intercepts were (-59511.2, -42530.0, -112380.1, and -315118.8 J/mol) for the samples cooled at 0.5°C/min, 10°C/min, 40°C/min, and by the external fan, respectively.

cooling rate	distance (A)
0.5°C/min	2.8
10°C/min	2.6
40°C/min	3.1
external fan	3.3

Table 6.12: Average distances between chains for the various cooling rates of interest. The errors were far from being negligible. In the case of the sample cooled by the fan, taking extreme points on the error bars of E_D for instance led to average distances ranging from 1.1Å to 10.3Å.

6.4. Conclusions

The ultimate objectives of the present study were to examine the relationships between the free volume contained in a polymeric matrix and the gas transport properties. The free volume content was changed by selecting various cooling rates. A particular

grade of bisphenol-A polycarbonate was chosen, and physical properties and gas transport parameters were determined as a function of the cooling rate.

On one hand, the physical properties of polycarbonate were found to be greatly affected by the time given to the polymer to cool down from 15°C above the glass transition temperature T_g to room temperature. The greater the cooling rate, the greater is the amount of free volume trapped into the polymeric matrix, the lower is the density, the lower is the T_g, and the greater is the breadth of the loss modulus E". No linear relationship was observed between the density and the T_g values. It was nevertheless determined that the breadth of E" was linearly correlated with the density.

On the other hand, the permeability coefficients through the polymer were not observed to be affected by the cooling rate. Although the diffusion coefficient and the solubility coefficient were found to be dependent on the cooling rate, their combined effects canceled out, and the permeability coefficient appeared to remain constant with an increase in free volume for all the gases studied, in contradiction with common expectations. The free volume present in polymers is commonly believed to allow molecular motions, to enhance the diffusional jumps, and to increase the permeability. This study points out that the permeability coefficient should not be directly related to the T_g or the free volume, as what is commonly done in the literature [69, 70]. However the solubility coefficient can be related to the free volume and its distribution. The free volume theory was not verified in this study however, indicating that the diffusion coefficient is not directly related to the free volume content, in contrast to the literature [29-33, 69, 101-105]. The increase in the diffusion coefficient with a decrease in the cooling rate, and thus with a decrease in the free volume amount, may be caused by the conformations and dynamics of the polymer segments. Quite surprisingly, the activation energies for gas transport were found to be greater for the samples with a higher amount of free volume. The results presented here are therefore in contradiction with what is usually written in the literature [70]. The behavior was explained in terms of the energy state of the polymer and the resulting relaxation times. The activation energies and corresponding preexponential factors were observed to verify well-established relationships, thus validating the experimental data. The average distance between chains was also determined from the knowledge of the activation energy for diffusion. As

expected, it was estimated that the chains were further apart for the sample with the higher cooling rate.

The gas transport results obtained in this study are in agreement with the ones obtained in Chapter 5. The free volume theory of diffusion may grossly apply to different polymer structures with different overall free volume contents but may not discern the subtle differences of a given polymer at different thermal histories. We postulate that the local chain dynamics are crucial for the gas transport process.

Furthermore, this study shows that the cooling rate is not an important polymer processing parameter, if one is interested in the permeability of freshly processed amorphous bisphenol-A polycarbonate only (used as a functional specialty polymer). Indeed P remains unaffected by the time given to the polymer to reach room temperature. However the cooling rate affects other properties such as density and T_g, and may affect the behavior of the polymer with time.

6.5. References

1. H. Hachisuka, H. Takizawa, T. Tsujita, A. Takizawa, T. Kinoshita, gas transport properties in polycarbonate films with various unrelaxed volumes, *Polymer*, 32, 13, 2383 (1991).
2. H. Hachisuka, Y. Tsujita, A. Takizawa, T. Kinoshita, Gas transport properties of annealed polyimide films, *Journal of Polymer Science: Part B: Polymer Physics*, 29, 11 (1991).
3. E. Ito, K. Sawamura and S. Saito, Effects of drawing on molecular motions in polycarbonate, *Colloid & Polymer Sci.*, 253, 480-484 (1975).
4. A. Bos, I. G. M. Punt, M. Wessling, H. Strathmann, CO_2-induced plasticization phenomena in glassy polymers, *Journal of Membrane Science*, 155, 67-78 (1999).
5. J. S. Chiou, J. W. Barlow and D. R. Paul, Plasticization of Glassy Polymers by CO_2, *Journal of Applied Polymer Science*, 30, 2633 (1985).
6. R. G. Wissinger and M. E. Paulaitis, Glass Transitions in Polymer/CO_2 Mixtures at Elevated Pressures, *Journal of Polymer Science, Part B: Polymer Physics*, 29, 5, 631 (1991).
7. E. S. Sanders, Penetrant-induced plasticization and gas permeation in glassy polymers, *Journal of Membrane Science*, 37, 63-80 (1988).
8. M. Wessling, S. Schoeman, Th. Van den Boomgaard, C. A. Smolders, Plasticization of gas separation membranes, *Gas Sep. Purif.*, 5, 222-228 (1991).

9. Y. P. Handa, S. Lampron, M. L. O'Neill, On the plasticization of poly(2,6-dimethyl phenylene oxide) by CO_2, *J. Polym. Sci., Polym. Phys. Ed.*, 32, 2549-2553 (1994).
10. W.-C. Wang, E. J. Kramer, W. G. Sachse, Effects of high –pressure CO_2 on the glass transition temperature and mechanical properties of polystyrene, *J. Polym. Sci., Polym. Phys. Ed.*, 20, 1371-1384 (1982).
11. J. R. Fried, H.-C. Liu, C. Zhang, Effect of sorbed carbon dioxide on the dynamic mechanical properties of glassy polymers, *J. Polym. Sci., Polym. Part C*, 27, 385-392 (1989).
12. T. S. Chow, Molecular interpretation of the glass transition temperature of polymerdiluent systems, *Macromolecules*, 13, 362-364 (1980).
13. M. Wessling, Z. Borneman, Th. Van den Boomgaard, C. A. Smolders, Carbon dioxide foaming of glassy polymers, *J. Appl. Polym. Sci.*, 53, 1497-1512 (1994).
14. H. Hachisuka, T. Sato, T. Imai, Y. Tsujita, A. Takizawa, T. Kinoshita, Glass transition temperature of glassy polymers plasticized by CO_2 gas, *Polymer Journal*, 22, 1, 77 (1990).
15. J.-S. Wang, Y. Kamiya, Y. Naito, Effects of CO_2 conditioning on sorption, dilation, and transport properties of polysulfone, *Journal of Polymer Science: Part B: Polymer Physics*, 36, 1695 (1998).
16. K. Tanaka, M. Ito, H. Kita, K. Okamoto, Y. Ito, The effects of CO2-conditioning of polymers on positron annihilation and gas permeation properties, *Bull. Chem. Soc. Jpn.*, 68, 3011-3017 (1995).
17. G. K. Fleming and W. J. Koros, Dilation of Polymers by Sorption of Carbon Dioxide at Elevated Pressures. 1. Silicone Rubber and Unconditioned Polycarbonate, *Macromolecules*, 19, 2285 (1986).
18. G. K. Fleming and W. J. Koros, Carbon Dioxide Conditioning Effects on Sorption and Volume Dilation Behavior for bisphenol A - Polycarbonate, *Macromolecules*, 23, 1353 (1990).
19. A. G. Wonders and D. R. Paul, Effects of CO_2 Exposure History on Sorption and transport in Polycarbonate, *Journal of Membrane Science*, 5, 63 (1979).
20. S. M. Jordan, W. J. Koros, J. K. Beasley, Characterization of CO_2-induced conditioning of polycarbonate films using penetrants with different solubilities, *Journal of Membrane Science*, 43, 103-120 (1989).
21. D. S. Pope, G. K. Fleming, W. J. Koros, Effect of various exposure histories on sorption and dilation in a family of polycarbonates, *Macromolecules*, 23, 2988 (1990).
22. W. R. Vieth, L. H. Dao, and H. Pedersen, Non-equilibrium microstructural and transport characteristics of glassy poly(ethylene terephthalate), *Journal of Membrane Science*, 60, 41-62 (1991).
23. P. Gotthardt, A. Grűger, H. g. Brion, R. Plaetschke, and R. Kirchheim, Volume change of glassy polymers by sorption of small molecules and its relation to the intermolecular space, *Macromolecules*, 30, 8058-8065 (1997).
24. S.-H. Chen, S.-L. Huang, K.-C. Yu, J.-Y. Lai, M.-T. Liang, Effect of CO_2 treated polycarbonate membranes on gas transport and sorption properties, *Journal of Membrane Science*, 172, 105-112 (2000).

25. B. G. Risch and G. L. Wilkes, Effects of physical aging and carbon dioxide absorption in bisphenol-A polycarbonate, *Journal of Applied Polymer Science*, 56, 1511 (1995).
26. A. H. Chan and D. R. Paul, Influence of history on the gas sorption, thermal, and mechanical properties of glassy polycarbonate, *Journal of Applied Polymer Science*, 24, 1539-1550 (1979).
27. J. S. Chiou, J. W. Barlow and D. R. Paul, Polymer Crystallization Induced by sorption of CO_2 Gas, *Journal of applied Polymer Science*, 30, 3911 (1985).
28. Christelle M. Laot, Understanding gas transport in physically aged, oriented and pressure densified amorphous glassy bisphenol-A polycarbonate, PhD preliminary examination thesis, Virginia Polytechnic Institute and State University, VA, USA, December 17, 1999.
29. J. L. Duda and J. M. Zielinski, Free-Volume Theory, *Plastics Engineering*, 32, 143 (1996).
30. M. H. Cohen and D. Turnbull, *J. Chem. Phys.*, 31, 1164 (1959).
31. J. S. Vrentas and J. L. Duda, *J. Polym. Sci.*, 15, 403 (1977).
32. J. S. Vrentas and J. L. Duda, *J. Polym. Sci.*, 15, 417 (1977).
33. H. Fujita, *Fortschr. Hochpolym. Forsch.*, 3, 1 (1961).
34. C. Nagel, E. Schmidtke, K. Gűnther-Schade, D. Hofmann, D. Fritsch, T. Strunskus, and F. Faupel, Free volume distributions in glassy polymer membranes: comparison between molecular modeling and experiments, *Macromolecules*, 33, 2242-2248 (2000).
35. T. Banerjee and G. G. Lipscomb, Calorimetric probes of carbon dioxide sorption in bisphenol-A based polymers, *Polymer*, 38, 23, 5807 (1997).
36. U. Kriesten and J. M. Hutchinson, On the use of a density gradient column to monitor the physical ageing of polystyrene, *Polymer*, 33, 22, 4875-4877 (1992).
37. Seungman Sohn, personal communication.
38. R. Wimberger-Friedl, G. Prast, A. V. Kurstjens, and J. G. de Bruin, Measurement of the density distributions in quenched polycarbonate specimens by a quantitative Schlieren optical technique, *Journal of Polymer Science: Part B: Polymer Physics*, 30, 83-90 (1992).
39. R. Wimberger-Friedl and J. G. de Bruin, The very long-term volume recovery of polycarbonate: is self-retardation finite? *Macromolecules*, 29, 4992-4997 (1996).
40. J. Bicerano, editor, Prediction of polymer properties, 2nd edition, revised and expanded, Marcel Dekker, Inc., New York, 1996.
41. S. Matsuoka, A. Hale, Cooperative relaxation processes in polymers, *Journal of Applied Polymer Science*, 77-93 (1997).
42. A. J. Kovacs, J. J. Aklonis, J. M. Hutchinson, and A. R. Ramos, Isobaric volume and enthalpy recovery of glasses. II. A transparent multiparameter theory, *Journal of Polymer Science: Polymer Physics Edition*, 17, 1097-1162 (1979).
43. A. J. Kovacs, A multiparameter approach for structural recovery of glasses and its implication for their physical properties, in Structure and mobility in molecular and atomic glasses, edited by J. M. O'Reilly and M. Goldstein, *Annals of the New York Academy of Sciences*, 371, 38-66 (1981).
44. Dr. Hervé Marand, lecture notes.

45. B.–S. Hsu, S.-H. Kwan, Directional anisotropy of dielectric β-relaxation in oriented poly(ethylene terephthalate), *Journal of Polymer Science: Polymer Physics Edition*, 14, 1591 (1976).
46. D. M. Bigg, A review of positron annihilation lifetime spectroscopy as applied to the physical aging of polymers, *Polymer Enginering and Science*, 36, 6, 737 (1996).
47. W. J. Davis and R. A. Pethrick, Investigation of physical ageing in polymethylmethacrylate using positron annihilation, dielectric relaxation and dynamic mechanical thermal analysis, *Polymer*, 39, 2, 255 (1998).
48. J. M. Hutchinson, J. J. Aklonis, and A. J. Kovacs, A new phenomenological approach to volume recovery in glasses, *Polymer preprints*, 16, 2, 94-99 (1975).
49. H. Hachisuka, H. Takizawa, Y. Tsujita, A. Takizawa, and T. Kinoshita, Gas transport properties in polycarbonate films with various unrelaxed volumes, *Polymer*, 32, 13, 2382-2386 (1991).
50. R. Greiner and F. R. Schwarzl, Thermal contraction and volume relaxation of amorphous polymers, *Rheologica Acta*, 23, 378-395 (1984).
51. J. H. Gibbs and E. A. DiMarzio, *J. Chem. Phys.*, 28, 3, 373 (1958).
52. J. M. Hutchinson, S. Smith, B. Horne, and G. M. Gourlay, Physical aging of polycarbonate: enthalpy relaxation, creep response, and yielding behavior, *Macromolecules*, 32, 5046-5061 (1999).
53. T. G. Fox and P. J. Flory, *J. Am. Chem. Soc.*, 70, 2384 (1948).
54. T. G. Fox and P. J. Flory, *J. Appl. Phys.*, 21, 581 (1950).
55. D. M. Colucci, G. B. McKenna, J. J. Filliben, A. Lee, D. B. Curliss, K. B. Bowman, J. D. Russell, Isochoric and isobaric glass formation: similarities and differences, *Journal of Polymer Science: Physics Edition*, 1561-1573 (1997).
56. P. Zoller, A study of the pressure-volume-temperature relationships of four related amorphous polymers: polycarbonate, polyarylate, phenoxy, and polysulfone, *Journal of Polymer Science: Polymer Physics Edition*, 20, 1453-1464 (1982).
57. J. A. Schouten, J. Scholten, N. Nelissen, and E. Nies, Influence of pressure on the thermal properties of polystyrene, *Polymer Communications*, 32, 14, 421-422 (1991).
58. A. Weitz, B. Wunderlich, Thermal analysis and dilatometry of glasses formed under elevated pressure, *Journal of Polymer Science: Polymer Physics Edition*, 12, 2473-2491 (1974).
59. J. J. Aklonis and A. J. Kovacs, A new look at the glass transition, 267- ( ).
60. O. Araki, M. Horie, T. Masuda, Physical aging of polycarbonate investigated by dynamic viscoelasticity, *Journal of Polymer Science: Part B: Polymer Physics*, 39, 337-341 (2001).
61. S. Matsuoka, Relaxation phenomena in polymers, Hanser Publishers, NY, 1992.
62. K. Takahara, H. Saito, T. Inoue, Physical aging in poly(methyl methacrylate) glass: densification via density fluctuation, *Polymer*, 40, 3729-3733 (1999).
63. M. D. Shelby and G. L. Wilkes, Thermodynamic characterization of the oriented state of bisphenol A polycarbonate as it pertains to enhanced physical aging, *Journal of Polymer Science: Part B: Polymer Physics*, 36, 2111 (1998).

64. E. Ito, T. Hatakeyama, Studies of the amorphous region of polymers- II - Relationship between change of structure and glass-transition temperature in polycarbonate, *Journal of Polymer Science: Polymer Physics Edition*, 13, 2313-2320 (1975).
65. H. H. Song and R.-J. Roe, Structural change accompanying volume change in amorphous polystyrene as studied by small and intermediate angle X-ray scattering, *Macromolecules*, 20, 2723-2732 (1987).
66. L. H. Sperling, *Introduction to physical polymer science*, Second edition, John Wiley and Sons, 1992.
67. Dr. G. L. Wilkes, lecture notes.
68. Dr. T. Ward, lecture notes.
69. J. Y. Park, D. R. Paul, Correlation and prediction of gas permeability in glassy polymer membrane materials via a modified free volume based group contribution method, *Journal of Membrane Science*, 125, 23-39 (1997).
70. Y. Yampolskii, S. Shishatskii, A. Alentiev, K. Loza, Correlations with and prediction of activation energies of gas permeation and diffusion in glassy polymers, *Journal of Membrane Science*, 148, 59-69 (1998).
71. W. J. Koros and G. K. Fleming, Membrane-based Gas Separation, *Journal of Membrane Science*, 83, 1-80, (1993).
72. W. J. Koros and M. W. Hellums, Transport Properties, Encyclopedia of Polymer Science and Engineering, 2nd Edition, H. F. Mark, N. M. Bikales, C. G. Overberger, G. Mendes, Eds., John Wiley and Sons, New York, Supplement volume, 1989.
73. D. W. Breck, Zeolite molecular sieves, John Wiley & Sons, Inc., New York, 1974.
74. W. J. Koros, A. H. Chan and D. R. Paul, Sorption and Transport of Various Gases in Polycarbonate, *Journal of Membrane Science*, 2, 165 (1977).
75. L. M. Costello and W. J. Koros, Temperature Dependence of Gas Sorption and Transport Properties in Polymers: Measurements and Applications, *Industrial Engineering Chemical Research*, 31, 2708 (1992).
76. S. A. Stern, Y. Mi, H. Yamamoto, A. K. St. Clair, *J. Polym. Sci., Polym. Phys. Ed.*, 27, 1887 (1989).
77. V. M. Shah, S. A. Stern and P. J. Ludovice, Estimation of the Free Volume in Polymers by Means of a Monte Carlo Technique, *Macromolecules*, 22, 4660 (1989).
78. D. Hofman, J. Ulbrich, D. Fritsch, D. Paul, Molecular modelling simulation of gas transport in amorphous polyimide and poly(amide imide) membrane materials, *Polymer*, 37, 21, 4773-4785 (1996).
79. A. Q. Tool, *J. Am. Ceram. Soci.*, 31, 177-186 (1948).
80. L. C. E. Struik, Physical aging in amorphous polymers and other materials, Elsevier, New York, 1978.
81. G. Strobl, The physics of polymers, Concepts for understanding their structures and behavior, Springer, NY, 1996.
82. J. Lu, Y. Wang, and D. Chen, Infrared spectroscopic and modulated differential scanning calorimetry study of physical aging in bisphenol-A polycarbonate, *Polymer Journal*, 32, 7, 610-615 (2000).

83. N. Heymans, FTIR investigation of structural modification of polycarbonate during thermodynamical treatments, *Polymer*, 38, 14, 3435 (1997).
84. N. Heymans and B. Dequenne, Relationship between conformation and enthalpy or volume relaxation in polycarbonate, *Polymer*, 42, 5337-5342 (2001).
85. C. A. Angell, The old problems of glass and the glass transition, and the many new twists, *Proc. Natl. Acad. Sci.*, 92, 6675-6682 (1995).
86. C. M. Roland, P. G. Santangelo, and K. L. Ngai, The application of the energy landscape model to polymers, *Journal of Chemical Physics*, 111, 12, 5593-5598 (1999).
87. Computational modeling of polymers, edited by Jozef Bicerano, Marcel Dekker, Inc., NY, 1992.
88. D. Hofmann, L. Fritz, J. Ulbrich, and D. Paul, Molecular modelling of amorphous membrane polymers, *Polymer*, 38, 25, 6145-6155 (1997).
89. E. Tocci, D. Hofmann, D. Paul, N. Russo, E. Drioli, A molecular simulation study on gas diffusion in a dense poly(ether-ether-ketone) membrane, *Polymer*, 42, 521-533 (2001).
90. P. S. Rallabandi, A. P. Thompson, and D. M. Ford, A molecular modeling study of entropic and energetic selectivities in air separation with glassy polymers, *Macromolecules*, 33, 3142-3152 (2000).
91. H. Higuchi, Z. Yu, A. M. Jamieson, R. Simha, and J. D. McGervey, Thermal history and temperature dependence of viscoelastic properties of polymer glasses: relation to free volume quantities, *Journal of Polymer Science: Part B: Polymer Physics*, 33, 2295-2305 (1995).
92. H. Higuchi, A. M. Jamieson, and R. Simha, Free volume quantities and viscoelasticity of polymer glasses, *Journal of Polymer Science: Part B: Polymer Physics*, 34, 1423-1426 (1996).
93. A. Bondi, Physical properties of molecular crystals, liquids, and glasses, Wiley, New York, 1968.
94. D. W. Van Krevelen, Properties of Polymers, Their correlation with chemical structure; their numerical estimation and prediction from additive group contributions, Third Ed, Elsevier, NY, 1990.
95. M. W. Hellums, W. J. Koros, G. R. Husk and D. R. Paul, Fluorinated polycarbonates for gas separation applications, *Journal of Membrane Science*, 46, 93 (1989).
96. M. D. Shelby, G. L. Wilkes, M. R. Tant, J. Zawada, T. J. Bastow and A. J. Hill, Amorphous orientation in glassy polycarbonate, *ACS, Polymeric Materials Science and Engineering, Conference Proceedings*, San Francisco, Spring 1997, 76, 485-6.
97. Y. C. Jean, J.-P. Yuan, J. Liu, Q. Deng, and H. Yang, Correlations between gas permeation and free-volume hole properties probed by positron annihilation spectroscopy, *Journal of Polymer Science: Part B: Polymer Physics*, 33, 2365-2371 (1995).
98. S. Arizzi, P. H. Mott, U. W. Suter, *J. Polym. Sci., Part B, Polym. Phys.*, 30, 415-426 (1992).
99. Y. C. Jean, Y. Rhee, Y. Lou, D. Shelby, G. L. Wilkes, Anisotropy of hole structures in oriented polycarbonate probed by two-dimensional angular

correlation of annihilation radiation, *Journal of Polymer Science: Part B: Polymer Physics*, 34, 2979-2985 (1996).
100. R. H. Gee and R. H. Boyd, Small penetrant diffusion in polybutadiene: a molecular dynamics simulation study, *Polymer*, 36, 1435 (1995).
101. D. R. Paul, Yuri P. Yampol'skii, editors, *Polymeric gas separation membranes*, CRC Press, Boca Raton, 1994.
102. Y. Kobayashi, K. Haraya, S. Hattori, *Polymer*, 35, 925-928 (1994).
103. S. Trohalaki, L. C. DeBolt, J. E. Mark, H. L. Frisch, *Macromolecules*, 23, 813-816 (1990).
104. Y. Maeda and D. R. Paul, Effect of AntiPlasticization on Gas Sorption and Transport. III. Free Volume Interpretation, *Journal of Polymer Science: Part B: Polymer Physics*, 25, 1005 (1987).
105. A. Thran, G. Kroll, F. Faupel, Correlation between fractional free volume and diffusivity of gas molecules in glassy polymers, *Journal of Polymer Science: Part B: Polymer Physics*, 37, 3344-3358 (1999).
106. W. J. Koros, M. R. Coleman, and D. R. B. Walker, *Ann. Rev. Mater. Sci.*, 22, 47 (1992).
107. W. J. Koros, G. K. Fleming, S. M. Jordon, T. H. Kim, and H. H. Hoehn, *Prog. Polym. Sci.*, 13, 339 (1988).
108. C. K. Kim, M. Aguilar-Vega, and D. R. Paul, Dynamic mechanical and gas transport properties of blends and random copolymers of bisphenol-A polycarbonate and tetramethyl bisphenol-A polycarbonate, *Journal of Polymer Science: Part B: Polymer Physics*, 30, 1131-1142 (1992).
109. Polycarbonates, Ullmann's Encyclopedia of Industril Chemistry, vol A21, 207 (1992).
110. H. Higuchi, A. M. Jamieson and R. Simha, Free volume quantities and viscoelasticity of polymer glasses, *Journal of Polymer Science: Part B: Polymer Physics*, 34, 1423-1426 (1996).
111. W. M. Lee, Selection of barrier materials from molecular structure, *Polym. Eng. Sci.*, 20, 65-69 (1980).
112. A. K. Doolittle, *J. Appl. Phys.*, 22, 1031 (1951).
113. A. K. Doolittle, *J. Appl. Phys.*, 22, 12, 1471 (1951).
114. A. Singh, and W. J. Koros, Significance of Entropic Selesctivity for Advanced Gas Separation Membranes, *Ind. Eng. Chem. Res.*, 35, 1231, (1996).
115. Handbook of chemistry & physics, 80th edition, D. R. Lide, editor, CRC Press, NY, 1999.
116. L. M. Costello and W. J. Koros, Comparison of Pure and Mixed Gas CO_2 and CH_4 Permeabilities in Polycarbonate: Effect of Temperature, *Ind. Eng. Chem. Res.*, 32, 2277 (1993).
117. C. Zener, *J. Appl. Phys.*, 22, 372 91951).
118. M. Pönitsch and R. Kirchheim, Relation between prefactor and activation energy for the diffusion of atoms and small molecules in polymers, *Scripta Materialia*, 34, 9, 1479-1482 (1996).
119. B. P. Tikhomirov, H. B. Hopfenberg, V. Stannett and J. L. Williams, *Makromol. Chem.*, 118, 177 (1968).
120. W. W. Brandt, *J. Phys. Chem.*, 63, 1080 (1959).

121. P. Meares, Diffusion of gases through polyvinyl acetate, *J. Am. Chem. Soc.*, 76, 3415 (1954).
122. V. Teplyakov, P. Meares, Correlation aspects of the selective gas permeability of polymeric materials and membranes, *Gas Sep. Purif.*, 4, 65 (1990).
123. A. Shimazu, T. Miyazaki, K. Ikeda, Interpretation of d-spacing determined by wide angle X-ray scattering in 6FDA-based polyimide by molecular modeling, *Journal of Membrane Science*, 166, 113-118 (2000).
124. N. Muruganandam, W. J. Koros and D. R. Paul, *J. Polym. Sci., Polym. Phys. Ed.*, 25, 1999 (1987).
125. N. Muruganandam and D. R. Paul, *Journal of Membrane Science*, 34, 185 (1987).

Chapter 7

Physical aging in amorphous glassy bisphenol-A polycarbonate as revealed by gas transport measurements

7.1. Introduction

Glassy polymers tend to decrease their excess free volume with time by undergoing further chain packing, without crystallization. This phenomenon is referred to as physical aging or structural relaxation. A background has been provided in Chapter 3. Below the glass transition temperature T_g, some free volume still remains allowing local motions and therefore conformational rearrangements. The molecules can oscillate between a limited number of conformations with minimum energy [1-3]. Obviously, the relaxation towards equilibrium takes an extremely long time since polymers below their glass transition temperature do not have sufficient thermal energy to attain equilibrium rapidly.

The effects of physical aging on the gas transport properties have been reported in Chapter 3. The gas transport parameters that are the permeability coefficient P, the diffusion coefficient D and the solubility coefficient S were generally observed to decrease with aging. The decrease in the gas transport properties was attributed to the loss of free volume with sub-T_g annealing. However most of the published data were complicated by several factors, such as conditioning, samples used as-received or cast

from solution, plasticization induced by carbon dioxide, or sorption experiments themselves. The reader should consult Chapter 3 for more details. New studies free of the above complications should be conducted in order to confirm the trends reported in the literature. We do expect that permeation experiments are more accurate than sorption experiments (whose problems have been mentioned in Chapter 3) and can be used as a tool to investigate the process happening at the molecular level with physical aging. Inert gases with different kinetic diameters will be used to probe the free volume of polymers. The same membrane will be used twice to make it possible to compare data within a limited error range. A recapitulation of the procedure selected in this project is shown in Table 7.1 and compared with the literature.

	Literature	This project
processing	solvent cast	hot press
preparation	conditioning	no conditioning
gas	CO_2	inert gases
membrane	different membranes	same membrane used twice
apparatus	sorption	permeation

Table 7.1: Comparison of the methods commonly found in the literature to study aging compared to the one chosen in this research.

As pointed out in Chapter 3, there still remain several unanswered questions about physical aging, such as which cavity sizes are more likely to be affected by the aging phenomena. According to Curro and Roe [4], thermal density fluctuations in polycarbonate on isothermal sub-T_g annealing were observed by small-angle X-ray scattering (SAXS) measurements in a narrow range from about 130^{o}C to 147^{o}C only. Although other properties such as specific volume or density did not change much in that limited temperature interval, they did change significantly at lower temperatures. SAXS data were collected for up to 200min for each annealing temperature. A model was developed by the researchers to interpret the density fluctuations in terms of the free volume concept. The conclusions indicated that although the amount of free volume decreased with aging at sub-T_g annealing temperatures below the glass transition range, the average free volume hole size increased with aging. An increase in the average hole size was attributed to two possible factors: either a coalescence of the cavities or an

elimination of the small cavities, with the larger ones remaining unchanged. Wendorff [5] could not observe any changes in the electron density fluctuations of polycarbonate annealed at 124^{o}C for up to 1000h either. Different conclusions were obtained by positron annihilation lifetime spectroscopy (PALS). It was found that on aging at temperatures below the glass transition range, the holes in polycarbonate did not really decrease in size but in number [6-11]. Indeed, τ_3 was reported to remain pretty much constant with aging whereas I_3 was significantly reduced. Therefore, the free volume was reduced with aging as similarly concluded from the SAXS results, but the average hole size remained unaffected by aging. Nevertheless, the existence of a distribution of τ_3 lifetimes and thus hole sizes has been suggested [11]. Similarly, all the cavities in polycarbonate were reported to decrease equally with physical aging by photochromic probes [12]. The average cavity size was suggested to remain constant. A PALS study on polycarbonate has nevertheless shown that the average hole size was reduced with physical aging at 120^{o}C [13]. The SAXS, PALS, and photochromic probe results showed therefore that below the glass transition region the average hole sizes in polycarbonate probed by those three techniques do not appear to be similarly affected by aging. The different behaviors may be caused by the range of hole sizes probed by each technique. Nevertheless, the data should be looked at with scrutiny since several complications arise in the analysis, such as assumption of spherical cavities and radiation effects for PALS, etc (see Chapter 3 for details).

Furthermore, differences between PALS or SAXS results and gas transport properties can also be noticed. At the glass transition temperature T_g of polycarbonate, a change in the slope of τ_3 versus temperature is noticed by PALS measurements [10, 11] and a change in the slope of the X-ray intensity I(0) versus temperature is seen by SAXS measurements (I(0) was obtained by extrapolation of the observed intensity I(s) to $s \rightarrow 0$, with $s = 2\sin\theta/\lambda$) [4]. Nevertheless no change in the slope of the permeability coefficient P versus temperature is noticed at T_g for polycarbonate using various gases [14]. The curve was observed to increase gradually at the T_g, in contrast with mechanical or thermal properties that vary non-linearly in the transition region.

Probing the free volume with gas molecules of different sizes can give information on the size of the microvoids and on the structural scale of changes occurring during physical aging. Gas permeation can be used as a tool to probe the free volume of polymeric materials on a microscopic level since the diffusion and the solubility coefficients themselves can be evaluated from permeation results.

Emphasis will be placed in this study on the sub-T_g annealing at the annealing temperature of 120^{o}C. Polymeric films are usually used for practical applications in the glassy state and not in the glass transition range where properties such as the storage modulus E' decrease tremendously. No drop in E' can already be seen at 120^{o}C on the DMTA curve. The effects of physical aging should be clearly visible at 120^{o}C. In addition, the effect of the cooling rate on the physical aging rate will also be examined, since this may affect the aging rate in an unexpected way. As the permeability coefficient corresponds to the product of the diffusion D and the solubility S coefficients, the combined effects of D and S may not result in common trends seen for physical properties most likely directly linked with the free volume content.

The first section of this chapter gives the experimental details. The results are presented and discussed in the second section.

7.2. Experimental details

The following subsections mention briefly the materials and the instrumental methods. The complete experimental details have been provided in Chapter 4. The reader should refer to this particular chapter for deeper understanding of the materials and the instrumental methods used in this research.

7.2.1. The materials

Bisphenol-A polycarbonate (BPA-PC) pellets were purchased from Aldrich. The density was given as 1.2 g/cm^3 at 20^{o}C, the refractive index n_D^{20} as 1.585, and the glass

transition temperature T_g as 150°C. The weight average molecular weight M_w was determined by GPC to be about 34,000 g/mol, and the polydispersity index about 2.2.

Sheets originating from the Aldrich pellets were compression-molded. The polymeric sheets were kept in a dessicator at all time to avoid any water moisture uptake. Prior to experiments, polymeric sheets were put between Kapton® sheets and copper metal plates, and suspended in the center of an internal fan oven. The samples were heated in the oven from room temperature (30°C) to 165°C at a heating rate of 40°C/min, kept at 165°C for 15min to remove thermal history, and cooled within the oven at a controlled rate of typically 40°C/min to room temperature (30°C). While studying the influence of the cooling rate on the physical aging rate, the samples were cooled from 165°C at the following controlled rates: 0.5°C/min, 10°C/min, and 40°C/min. The system consisting of the polymer sandwiched between the Kapton® sheets and the metal plates was also cooled by opening the door of the oven and by blowing air immediately inside the oven with an external fan. The cooling rate was in excess of 40°C/min. The polymer films were used immediately once taken from the oven.

The thicknesses of the sheets were about 130μm.

Samples to be used for permeation experiments were treated as follows. Permeation was performed at 35°C on the polycarbonate films described above, and thus freshly processed. Once the permeation data had been collected, the films were put back between the Kapton® sheets and the copper metal plates, together with the remaining samples to be used for density measurements, and the metal plates were suspended in the center of the internal fan oven. The “remaining samples” refer to the fresh polycarbonate samples that were left at room temperature in a dessicator while the membranes were studied by permeation experiments at 35°C. The samples were heated in the internal fan oven from room temperature (30°C) to the sub-T_g annealing temperature T_e at a heating rate of 40°C/min, kept at T_e for a defined annealing time t_e, and cooled within the oven at a cooling rate of 40°C/min to room temperature (30°C). Permeation was performed immediately at 35°C on the aged films. A schematic of the temperature program is given in Figure 7.1. As mentioned previously, since the thickness is crucial in permeation experiments, the same membrane was used twice in permeation experiments: once as the

sample described in the beginning of this subsection and then as the aged sample. This procedure made it possible to compare data within a limited error range. The error was believed to be lower than the one introduced if two films are used. It is indeed rather difficult to generate films of identical thicknesses and perfectly flat by hot press. It is assumed that the low applied pressures used in permeation experiments do not modify the structure of the polymer. No change in thickness could be detected after sub-T_g annealing.

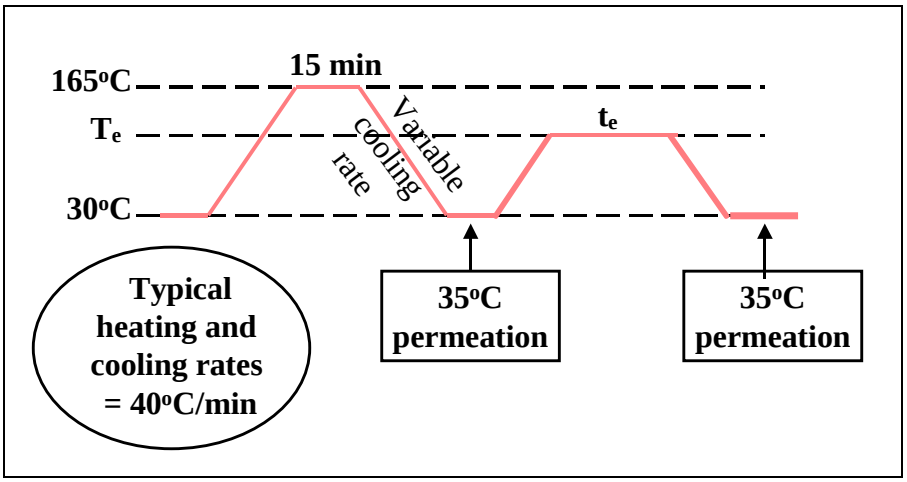

Figure 7.1: Schematic of the preparation of the samples for permeation experiments. The cooling and heating rates were typically chosen as 40°C/min, except for the following. The cooling rates from 165°C to 30°C were chosen as 0.5°C/min, 10°C/min, or 40°C/min. Another cooling rate in excess of 40°C/min was also achieved by blowing air inside the oven with an external fan.

Please note that it was not possible to heat the fresh samples from room temperature to 165°C at a heating rate of 40°C/min, leave them at 165°C for 15min, cool them at a controlled rate to T_e, leave them at T_e for t_e, cool them to room temperature, perform permeation experiments at 35°C on them, heat the samples back above T_g to remove thermal history, and finally perform permeation at 35°C again after this. Indeed, the shapes and the thicknesses of the films changed between the aged samples and the fresh samples because of the softening taking place in the polymeric matrix above T_g. And such a change is crucial in permeation experiments. The change in the permeation profile with aging needs to be determined in the present study. And for this to be done,

the change in thickness needs to be negligible with aging. Since the thickness is crucial in permeation studies, the option given above could not be considered.

Because the aged samples could not be refreshed for permeation experiments, we are aware that memory effects may come into play into our experimental data [15].

7.2.2. The instrumental methods

The densities were obtained at 18^{o}C using a linear density gradient column made of an aqueous solution of sodium bromide. The theoretical resolution of the column was about 5×10^{-5} g/cm^3. At least three samples of the same thermal history were dropped in the column to verify reproducibility.

In order to look for any conformational changes, FTIR spectra were collected in the ATR (attenuated total reflectance) mode using a zinc selenide ZnSe crystal.

The dynamic mechanical experiments were carried out in the tensile mode. While studying physical aging effects however, no calibration check was performed on the DMTA apparatus before collecting all the data for the set of samples. This ensured that the DMTA internal parameters remained unchanged between sample runs.

Dynamic temperature ramp experiments were carried out with the following conditions. A torque of 10cNm was used on each clamp. The frequency was chosen as 1Hz, the heating rate as 2^{o}C/min, and the initial temperature as 25^{o}C. The static force was optimized at room temperature by dynamic frequency sweep test (strain control). The strain was chosen as 0.025%, unless indicated. In the aging experiments, an extremely low strain level of 0.004% was selected in order to avoid any structural rearrangements that may occur at a higher strain level and hence destroy aging. The data were reproducible within 0.3%.

Dynamic time sweep tests performed on samples cooled at different rates required preliminary data. The static force was determined at the chosen annealing temperature T_e by dynamic frequency sweep test (strain control). The strain was chosen as 0.025%. The sample was left for 5min at T_e before starting the test itself in order to reach the desired

annealing temperature T_e indeed. The resulting force at 3Hz was recorded for further testing. Once the previous test was finished, the gap between the grips was put back to 12mm without opening the compartment of the DMTA in order to maintain the temperature at T_e. Dynamic time sweep experiments were immediately carried out with the following conditions. A torque of 15cNm was used on each clamp. The frequency was chosen as 3Hz, the strain as 0.025%, the static force as determined above, and the temperature as the annealing temperature T_e. Data were collected every 10s for 20h. It was determined by GPC that the samples did not degrade after this time at T_e. No change in color was noticed on the samples either. The time needed between both DMTA tests given above was evaluated to be 5min. For each cooling rate treatment, at least two samples were run in the DMTA to verify reproducibility.

Dynamic time sweep experiments were performed at various temperatures for samples cooled at 40^{o}C/min. 5min were allowed prior to testing for temperature equilibrium. The strain was chosen as 0.025%, and the frequency was fixed at 5Hz.

Dynamic time sweep experiments were also carried out in order to possibly determine the aging shift rate. The experiments were performed on a fresh sample at a given annealing temperature as a function of the logarithm of the annealing time for several frequencies. About 6 minutes were allowed prior to testing to ensure temperature equilibrium. The analysis was similar as the one used to build master curves of a fresh polymer (see Chapter 5 for details). The data were plotted back as a function of the logarithm of the frequency for different annealing times. A reference annealing time was selected and the curves were moved horizontally around the particular reference curve. While conducting isothermal DMTA experiments, the storage modulus increased with aging time, whereas the loss modulus decreased. The decrease in E" originated from the absorption of heat by the sample, as what is measured in DSC experiments. The polycarbonate samples were not found to be degraded under atmospheric pressure by GPC measurements for the annealing times chosen in the time sweep experiments.

Permeation experiments were carried out at 35^{o}C using He, O_2, and N_2, in that given sequence. The applied pressures were kept constant at about 2.5atm for He and about 3.9atm for both O_2 and N_2. Three measurements were taken for each gas to ensure

reproducibility and to calculate the error involved in the permeation results. Permeation experiments were carried out twice on the same membrane (fresh and aged) in order to evaluate the percent change with aging within a limited error range. Once permeation data were obtained on the fresh sample, the membrane was degassed for a few hours before putting it in the oven for sub-T_g annealing. This ensured that the gas trapped inside the polymeric matrix did not interfere with the typical aging process. While collecting data a second time on the aged polymer, the membrane was placed exactly at the same position it was before in the permeation cell in order to avoid permeating gas molecules through the possibly present vacuum grease. Permeation experiments were also carried out on the same aged membrane at 40, 45, and 55^{o}C, right after the experiment at 35^{o}C in order to determine the activation energy for permeation. Deaging was assumed to be negligible at those temperatures within the timeframe of the experiments.

7.3. Results and discussion

Physical aging was investigated with time at a sub-T_g annealing temperature T_e of 120^{o}C on samples cooled at 40^{o}C/min. In addition, data obtained after a fixed annealing time for polycarbonate samples cooled at different cooling rates are also discussed.

Physical aging was characterized by measuring bulk properties as well as by probing the molecular level with gases using gas permeation experiments.

7.3.1. Annealing temperature determination

Samples cooled at 40^{o}C/min were chosen to be aged at sub-T_g annealing temperature T_e of 120^{o}C. Therefore, T_e corresponded to a temperature of (T_g – 33.3^{o}C), as calculated from the glass transition temperature of 153.3^{o}C reported in Chapter 6.

The value of T_e needed to be adjusted for samples cooled at different rates. We have:

$$T_e = T_g - xx\,^oC \qquad \text{Eq (7.1)}$$

where xx is a fixed number. The T_g values of the various samples are recapitulated in Table 7.2. Those numbers were extracted from the work presented in Chapter 6. Unfortunately, the gas chromatograph (GC) oven used to control the cooling rate could be programmed with 1°C resolution only. As a consequence, a common temperature of 120°C was chosen for T_e for all the samples of this research despite of the slight differences in their $T_{g's}$. The maximum T_g difference between samples was of about 0.8°C.

cooling rate	T_g (°C)
0.5	153.57
10	153.41
40	153.32
fan	152.79

Table 7.2: T_g as determined by DMTA experiments on the fresh samples (data taken from Chapter 6). The cooling rates are given in °C/min.

7.3.2. Density results

Changes in density with aging time were clearly observed at 120°C (see Figure 7.2). The density was found to increase linearly with the logarithm of aging time, in agreement with the literature [16-26]. The loss in the amount of free volume was thus linear with log t_e. The densification rate was evaluated to be around 0.00034 g/cm^3 for one decade for our samples cooled at 40°C/min. For comparison, the densification rates evaluated from specific volume data [27] can be estimated to be about 0 g/cm^3, 0.000177 g/cm^3, and 0.00035 g/cm^{3}per decade for polycarbonate samples cooled at 1°C/min, 10°C/min, and 80°C/min, respectively. Our results are therefore in "fair" agreement with the literature.

Furthermore, although the fresh polycarbonate samples were left at room temperature in a dessicator during about 16h before aging while other samples were in the permeation apparatus (see details in the experimental section), no deaging effects can be seen on the density data of Figure 7.2, at least in the timeframe selected here. Furthermore it is well-known that aging occurs very slowly in polycarbonate at room temperature, at least for aging periods under six months [27].

No crystallinity is believed to be present in the polycarbonate material, as this particular polymer is one of the most difficult to crystallize under normal conditions.

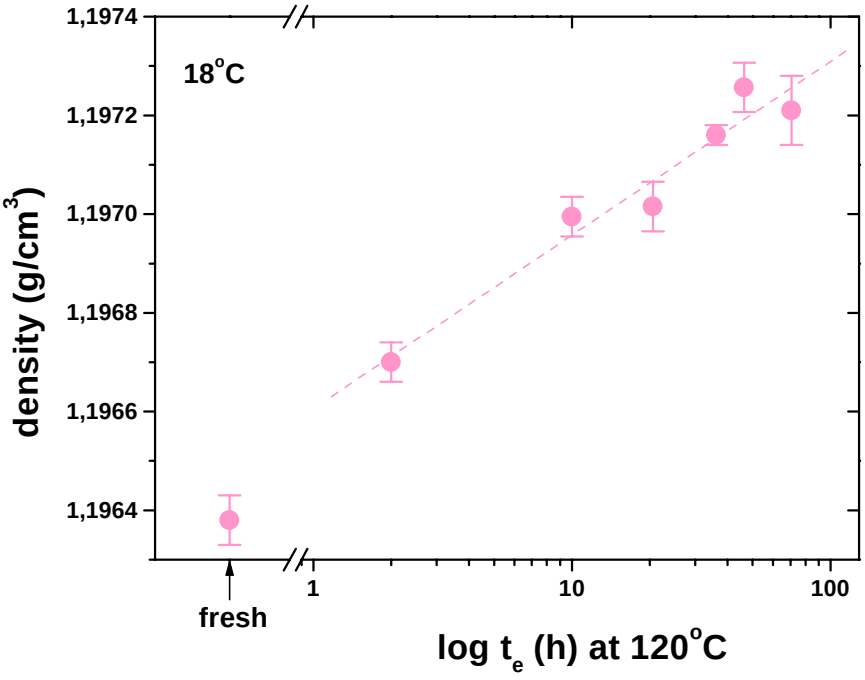

Figure 7.2: Density as a function of the aging time for a sample cooled at 40°C/min and aged at 120°C. The densities were measured at 18°C using a linear density gradient column.

In our attempts at investigating the effect of the cooling rate on the physical aging rate, the densities were measured as a function of log t_e for a sample initially cooled at 0.5°C/min. Unfortunately the data points remained within the experimental error range. As a consequence, it was not possible to determine the densification rate for that particular sample. We expect that the greater the initial free volume content, the greater the loss of this free volume with physical aging [27, 28].

7.3.3. FTIR results

In order to verify any conformational changes occurring within the sample with aging, ATR-FTIR spectra were collected for all the aged samples. Indeed, it has been shown that aging in polycarbonate is accompanied by local rearrangements [1, 2].

However no detectable changes could be noticed in this research in the peaks of interests. The fact that the contact pressure changed from one sample to another with the ATR technique induced some complications in comparing the intensity of the absorption bands. In addition since the spectra were not taken in situ as a function of aging but directly on aged samples instead it was more difficult to detect any conformational changes. It was not possible to collect spectra in the transmission mode due to the strong absorption of polycarbonate in the infrared range.

7.3.4. DMTA results

7.3.4.1. Physical aging characterization

Dynamic mechanical analysis provides information about molecular motions and morphology [29-31]. It has been shown in the literature that the intensity and the position of the β-relaxation for polycarbonate does not depend on the free volume and is not affected by aging [17, 32-34]. Therefore only the α-relaxation has been investigated in this research. The α-relaxation results from motions of the large segments of the polymer backbone whereas the β,γ,etc-relaxations are attributed to local motions. Polycarbonate does not exhibit any coupling between the β- and the α-relaxations. At room temperature the secondary relaxation is complete, while the α-relaxation does not contribute yet; there are no overlap between the two peaks. Actually one of the unique features of bisphenol-A polycarbonate is that its main and secondary relaxations are well separated in the thermal response. This makes aging easier to follow.

Although the effects of aging have been reported to be difficult to observe with DMTA because of the elevated frequencies involved in the experiments, aging of polycarbonate could be characterized in this research using DMTA. An extremely low strain level of 0.004% was selected in order to avoid any structural rearrangements that may occur at a higher strain level and hence destroy aging. Aging was followed closely as a function of the aging time at constant temperature. DMTA experiments were

performed at random on the aged samples. The DMTA traces happened to be more sensitive to the loss modulus E" than to the storage modulus E', and therefore only E" is shown in this study. E' is related to the mechanical energy stored per cycle whereas E" is related to the energy dissipated or converted to heat through viscous dissipation. Figure 7.3 shows the data obtained at an annealing temperature of 118^{o}C. Please note that a sub-T_g annealing temperature of 118^{o}C was chosen instead of 120^{o}C, because this was the temperature used in the preliminary studies. Unfortunately the DMTA apparatus did not function anymore later on. As seen in Figure 7.3, the width of the E" peak decreased with aging and the E" peak shifted to higher temperatures, hence indicating a greater value of the glass transition temperature T_g. These observations can be attributed to the decrease in the amount of the free volume with aging, as suggested from the Fox and Flory theory [35, 36]. Some confusion may here arise as one visualizes the typical specific volume / temperature curve drawn in Chapter 3. The fictive temperature reduces its value with sub-T_g annealing time. However here the observed T_g is seen to increase with aging. Problems of similar nature have been explained in Chapter 6 while discussing how the T_g value changes as the value is obtained on cooling or on heating.

The aging rates seemed to go through a maximum between 27h and 53h of aging. A sufficient amount of thermal energy may be needed to allow further conformational changes or cooperative motions. The change in the breath of the E" peak at 10^9 dyn/cm^2 is shown in Figure 7.4 as a function of log annealing time, along with the T_g values. The slope of the breadth of E" as a function of log t_e became strictly linear after 27h at 118^{o}C. However the fact that the breadth did not appear to be linear below 27h may be due to the fact that the DMTA traces were not normalized. At long aging times the E" peak was quite steep and therefore the breadth did not vary much from one fixed value of E" to another close one. However at lower aging times a slight change in the value of E" may affect the value of the breadth tremendously. From conclusions reached in Chapter 6, the breadth of the loss modulus E" peak obtained on heating may be an indication of the amount of free volume contained in the polymer, and therefore a linear decrease in this breadth should be observed with aging, as the density increases linearly with log (aging time) (see above). The observed T_g increased with aging, in agreement with published results [6, 37-41]. Nevertheless, this increase in T_g was not observed to be linear with log

t_e. This observation was actually expected from the results seen in previous chapters, which placed emphasis on showing that T_g and density were not directly correlated. Please note that the value of the T_g for the fresh polycarbonate differed from the one reported in Chapters 5 and 6 because of a slight change in the position of the DMTA thermocouple. Furthermore, the strain level selected in aging studies was more than six times lower than the one used in Chapters 5 and 6 (0.004% versus 0.025%). The magnitude of the modulus was found to decrease with annealing time, as shown in Figure 7.5.

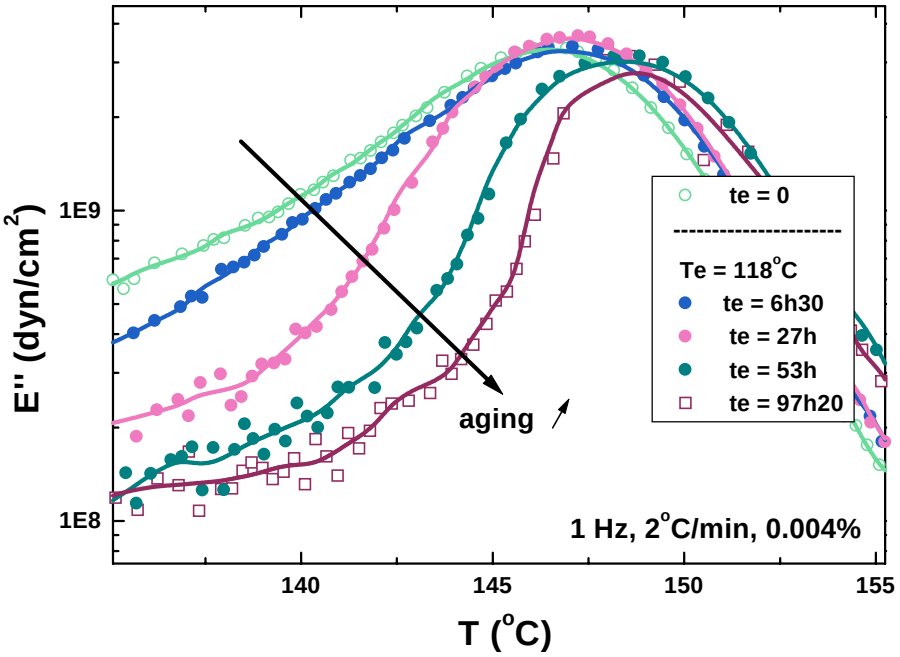

Figure 7.3: Effect of aging at 118°C on the loss modulus of polycarbonate. The DMTA conditions were the following: frequency = 1Hz, strain = 0.004%, initial temperature = 25°C, heating rate = 2°C/min, torque = 10cNm. Samples were tested in the DMTA in a random order.

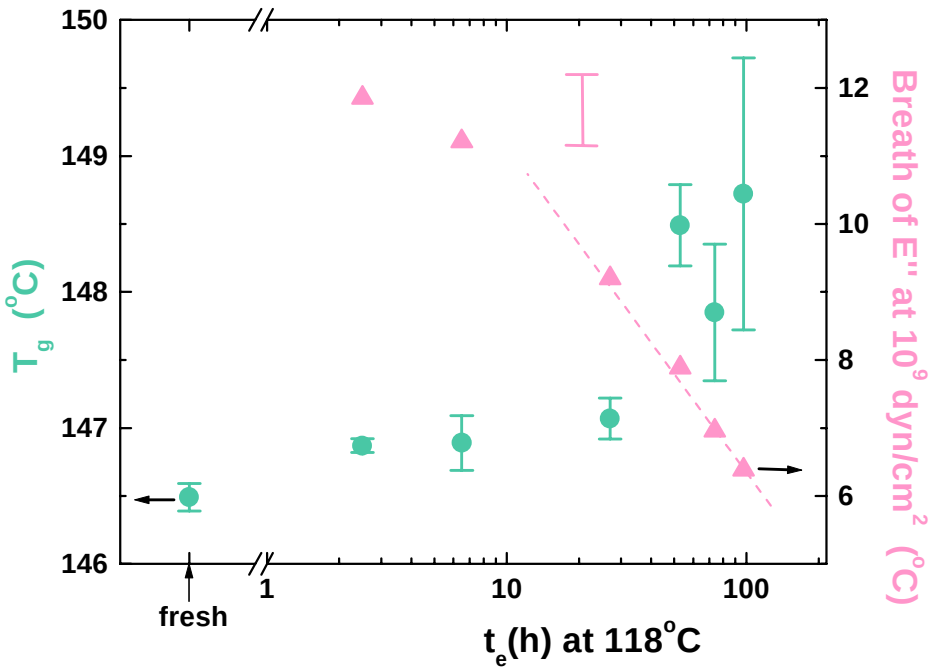

Figure 7.4: Change in the T_g (left axis) and in the breath of the loss modulus of polycarbonate at 10^9 dyn/cm^2 (right axis) as a function of annealing at 118°C. The T_g was taken as the maximum of the glass transition. The DMTA conditions were the following: frequency = 1Hz, strain = 0.004%, initial temperature = 25°C, heating rate = 2°C/min, torque = 10cNm.

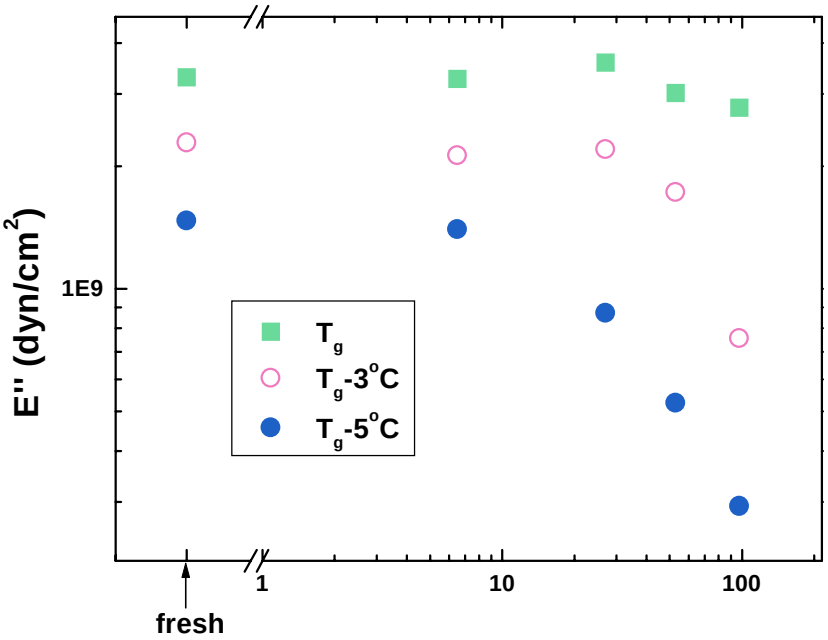

Figure 7.5: Change in the magnitude of the loss modulus as a function of annealing at 118°C for different temperatures (namely T_g, T_g-3°C, and T_g-5°C). The DMTA conditions were the following: frequency = 1Hz, strain = 0.004%, initial temperature = 25°C, heating rate = 2°C/min, torque = 10cNm. The T_g was taken as the maximum of the glass transition.

Aging studies were carried out at 140°C as well. However in this case no change in the temperature ramp DMTA traces could be observed. The fresh sample and the sample annealed at 140°C for up to 329h gave the same response. Other curves were collected between 1h and 329h and the same response was obtained. Therefore, aging performed in the neighborhood of T_g did not seem to show any changes with aging time, probably because the temperature was too high. Schultheisz and McKenna have actually shown that no aging was detectable above 137°C with stress relaxation experiments [42].

7.3.4.2. Memory effects characterization

In order to see if memory effects could be observed by DMTA, and therefore prove that the aging phenomenon was indeed the phenomenon observed by DMTA in the previous figures, the temperature in the aging oven was increased from 118°C to 127°C after 97h20 at 118°C. The new aging temperature was therefore still below T_g but above the previous aging temperature. DMTA measurements were collected on samples aged for various times at 127°C. As seen in Figure 7.6, the width of the α-relaxation peak first increased at short aging times, and the T_g decreased as well. This corresponded to the memory effects extensively studied by Kovacs [15]. Matsuoka [43] explained deaging effects by noting that they are related to the distribution of domain sizes. Since the polymer possesses a wide distribution of relaxation times, smaller domains with rapid relaxation times have already densified and reached equilibrium after some time at a particular aging temperature, while larger domains with slower relaxation times are still progressing towards equilibrium. Therefore as the temperature is increased to a temperature greater than the previous annealing temperature but still below T_g, the domains with short relaxation times that are in or near equilibrium have to expand because of the increase in temperature. Since those domains have rapid relaxation times, their response can be clearly seen only at initial times (as observed in Figure 7.6) since they reach equilibrium faster. The domains with longer relaxation times keep densifying towards the equilibrium value. As seen in Figure 7.6, the process of deaging took a rather long time, even at those elevated temperatures, since the T_g decreased up to 22h30. Aging started over again between 22h30 and 46h30 at 127°C. The slope seemed to change

though at the new aging temperature, as observed by comparing the data at 4h30 and 46h30, as if the path to reach to equilibrium was different.

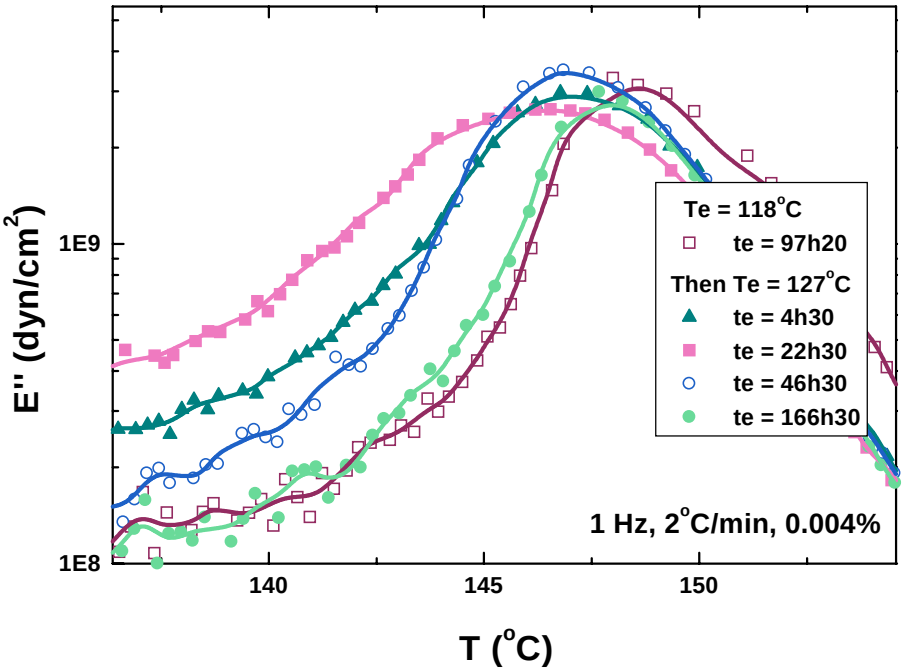

Figure 7.6: Loss modulus traces showing memory effects in polycarbonate as the temperature is increased from 118°C to 127°C. The DMTA conditions were the following: frequency = 1Hz, strain = 0.004%, initial temperature = 25°C, heating rate = 2°C/min, torque = 10cNm.

7.3.4.3. Isothermal experiments

Whenever a constant heating scan mode is used, interpretation of the aging results becomes complicated because of the interaction of this heating scan with the aging process. The structure of the sample may change, especially at temperatures close to the T_g. In order to access the aging behavior at different temperatures within the glassy state, isothermal DMTA experiments were carried out at 120°C and 80°C. As expected, fresh polycarbonate samples were determined to age faster at 120°C than at 80°C (see Figure 7.7). Quite interestingly, the decrease in tan δ with annealing time was observed to be linear with log t_e for the temperature of 80°C only. The linearity of tan δ with log t_e has been reported elsewhere [44]. The increase in tan δ at short aging time for T_e = 120°C was attributed to internal stresses. The samples were put between the grips of the DMTA

apparatus at room temperature, they were heated to T_e relatively fast and left at T_e for a few minutes before starting the test itself. Since the samples were constrained between the grips, it is possible that 20min may be needed for the polymer to relax at T_e.

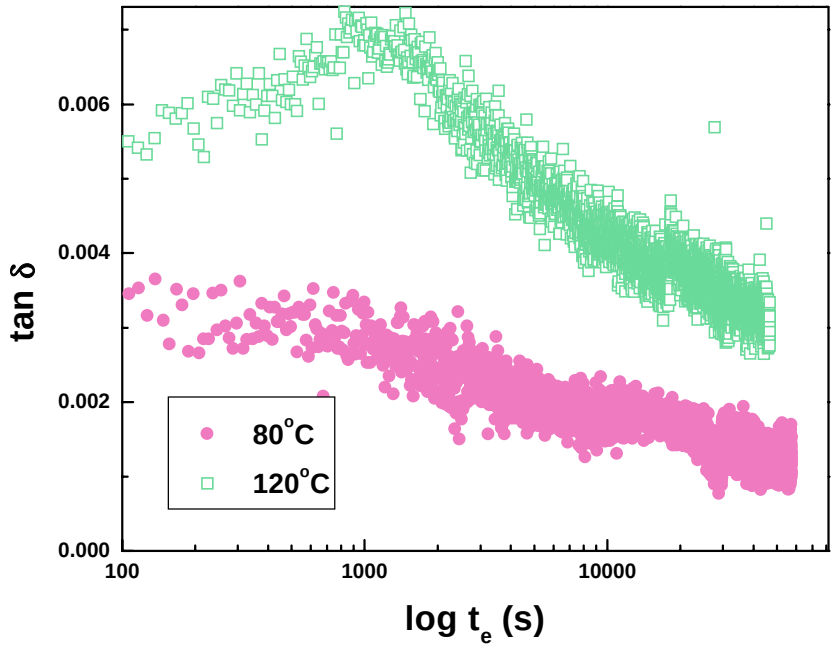

Figure 7.7: Change in tan δ as a function of annealing time at 80°C and 120°C. The sample was initially cooled at 40°C/min. The DMTA conditions were the following: strain = 0.025%, frequency = 5Hz, torque = 10cNm, static force = 40g.

Attempts were made to determine the aging shift rate at 120°C by isothermal DMTA experiments. The shift rate is given as the ratio of the derivative of the logarithm of the shift factor divided by the derivative of the logarithm of the annealing time (assuming that the relaxation time distribution does not change in shape during aging). The master curves [45, 46] can be built by using several frequencies. By increasing the frequency, the sample has less time to respond, and therefore an increase in frequency is similar to a decrease in temperature, as illustrated in Figure 7.8. As the frequency increased, the T_g was observed at a higher temperature. Moreover, the intensity of E" decreased, the peak broadened, and the slope of E' decreased. Unfortunately, the shifting procedure was not successful. It was indeed impossible to superimpose the various curves. Vertical shifts did not significantly improve the master curve. The problem may have come from the fact that the DMTA equipment did not allow us to run several

frequencies at a time on the same sample. Unlike the dynamic frequency-temperature sweep experiments analyzed in Chapter 5, several samples had to be run in the aging studies one after another in order to gather all the needed information to build the master curve. This may have generated some errors due to the slight differences in sample dimensions. Moreover, it was observed that the values of the loss modulus E" became negative at frequencies higher than 10Hz, attributed to the limitations of the DMTA equipment itself.

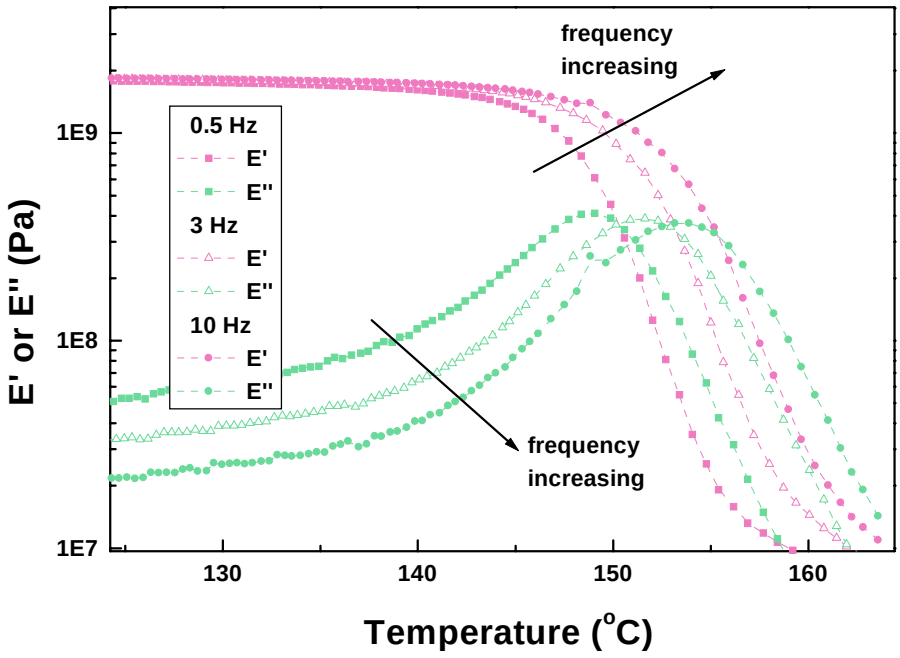

Figure 7.8: Effect of frequency on the DMTA traces. The DMTA conditions were the following: strain = 0.025%, initial temperature = 25°C, heating rate = 1°C/min, torque = 10cNm.

Isothermal DMTA experiments were performed at 120°C as a function of the annealing time for the samples cooled at different rates and hence representing different histories. Obviously, the thermal cycle was different from the one used for permeation or density measurements since it was controlled by the DMTA apparatus itself and not by the internal fan oven, as used to prepare the other aged samples. The freshly processed samples were directly aged at 120°C without waiting at room temperature for a period of 16h (as what was done for samples to be used in density measurements in order to allow comparison with samples used in permeation). The resulting DMTA traces of tan δ are

provided in Figure 7.9. It appeared that the samples cooled faster and thus containing the greatest amount of free volume aged faster. Moreover, one observed that the behavior became linear with the logarithm of the annealing time t_e for the slow-cooled sample only. Recall, a linear decrease in the tan δ response was observed at an annealing temperature of 80°C but not at 120°C for the sample cooled at 40°C/min. Therefore it seems that aging of a 40°C/min-cooled sample at low temperatures in the glassy state reflects aging of the slow-cooled sample at higher temperatures. The initial increase in tan δ observed on Figure 7.9 at annealing times under 0.3h could be attributed to internal stresses as discussed previously.

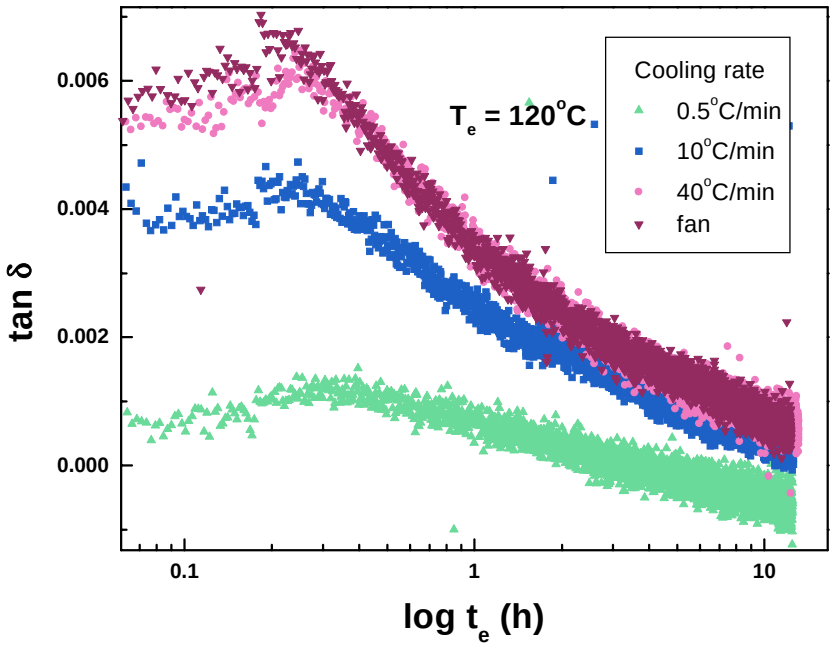

Figure 7.9: tan δ as a function of the annealing time t_e for the samples cooled at different cooling rates. The annealing temperature T_e was chosen as 120°C. The DMTA conditions were the following: frequency = 3Hz, strain = 0.025%, data points collected every 10s.

7.3.5. Permeation results

The following sections report how the gas transport coefficients are affected by aging for a sample cooled at a fixed rate, as well as for samples cooled at different rates

and evaluated after a given sub-T_g annealing time. The experimental results are then discussed. Changes in activation energies are also reported.

7.3.5.1. Physical aging characterization

Information about the amount of free volume and its size distribution can be assessed in permeation experiments by using inert gases. As explained in the experimental section of this chapter, permeation profiles were obtained twice on the same membrane: once on the freshly processed polycarbonate and then on the aged one. This procedure allowed us to investigate the effects of aging within a limited error range. No change in thickness could be detected with sub-T_g annealing. As seen in Figure 7.10, the permeation profiles were observed to be affected with physical aging. After 70h40 at 120^{o}C the slopes decreased with aging, but this decrease depended on the nature of the gas. The experimental permeation profile of N_2 dropped more than those of He and O_2. Please note that although the decrease for N_2 appeared to be much greater in Figure 7.10 than that of the other gases, this is not strictly true since the x-axis was not the same for each gas. To our knowledge those results are the first ones to show how the experimental permeation profile is really affected by aging. Data published in the literature obtained with a permeation apparatus usually report values of the permeability coefficient directly. However, such data were obtained within a greater error margin.

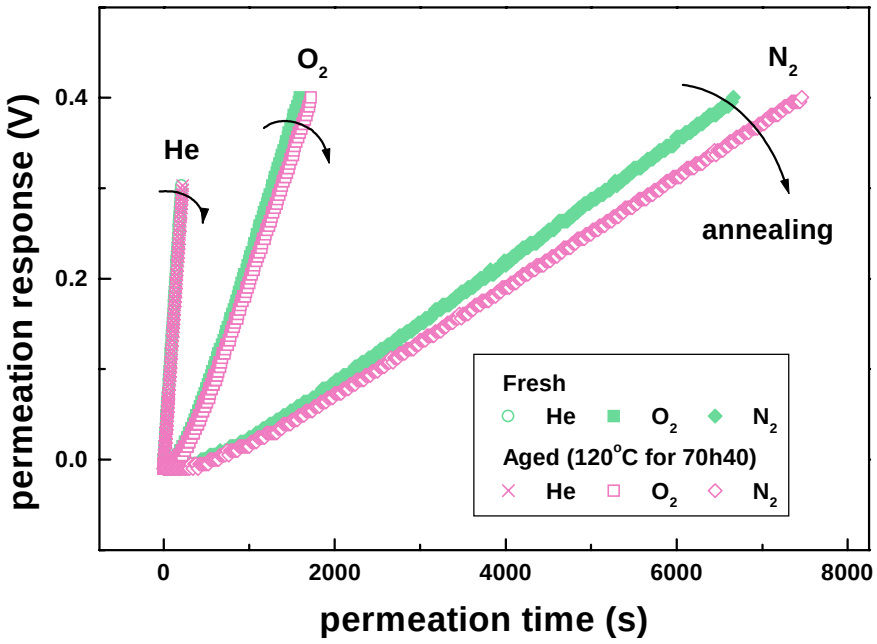

Figure 7.10: Permeation profile as a function of the permeation time. The permeation experiments were carried out at 35°C. The difference in profile between a fresh membrane (cooling rate from 165°C = 40°C/min) and a membrane annealed at 120°C for 70h40 is clearly seen. The profile was averaged for each gas at each condition. The effect of annealing appeared to be greater for N_2. The applied pressures were chosen as 3.9atm for He, and 2.5atm for both O_2 and N_2.

7.3.5.2. Aging results as a function of time

The percent (%) change in the slope of the experimental permeation profile was determined by comparing the responses of the freshly processed (cooling rate from 165°C = 40°C/min) and the aged samples for each aging time t_e at the given sub-T_g annealing temperature of T_e = 120°C. The % in the permeation profile slope change as a function of aging at 120°C is shown in Figure 7.11. The slope was found to decrease for the three gases used in this research. Furthermore, the greater the kinetic diameter of the gas, the greater the decrease in the permeation profile slope. However this does not necessarily mean that the larger free volume holes are eliminated first during physical aging since the permeation process is a more complex phenomena. The % permeance change did not appear to decrease linearly with log t_e though. This may reflect the conformational changes taking place within the polymeric matrix with aging [2]. If one removes the first data points up to t_e = 10h, the rest of the data could be fitted on a linear line though. The behavior observed at short aging times could be either due to some deaging effects or to

some induction period (acquisition of enough energy to move the chains at a local level). However no deaging effects were observed by density measurements. Indeed, the density was not observed to decrease at short aging times and then increase with further times. Instead, the density was found to increase linearly with log t_e, even though the samples were left for a couple of hours at room temperature before aging at 120°C while the other samples were tested in the permeation apparatus. This seems to indicate that deaging may not have taken place in the samples, at least at the macroscopic level. The % profile slope change is shown as a function of the kinetic diameter in Figure 7.12.

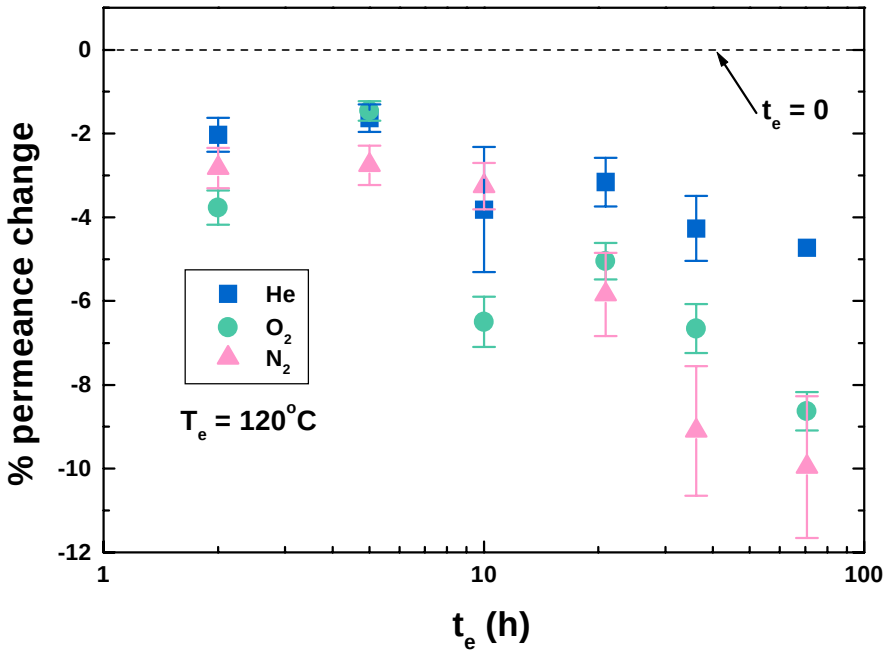

Figure 7.11: Percentage of the permeance change as a function of annealing time at 120°C for the gases studied in this research. The permeation slopes were obtained at 35°C and averaged. As apparent from the figure, the permeation slope was reduced with annealing time.

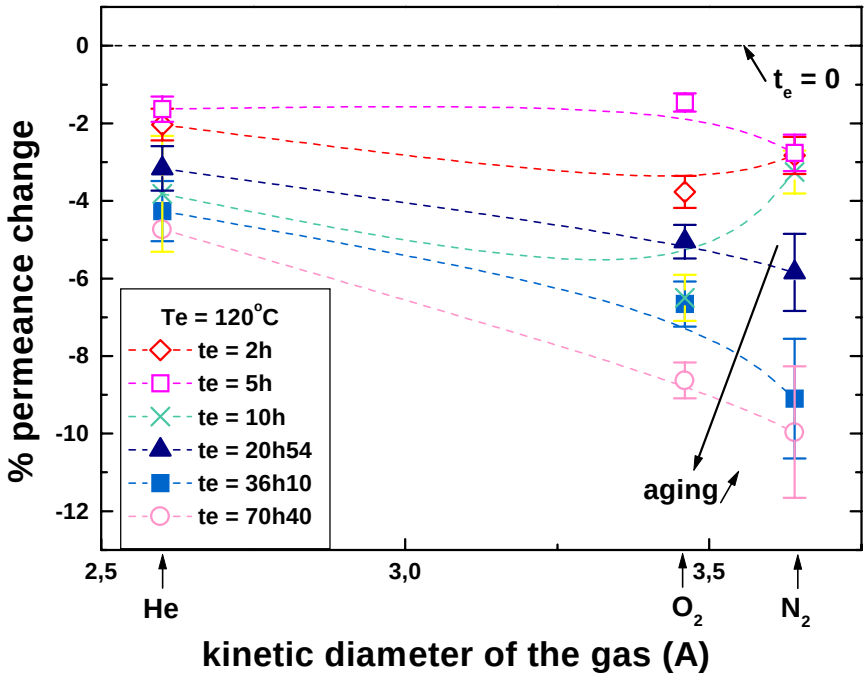

Figure 7.12: Percentage of the permeance change as a function of the kinetic diameter of the penetrant gas in Å for various annealing times at 120°C. The permeation slopes were obtained at 35°C and averaged. The greater the kinetic diameter, the greater the change at long annealing times.

The % change in the permeability coefficient P was calculated for each aging time t_e at 120°C. Obviously the results in terms of % corresponded exactly to the ones shown above for the permeation profile slope since P and the experimental permeation profile slope are directly correlated (see Chapter 4 for details). What is important to note for practical applications is that the permselectivity is highly affected by aging. The permeability coefficient of bigger gas molecules is more reduced by aging than those of smaller size molecules.

The effects of aging on the diffusion and the solubility coefficients are shown in Figure 7.13 and Figure 7.14, respectively.

The diffusion coefficient appears to decrease with aging for both O_2 and N_2. This observation is in agreement with the literature. Nevertheless, an increase in the diffusion coefficient with aging can also be distinguished at shorter aging times. This fact will be discussed later on. The data points suggest that the solubility coefficient may increase with the logarithm of sub-T_g annealing time. This is not expected since the density actually increased with aging time, hence indicating a loss of free volume. Since we did

not change the temperature of the permeation experiments or the interactions between the gas and the polymer, changes in the solubility coefficient S can only be attributed to changes in free volume. At this point we think that the increase in the solubility coefficient S is attributed to a change in the free volume distribution on aging.

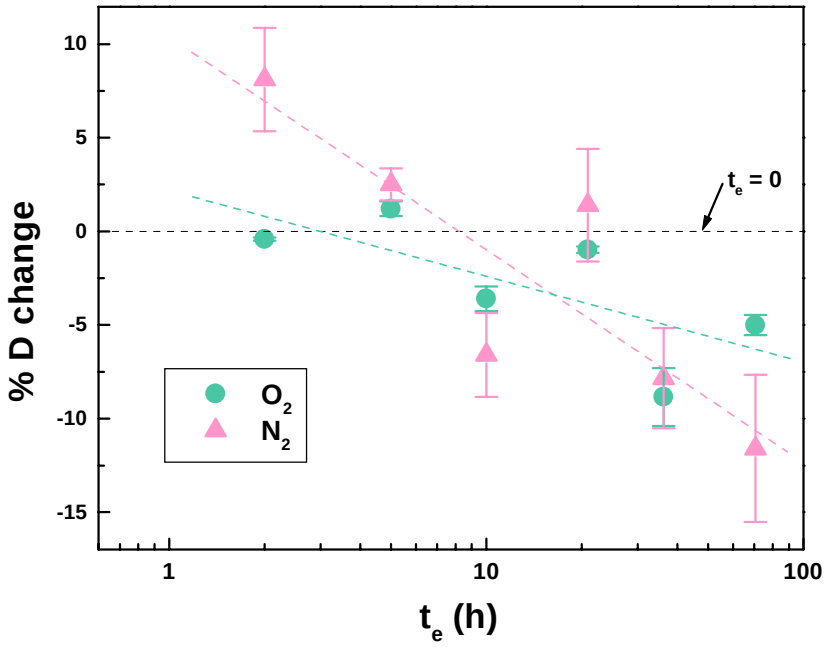

Figure 7.13: Percentage of diffusion coefficient D change as a function of annealing time at 120°C for the gases studied in this research. The permeation slopes were obtained at 35°C and averaged for each gas.

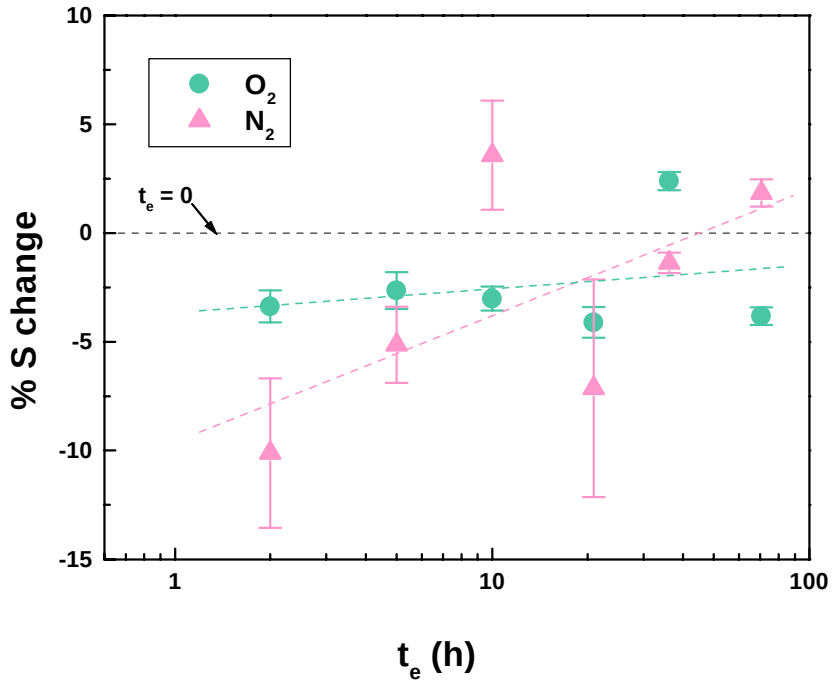

Figure 7.14: Percentage of solubility coefficient S change as a function of annealing time at 120°C for the gases studied in this research. The permeation slopes were obtained at 35°C and averaged for each gas.

7.3.5.3. Cooling rate / aging results

Polycarbonate samples cooled at different rates and hence with different histories were aged at T_e = 120°C for t_e = 10h. The change in the permeation profile slope is shown as a function of the cooling rate in Figure 7.15 for N_2. The experimental permeation profile slopes were found to decrease with 10h of aging at 120°C for all four samples. Recall, the permeation slope is directly related to the permeability coefficient P. Therefore the above results mean that the permeability coefficient decreased with aging as well for the cooling rates selected in this study. In contrast with previous properties such as density and tan δ showing that the sample containing the greatest amount of free volume aged faster, Figure 7.15 shows that the permeation of the sample containing an initial greater free volume content was less affected by aging than the other samples containing a lower initial free volume content. The permeation of N_2 in the sample cooled by the fan did not actually appear to be affected at all by 10h of aging at 120°C. In general, the greater the kinetic diameter, the greater the slope decrease.

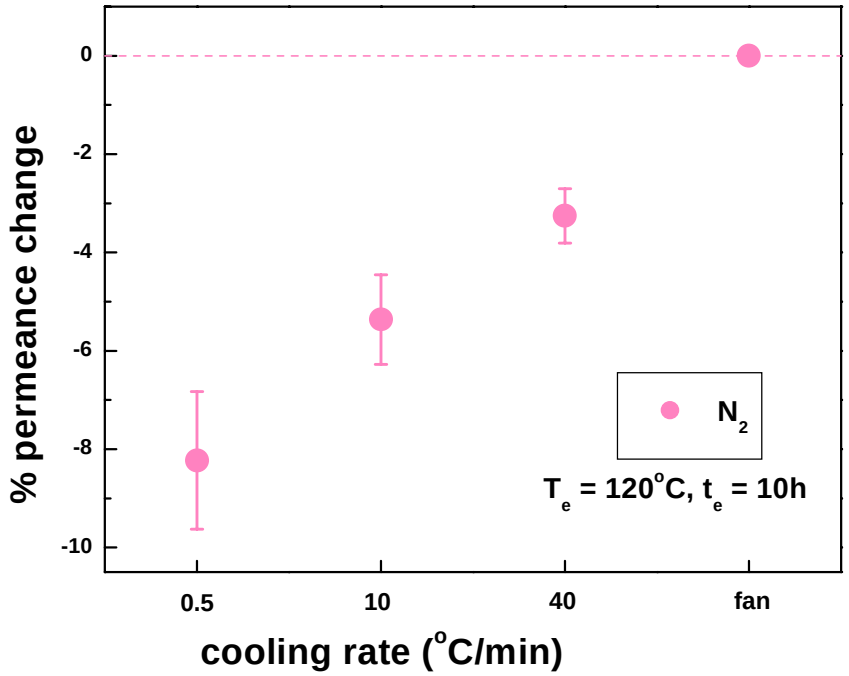

Figure 7.15: Percent in permeance change as a function of the cooling rate for N_2 (note that the x-axis is not a continuous axis). The samples had been annealed at 120°C for 10h. The permeation experiments were carried out at 35°C. The applied pressure was taken as 3.9atm for N_2.

The responses observed for the diffusion D and the solubility S coefficients of O_2 and N_2 are shown in Figure 7.16 and Figure 7.17. As mentioned previously, it was not possible to evaluate D and S for He due to the short value of the time-lag. The diffusion coefficients of O_2 and N_2 were found to be increased after 10h at 120°C for the sample cooled by the fan. However the other three samples did show a decrease in D after the same time at 120°C. The slower the cooling rate, the greater is the decrease in D. Also, the diffusion coefficient was found to decrease much more for N_2 than for O_2. The solubility coefficient S is expected to relate to the free volume content. The decrease in S should therefore be highly affected by the initial amount of free volume. And indeed, S decreased the most for the high free volume material (see Figure 7.17). The behaviors of O_2 and N_2 appeared to be quite different though since S was found to increase for some samples for N_2, in contrast with O_2 that always probed a decrease in S. S was found to increase for N_2 in samples cooled from 0.5°C/min to 40°C/min (about 6.5% increase for N_2 in the sample cooled at 0.5°C/min after 10h at 120°C).

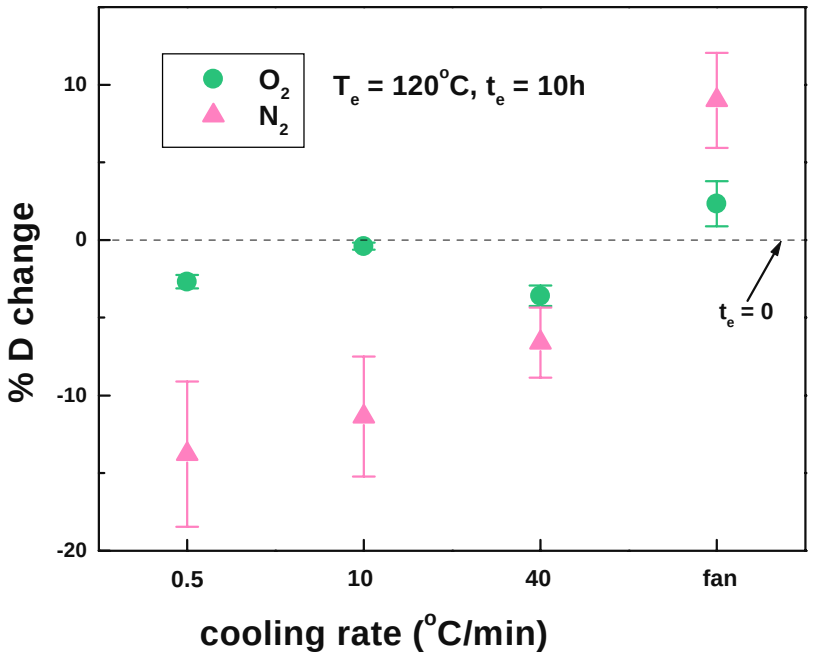

Figure 7.16: Percent in diffusion coefficient change as a function of the cooling rate for the various gases of interest (note that the x-axis is not a continuous axis). The samples had been annealed at 120°C for 10h. The permeation experiments were carried out at 35°C.

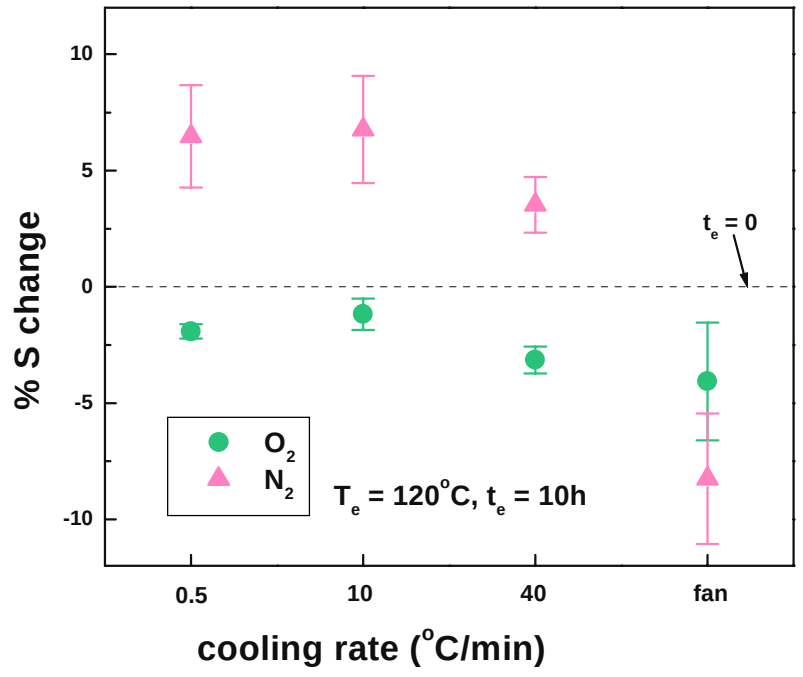

Figure 7.17: Percent in solubility coefficient change as a function of the cooling rate for the various gases of interest (note that the x-axis is not a continuous axis). The samples had been annealed at 120°C for 10h. The permeation experiments were carried out at 35°C.

7.3.5.4. Permeation data discussion

Diffusion and solubility coefficients of O_2 and N_2 can provide information on the structural rearrangements and scales taking place in polycarbonate with physical aging. The average hole size has been determined by two-dimensional angular correlation of annihilation radiation (2D-ACAR) to be about 2.9Å for polycarbonate [47], thus outside the range between the size of O_2 (3.46Å) and N_2 (3.64Å). Nevertheless, the gas permeation data shown above presented dramatically different behaviors for O_2 and N_2.

The solubility coefficient S of O_2 decreased overall with aging, but the decrease appeared to remain at rather constant level with aging time (see Figure 7.14). Whereas the solubility coefficient of N_2 showed a decrease at shorter aging times and then actually tended to increase with aging time after some particular point (see Figure 7.14). Similarly, the cooling rate / aging studies showed that as the cooling rate decreased, the solubility coefficient of N_2 increased for the same fixed annealing time (see Figure 7.17). Recall, the solubility coefficient S has been shown to be related to the amount of free volume (see Chapters 5 and 6).

The fact that the solubility coefficient S of N_2 tends to show an increase with physical aging despite of the decrease in free volume (as seen from the density values) may reflect the dynamics of the redistribution of free volume and the shape of the free volume voids. With aging, the size distribution of the cavities may become narrower and of a size close (but greater) to that of the N_2 gas molecule. A rapid reduction in the amount of larger free volume sites is likely to occur with aging in order to account for the decrease in the concentration of microvoids. The density has indeed been found to increase with aging (see Figure 7.2) with $(d\rho / d\log t_e)$ = constant, indicating a loss in the free volume amount with time. Since the solubility coefficient of O_2 appears to remain rather constant with aging time and that of N_2 increases, this seems to indicate that cavity sizes larger than the size of the N_2 gas molecule have to decrease tremendously with aging time to compensate for the reduction in free volume. The bigger cavities may decrease in size whereas the small ones may group together to form bigger cavities (new large cavities could indeed be formed by cavity coalescence). A possible schematic of the

aging process is provided in Figure 7.18. Spherical cavities are drawn to represent the fresh sample, but actually the cavities should have a distribution of sizes and shapes. One needs to be cautious in interpreting the solubility data though, since the data points only suggest that the solubility coefficient may increase with aging time; the trends remains ambiguous.

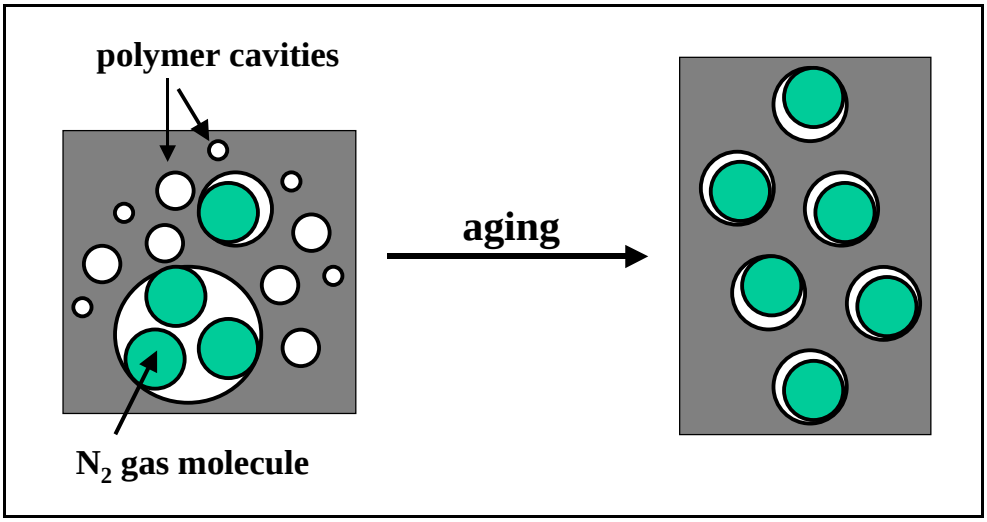

Figure 7.18:. Schematic of the aging process. With aging the size distribution of the cavities may become narrower and of a size close to that of the N_2 gas molecule. The grey matrix corresponds to the polycarbonate, the green spheres to the gas molecules, and the white spheres to the free volume.

On the other hand, the diffusion coefficients of both O_2 and N_2 decreased with aging time (see Figure 7.13). Nevertheless, an increase at shorter aging time was also observed. The cooling rate/aging studies showed that the diffusion coefficient of N_2 was much more reduced than that of O_2 in slower cooled samples (see Figure 7.16). An increase in diffusion coefficients was also seen in the sample cooled by the fan.

The fresh sample cooled at 40^{o}C/min may initially contain conformations of the trans-trans and trans-cis types. It has been shown in the literature that with sub-T_g annealing in polycarbonate the population of trans-trans conformers increases whereas that of trans-cis conformers decreases [1, 48]. And from the conclusions reached in Chapter 6, it seems that the polymer chains in the trans-trans conformation can vibrate at a greater frequency than those in the trans-cis conformation (at least in the freshly 40^{o}C/min-cooled samples, and also possibly in the initial stages of aging), hence creating

fluctuations large enough to allow the passage of a gas molecule from one cavity to another and resulting in a greater diffusion coefficient. The degrees of freedom associated with the trans-trans conformations may be lost with further sub-T_g annealing. An increase in relaxation times is indeed observed with physical aging [17]. This would induce a reduction in segmental mobility and thus in the diffusion coefficient, as seen here.

As far as the cooling rate / aging studies are concerned, the slowly cooled sample was already mainly in the lowest energy conformation, namely the trans-trans conformation. As the sample is annealed, more and more degrees of freedom or fluctuations within a limited range around the minimum are lost, hence resulting in a reduced diffusion coefficient. The polymer chains may even become capable of lying parallel to one another on a local level and decrease this distance with time. If indeed bigger cavities are formed with sub-T_g annealing as suggested above, this would mean that the distance between the chains keeps decreasing with time, and may even become too narrow to allow large kinetic diameter gas molecules (such as N_2) to go through the polymer rapidly. This high concentration of locally oriented chains (corresponding to local density fluctuations) could possibly act as an obstacle for the gas molecule, which would have to contour the obstacles, and therefore increase the diffusion path length by a tortuosity factor, as seen in the diffusion process through semi-crystalline polymers. The aging phenomenon would resemble a crystallization process, but on a greater length scale. In contrast, the sample cooled by the fan may increase the population of trans-trans conformers at early aging times. Again, from the conclusions reached in Chapter 6, this would imply an enhanced diffusion coefficient. This could explain the enhanced diffusion coefficient seen after 10h at 120^{o}C.

Please note that in the case of deaging effects the diffusion coefficient would be expected to decrease and not to increase. Therefore this reinforces the idea that the first data points of Figure 7.13 and Figure 7.16 could not be attributed to deaging effects. No deaging effects could be seen either on the density measurements.

The fact that P appeared to decrease with aging for all the gases (see Figure 7.11) even though the behaviors of D and S were opposite is attributed to the fact that D has a

greater influence on P than S [49-51]. And indeed, the quantitative absolute decreases in D appeared to be greater than those in S (see Figure 7.13 and Figure 7.14).

Quite interestingly, the permeability coefficient was found to decrease more after 10h at 120^{o}C for the sample initially cooled at 0.5^{o}C/min than for the one initially cooled by the fan, despite of the lower free volume content in the slowly cooled sample. In contrast, properties directly related to the free volume content, such as density or isothermal DMTA measurements actually showed a greater aging rate in the sample containing the greatest amount of free volume (see above). This observation proves that once again the permeability coefficient should not be directly correlated with the free volume content of the material, as already discussed in Chapters 5 and 6. The fact that the permeability coefficient shows a different behavior than properties more related to the macroscopic level (such as density) should be considered for future industrial applications. The difference may originate in part from cooperativity concepts. Although the gas transport process is not believed to require cooperativity but rather extremely local rearrangements, other properties may require cooperative motions. And a greater decrease in the free volume content is likely to necessitate an enhanced number of segments to relax together, hence a greater cooperativity. A minimum free volume content may indeed be needed to enable cooperative motions to take place.

To summarize, the gas permeation results suggest that with sub-T_g annealing the polymer chains may rearrange their conformations and thereafter loose progressively their degrees of freedom. The size distribution of the cavities may also become narrower and of a size close to that of the N_2 gas molecule.

The above conclusions are in agreement with the results of Neki and Geil [52] on the physical aging of polycarbonate. The researchers reported that the surface of polycarbonate initially appeared by electron micrographs to have various cavity sizes and shapes. With aging in the glassy state those cavities were becoming well-defined and with similar sizes. However the question remained if this phenomenon was actually taking place with aging or if the results were artifacts of the etching process used by the researchers.

The possibility that bigger cavities are formed with aging in polycarbonate would agree with the conclusions of Curro and Roe using small-angle X-ray scattering (SAXS) [4]. The fact that SAXS results indicated an increase in the average free volume hole size of polycarbonate with sub-T_g annealing time [4], and positron annihilation lifetime spectroscopy (PALS) and photochromic probe results a constant free volume hole size with aging [6-12] may be caused by the differences in the probing ranges of the techniques. The average hole size in one technique may represent a different value than the average in another one. And therefore the behavior may appear as different depending on where the average is located. In this research for instance, if the initial average size corresponds to the size of N_2 (3.64Å), the average size may appear as constant with aging. Whereas an initial average size of about 3Å would appear to become increased with aging time. Finally, giving an average is always discutable since it does not reflect the distribution.

If the bigger cavities are indeed disappearing first with sub-T_g annealing in order to account for the densification process, this may in part elucidate why enthalpy and volume relaxation rates are different [16, 53]. It has been established that the domain sizes for volume relaxation are greater than those for enthalpy relaxation, based on the difference in activation energies [54]. Only cavity sizes above a critical size may contribute to volume relaxation. Therefore, at some particular aging time the bigger cavities may have all disappear and no change in volume can be easily observed by non-sensitive enough dilatometers. Nevertheless, some molecular motions can keep contributing to the enthalpy relaxation.

The fact that published data concerning physical aging have shown a decrease in the sorption properties of the polymer with aging, thus in contrast with the N_2 data shown in this work, may be caused by the conditions chosen by the researchers. The problems associated with the sorption process have been discussed in Chapter 3.

The fact that the samples cooled slowly and thus containing the lowest amount of free volume show a greater decrease in the permeability coefficient with sub-T_g annealing seems somehow similar to the “mobility paradox” observed for annealed oriented samples [55, 56]. Shelby and co-workers [57] have distinguished two types of trends as hot-drawn polycarbonate is aged below T_g. On one hand, the properties related to the α-

type of motions (such as creep aging rate and T_g) are observed to become less mobile with aging time compared to those of isotropic samples. On the other hand the properties related to the β-type of motions (such as volume relaxation rate) show a greater mobility with aging time. As a recall, the α and the β relaxations have different origins. The α-relaxation occurring around T_g corresponds to long-range or large scale motions and is a cooperative phenomenon involving several polymer segments. Whereas the β-relaxation corresponds only to localized motions which may involve the repeat unit of polycarbonate only. Moreover the β-relaxation can be described by an Arrhenius-type equation, but the α-relaxation not [58]. The density of uniaxially hot-drawn polycarbonate was found to increase with stretching, hence indicating a lower free volume content [55, 56]. The fact that a property can show a greater mobility with aging for oriented materials is rather unexpected since usually one associates a greater physical aging rate with a greater free volume content, and thus a greater mobility. Solid state ^{1}H-NMR and dynamic mechanical measurements (DMA) were used by the researchers to probe the motions of the polymer chains [57]. The mobility paradox was explained in terms of the increased size of the cooperative domains associated with the α-relaxation with stretching versus the increased number of localized relaxing segments caused by the larger ellipsoidal holes created from the orientation process and which provide additional space for the samples to relax (then linked with the β-relaxation). Quite interestingly, the volume relaxation rates were not found to be a function of the degree of orientation, but instead on whether the samples had been stretched or not [57]. It has been shown in the literature that the timescale of conformational rearrangements is similar to that of volumetric relaxation for isotropic polycarbonate [59]. However the timescale of enthalpy relaxation was found to be greater for the same samples [59]. A modification of the interchain interactions without a change in population with sub-T_g annealing has been suggested in order to explain the greater timescale of the enthalpic relaxation [59]. The important fact here is that conformational rearrangements and volumetric relaxation are linked. If one applies this conclusion to the results obtained by Shelby and co-workers [57], this suggests that the conformation of the polycarbonate chains changes only as the sample is initially stretched. Another unexpected behavior has been reported in the literature [60]. When polycarbonate samples are aged for 50min at 20.3^{o}C and for about

100min at 22.5°C, the stress relaxation occurs more rapidly at the lower temperature at the point at which both samples possess the same overall free volume content.

7.3.5.5. Activation energies

In order to confirm recent data published in the literature showing a decrease in the activation energy of diffusion with aging for polycarbonate [61], gas transport activation energies were determined at 120°C for the samples aged as a function of time. The permeation temperatures were taken in a narrow temperature window in order to avoid aging and/or deaging, although such a reduced temperature range may have increased the errors associated with the gas transport properties. Gas transport activation energies are shown below from Figure 7.19 to Figure 7.21. Please note that the results obtained for the fresh membrane were obtained by permeating gases at 35°C only once. In contrast, aged membranes were run twice at 35°C (fresh + aged).

The activation energy of permeation E_P appeared to remain relatively constant with aging for the three gases selected (see Figure 7.19). Obviously, the greater the kinetic diameter of the gas molecules, the greater the activation energy. E_D and ΔH_s appeared to remain constant with aging for O_2, but changed tremendously for N_2 (see Figure 7.20 and Figure 7.21). A possible explanation for the increase in E_D is that the increase in the relaxation times with aging [17] requires more energy to dilate the chains and enable the diffusion process to take place. It is well-established indeed that physical aging involves relaxation processes. Explanations based on the free volume content alone [62] seem indeed invalid in light of the results presented in Chapters 5 and 6.

The fact that E_D increased with aging time is in contradiction with the recent published results of Pekarski and co-workers on the physical aging of polycarbonate [61]. E_D was found to be lower in an aged sample than in a conditioned one. As explained in Chapter 3, caution is however needed in interpreting the sorption results obtained with carbon dioxide. In addition, only two data points were obtained by the researchers (aged versus conditioned). More data points should have been collected to be able to identify a significant trend.

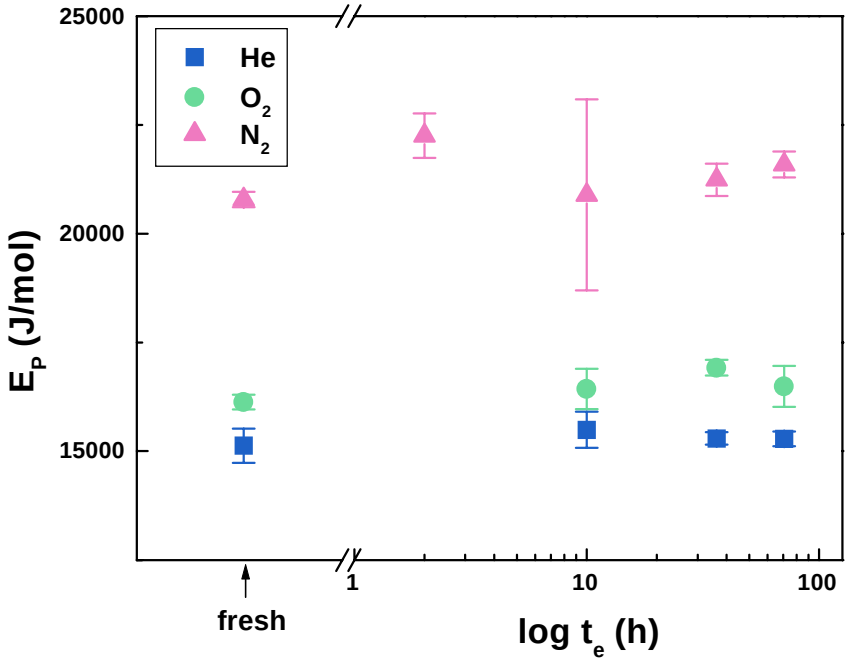

Figure 7.19: E_P as a function of annealing time at 120°C for the gases studied in this research. The permeation experiments were carried out at 35, 40, 45, and 55°C. At t_e = 2h, permeation experiments were carried out for N_2 only.

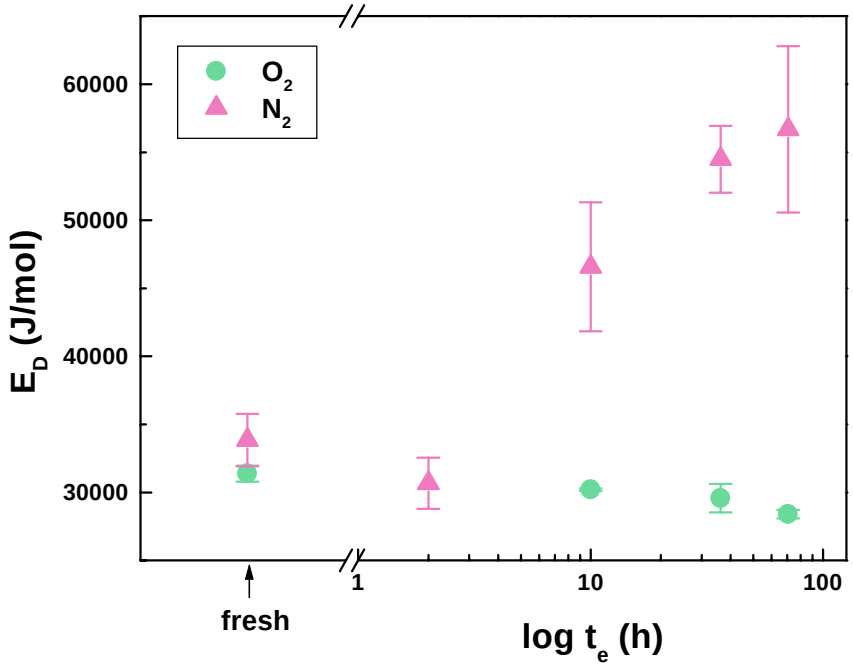

Figure 7.20: E_D as a function of annealing time at 120°C for the gases studied in this research. The permeation experiments were carried out at 35, 40, 45, and 55°C. At t_e = 2h, permeation experiments were carried out for N_2 only.

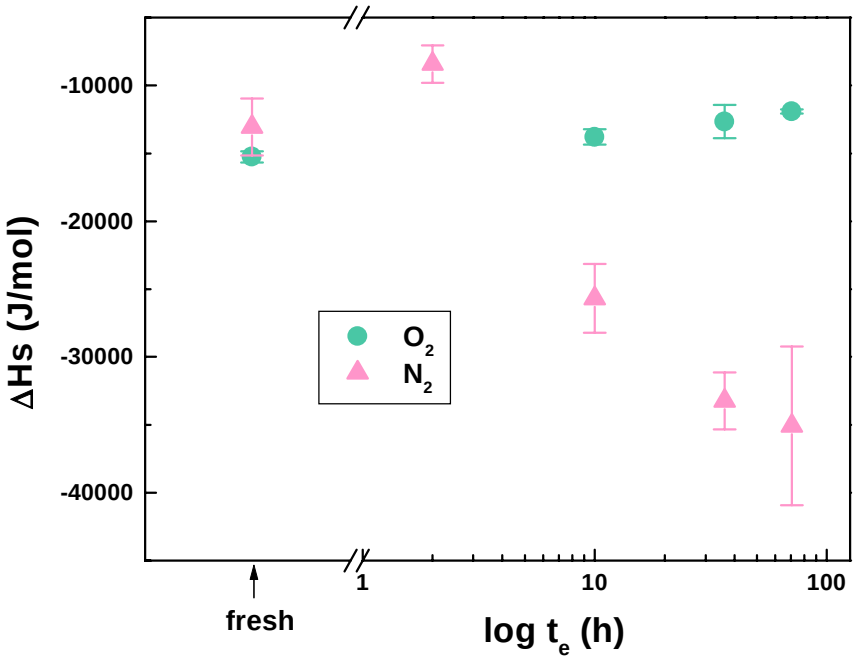

Figure 7.21: ΔHs as a function of annealing time at 120°C for the gases studied in this research. The permeation experiments were carried out at 35, 40, 45, and 55°C. At t_e = 2h, permeation experiments were carried out for N_2 only.

7.3.5.6. Other

Attempts were made to observe memory effects by gas permeation measurements. As seen previously from DMTA results, when a polymer is heated to a temperature greater than T_e but still below T_g, the polymer deages first before aging with further time. These memory effects have been attributed to the distribution of relaxation times [43]. The slope of the permeation profile is expected to decrease at T_e until equilibrium. Once the temperature is increased to a temperature above T_e but still below T_g, the permeation slope may first increase at short aging times, and then decrease again with further aging. Moreover, it has been shown in the literature that temperature jump studies are characterized by a nonlinear response [15]. The response observed by a $+\Delta T$ jump is indeed different from the one seen by a $-\Delta T$ jump (see Chapter 3 for more details). A nonlinear response could also be observed in permeation experiments. The % slope change should be plotted as a function of time for positive and negative changes in temperature (the y-axis would be at t_e = 0 with negative and positive x-axis). Taking

different temperatures should also affect the response. It has indeed been shown in the literature that the path to equilibrium is different depending on the temperature [15]. Unfortunately, the permeation experiments were unsuccessful. The membranes were refreshed after aging in order to simplify the thermal history, but changes in thickness made comparisons between samples impossible.

7.4. Conclusions

This study was concerned with the effect of physical aging on the gas transport properties. Polycarbonate samples with a well-defined thermal history were aged at 120^{o}C and the gas transport properties were evaluated as a function of aging time. In addition, the effect of the cooling rate on the physical aging process was examined after 10h at 120^{o}C. The use of gas permeation has been proven to be a versatile tool in providing a deeper fundamental understanding of the aging phenomena. This study showed that the permeability coefficient of molecules, the size of N_2, was more affected by aging that that of smaller size molecules. The diffusion coefficients of both O_2 and N_2 were observed to initially increase at short aging times and to decrease with further sub-T_g annealing. In contrast, the solubility coefficient of N_2 (and that of O_2 as well but to a smaller extent) was observed to increase with further aging time. Properties directly related to the free volume content of the polymers, such as density and DMTA measurements, were observed to age faster when the initial content of free volume in the materials was high. In contrast, the permeability coefficient was observed to be reduced the most with aging for polycarbonate samples possessing an initial lower free volume amount. Actually, the permeability coefficient of a sample cooled in excess of 40^{o}C/min appeared to be almost unaffected by aging after 10h at 120^{o}C. However the diffusion and the solubility coefficients were highly affected by aging for this particular sample. The trends seen in aging / cooling rate studies were similar to those observed for samples studied as a function of time, i.e. a decrease in the diffusion coefficient and an increase in the solubility coefficient as the initial free volume content is reduced.

The gas transport results suggest that on sub-T_g annealing the polycarbonate chains may adopt the trans-trans conformation (possibly fluctuating more rapidly than the

trans-cis conformation around the minima) and loose progressively their degrees of freedom. The free volume distribution may become narrower and favor the formation of cavities of a size similar (but greater) to that of the N_2 gas molecule. The increase in the activation energy of diffusion with aging time was explained in terms of the increase in the relaxation times.

For practical purposes, this study points out that gas transport properties are affected by physical aging in a different way than for instance the density. The greater the initial free volume amount in polycarbonate, the greater is the densification rate, but the lower is the decrease in the permeability coefficient with aging time. This observation proves that the permeability coefficient should not be directly correlated with the free volume content of the material, but rather with the molecular chain dynamics. This also suggests that the various "static" models of gas diffusion in polymers are inappropriate.

7.5. References

1. N. Heymans, FTIR investigation of structural modification of polycarbonate during thermodynamical treatments, *Polymer*, 38, 14, 3435 (1997).
2. V. Stolarski, A. Letton, S. N. Lee, J. Laane, Conformational changes and physical aging in bisphenol-A polycarbonate; origins of mechanical properties, *Polym. Mater. Sci. Eng.*, 71, 479-480 (1994).
3. V. Stolarski, A. Letton, E. Nour, J. Laane, Conformational changes and physical aging in bisphenol-A polycarbonate; origins of mechanical properties, *ANTEC'94*, 2077 (1994).
4. J. J. Curro and R.-J. Roe, Isothermal relaxation of specific volume and density fluctuation in poly(methyl methacrylate) and polycarbonate, *Polymer*, 25, 1424 (1984).
5. J. H. Wendorff, *J. Polym. Sci., Polym. Lett. Ed.*, 17, 765 (1979).
6. A. J. Hill, I. M. Katz and P. L. Jones, Isothermal volume relaxation in aged polycarbonate measured by positron annihilation lifetime spectroscopy, *Polymer Enginering and Science*, 30, 13, 762 (1990).
7. T. C. Sandreczki, X. Hong, and Y. C. Jean, Sub-glass-transition-temperature annealing of polycarbonate studied by positron annihilation spectroscopy, *Macromolecules*, 29, 4015-4018 (1996).
8. A. J. Hill, C. M. Agrawal, Positron lifetime spectroscopy characterization of thermal history effects on polycarbonate, *Journal of Materials Science*, 25, 5036-5042 (1990).
9. J. E. Kluin, H. Moaddel, M. Y. Ruan, Z. Yu, A. M. Jamieson, R. Simha, J. D. McGervey, Probe spectroscopy, free volume concepts, and physical aging of

polymer glasses, in Structure-property relations in polymers: spectroscopy and performance, ACS, 236, 535-555 (1993).

10. T. C. Sandreczki, X. Homg, and Y. C. Jean, Sub-glass-transition temperature annealing of polycarbonate studied by positron annihilation spectroscopy, *Macromolecules*, 29, 4015-4018 (1996).
11. J. E. Kluin, Z. Yu, S. Vleeshouwers, J. D. McGervey, A. M. Jamieson, R. Simha, Temperature and time dependence of free volume in bisphenol A polycarbonate studied by positron lifetime spectroscopy, *Macromolecules*, 25, 19, 5089 (1992).
12. J. S. Royal and J. M. Torkelson, Photochromic and fluorescent probe studies in glassy polymer matrices. 5. Effects of physical aging on bisphenol-A polycarbonates and poly(vinyl acetate) as sensed by a size distribution of photochronic probes, *Macromolecules*, 25, 4792 (1992).
13. L. B. Liu, D. Gidley, A. F. Yee, Effect of cyclic stress on structural changes in polycarbonate as probed by positron annihilation lifetime spectroscopy , *Journal of Polymer Science: Part B: Polymer Physics*, 30, 231 (1992).
14. L. M. Costello and W. J. Koros, Temperature Dependence of Gas Sorption and Transport Properties in Polymers: Measurements and Applications, *Industrial Engineering Chemical Research*, 31, 2708 (1992).
15. A. J. Kovacs, Transition vitreuse dans les polymeres amorphes- Etude phenomenologique, *Fortschr. Hochpolym.- Forsch.*, 394-507 (1963).
16. J. M. Hutchinson, Physical aging of polymers, *Prog. Polym. Sci.* , 20, 703 (1995).
17. L. C. E. Struik, Physical aging in amorphous polymers and other materials, Elsevier, New York, 1978.
18. M. R. Tant and G. L. Wilkes, An overview of the nonequilibrium behavior of polymer glasses, *Polymer Engineering and Science*, 21, 14, 874 (1981).
19. J. M. Hutchinson, Relaxation processes and physical aging, in The Physics of Glassy Polymers, edited by R. N. Haward and R. J. Young, Chapman & Hall, London, 1997.
20. R. P. Chartoff, Thermoplastic polymers, in Thermal characterization of polymeric materials, E. A. Turi, edt, Academic Press, NY, 548-573 (1997).
21. L. C. E. Struik, Aging, Physical, *Encyclopedia of Polymer Science and Engineerin*g, vol 1, 595-611, Wiley, NY (1985).
22. J. M. O'Reilly, Review of structure and mobility in amorphous polymers, *CRC critical reviews in solid state and materials sciences*, 13, 3, 259-277 (1987).
23. J. Mijovic, L. Nicolais, A. D'Amore, J. M. Kenny, Principal features of structural relaxation in glassy polymers- A review, *Polymer Enginering and Science*, 34, 5, 381 (1994).
24. S, Matsuoka, Free volume, excess entropy and mechanical behavior of polymeric glasses, *Polymer Engineering and Science*, mid-october, 21, 14, 907-921 (1981).
25. J.-C. Bauwens, Physical aging: relation between free volume and plastic deformation, in Failure of plastics, W. Brostow and R. D. Corneliussen, edts, Hanser Publishers, Munich (1986).
26. L. C. E. Struik, Physical aging: influence on the deformation behavior of amorphous polymers, in Failure of plastics, W. Brostow and R. D. Corneliussen, edts, Hanser Publishers, Munich (1986).

27. R. Wimberger-Friedl and J. G. de Bruin, The very long-term volume recovery of polycarbonate: is self-retardation finite? *Macromolecules*, 29, 4992-4997 (1996).
28. U. Kriesten and J. M. Hutchinson, On the use of a density gradient column to monitor the physical ageing of polystyrene, *Polymer*, 33, 22, 4875-4877 (1992).
29. T. Murayama, Dynamic mechanical analysis of polymeric materials, Elsevier, NY, 1978.
30. Edith A. Turi, Editor, Thermal characterization of polymeric materials, Academic Press, New York, 1981. 2nd Edition, vol 1, 1997.
31. G. L. Wilkes, Polymers, Mechanical behavior, Encyclopedia of physical science and technology, vol 11, 61-84.
32. M. Trznadel, T. Pakula, M. Kryszewski, *Polymer*, 29, 619 (1988).
33. C. Bauwens-Crowet, J. C. Bauwens, *Polymer*, 24, 921 (1983).
34. A. F. Yee and S. A. Smith, *Macromolecules*, 14, 54-64 (1981).
35. T. G. Fox and P. J. Flory, *J. Am. Chem. Soc.*, 70, 2384 (1948).
36. T. G. Fox and P. J. Flory, *J. Appl. Phys.*, 21, 581 (1950).
37. A. H. Chan and D. R. Paul, Effect of sub-Tg annealing on CO_2 sorption in polycarbonate, *Polymer Enginering and Science*, 20, 1, 87 (1980).
38. A. J. Hill, K. J. Heater, C. M. Agrawai, The effects of physical aging in polycarbonate, *Journal of Polymer Science: Part B: Polymer Physics*, 28, 387 (1990).
39. H. Hachisuka, Y. Tsujita, A. Takizawa, T. Kinoshita, CO_2 properties and enthalpy relaxation in alternating copoly(vinylidene cyanide-vinyl acetate)s, *Polymer*, 29, 2050 (1988).
40. R. A. Pethrick, Physical aging – an old problem revisited, *TRIP*, 1, 8, 226-227 (1993).
41. T. W. Cheng, H. Heskkula, and D. R. Paul, Thermal aging of impact-modified polycarbonate, *Journal of Applied Polymer Science*, 45, 531-551 (1992).
42. C. R. Schultheisz and G. B. McKenna, Volume recovery and physical aging in glassy polycarbonate following temperature jumps, Polymeric materials science and engineering, ACS, 76, 221 (1997).
43. S. Matsuoka, Relaxation phenomena in polymers, Hanser Publishers, NY, 1992.
44. W. J. Davis and R. A. Pethrick, Investigation of physical ageing in polymethylmethacrylate using positron annihilation, dielectric relaxation and dynamic mechanical thermal analysis, *Polymer*, 39, 2, 255 (1998).
45. M. L. Cerrada and G. B. McKenna, Physical aging of amorphous PEN: isothermal, isochronal and isostructural results, *Macromolecules*, 33, 3065-3076 (2000).
46. M. M. Santore, R. S. Duran, G. B. McKenna, Volume recovery in epoxy glasses subjected to torsional deformations: the question of rejuvenation, *Polymer*, 32, 13, 2377 (1991).
47. Y. C. Jean, Y. Rhee, Y. Lou, D. Shelby, G. L. Wilkes, Anisotropy of hole structures in oriented polycarbonate probed by two-dimensional angular correlation of annihilation radiation, *Journal of Polymer Science: Part B: Polymer Physics*, 34, 2979-2985 (1996).

48. J. Lu, Y. Wang, and D. Chen, Infrared spectroscopic and modulated differential scanning calorimetry study of physical aging in bisphenol-A polycarbonate, *Polymer Journal*, 32, 7, 610-615 (2000).
49. Y. Maeda and D. R. Paul, Effect of AntiPlasticization on Gas Sorption and Transport. III. Free Volume Interpretation, *Journal of Polymer Science: Part B: Polymer Physics*, 25, 1005 (1987).
50. J. M. Mohr, D. R. Paul, G. L. Tullos, and P. E. Cassidy, Gas transport properties of a series of poly(ether ketone) polymers, *Polymer*, 32, 13, 2387-2394 (1991).
51. J. S. McHattie, W. J. Koros and D. R. Paul, Gas transport properties of polysulphones: 1. Role of symmetry of methyl group placement on bisphenol rings, *Polymer*, 32, 5, 840-850 (1991).
52. K. Neki and P. H. Geil, Morphology – Property studies of amorphous polycarbonate, *J. Macromol. Sci.- Phys.*, B8(1-2), 295-341 (1973).
53. S. L. Simon, D. J. Plazek, B. J. Harper, and T. Holden, Physical aging of polystyrene: volume and enthalpy recovery, *PSME Preprints*, 76, 334 (1997).
54. T. S.-K. Lo, M. S. Thesis, University of Cincinnati, Cincinnati, OH (1978).
55. M. D. Shelby and G. L. Wilkes, Thermodynamic characterization of the oriented state of bisphenol A polycarbonate as it pertains to enhanced physical aging, *Journal of Polymer Science: Part B: Polymer Physics*, 36, 2111 (1998).
56. M. D. Shelby and G. L. Wilkes, The effect of molecular orientation on the physical ageing of amorphous polymers - dilatometric and mechanical creep behaviour, *Polymer*, 39, 26, 6767-6779 (1998).
57. M. D. Shelby, A. J. Hill, M. I. Burgar, G. L. Wilkes, The effects of molecular orientation on the physical aging and mobility of polycarbonate – solid state NMR and dynamic mechanical analysis, *Journal of Polymer Science: Part B: Polymer Physics*, 39, 32-46 (2001).
58. J. J. Aklonis, W. J. MacKnight, M. Shen, Introduction to polymer viscoelasticity, Wiley-Interscience, NY, 1972.
J. J. Aklonis and W. J. MacKnight, Introduction to polymer viscoelasticity, 2nd edition, John Wiley & Sons, NY, 1983.
59. N. Heymans and B. Dequenne, Relationship between conformation and enthalpy or volume relaxation in polycarbonate, *Polymer*, 42, 5337-5342 (2001).
60. H. Higuchi, Z. Yu, A. M. Jamieson, R. Simha, and J. D. McGervey, Thermal history and temperature dependence of viscoelastic properties of polymer glasses: relation to free volume quantities, *Journal of Polymer Science: Part B: Polymer Physics*, 33, 2295-2305 (1995).
61. P. Pekarski, J. Hampe, I Böhm, H.-G. Brion, and R. Kirchheim, Effect of aging and conditioning on diffusion and sorption of small molecules in polymer glasses, *Macromolecules*, 33, 2192-2199 (2000).
62. Y. Yampolskii, S. Shishatskii, A. Alentiev, K. Loza, Correlations with and prediction of activation energies of gas permeation and diffusion in glassy polymers, *Journal of Membrane Science*, 148, 59-69 (1998).

Chapter 8

Effect of orientation on the transport of gas molecules through amorphous glassy bisphenol-A polycarbonate

8.1. Introduction

Knowledge of the effect of orientation on gas transport is more than necessary since commercial films are always oriented to some degree. Such knowledge would make it possible to optimize the properties of the polymeric materials. A literature review concerning orientation and gas transport has been provided in Chapter 3. The few results reported in the literature suggest that the influence of orientation on the gas transport parameters is rather complex. Since the permeability coefficient is the product of a solubility and a diffusion coefficients, the contribution of orientation on both parameters has to be evaluated separately. As a sample is stretched uniaxially, the polymer chains orient themselves in the draw direction and the sample becomes anisotropic. Two-dimensional angular correlation of annihilation radiation (2D-ACAR) has been used to give information on the structure of the microvoids dispersed inside a polycarbonate matrix [1]. The hole structure has been shown to become ellipsoidal with uniaxial orientation, whereas it was spherical in unoriented samples. The radius of the sphere was determined to be about 2.9 Å, whereas the radii of the ellipsoid axis were 2.3 Å and 3.8

Å. The corresponding Herman's orientation function was 0.2. Changes in the shape of the microvoids may affect the diffusion coefficient. We expect that the diffusion coefficient will be affected by the orientation process, because of the orientational and conformational changes of the polymer chains induced by drawing.

This study is aimed at providing some information on the effect of orientation on the gas transport parameters. Polycarbonate will be stretched both below and above T_g. The resulting orientation is referred to as cold-drawing and hot-drawing, respectively. Hot-drawing is simpler in the sense that it avoids complications arising from residual stresses. Stretching a polymer below T_g slightly changes the intermolecular distances between bond angles and lengths of the polymer backbone. The bond angles are slightly increased because of the restricted rotations between bonds. Some level of distortional birefringence can be observed [2]. The stretching temperatures were chosen as 130^{o}C (cold-drawing), and 160^{o}C and 180^{o}C (hot-drawing), which are in the vicinity of the T_g of polycarbonate, which is about 150^{o}C. The temperature of 160^{o}C was selected in this study because some orientation studies have already been carried out at that particular temperature [1-4]. This should allow us to compare our results with those published elsewhere. The temperature of 180^{o}C was chosen in order to possibly achieve the global orientation–local random (GOLR) state in the amorphous polycarbonate. This particular state corresponds to a high global chain orientation but to a nearly random local segmental orientation. The GOLR state of polycarbonate has been shown to exist at temperatures of about 20 to 30^{o}C above T_g [5], and had a corresponding birefringence on the order of 10^{-4}. Song and Fan [5] observed that although some properties of the polycarbonate samples such as birefringence, linear dichroism, and X-ray diffraction pattern were nearly isotropic at the GOLR state, other properties such as thermal expansion, solvent-swelling, and stress-strain behavior showed strong anisotropic behaviors. The difference in the property behaviors was attributed to the difference in the relaxation rates of the oriented chains versus the local polymer units. It would be interesting to determine whether or not gas transport properties are affected by this GOLR state and to compare the gas transport results with other physical properties. Since gas transport should affect only a local portion of the polymer chains, if there is any

difference between the sample in the GOLR state and an isotropic sample, the difference could be possibly attributed to conformational changes.

To our knowledge, the effects of orientation on polymer physical aging and the corresponding gas transport properties of polymers have not been examined in the literature. Using gas transport should provide information on how physical aging is affected by orientation from a molecular point of view. Indeed, as discussed in Chapter 3, inconsistencies in the free volume theory have been reported for uniaxially oriented amorphous glassy polymers subjected to aging [2-4, 6-9].

8.2. Experimental details

The following subsections mention briefly the materials and the instrumental methods used in this study. The complete experimental details have been provided in Chapter 4. The reader should refer to this particular chapter for deeper understanding of the materials and the instrumental methods used in this research.

8.2.1. The materials

Lexan 8010 bisphenol-A polycarbonate sheets were ordered from General Electric (GE). The weight average molecular weight M_w was determined by GPC to be about 43,700 g/mol and the polydispersity index about 2.1. The glass transition temperature was given as 150^{o}C by the supplier, as obtained by DSC from the second heating scan at a heating rate of 10^{o}C/min. The density was given as 1.2 g/cm^3 at 20^{o}C. The molecular weight was believed to be high enough to prevent crystallization from happening because of the entanglement effects. Please note that it was not possible to process polycarbonate films from pellets by hot press in this study. Films processed by compression molding were not flat through the whole surface area of the hot plates and this difference in thickness affected the film during stretching. Moreover, the surface area of the hot press was not large enough to make stretched films for further permeation

experiments. The permeation set-up required indeed bubble-free polymeric circles of diameter 4.8cm.

The polymeric sheets were kept in a dessicator at all time after purchase in order to avoid any more water moisture uptake. Prior to experiments, the polymeric sheets were dried at room temperature for one day in a vacuum oven. It was not recommended to heat the GE polycarbonate at higher temperatures for a prolonged time because of the possible reaction of the polymeric components. Indeed, Lexan can react easily at high temperature to give rise to "fries rearrangement", involving the formation of small branches [10]. Following drying the sheets were put between Kapton® sheets and copper metal plates, as explained in Chapter 4. The metal plates were suspended in the center of a circulating air gas chromatograph (GC) oven to improve heat transfer on both sides of the plates. The samples were heated in the GC oven from room temperature to 165^{o}C at a heating rate of 40^{o}C/min, kept at 165^{o}C for 15min to remove thermal history and possible orientation, and cooled within the oven at a controlled rate of 40^{o}C/min to room temperature. The room temperature was about 30^{o}C. The polymer films were used immediately.

The thicknesses of the initial sheets (before stretching) were about 190μm.

8.2.2. The instrumental methods

Stretching, density, FTIR, birefringence, DMTA, and permeation conditions are presented below.

8.2.2.1. Stretching

A stretcher was built in the Physics Department of Virginia Tech based on the design of the one used in Dr. Wilkes' lab in the Chemical Engineering Department at Virginia Tech. A schematic of the stretcher used in this research is provided in Figure 8.1. The stretched surface area required for permeation experiments necessitated very large samples, which could not be stretched with commercially available Instron equipment on campus.

The stretcher was placed in an oven insulated by aluminium metal plates to limit heat loss. A thermocouple was attached to the system to read the temperature inside the oven near the grips of the stretcher. The oven was heated to the desired stretching temperature. The heating process of the system consisting of the stretcher and the oven took at least one hour, but usually the oven was heated overnight to allow the temperature to reach equilibrium. The temperature gradient inside the oven at the grips level was found to be negligible. As written before, the stretching temperatures in this study were chosen as 130^{o}C (cold-drawing), and 160^{o}C and 180^{o}C (hot-drawing). Some films stretched at other temperatures than the ones given above will also however be shown in the section dealing with the DMTA results.

Polycarbonate samples were cut into rectangular shapes. The samples had to be at least 10cm long, but the width could vary. Nevertheless the wider the width, the more difficult the stretching process. Furthermore, whitening of the material in the transverse direction was observed on stretched samples with a large width. This whitening was not however attributed to strain-induced crystallization, but rather to a change in refractive index with void formation [11]. An approximate length to width ratio was determined to avoid loosing transparency at all time. A ratio of three between the length and the width was verified for the samples. Lines were drawn on the polycarbonate samples with waterproof ink every 5mm. The distance between these lines after stretching provided information about the draw ratio.

The stretching was performed as follows. Once the temperature in the oven had been established, the stretcher was taken out of the oven and the film was rapidly placed between the two grips. The stretcher was then put back in the oven. Ten minutes were allowed for temperature equilibrium of the system, and stretching was performed for about one minute at a constant overhead speed. This overhead speed (in turns/min) varied from one sample to another in order to achieve various draw ratios. Obviously, the stretching was performed without opening the oven and thus without disturbing the temperature inside the oven. Please note that the stretching rate was not constant since the initial length l_o was changing throughout the stretching. Indeed, if one calculates the draw

ratio, which corresponds to the ratio of the length at some time divided by l_o, l_o changes its value for each time increment Δt. The stretching rate corresponded actually to an exponential decay. When undrawn isotropic samples were to be studied, samples were left for eleven minutes inside the oven. This ensured that the same thermal treatment was given to unoriented samples. This time was believed to be small enough to avoid any form of aging (in the case of cold-drawing) or crystallization (in the case of hot-drawing) in the unstretched polycarbonate film. A drill and a variable autotransformer were initially used to control the speed at which the samples were stretched uniaxially. However the speed could not be controlled uniformly. As a consequence, it was decided to turn the stretcher by hand at a uniform rate. As soon as the stretching was completed, the thermocouple and the metal plates were removed, the stretcher was taken out of the oven, and the specimen was immediately cooled by blowing air to freeze-in orientation. The cooling rate was maintained constant and was evaluated to be in excess of 50^oC/min, in agreement with values reported in the literature for a typical fan [12]. It should be pointed out that oriented samples may have cooled faster than isotropic ones because of the reduced thickness. No correction was considered in this study to account for the differences in the cooling rates. The time needed after stretching and before cooling was evaluated to be about five seconds. This corresponded to the time needed to remove the parts attached to the oven, to put the stretcher on the laboratory bench, and to start the fan. This time was assumed to be short enough to prevent the polymer chains from completely relaxing. Cooling was performed for at least five minutes on the specimen under constant stress. The film was finally removed from the apparatus. A schematic of the stretching process is shown in Figure 8.2. The appearance of the films before and after stretching is sketched in Figure 8.3. The distance between the lines after stretching provided information about the draw ratio. Circles drawn on the specimen prior to drawing became ellipsoidal after stretching.

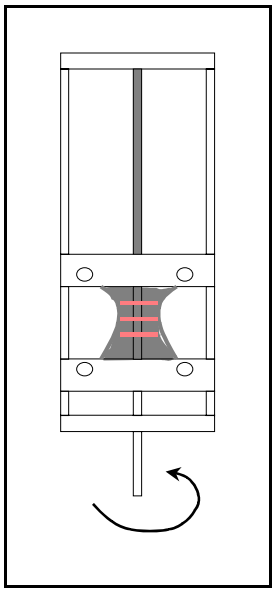

Figure 8.1: Schematic of the stretcher.

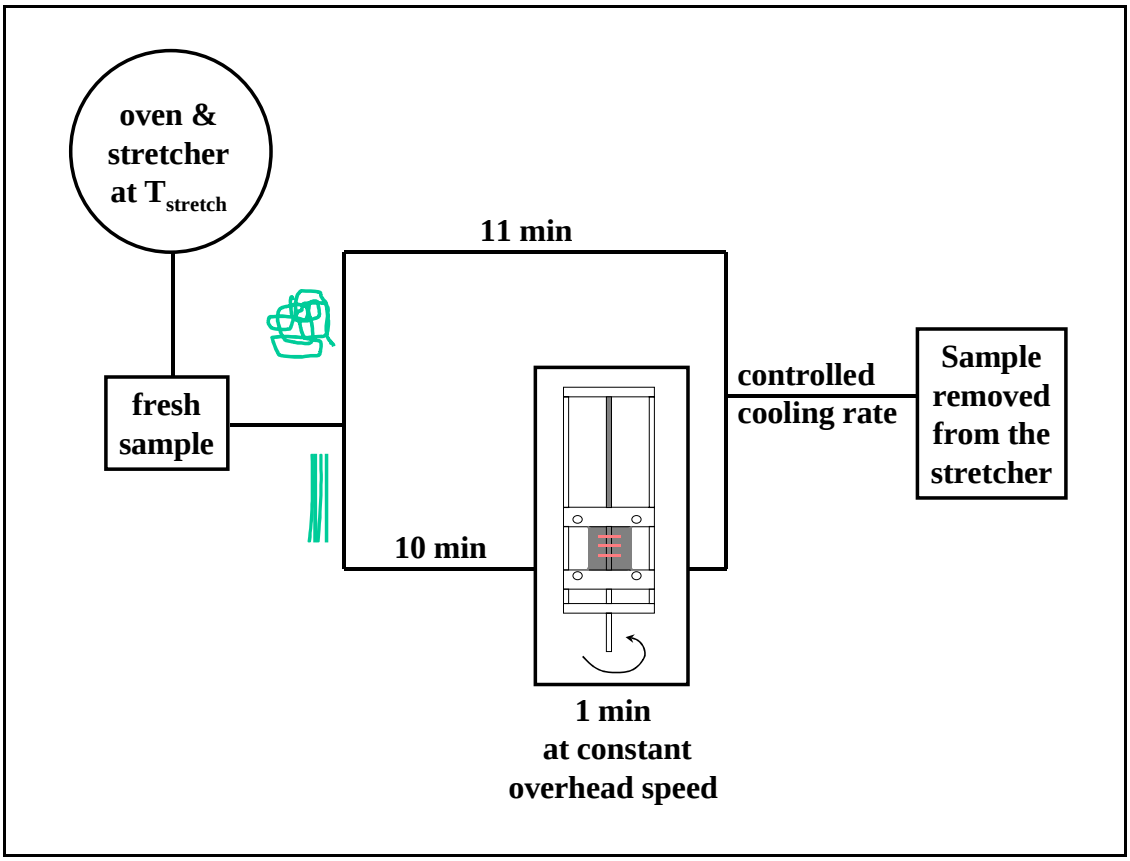

Figure 8.2: Schematic of the stretching process.

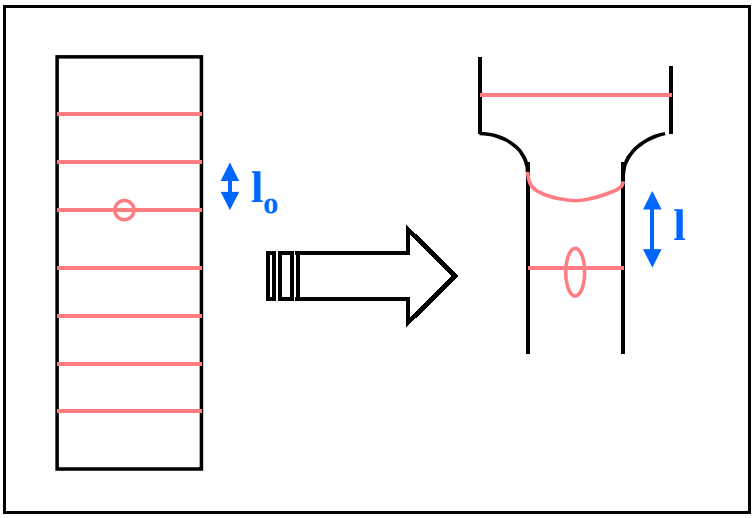

Figure 8.3: Schematic of the samples prepared for stretching and resulting appearance after drawing. Before stretching, lines were drawn every 5mm. The distance between those lines after stretching provided information about the draw ratio λ ($=l/l_o$). Circles drawn on the specimen prior to drawing became ellipsoidal with stretching.

8.2.2.2. Density

The densities were measured at 18°C in a linear density gradient column made of an aqueous solution of sodium bromide. The theoretical resolution of the column was about 5×10^{-5} g/cm^3. The values of the densities gave indication about the presence or lack of crystallinity in the bulk samples.

8.2.2.3. FTIR

In order to verify the absence of strain-induced crystallization at the surface, FTIR spectra were collected in the ATR (attenuated total reflectance) mode using a zinc selenide ZnSe crystal.

8.2.2.4. Birefringence

The average degree of orientation was determined from a birefringence apparatus using a Babinet compensator. The sample was always introduced in the beam path with

the machine direction placed horizontally for consistency in the measurements. The birefringence Δ was determined in the center of the membrane, at the top, bottom, right, and left, as seen in Figure 8.4. Three measurements were taken and averaged for each of the five positions. The measurements were taken at 23^{o}C.

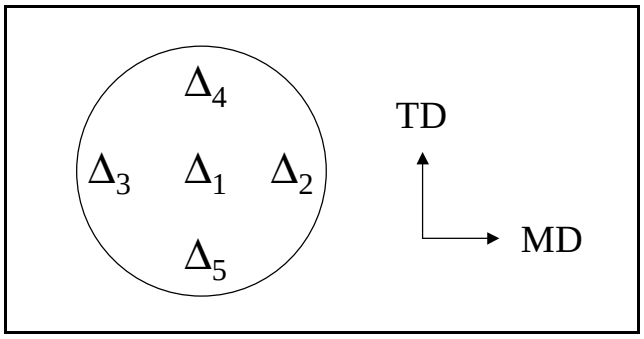

Figure 8.4: Location of the five birefringence measurements taken on the membrane. The area of the membrane was about 18.10 cm^2. MD and TD stand for the machine and the transverse directions, respectively.

8.2.2.5. DMTA

The dynamic mechanical experiments were carried out in the tensile mode. The location of the sample cut for DMTA experiments was clearly written down on the schematic shown in Figure 8.3 for further estimation of the draw ratio.

Dynamic temperature ramp experiments were performed with the following conditions. A torque of 10 cNm was used on each clamp. The frequency was chosen as 1Hz, the heating rate as 2^{o}C/min, the initial temperature as 25^{o}C, the strain as 0.025%, and the static force as 40g. The static force was determined at room temperature by dynamic frequency sweep test (strain control). The strain level was assumed to be low enough to not interfere with the strain induced by orientation and to avoid any structural breakdowns.

8.2.2.6. Permeation

The polycarbonate samples were prepared as follows for permeation experiments. A circle of diameter 4.8cm was cut on the center of the stretched polymer films. The central part of the film was believed to be more uniaxially oriented than the sides or the extremities. The location of the circle was clearly indicated on the schematic provided in Figure 8.3 for further calculation of the draw ratio.

Samples to be used in the permeation apparatus were originally masked off to reduce the permeation area and thus improve the accuracy in the value of the draw ratio. A circle of about 14mm diameter was cut from the central part of the stretched film. Its location was clearly indicated on the schematic provided in Figure 8.3 for estimation of the draw ratio. Its thickness was also recorded. An aluminium foil circle of 4.8cm diameter was cut, folded in twice, and a semi-circle of 4mm radius was drawn on it, and cut. Thereafter, the aluminium foil circle presented a hole of 8mm diameter in its center. Some glue was applied on the edges of the hole, the polymer was put into contact with the glued contour, and both surfaces were hold together for about 15 seconds. The glue was a Duro quick gel / No-run super glue equipped with a small pipe. Complete drying took about 5 minutes. While doing permeation experiments, the side with the glue visible was exposed to the gas feed. Unfortunately, the permeation experiments did not always work on such masked samples, mainly because of the glueing procedure. Using aluminium foil also introduced additional problems. The presence of small wrinkles on the aluminium created leaks in the permeation set-up. Furthermore, the pressure transducers were not sensitive enough to the reduced permeate stream. Indeed, no time-lag could be observed on either unoriented or oriented specimens. The permeation profile appeared to be linear with time. Decreasing the permeation volume was impossible since the volume was already minimized and originated mainly from the inside of the pressure transducer itself, and increasing the feed pressure could modify the polymer and possibly destroy the pressure transducers in case of leaks. The polymeric samples could not therefore be prepared this way, rather as explained in the previous paragraph. The surface area of the membrane had to be taken as about 18.10 cm^2. Obviously, the degree of orientation could not be assumed to remain constant all over the area.

Permeation experiments were carried out at 35°C using He, O_2, and N_2, in that given sequence. The applied pressures were fixed at about 2.5 atm for He, and 3.9 atm for O_2 and N_2. Three measurements were taken for each gas to ensure reproducibility and to calculate the error involved in the permeation results. Please note that the degassing time between N_2 runs was fixed at 120min in this particular study, and not 90min as reported in Chapter 4. Permeation experiments were also carried out on the same membrane at several temperatures, right after the experiment at 35°C, in order to determine the temperature dependent activation energies. Those temperatures were chosen as 45°C and 55°C for the samples stretched at 130°C and 160°C. Temperatures of 40, 45, and 55°C were selected for the samples stretched at 180°C. Aging was found to be negligible at those temperatures within the timeframe of the experiments. It was assumed that deorientation and shrinkage did not have time to take place within the timeframe of the permeation experiments.

8.3. Results and discussion

8.3.1. FTIR results

Comparisons of spectra of amorphous and semi-crystalline samples are shown in Figure 8.5. The semi-crystalline samples were supplied by Dr. Marand's lab in the Chemistry Department of Virginia Tech. Although these samples possessed a lower molecular weight than the polycarbonate selected in the current research, this was not expected to affect the wavenumbers of the amorphous bands. The crystallinities of the two semi-crystalline samples were determined to be 5% and 18% [13]. The spectra shown in Figure 8.5 could not, however, be compared quantitatively since the contact was different for each sample. However changes in the peak assignments were easily visible. The peak assignments of polycarbonate can be found in the literature [14, 15]. As expected, there were more trans-trans contributions (1767cm^{-1}, 1594cm^{-1}, 1252cm^{-1}) with crystallinity than trans-cis contributions (1785cm^{-1}, 1604cm^{-1}, 1223cm^{-1}), indicating that ordering was taking place within the material. Trans-trans and trans-cis refer to the

conformation of the carbonate group. The band around 1785 cm^{-1} was assigned to the vibration of the carbonyl group C=O, the band at 1604 cm^{-1} to the C-C aromatic in-plane, and the band at 1223 cm^{-1} to the C-O-C antisymmetric [14].

No signs of strain-induced crystallization at the surface could be detected by FTIR-ATR spectroscopy on any of the samples stretched in this work. Crystallinity in polycarbonate is actually reported to be very difficult to achieve, at least under normal stretching conditions. Wu [2] could not detect any signs of strain-induced crystallization in cold and hot-drawn polycarbonate samples using experimental techniques such as DSC, X-ray diffraction, and FTIR spectroscopy. Since the ATR technique provided information about the absence of crystallization at the surface only, density measurements were carried out as well.

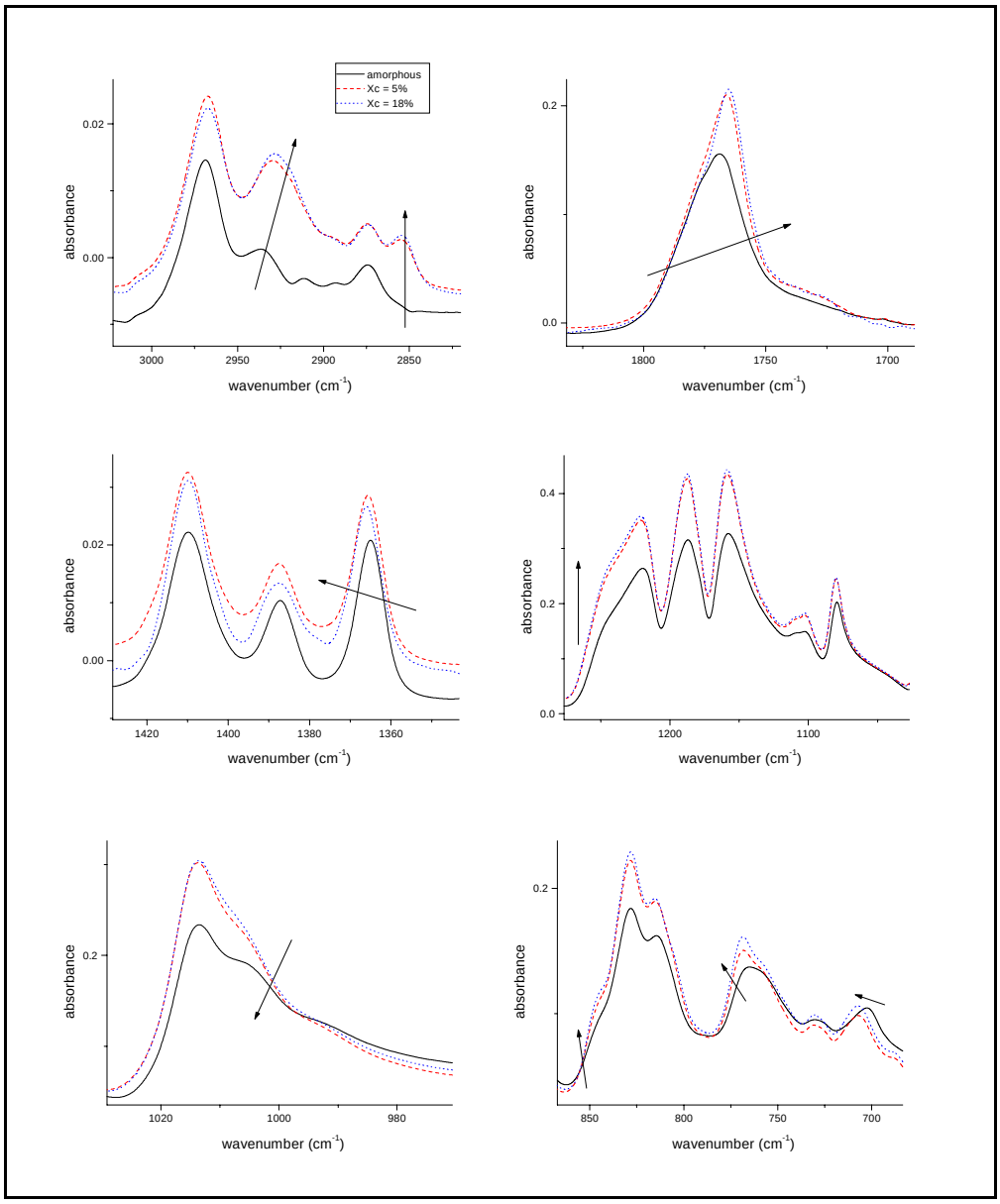

Figure 8.5: Spectral changes induced with crystallization as observed by ATR for several absorption bands of polycarbonate (ZnSe crystal, 50°, no polarizer). The critical angle of incidence was calculated to be 40.92°. The refractive indices of the ZnSe ATR crystal and the polycarbonate were taken as 2.42 and 1.585, respectively.

8.3.2. Orientation results

The degree of orientation in the polycarbonate films was defined by calculating the draw ratio λ and the Hermans' orientation function f. The general definition of those quantities has been given in Chapter 3. Nevertheless a background is provided here about

the calculation of f from the birefringence technique. The values obtained for f in this study are provided. Finally, λ and f values are compared.

8.3.2.1. Background

Due to the high absorption of polycarbonate in the infrared range and fairly thick samples, it was not possible in this study to determine orientation by FTIR transmission techniques. The 1364cm^{-1} and 2971 cm^{-1} peaks used in other studies involving polycarbonate [2, 5, 16-18] saturated in the IR range. FTIR-ATR spectroscopy was not used to look at the surface orientation since the contact is a serious limitation of the technique. Therefore the level of orientation was assessed from birefringence measurements. One has to keep in mind that the birefringence method provides only information about an average orientation of the molecules.

The Hermans' orientation function f measured by birefringence is given by the following relation:

$$f = \left(\frac{\Delta_f}{\Delta^o} \right) \qquad \text{Eq (8.1)}$$

where Δ_f is the orientational birefringence and Δ^o the intrinsic birefringence. The intrinsic birefringence Δ^o corresponds to the birefringence of a perfectly oriented polymer. Δ^o was taken as 0.16, as reported by Shelby and Wilkes on hot-drawn polycarbonate by combining birefringence and sonic modulus results [3]. The theoretical value of the intrinsic birefringence Δ^o of polycarbonate has been calculated from the bond polarizabilities of the polycarbonate repeat unit to be 0.207 [19]. An experimental value of 0.236 was found by Biangardi [20] using WAXS. Unfortunately, Biangardi calculated the value of Δ^o by fitting data obtained while stretching polycarbonate both below and above T_g. As stated earlier, distortional birefringence cannot be neglected below T_g [2]. Wu [2] determined Δ^o to be equal to 0.192 for polycarbonate. The value was obtained from birefringence and linear dichroism measurements. The total birefringence of hot-drawn samples (shown to be due to orientational effects only) was plotted as a function of

f (determined from linear dichroism) and the resulting slope corresponded to the intrinsic birefringence.

8.3.2.2. Hermans' orientation function results

The Hermans' orientation function was calculated for the anisotropic samples. As mentioned in Chapter 4, it was found that the measured birefringence Δ of hot-drawn samples was equal to the orientational birefringence Δ_f in this study. Experimental birefringences were taken at five different selected areas for each polymer film, as explained in the experimental section of this chapter. An average value of f was calculated for each polymer film by taking the average of the five Hermans' orientation functions.

The orientation results are summarized in Table 8.1. The values of f may appear as being rather low, but amorphous polymer chains cannot be oriented that much by hot-drawing. Furthermore, the presence of entanglements restricts the alignment of the chains. The entanglements remain intact with stretching. However, when one chain is stretched, at least another one moves too because they are connected through those entanglements. The presence of entanglements limits the motion of the polymer chains. f was observed to be greater at 160^{o}C than at 180^{o}C. Indeed, thermal motions become more rapid at higher temperatures and "destroy" the orientation. Also, it was observed that the membranes were typically more stretched in the middle than on the sides. This may have originated from an unhomogeneous pressure near the grips. The orientation function f was also on average higher in the MD direction than in the TD direction.

The values of f at 160^{o}C are consistent with those reported in the literature from birefringence measurements [1-4]. However they are about two times greater than the values determined by linear dichroism by Lundberg and Jansson [17]. However, one has to keep in mind that linear dichroism measures the orientation of a particular structure of the molecular chain, in contrast to birefringence that gives an indication of the average orientation. Moreover, although the stretching temperature is the same, results from the literature cannot be strictly compared because of differences in stretching and cooling procedures, molecular weights, suppliers, intrinsic birefringence values, etc.

The values of f at 180°C are about ten times greater than those observed in the GOLR state of polycarbonate at about the same strain levels [5]. Therefore this particular state was not achieved in this work.

The birefringence of the cold-drawn sample ($T_{stretch}$ = 130°C) could not be determined by use of the Babinet compensator. This was initially attributed to turbidity. However with the use of a microscope, it was noticed that crazing was taking place within the material. Some silicon oil was put on the surface of the sample to facilitate the measurement by avoiding scattering. Unfortunately, measurements were still not possible. Had it been possible to measure the birefringence of the cold-drawn polycarbonate samples, the value of the birefringence could have been corrected for deformation or distortional birefringence Δ_d. This particular type of birefringence (which can be observed in isotropic materials as well), arises from a change in packing caused by an external deformation. Distortions of bond angles and/or bond lengths from equilibrium are indeed observed in materials containing residual stresses. This can be observed for instance in materials quenched from the rubbery state. The skin and the core may be cooled at different rates and the resulting thermal gradient may generate residual stresses. Δ_d is usually in the order of 10^{-4} [21]. However Δ_d cannot be neglected in cold-drawn polymer films. In the case of cold-drawn polycarbonate, Δ_d has been shown to represent about 25% of the intrinsic birefringence [2].

		center	MD		TD		average
		f1	f2	f3	f4	f5	f
$T_{stretch}$ = 160°C	2t/5s for 19s	0.26196	0.16890	0.24081	0.20364	0.21070	0.21720
	2t/5s for 38s	0.25544	0.23712	0.25383	0.23439	0.22185	0.24053
	2t/5s for 56s	0.13673	0.13129	0.13301	0.11735	0.11715	0.12711
$T_{stretch}$ = 180°C	1t/5s for 75s	0.08708	0.06607	0.08019	0.06740	0.07761	0.07567
	2t/5s for 38s	0.11160	0.08333	0.08703	0.07348	0.08893	0.08887
	2t/5s for 75s	0.03993	0.03250	0.04234	0.01667	0.01870	0.03003
	3t/5s for 25s	0.10097	0.07819	0.08724	0.07867	0.07770	0.08456

Table 8.1: Orientation results giving the Hermans' orientation function f in the five different selected areas. Results are given as a function of the stretching temperature ($T_{stretch}$), and the number of turns per second in a given time (x t/s for x s). The membrane was typically found to be more oriented in the middle than on the sides. f was also on average higher in the MD direction than in the TD direction.

8.3.2.3. Comparison between λ and f values

No simple correlation existed between the draw ratio λ and the Hermans' orientation function f in this study, as indicated from the results given in Figure 8.6 and Figure 8.7. The calculated draw ratio and the Hermans' orientation function do not give the same values for the orientation; trends are not even respected. The stretching time seems to play an important role since chains are likely to relax at long stretching times. The fact that λ and f are not linearly correlated is in agreement with the literature [3].

Since the Hermans' orientation function characterizes the level of orientation much more accurately than the draw ratio, the results of characterization studies will be reported from now on as a function of f and not λ.

It has been shown in the literature that data obtained at different stretching rates do fit on a same line while plotted as a function of f [2]. Therefore experimental data can be plotted as a function of f even though the stretching rates were different.

Data reported in the literature are sometimes given as a function of the draw ratio [18, 22-26]. Such data make comparisons difficult between research groups since knowledge of the draw ratio alone is not sufficient to characterize the degree of orientation in polymeric materials. Giving the draw ratio should make sense within the same film though.

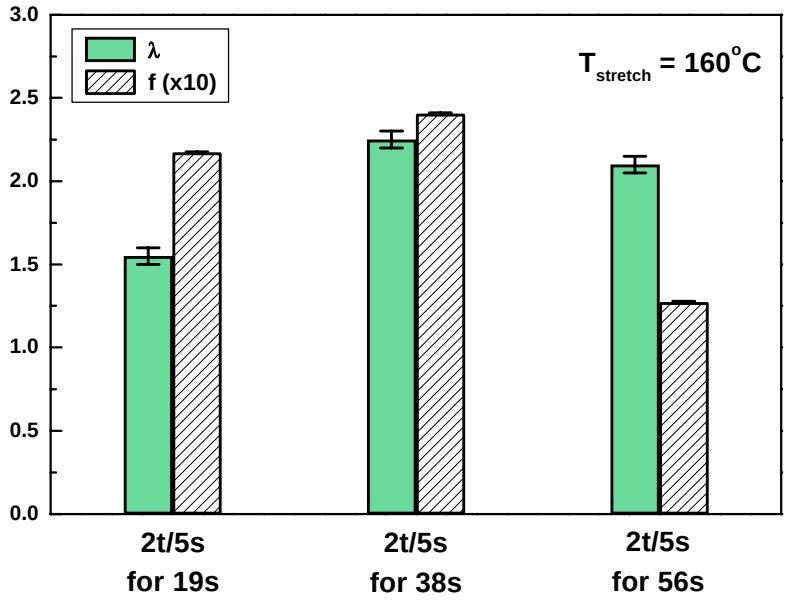

Figure 8.6: Comparison of the draw ratio λ and the Hermans' orientation function f. The samples were stretched at 160°C.

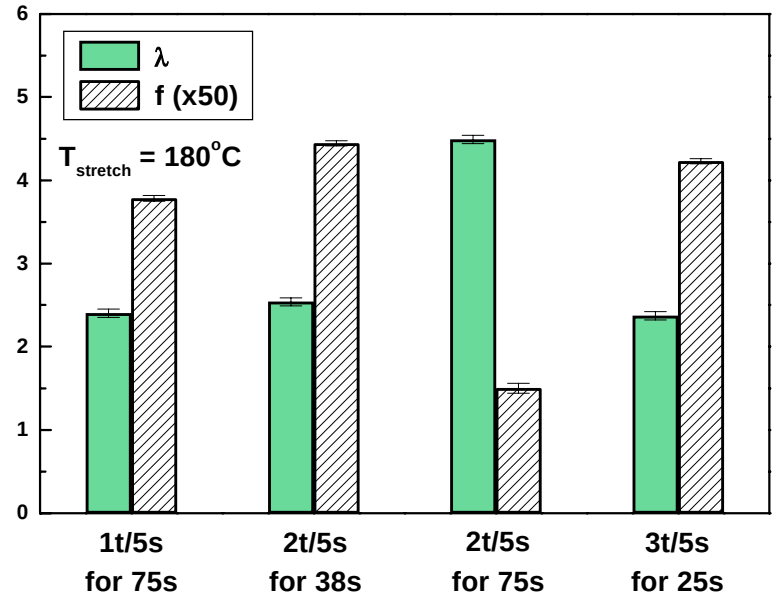

Figure 8.7: Comparison of the draw ratio λ and the Hermans' orientation function f. The samples were stretched at 180°C.

8.3.3. Density results

8.3.3.1. Isotropic samples

The densities of the isotropic samples are shown in Figure 8.8 for the various stretching temperatures chosen in this study. In this case, the samples were not stretched though, but just left in the stretcher inside the oven for the same amount of time as stretched samples in order to remove any thermal effects. The density was found to decrease with the stretching temperature (or here the term of oven temperature should be used instead). As the temperature increases, it is well-established that the specific volume increases, as measured by dilatometric measurements [27, 28]. And therefore the density decreases since density and specific volume are inversely related. If polymeric samples are quenched by blowing air at the same cooling rates but from different starting temperatures, the material cooled from the highest temperature will contain the greatest overall free volume content and hence the lowest density. This is what is observed in this study.

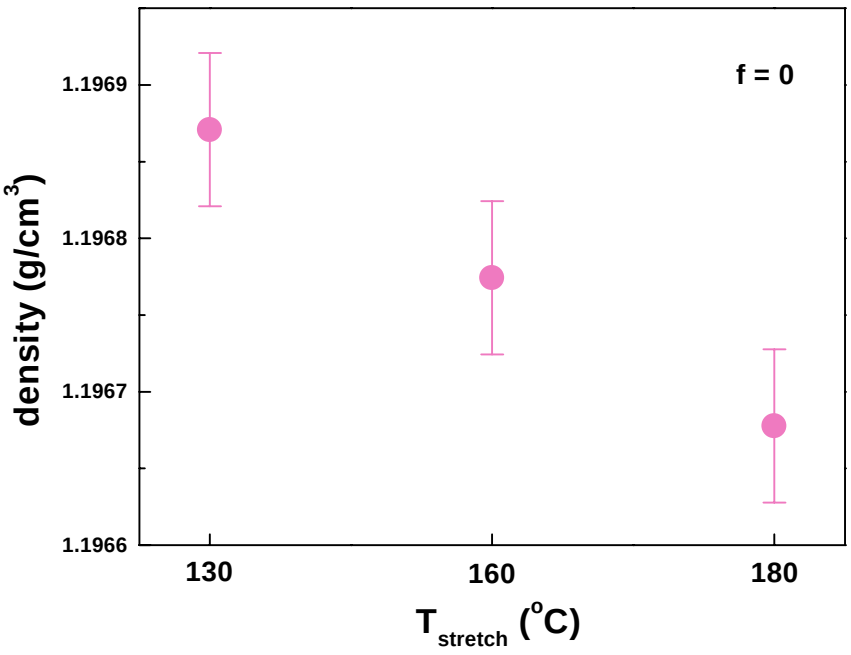

Figure 8.8: Density as a function of $T_{stretch}$ for isotropic samples. The densities were measured at 18°C in a linear density gradient column.

8.3.3.2. Anisotropic samples

Densities were determined for the stretched samples. Results are shown in Figure 8.9 through Figure 8.11. The densities were found to remain constant with stretching for hot-drawn samples whereas the density did increase for cold-drawn samples. The fact that the densities of hot-drawn polycarbonates remained at values similar to those of the undrawn samples seems reasonable. Indeed, hot-drawing is generally considered to be a constant volume process, as assumed from the Poisson's ratio value of 0.5, corresponding to a nearly incompressible process. On the other hand, drawing below T_g is not a constant volume deformation and is typically characterized by a Poisson' s ratio of 0.33. The densities of hot-drawn polycarbonate were too low for crystallinity to have occurred with orientation [13].

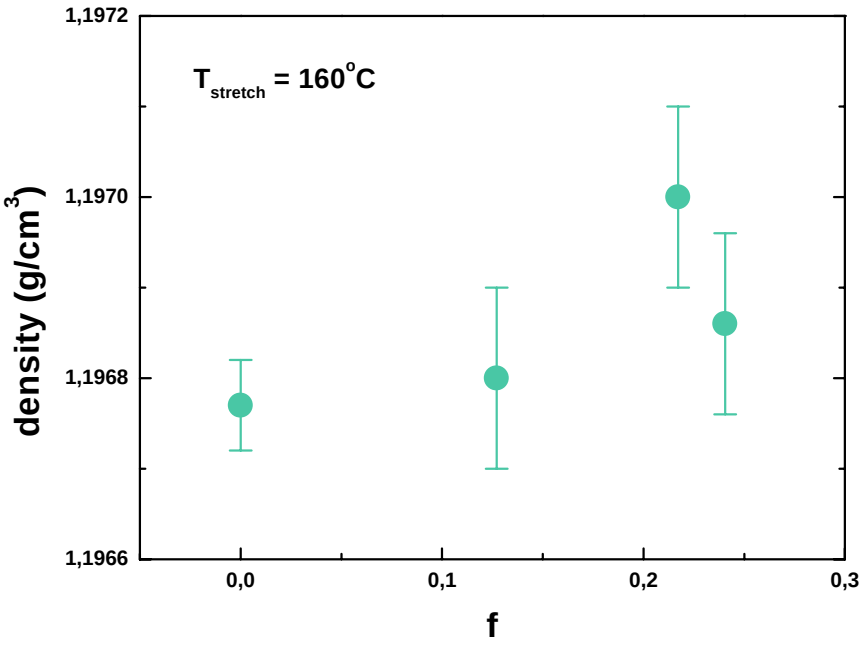

Figure 8.9: Density as a function of the Hermans' orientation function f. The stretching temperature was 160°C.

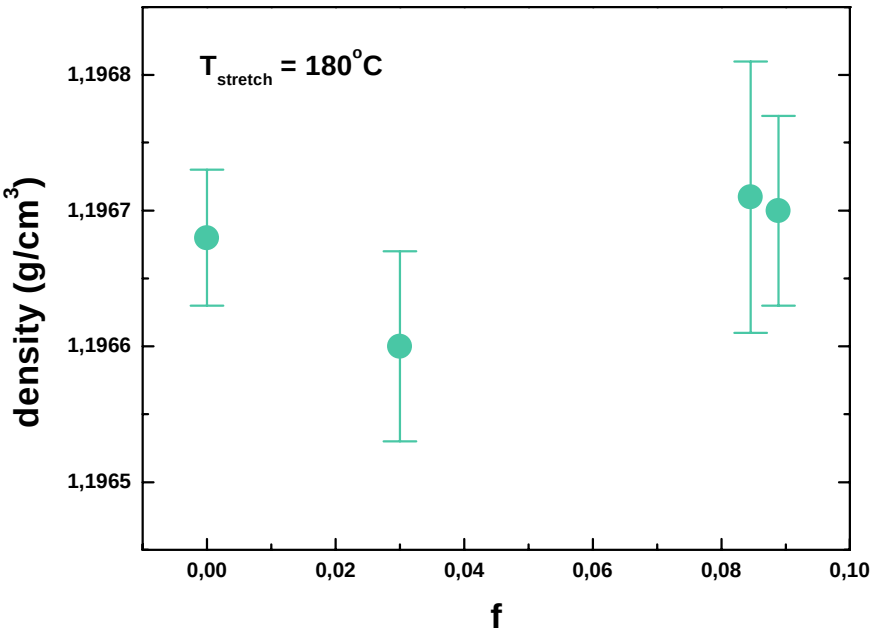

Figure 8.10: Density as a function of the Hermans' orientation function f. The stretching temperature was 180°C. The density of the sample characterized by a f value of 0.07567 could not be taken since vacuum grease was covering the membrane.

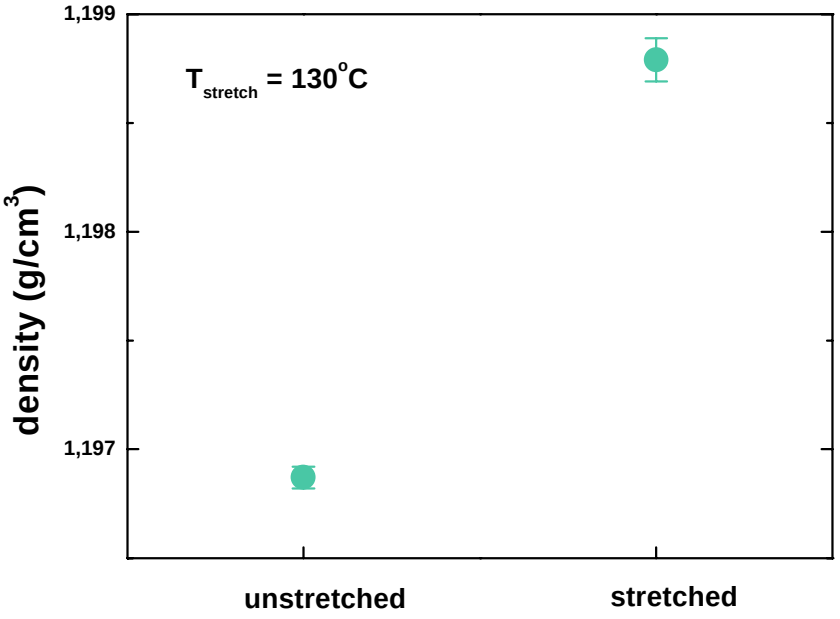

Figure 8.11: Density of unstretched and stretched samples. The stretching temperature was 130°C. It should be pointed out that the stretched sample was not taken from the membrane used in permeation experiments since the membrane was destroyed by oil while attempting to measure birefringence (see above). Nevertheless, the same experimental conditions were repeated in order to generate the same sample.

The experimental results are supported by the work of Wu. Wu [2] reported that any changes in the density of polycarbonate with stretching were highly dependent on the stretching temperature. In fact, the researchers did not observe any significant changes in the density of hot-drawn polycarbonate, whereas the density was slightly higher in cold-drawn samples. The resolution of the density gradient column was 5×10^{-4} g/cm^3. The increase in the density with cold-drawing can be attributed to the bond distortions, that may allow better packing of the polymer chains and thus give a higher density.

An increase in the density of polycarbonate with cold-drawing has been reported by Bartos et al [6]. Polycarbonate was stretched at room temperature and an increase in density of about 0.3% was observed compared to that of the isotropic sample. Quite interestingly, the T_g was not found to be influenced by drawing. A densification in cold-drawn polycarbonate was also reported by Pixa et al [7], although not quantified.

Interestingly, Shelby and co-workers [1, 3, 4] observed an increase in the density of hot-drawn polycarbonate samples with stretching. The density was found to increase almost linearly with the orientation function [3, 4]. A slight decrease in the density at a low f value was reported. The density increased from about 1.1982 g/cm^3 for an undrawn sample to about 1.1994 g/cm^3 for a sample with a f value of 0.2. The stretching temperature was set as 160^{o}C. Unfortunately the time given for temperature equilibrium of the samples in the oven was not mentioned and it is not clear whether or not the samples had reached the desired temperature of 160^{o}C at the time of drawing. Also, it was not specified whether the anisotropic samples did undergo exactly the same thermal treatment as the isotropic samples. The time left at 160^{o}C is indeed given for the isotropic samples, but not for the anisotropic ones [1]. The T_g (determined from DSC measurements) was also observed to increase slightly with f [3]. An orientation function of about 0.15 corresponded to an increase in T_g of about 0.8^{o}C compared to the isotropic sample. The fact that the density went through a minimum at a f value of about 0.03 and the changes in T_g suggest that density and T_g are not directly correlated for oriented samples. This point has already been discussed in Chapter 6 for isotropic samples.

In another study by Ito et al [22] the density of hot-drawn polycarbonate samples was also found to increase with the draw ratio. The samples were stretched at 170^{o}C at constant speed to various draw ratios ranging from 1 to about 3. The resulting densities

increased from about 1.193 to about 1.202 g/cm^3, which is quite a significant change. The stretching and the cooling procedures were not defined in the work of Ito et al [22], although those factors are highly significant. The researchers observed that the frequency of the maximum in the β-relaxation peak reached a minimum at a draw ratio of about 2. In another publication published at about the same time by Ito and co-workers again [18], an increase in density with the draw ratio was again observed for hot-drawn polycarbonate samples. Although the samples and their preparations and stretching procedures appear to be the same in both publications [18, 22], the density in the second paper ranged from about 1.192 to 1.194 g/cm^3 only, and not from about 1.193 to about 1.202 g/cm^3 anymore (see above). In both cases, the densities were obtained by the same technique. The difference in the temperature at which the densities were obtained (25^{o}C versus 30^{o}C) is unlikely to explain the density differences between both publications. Please note that the resolution of the flotation method was not given, and error bars were not reported either. Quite interestingly, the T_g of polycarbonate determined from DSC measurements was observed to go through a maximum at a draw ratio of about 2 [18]. In contrast, the density values did not present any particular point at the same draw ratio of 2. Since density and free volume are assumed to be directly correlated, such a difference in the behavior of T_g seems to suggest that density and T_g are two distinct quantities, not linearly correlated with one another. This point has been raised in Chapter 6. Please note that using draw ratios in the above publication instead of the Hermans' orientation function is not expected to be a limitation while comparing density and T_g since the measurements should have been done on the same films. Of course, better determination of the degree of orientation should have been done in order to determine if a critical point was still observed for the T_g for instance.

8.3.4. DMTA results

DMTA experiments were performed on the stretched membranes after permeation data and birefringence measurements had been collected. Stretched samples to be used in the DMTA apparatus were cut in the machine direction (MD) as well as in the transverse direction (TD). Samples that had been inside the oven but not stretched were denoted as

isotropic. The draw ratio was determined for each sample. A schematic of the DMTA set-up is provided in Figure 8.12.

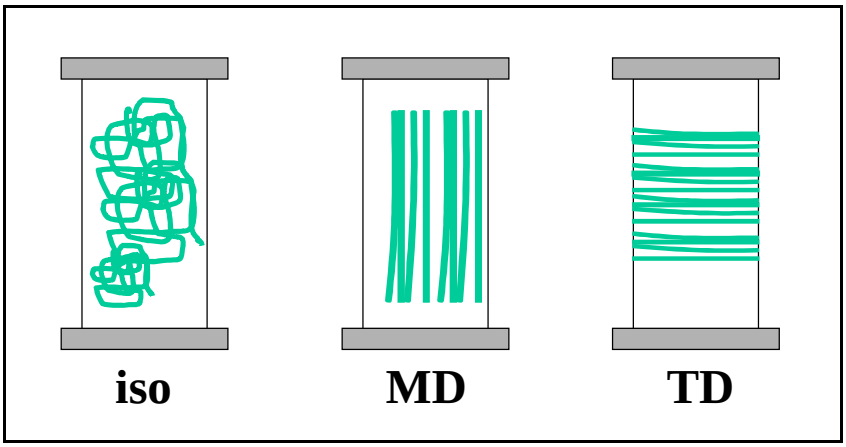

Figure 8.12: Schematic of the DMTA set-ups. Iso, MD, and TD stand for isotropic, machine direction, and transverse direction, respectively. The chains were drawn as perfectly oriented in order to emphasize the orientation direction. Nevertheless one has to keep in mind that the Hermans' orientation function of the polycarbonate films was very low (about 0.2) and therefore the polymer chains should be only slightly oriented.

The glass transition temperature varied as $T_{gTD} \leq T_{giso} < T_{gMD}$, where TD, iso, and MD stand for transverse direction, isotropic, and machine direction, respectively. The maximum difference between T_{gMD} and T_{giso} was about 3.5°C for $T_{stretch}$ = 130°C, 2.5°C for $T_{stretch}$ = 160°C, and 0.7°C for $T_{stretch}$ = 180°C. Also, typically $E'_{TD} \leq E'_{iso} < E'_{MD}$, in agreement with stress-strain curves commonly seen in the literature for ductile semi-crystalline polymers [29]. However, the α' peak appearing at around 80°C on the loss modulus E" trace of oriented samples and believed to originate from the local orientation of chain segments [3, 23, 24, 30] could not be clearly distinguished on our DMTA traces due to a scatter of the data. The fact that the $T_{g's}$ were affected by hot-drawing and that the densities were not (see above) suggests that those two quantities may not be directly related. This point has already been raised in Chapter 6.

An example of the DMTA traces is shown in Figure 8.13 and Figure 8.14 for $T_{stretch}$ = 160°C, and f = 0 and 0.2172. Traces obtained at other Hermans' orientation functions and other stretching temperatures were rather similar.

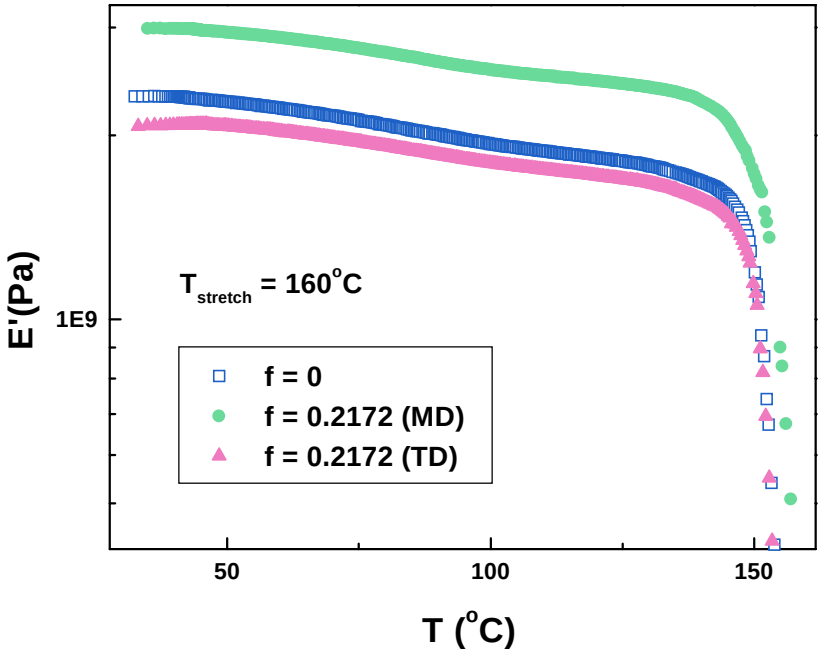

Figure 8.13: Storage modulus of isotropic and anisotropic polycarbonate (Lexan) as a function of temperature. The stretching temperature was set at 160°C. The Hermans' orientation function of the oriented sample was determined from birefringence measurements to be 0.2172. The DMTA traces of the oriented sample were performed in both the machine (MD) and the transverse (TD) directions. The DMTA conditions were the following: frequency = 1Hz, strain = 0.025%, initial temperature = 25°C, heating rate = 2°C/min, static force = determined at room temperature by dynamic frequency sweep test (strain control), torque = 10 cNm.

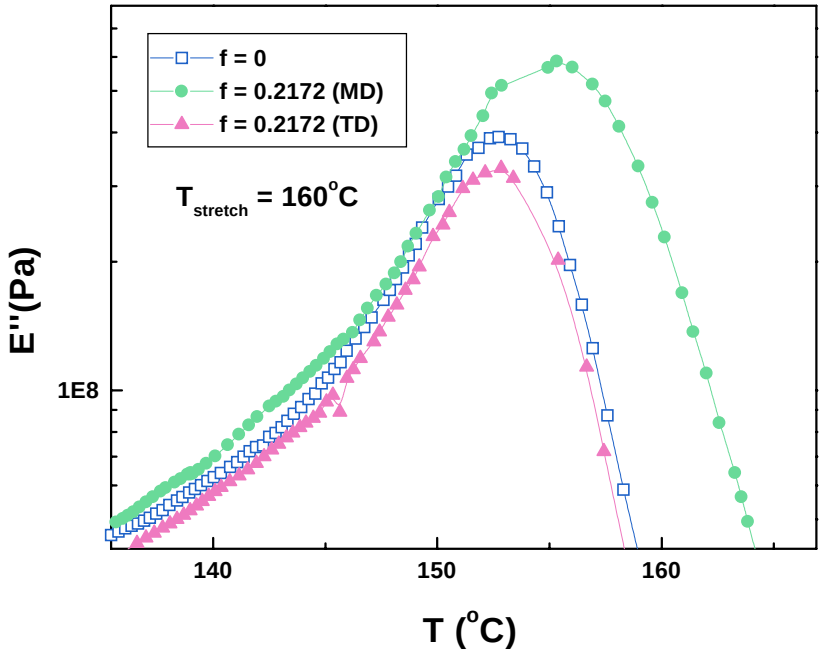

Figure 8.14: Loss modulus of isotropic and anisotropic polycarbonate (Lexan) as a function of temperature. The stretching temperature was set at 160°C. The Hermans' orientation function of the oriented sample was determined from birefringence measurements to be 0.2172. The DMTA traces of the oriented sample were performed in both the machine (MD) and the transverse (TD) directions. The DMTA conditions were the following: frequency = 1Hz, strain = 0.025%, initial temperature = 25°C, heating rate = 2°C/min, static force = determined at room temperature by dynamic frequency sweep test (strain control), torque = 10 cNm.

8.3.5. Permeation results

In the absence of crystallinity, the densities of polycarbonate were not observed to change significantly for hot-drawn samples, whereas the density increased in the cold-drawn sample. Interestingly, the T_g values were found to increase in the machine direction for both hot- and cold-drawn samples compared to those of isotropic samples. As a consequence, we would expect to see changes in the gas transport properties with hot-drawing. Gas transport coefficients and activation energies are reported below for both isotropic and anisotropic samples.

8.3.5.1. Isotropic samples

8.3.5.1.1. Determination of the gas transport coefficients (P,D,S)

Gas transport coefficients were plotted as a function of the oven temperature for isotropic samples. Results are provided in Figure 8.15 through Figure 8.17. Again, these samples were not oriented, but just left at a given temperature for a fixed time. In addition, the experimental data were obtained at 35°C, and not at the temperatures written on the figures. The dynamic free volume was frozen. Data can be compared since the condensability of the gas in the polymer does not have to be corrected for temperature.

The density was found to decrease with the temperature for isotropic samples, indicating an increase in the overall free volume content with a greater oven temperature. An increase in free volume should correspond to an increase in solubility coefficients. However here the solubility coefficient is observed to slightly increase for O_2 and to decrease for N_2 (see Figure 8.17). A possible explanation is that the redistribution of free volume with an increase in temperature may favor smaller molecular cavities than the size of the N_2 molecule (kinetic diameter = 3.64Å). This conclusion would be in contradiction with PALS data that have shown that the hole size and concentration increase with temperature for polycarbonate [31-35]. On the other hand, the diffusion coefficient of O_2 appeared to remain constant with temperature. An increase in D was nevertheless observed with temperature for N_2. As suggested above, the free volume may have been more uniformly redistributed inside the polymeric matrix as the temperature was higher, enabling molecular motions to take place more easily due to the decrease in the local stiffness. The permeability coefficient was observed to remain relatively constant with the temperature for N_2. However, as the size of the gas molecule decreases, P was found to increase with the temperature.

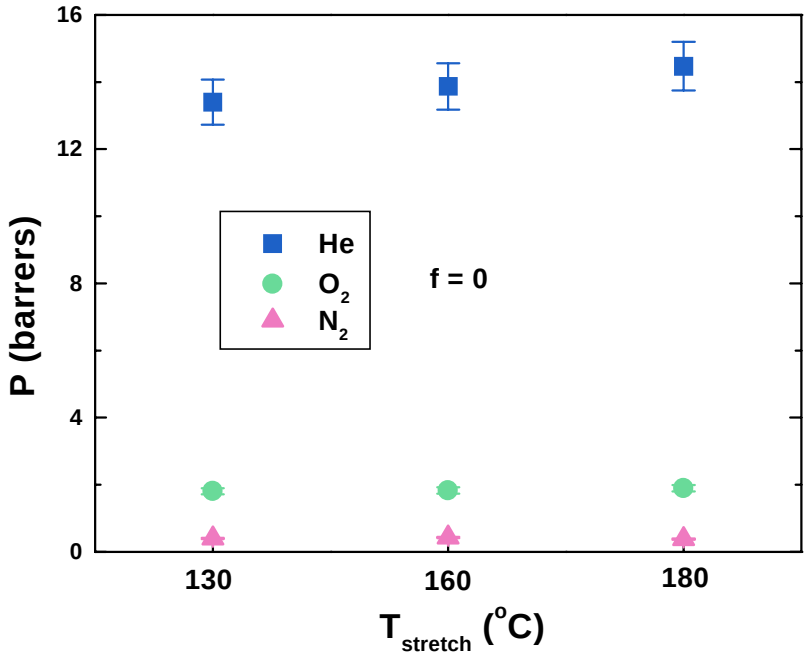

Figure 8.15: Permeability coefficient P as a function of $T_{stretch}$ for isotropic samples. Permeation experiments were performed at 35°C.

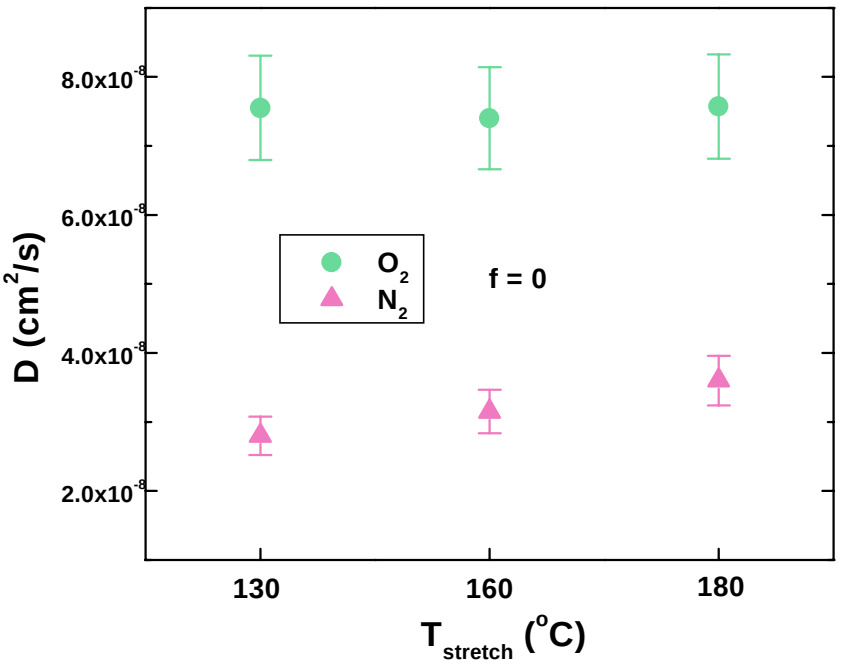

Figure 8.16: Diffusion coefficient D as a function of $T_{stretch}$ for isotropic samples.

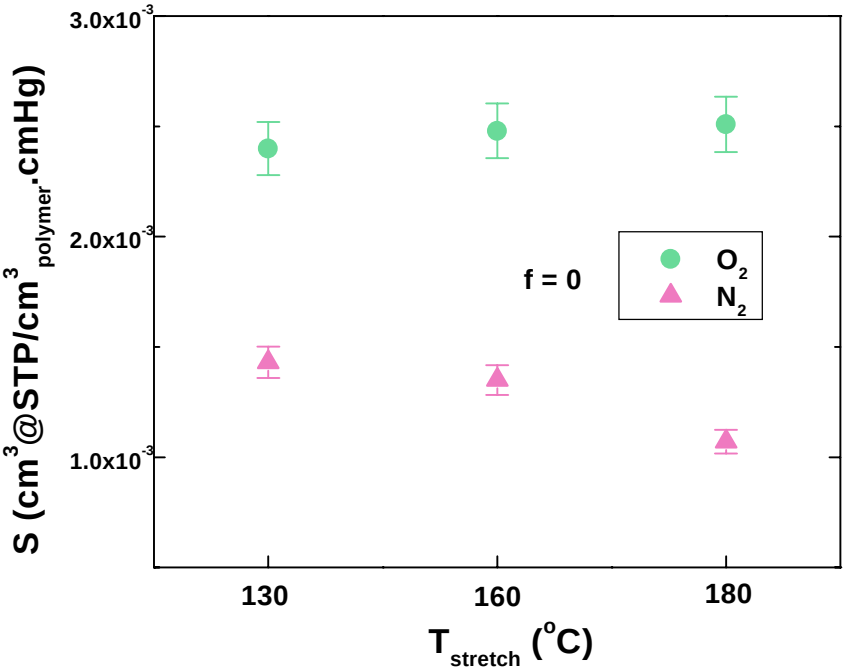

Figure 8.17: Solubility coefficient S as a function of $T_{stretch}$ for isotropic samples.

8.3.5.1.2. Determination of the gas transport activation energies (E_P, E_D, ΔH_s)

Activation energy data obtained on isotropic samples are presented in Figure 8.18 through Figure 8.20. Gas transport activation energies do not seem to be affected by the annealing at elevated temperatures for smaller size gas molecules (He and O_2). However, E_D decreases and ΔH_s increases significantly for N_2 as the temperature of the oven increased.

The data suggest that the energy needed for diffusion to occur in polycarbonate is reduced with the temperature at which cooling started, and this for larger size molecules. The relaxation times are being reduced with an increase in temperature, resulting in a decrease in E_D. The decrease in the local stiffness makes it easier for activated diffusion to take place.

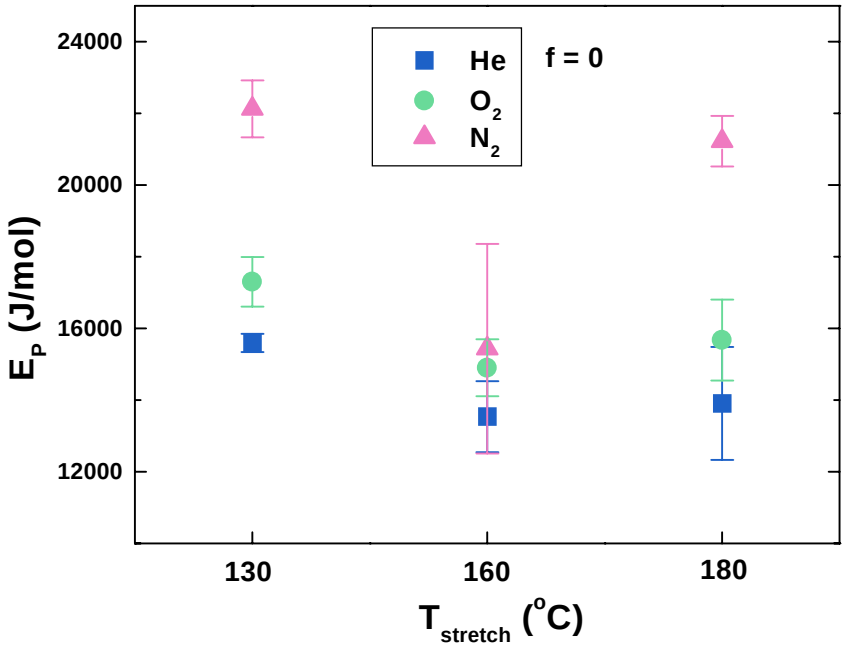

Figure 8.18: E_P as a function of $T_{stretch}$ for isotropic samples.

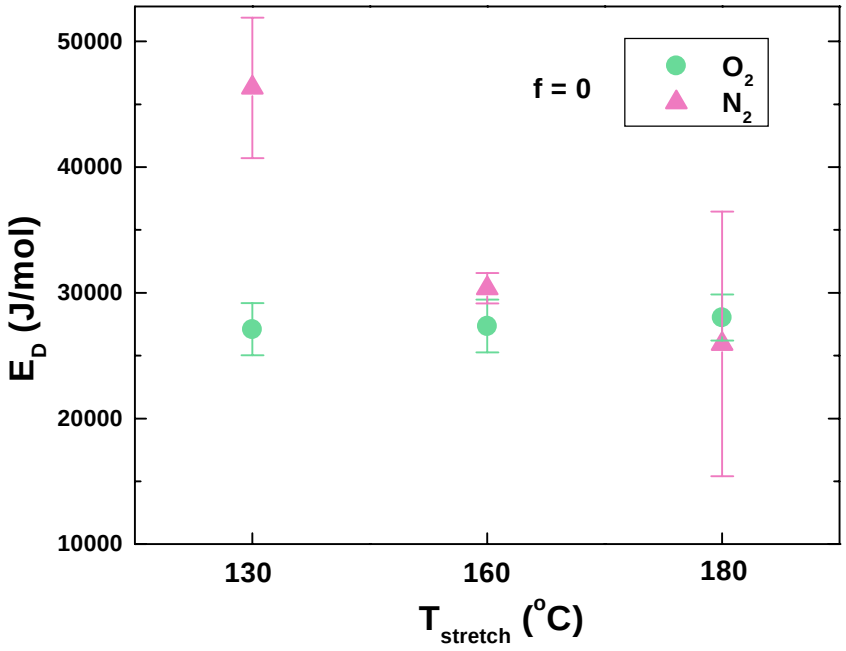

Figure 8.19: E_D as a function of $T_{stretch}$ for isotropic samples.

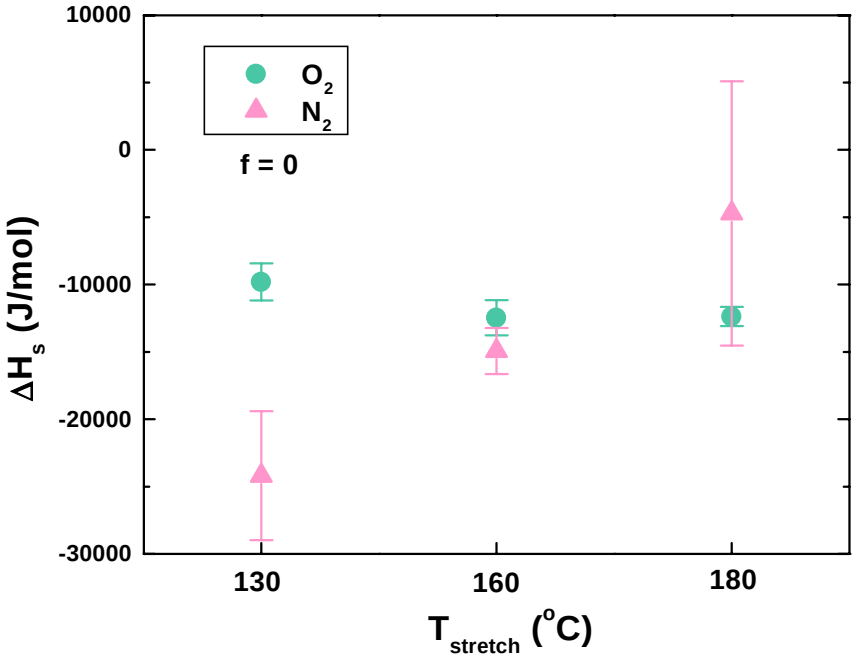

Figure 8.20: ΔH_s as a function of $T_{stretch}$ for isotropic samples.

8.3.5.2. Anisotropic samples

8.3.5.2.1. Determination of the gas transport coefficients (P,D,S)

The gas transport coefficients P, D, and S were calculated as a function of the Hermans' orientation function f for hot-drawn samples. Since it was impossible to determine f for cold-drawn samples (see previous remarks), the results of the cold-drawn samples were just given as stretched or unstretched. The degree of orientation did not change before and after the gas transport measurements. Since the thickness of the samples changed as the samples were stretched, the permeation slope could not be compared before and after stretching. Instead the permeability was calculated directly. The error bars reflect the precision of the thickness measurements.

The permeability coefficient P results are reported from Figure 8.21 to Figure 8.23. P seems to remain constant with stretching for both cold- and hot-drawn samples. What is rather interesting for practical applications is that the permselectivity appears to remain constant with stretching. One has to keep in mind that the permeation experiments were

performed perpendicularly to the polymer chain orientation. Still, the fact that orientation does not seem to affect the permeability coefficient is rather unexpected. Even though the f values are not that high, orientation effects should still be there. Stretching is expected to affect the distribution of free volume to some extent. It has actually been shown in the literature that cold-drawing increased the width of the free volume distribution of polycarbonate when the drawing was performed at room temperature [6, 8]. However, the thermal density fluctuations were observed to remain at values similar to those of undrawn samples when the drawing was performed at temperatures of 90^{o}C and 120^{o}C, thus still in the glassy state [8]. Therefore at the temperatures selected in this study the density fluctuations can be expected to remain unaffected by drawing. In addition, the densities were found to be unaffected by hot-drawing. Therefore, it seems possible that the permselectivities remain constant with drawing at the experimental stretching temperatures.

Discussing the effect of cold-drawing on gas transport may be more complex. In the present research work, crazing was observed to take place in the cold-drawn sample (see above). A study by Muzovskaya and Malkin [36] revealed that CO_2 transport in polycarbonate films was complicated by the fact that two different transfer mechanisms occurred in the cold-drawn films. Indeed, one needed to separate the orientation effects from the crazing effects. This crazing phenomenon has also been pointed out for the permeation of nitrogen in cold-drawn polycarbonate above a particular strain level [37]. As a film is being uniaxially oriented, microdefects or cracks may appear in the film to various extents. It has been shown that cracks appear when the viscoelasticity becomes clearly non-linear [38]. Those micropores are expected to appear under large deformations, i.e. mainly with cold-drawing. The presence of crazing could enhance the transport rate. Nevertheless, a study by Smith and Adam [37] did not notice a real change in the slope of the permeability coefficient P versus stretching for polycarbonate. P was said to increase with stretching at 128^{o}C because of two reasons: the increase in free volume first and crazing itself. The transport of gas molecules through films with crazing could also maybe be considered as gas transport through porous and not through dense material after some critical point. The gas transport results are therefore complicated. In

this study however a time-lag could still be distinguished in permeation experiments, thus indicating that no pores were present in the cold-drawn material.

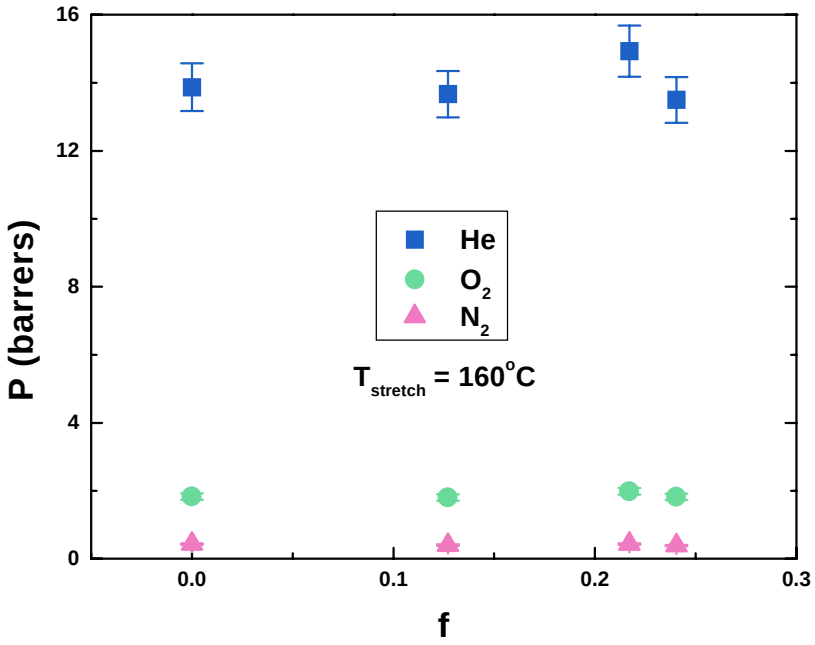

Figure 8.21: Permeability coefficient P as a function of the Hermans' orientation function f. The stretching temperature was 160°C. Results are plotted for the three gases studied in this research. Permeation experiments were performed at 35°C.

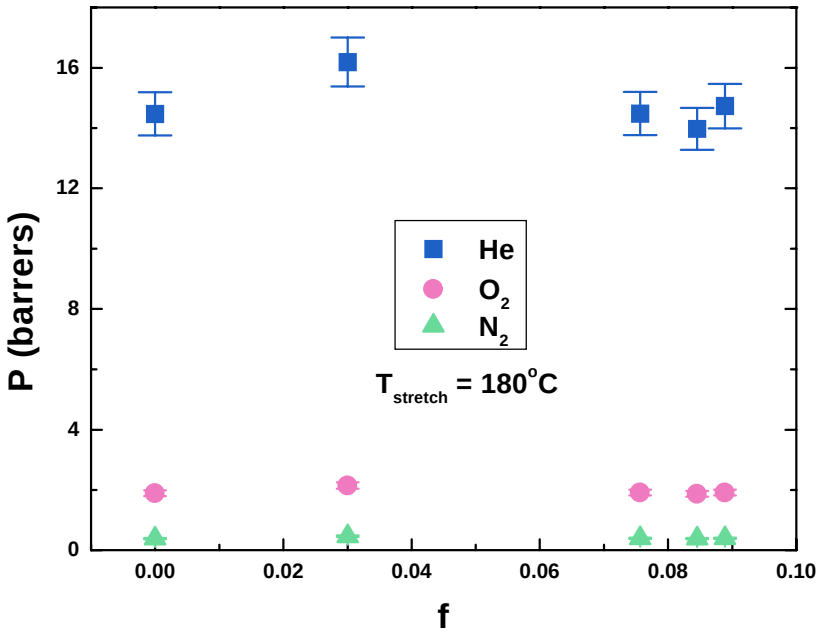

Figure 8.22: Permeability coefficient P as a function of the Hermans' orientation function f. The stretching temperature was 180°C. Results are plotted for the three gases studied in this research. Permeation experiments were performed at 35°C.

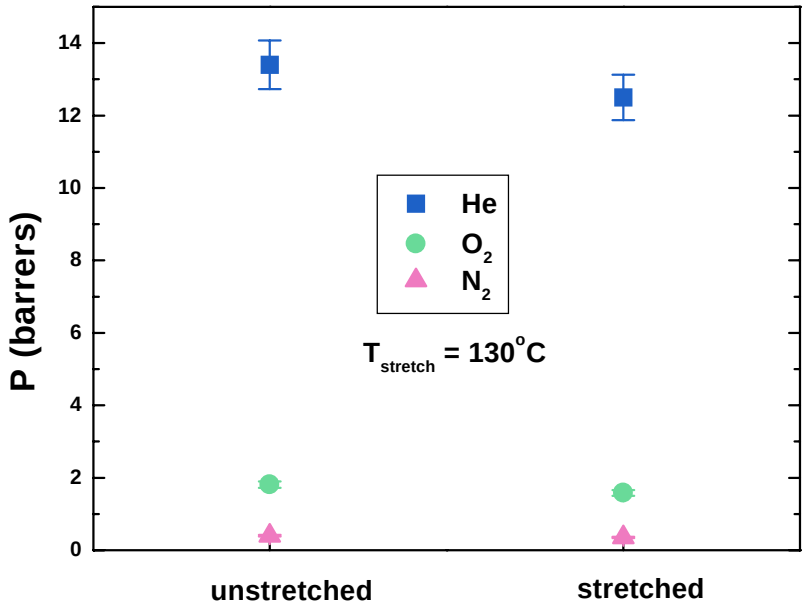

Figure 8.23: Permeability coefficient P of an unstretched versus a stretched sample. The stretching temperature was 130°C. Results are plotted for the three gases studied in this research. Permeation experiments were performed at 35°C.

The diffusion coefficient results are presented in Figure 8.24 through Figure 8.26. Again, no real trends can be distinguished with cold- and hot-drawing for the diffusion coefficient. Permeation experiments were performed perpendicularly to the polymer chain orientation. We believe that if the permeation experiments could have been performed in the direction parallel to the alignment of the polymer chains and not perpendicularly to them, the diffusion coefficient would have been affected by orientation. The $T_{g's}$ showed for instance a strong difference between the machine and the transverse directions. The $T_{g's}$ of the isotropic sample and that of the stretched sample tested in the TD direction had similar values, whereas the T_g of the stretched sample tested in the MD direction was greater.

The solubility coefficient results are presented in Figure 8.27 through Figure 8.29. Again, the changes induced by drawing do not appear to be statistically significant.

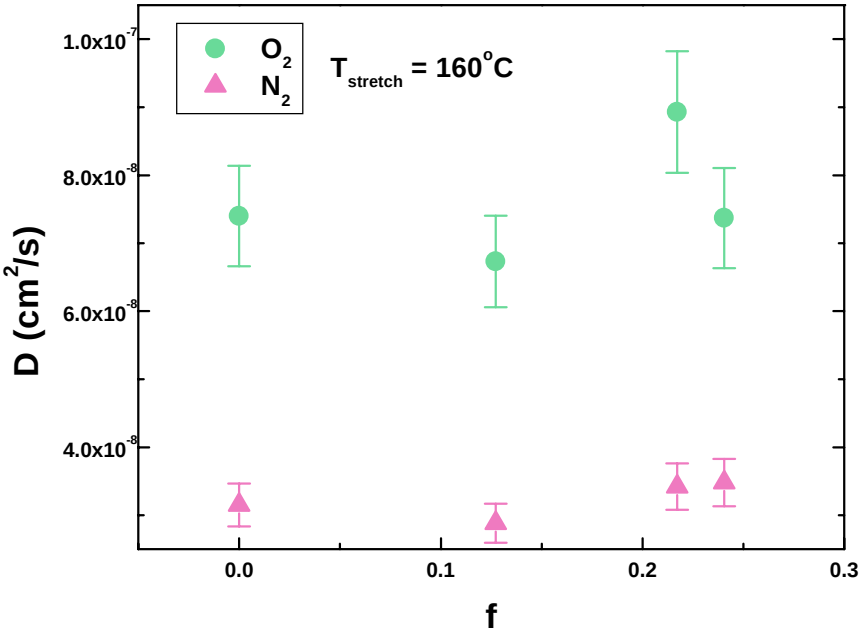

Figure 8.24: Diffusion coefficient D as a function of the Hermans' orientation function f. The stretching temperature was 160°C. Results have been obtained for O_2 and N_2 only.

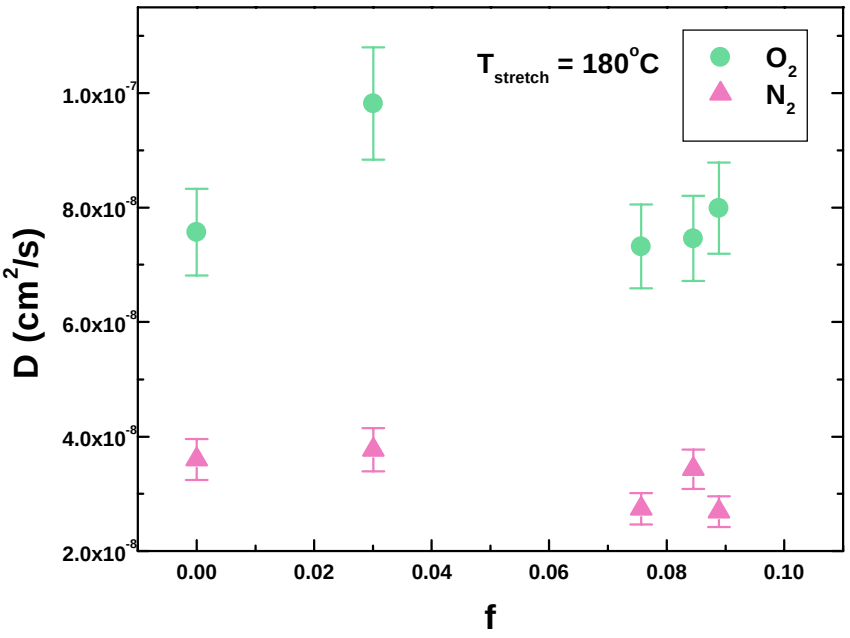

Figure 8.25: Diffusion coefficient D as a function of the Hermans' orientation function f. The stretching temperature was 180°C. Results have been obtained for O_2 and N_2 only.

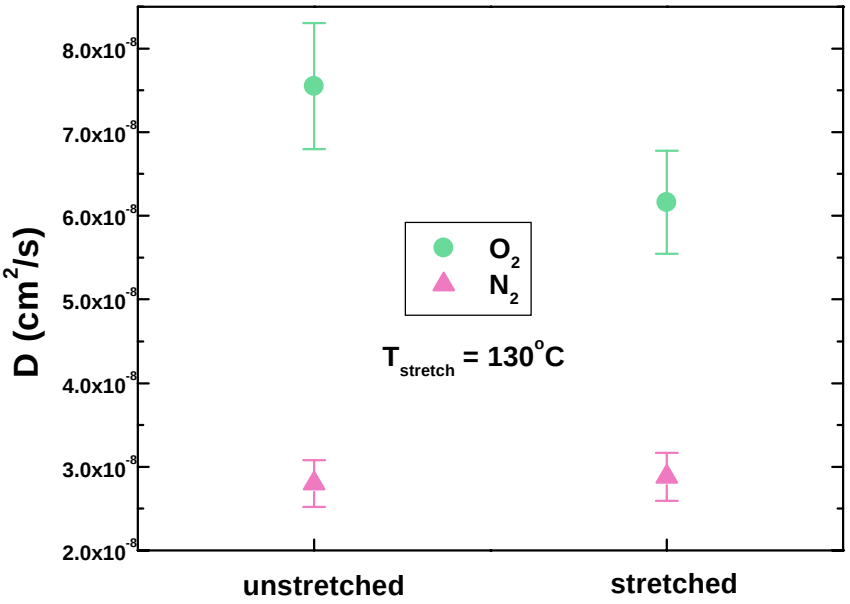

Figure 8.26: Diffusion coefficient D of an unstretched versus a stretched sample. The stretching temperature was 130°C. Results have been obtained for O_2 and N_2 only.

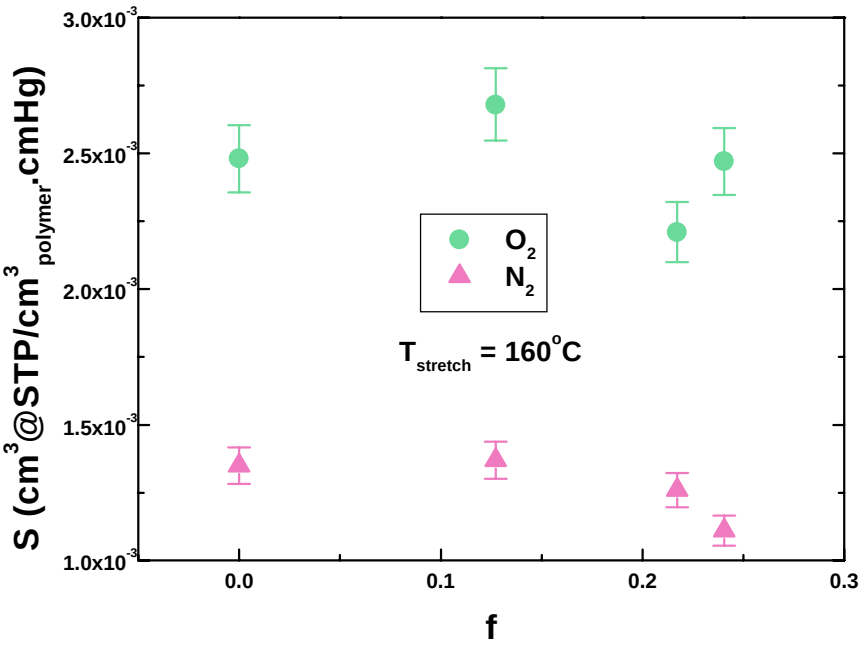

Figure 8.27: Solubility coefficient S as a function of the Hermans' orientation function f. The stretching temperature was 160°C. Results have been obtained for O_2 and N_2 only.

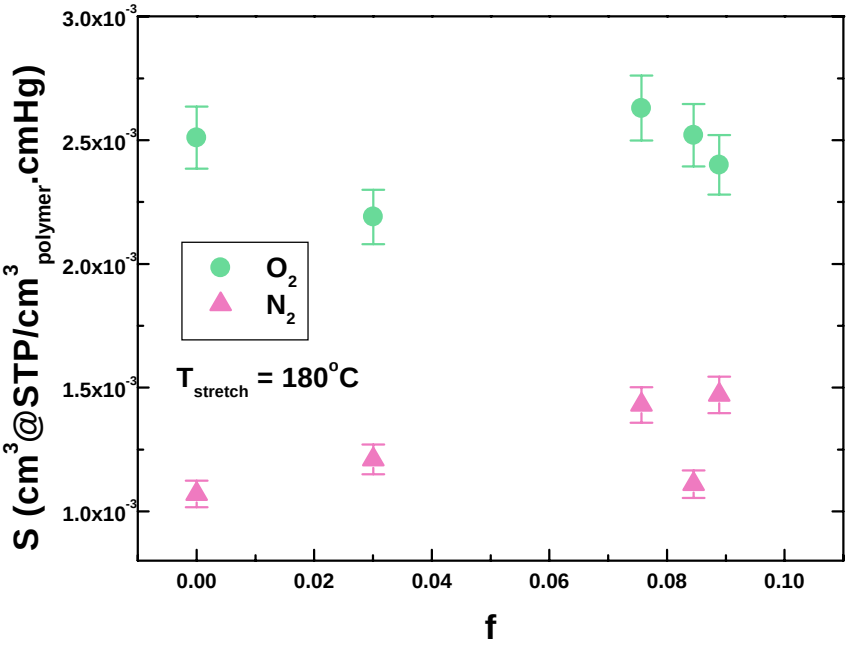

Figure 8.28: Solubility coefficient S as a function of the Hermans' orientation function f. The stretching temperature was 180°C. Results have been obtained for O_2 and N_2 only.

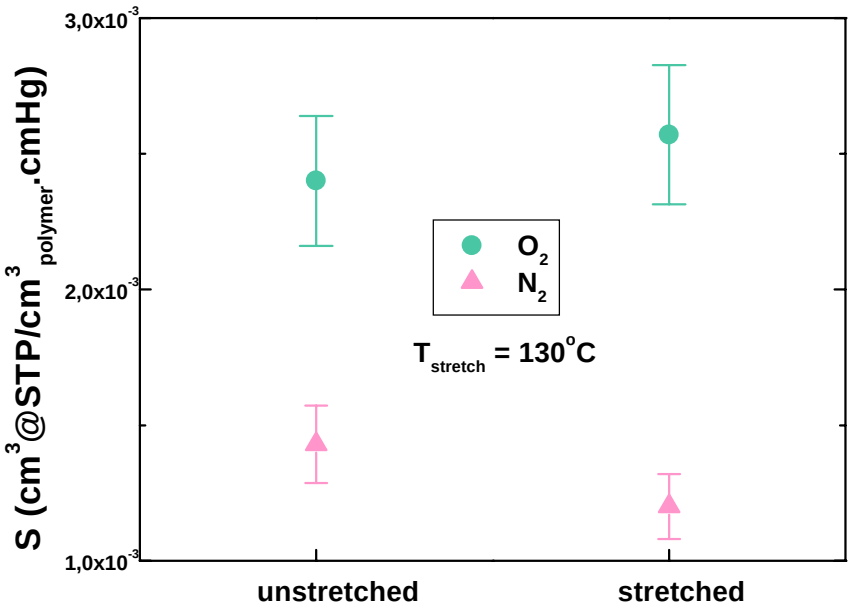

Figure 8.29: Solubility coefficient S of an unstretched versus a stretched sample. The stretching temperature was 130°C. Results have been obtained for O_2 and N_2 only.

8.3.5.2.2. Determination of the gas transport activation energies (E_P, E_D, ΔH_S)

Results of activation energy calculations are shown from Figure 8.30 to Figure 8.35. The activation energy data appear to be too scattered to draw conclusions, because the error bars are large. The estimation of the error was mainly based on the linear regressions. The errors may have come from the fact that the permeation temperatures were too close to one another to really measure significant changes in the gas transport parameters. The permeation temperatures were chosen as 35, 40, 45, and 55°C. The fact that the errors for the isotropic samples are on the same order of magnitude as the errors for the anisotropic samples supports this idea. Orientation is likely to increase the polymer relaxation times and make it more difficult for the gas molecules to move through the chains.

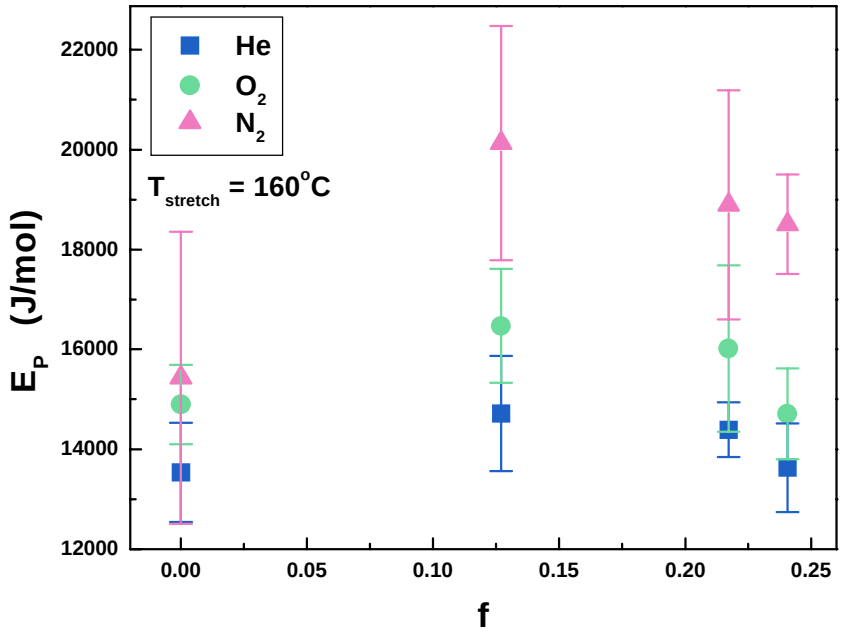

Figure 8.30: E_P as a function of the Hermans' orientation function f. The stretching temperature was 160°C. Results are plotted for the three gases studied in this research.

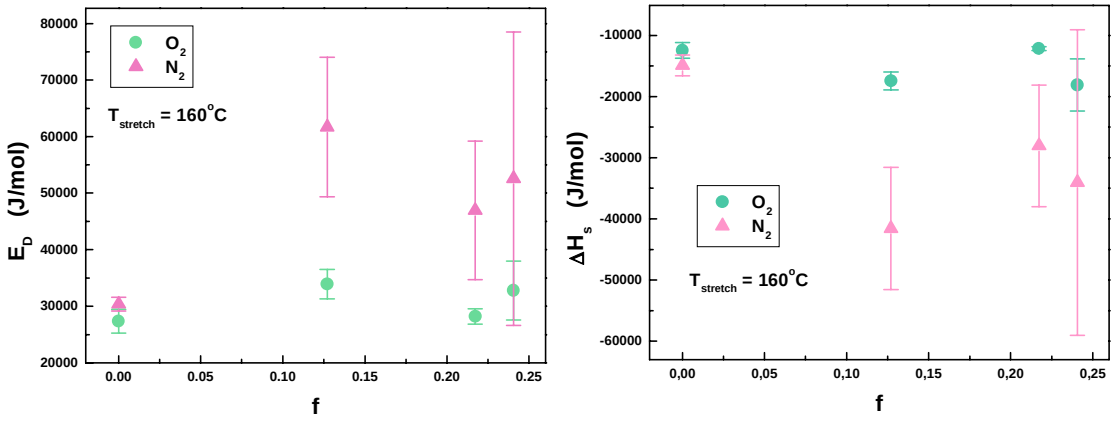

Figure 8.31: E_D (left) and ΔHs (right) as a function of the Hermans' orientation function f. The stretching temperature was 160°C. Results have been obtained for O_2 and N_2 only.

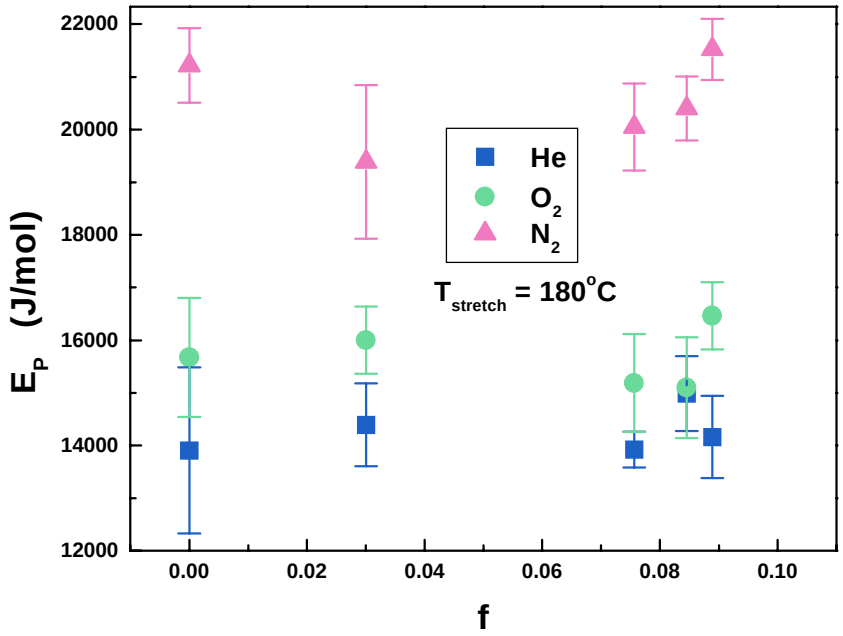

Figure 8.32: E_P as a function of the Hermans' orientation function f. The stretching temperature was 180°C. Results are plotted for the three gases studied in this research.

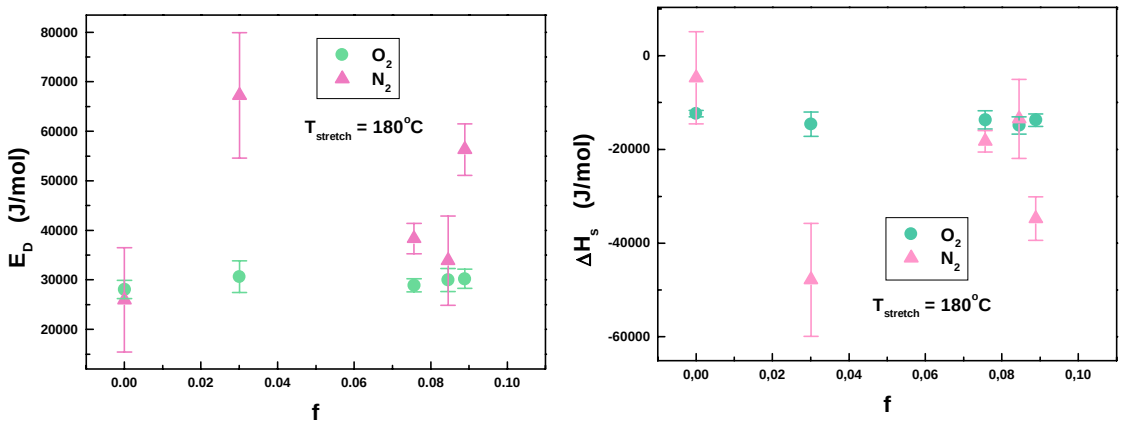

Figure 8.33: E_D (left) and ΔHs (right) as a function of the Hermans' orientation function f. The stretching temperature was 180°C. Results have been obtained for O_2 and N_2 only.

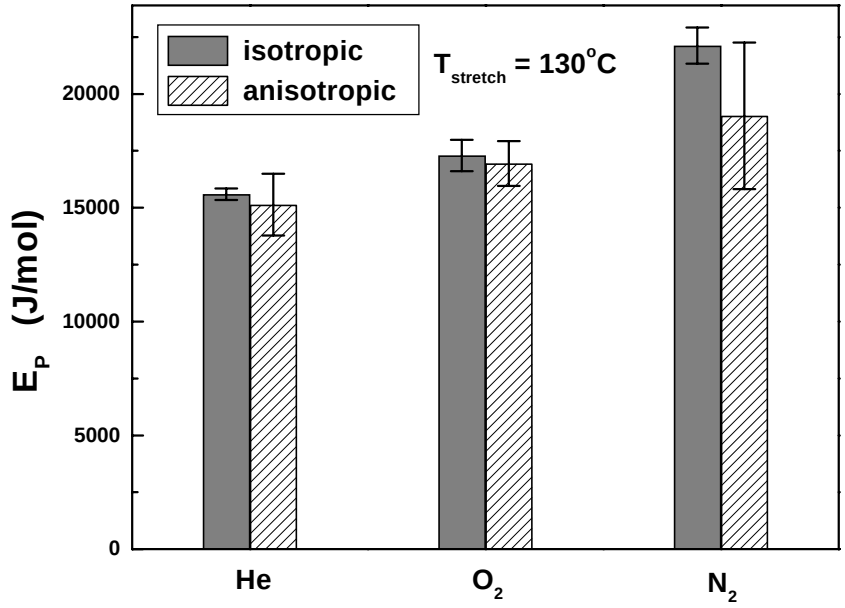

Figure 8.34: E_P of isotropic and anisotropic samples. The stretching temperature was 130°C. Results are plotted for the three gases studied in this research.

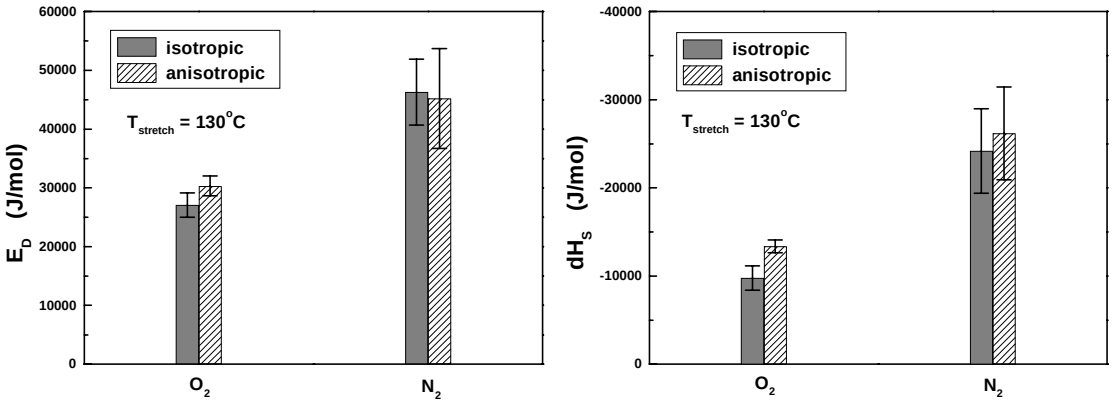

Figure 8.35: E_D (left) and ΔHs (right) of isotropic and anisotropic samples. The stretching temperature was 130°C. Results have been obtained for O_2 and N_2 only.

8.3.6. Orientation and physical aging

The experimental data given in this chapter do not show a change in density with stretching above T_g. The literature is actually divided concerning this increase in density with hot-drawing in polycarbonate, as discussed previously. As a consequence it is impossible to link the aging rate with the free volume content and its distribution

contained in the materials since the density (and thus the free volume content) do not appear to be affected by orientation. In addition, the gas transport data concerning freshly oriented samples were too scattered to really distinguish any trends.

Furthermore, annealing oriented samples is a rather complicated process since the material can relax during the experiments. As seen in Figure 8.36 and Figure 8.37, deorientation of the polymer chains in samples cold-drawn at 126^{o}C occurs during the DMTA experiments, as well as shrinkage of the samples. The appearance of new relaxations can be attributed to orientational stresses. Orientational stresses in plastics can be attributed to several factors. Four of them have been listed by Struik [39]: volume relaxation, thermal stresses due to rapid inhomogeneous cooling, shrinkage of the material after removing of the stress, and orientation of the polymer chains. Since the DMTA uses a constant heating scan, the thermal history can be quite complicated. Isothermal DMTA experiments would actually be easier to interpret. Still, the results of Figure 8.36 and Figure 8.37 point out that aging measurements, would they be DMTA or not, should be rather difficult to carry out on oriented samples. A fixed value cannot be given to characterize the orientation of the polymer chains since this orientation is likely to change during the measurement. Furthermore, as the sample shrinks the density may increase as well. And the relaxation time needed to accomplish a particular rearrangement and disorient the chains (as sketched in Figure 8.38) decreases as the temperature is increased. The timescale of the measurement is an important parameter to consider. The Deborah number D_e, which represents the ratio of the relaxation time divided by the observation time, should be ideally high. The timescale needed for a change in conformation has to be large compared to the duration of the test.

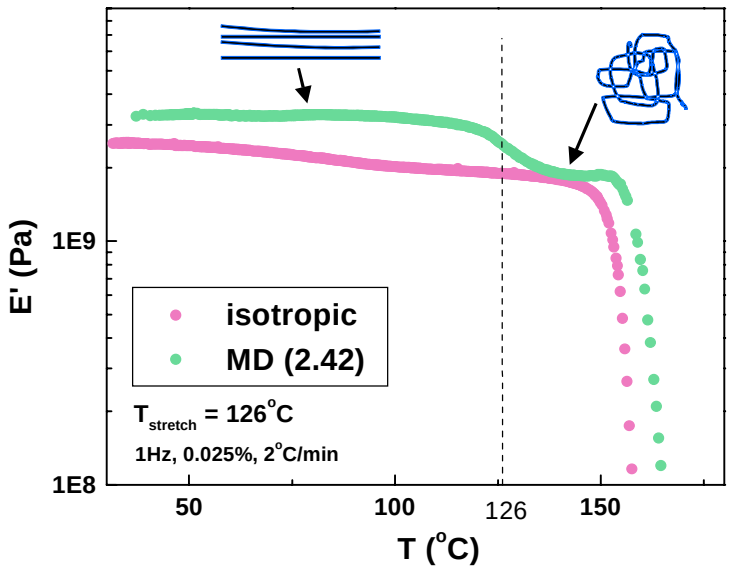

Figure 8.36: Storage modulus of isotropic and anisotropic polycarbonate (Lexan) as a function of temperature. As expected, the storage modulus at room temperature was greater in the oriented sample than in the isotropic one. Deorientation of the anisotropic samples is clearly seen on the figure, as the storage modulus dropped around the stretching temperature and reached the level of that of the isotropic sample. The fact that the drop of E' occurred around $T_{stretch}$ is believed to be a coincidence rather than a general rule. Indeed, this drop should depend on the heating rate for instance, and a higher heating rate should show a drop at higher temperatures. The stretching temperature was set at 126°C, the stretching rate was 15 turns/min. The DMTA trace of the oriented sample was performed in the machine direction. The draw ratio is indicated into brackets. The thicknesses of the fresh and the stretched samples were 150μm and 90μm, respectively. The DMTA conditions were the following: frequency = 1Hz, strain = 0.025%, initial temperature = 25°C, heating rate = 2°C/min, static force = 40g, torque = 10 cNm.

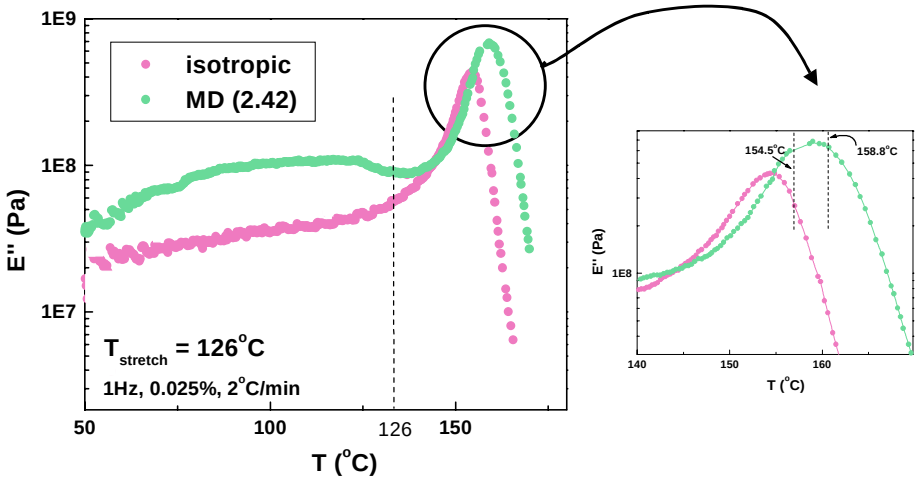

Figure 8.37: Loss modulus of isotropic and anisotropic polycarbonate (Lexan) as a function of temperature (see Figure 8.36 for experimental details). The loss modulus trace indicated that energy was dissipated in the material with deorientation of the chains (see previous figure), suggesting that shrinkage was taking place in the anisotropic samples during the measurements. The T_g of the stretched sample (MD direction) was higher by about 4°C.

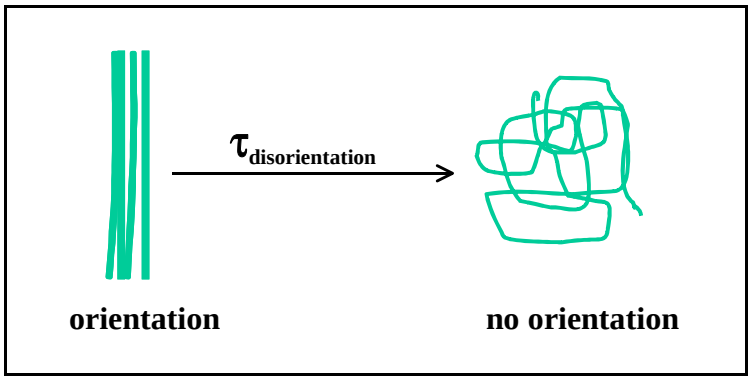

Figure 8.38: Schematic showing the relaxation of oriented polymer chains.

Data published on the enhancement of volume relaxation for oriented materials have sometimes been obtained on samples stretched at room temperature and annealed at room temperature or at higher temperatures. This is for instance the case in the work of Pixa et al [7] or Müller, Wendorff et al [6, 8], who focused their studies on cold-drawn polycarbonate. Obviously, such data are rather complicated to interpret since shrinkage is more than likely to occur with time. DMTA responses of polycarbonate stretched at room temperature are shown in Figure 8.39 through Figure 8.41 for reference. A study by Lunn and Yannas [16] has pointed out that the temperature at which the polycarbonate films were stretched had a profound influence on the relaxation rate during sub-T_g annealing. The higher the stretching temperature, the higher the temperature at which relaxation takes place. The orientation function was observed to decrease with annealing time, at any annealing temperature up to the T_g value. Obviously, the decrease in the orientation function became more pronounced close to the T_g for hot-drawn samples.

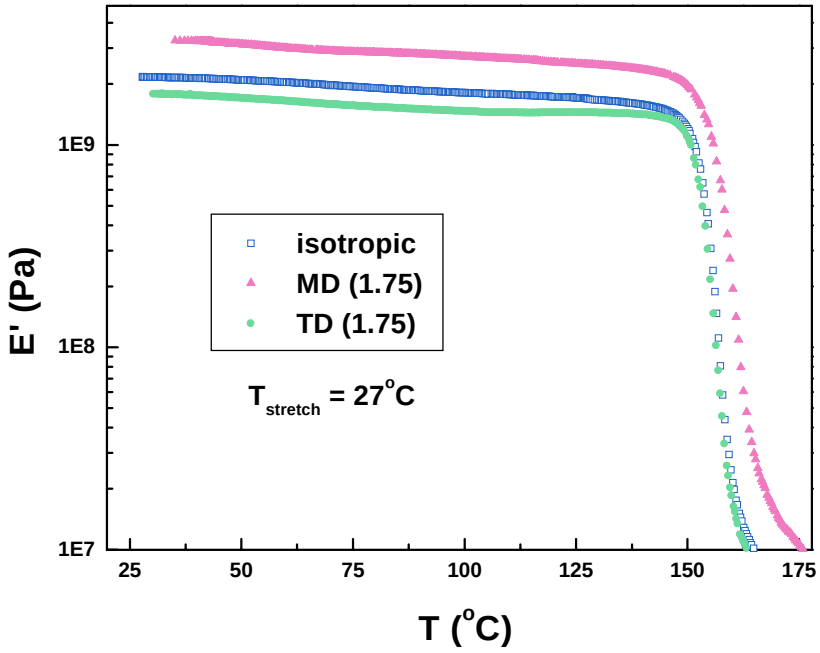

Figure 8.39: Storage modulus E' of isotropic and anisotropic polycarbonate (Lexan) as a function of temperature. No direct evidence of deorientation of the polymer chains could be noticed. The stretching was done at room temperature (27°C), the stretching rate was 7 turns/min. The draw ratio of the oriented samples are indicated into brackets. DMTA measurements were performed in both the machine (MD) and the transverse (TD) directions. The DMTA conditions were the following: frequency = 1Hz, strain = 0.025%, initial temperature = 25°C, heating rate = 2°C/min, torque = 10 cNm.

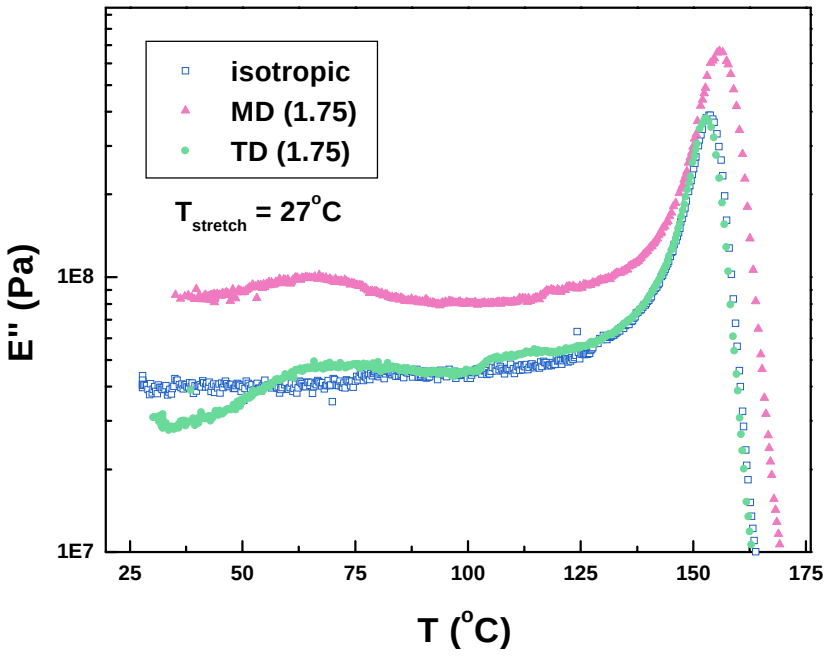

Figure 8.40: Loss modulus E" of isotropic and anisotropic polycarbonate (Lexan) as a function of temperature. The samples were stretched at room temperature (see Figure 8.39 for experimental details). New relaxations between 50 and 120°C appeared on the traces with orientation.

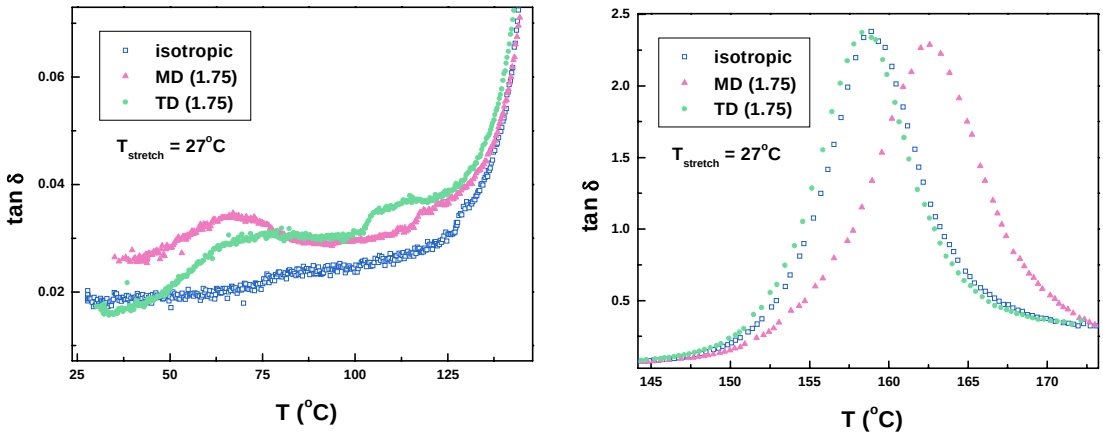

Figure 8.41: Tan δ of isotropic and anisotropic polycarbonate (Lexan) as a function of temperature. The samples were stretched at room temperature (see Figure 8.39 for experimental details).

8.4. Conclusions

The objectives of this study were to investigate the effect of amorphous orientation on the gas transport properties of polycarbonate. Both hot- and cold-drawing were performed on polycarbonate samples. The permeation data on a cold-drawn sample was complicated by the fact that crazing was present in the oriented material. Orientation studies on hot-drawn polycarbonate samples did not appear to affect the gas transport properties. The gas transport coefficients seemed to remain unaffected by hot-drawing, hence indicating a constant permselectivity with stretching. Please note that no change in density was noticed with hot-drawing either. We expect that the gas results would have been affected by orientation though if permeation experiments could have been performed in the direction parallel to the alignment of the polymer chains, and not perpendicularly to them.

Studies investigating the physical aging of oriented samples were not carried out since the density of polycarbonate was not found to be affected by hot-drawing. Therefore, it was impossible to link the aging rate with the free volume content. In addition, studying the physical aging of oriented samples appears to be rather complex since deorientation and shrinkage have been shown in this study to take place during sub-T_g annealing.

8.5. References

1. Y. C. Jean, Y. Rhee, Y. Lou, D. Shelby, G. L. Wilkes, Anisotropy of hole structures in oriented polycarbonate probed by two-dimensional angular correlation of annihilation radiation, *Journal of Polymer Science: Part B: Polymer Physics*, 34, 2979-2985 (1996).
2. M.-S. S. Wu, Intrinsic birefringence of amorphous poly(bisphenol-A carbonate), *Journal of Applied Polymer Science*, 32, 3263-3275 (1986).
3. M. D. Shelby and G. L. Wilkes, Thermodynamic characterization of the oriented state of bisphenol A polycarbonate as it pertains to enhanced physical aging, *Journal of Polymer Science: Part B: Polymer Physics*, 36, 2111 (1998).
4. M. D. Shelby and G. L. Wilkes, The effect of molecular orientation on the physical ageing of amorphous polymers - dilatometric and mechanical creep behaviour, *Polymer*, 39, 26, 6767-6779 (1998).
5. R. Song, Q. Fan, Polycarbonate films in the state of high global chain orientation but nearly random segmental orientation, *European Polymer Journal*, 36, 1463-1470 (2000).
6. J. Bartos, J. Muller, J. H. Wendorff, Physical ageing of isotropic and anisotropic polycarbonate, *Polymer*, 31, 1678 (1990).
7. R. Pixa, B. Grisoni, T. Gay, and D. Froelich, Influence of deformation on physical aging of polycarbonate- 2 - Volume recovery near ambient temperature, *Polymer Bulletin*, 16, 381-387 (1986).
8. J. Muller, J. H. Wendorff, Thermal density- Fluctuations in rejuvenated and aged polycarbonate, *Journal of Polymer Science: Part C: Polymer Letters*, 26, 421 (1988).
9. J.-J. Pesce and G. B. McKenna, Prediction of the subyield extension and compression responses of glassy polycarbonate from torsional measurements, *J. Rheol.*, 41, 5, 929-942 (1997).
10. Dr. Georgiev, GE Plastics, personal communication.
11. G. L. Wilkes, Polymers, Mechanical Behavior, in Encyclopedia of physical science and technology, vol II, 61-84, ( ).
12. M. J. El-Hibri and D. R. Paul, Effects of uniaxaial drawing and heat-treatment on gas sorption and transport in PVC, *Journal of Applied Polymer Science*, 30, 3649-3678 (1985).
13. Seungman Sohn, personal communication.
14. N. Heymans, FTIR investigation of structural modification of polycarbonate during thermodynamical treatments, *Polymer*, 38, 14, 3435 (1997).
15. J. Dybal, P. Schmidt, J. Baldrian and J. Kratochvil, Ordered structures in polycarbonate studied by infrared and raman spectroscopy, wide-angle X-ray scattering, and differential scanning calorimetry, *Macromolecules*, 31, 6611-6619 (1998).
16. A. C. Lunn and I. V. Yannas, Chain-backbone motion in glassy polycarbonate studied by polarized infrared spectroscopy, *Journal of Polymer Science: Polymer Physics Edition*, 10, 2189-2208 (1972).

17. L. Lundberg and J.-F. Jansson, Anisotropic creep behaviour of oriented polycarbonate, *Polymer*, 35, 10, 2084-2089 (1994).
18. E. Ito, T. Hatakeyama, Studies of the amorphous region of polymers- II - Relationship between change of structure and glass-transition temperature in polycarbonate, *Journal of Polymer Science: Polymer Physics Edition*, 13, 2313-2320 (1975).
19. B. von Falkai, G. Spilgies, and H. J. Biangardi, *Angew. Makromol. Chem.*, 108, 41 (1982).
20. H. J. Biangardi, *Makromol. Chem.*, 183, 1785 (1982).
21. Dr. G. L. Wilkes, lecture notes.
22. E. Ito, K. Sawamura and S. Saito, Effects of drawing on molecular motions in polycarbonate, *Colloid & Polymer Sci.*, 253, 480-484 (1975).
23. G. Yianakopoulos, J. Vanderschueren, and J. Niezette, Effect of mechanical deformations on thermally stimulated currents in polymers. 1. Uniaxially cold-drawn polycarboante, *Proceedings of the 6th International Symposium on electrets (ISE 6)*, Oxford, England, 131-136 (1988).
24. G. Yianakopoulos, J. Vanderschueren, and J. Niezette, Sub-Tg relaxation in cold-drawn polymers. Thermally-stimulated-current methods, *IEEE Transactions on electrical insulation*, 24, 3, 429-438 (1989).
25. L. H. Wang, R. S. Porter, On the CO2 permeation of uniaxially drawn polymers, *Journal of Polymer Science: Polymer Physics Edition*, 22, 1645-1653 (1984).
26. M. D. Shelby, G. L. Wilkes, M. R. Tant, J. Zawada, T. J. Bastow and A. J. Hill, Amorphous orientation in glassy polycarbonate, *ACS, Polymeric Materials Science and Engineering, Conference Proceedings,* San Francisco, Spring 1997, 76, 485-6.
27. D. M. Colucci, G. B. McKenna, J. J. Filliben, A. Lee, D. B. Curliss, K. B. Bowman, J. D. Russell, Isochoric and isobaric glass formation: similarities and differences, *Journal of Polymer Science: Physics Edition*, 1561-1573 (1997).
28. L. H. Sperling, *Introduction to physical polymer science*, Second edition, John Wiley and Sons, 1992.
29. Dr. T. Ward, lecture notes.
30. L. Lundberg and J.-F. Jansson, Influence of physical ageing on the non-linear viscoelasticity of polycarbonate, *Polymer*, 37, 8, 1311 (1996).
31. T. C. Sandreczki, X. Homg, and Y. C. Jean, Sub-glass-transition temperature annealing of polycarbonate studied by positron annihilation spectroscopy, *Macromolecules*, 29, 4015-4018 (1996).
32. J. E. Kluin, Z. Yu, S. Vleeshouwers, J. D. McGervey, A. M. Jamieson, R. Simha, Temperature and time dependence of free volume in bisphenol A polycarbonate studied by positron lifetime spectroscopy, *Macromolecules*, 25, 19, 5089 (1992).
33. A. J. Hill, C. M. Agrawal, Positron lifetime spectroscopy characterization of thermal history effects on polycarbonate, *Journal of Materials Science*, 25, 5036-5042 (1990).
34. J. E. Kluin, H. Moaddel, M. Y. Ruan, Z. Yu, A. M. Jamieson, R. Simha, J. D. McGervey, Probe spectroscopy, free volume concepts, and physical aging of polymer glasses, in Structure-property relations in polymers: spectroscopy and performance, ACS, 236, 535-555 (1993).

35. J. Bohlen and R. Kirchheim, Macroscopic volume changes versus changes of free volume as determined by positron annihilation spectroscopy for polycarbonate and polystyrene, *Macromolecules*, 34, 4210-4215 (2001).
36. N. Yu. Muzovskaya and A. Ya. Malkin, Influence of orientation on the diffusion characteristics of polycarbonate, *Polymer Science USSR*, 27, 12, 2950-2954 (1985).
37. T. L. Smith and R. E. Adam, Effect of tensile deformations on gas transport in glassy polymer films, *Polymer*, 22, 299-304 (1981).
38. G. Menges and F. Schmidt, *Plast. Polym.*, 38, 13 (1970).
39. L. C. E. Struik, Internal stresses, dimensional instabilities and molecular orientations in plastics, John Wiley and Sons, New York, 1990.

Chapter 9

Summary and recommendations for future work

9.1. Summary of the results

The objective of this work was to understand the molecular mechanism of gas transport in amorphous glassy polymers. Especially, one question that tried to be answered in this work was: is the gas transport process directly correlated with the overall free volume content of amorphous glassy polycarbonate? In order to understand the nature of the gas transport, three different conditions (cooling rate, physical aging, and orientation) were selected in order to manipulate the free volume.

To begin, the amount of free volume present in polycarbonate was modified by varying the cooling rate. The greater the cooling rate, the lower was the density, hence the greater was the amount of free volume trapped in the polymeric matrix as the material underwent a transition from the rubbery to the glassy state. An increase in the free volume amount induced by the cooling procedure resulted in an increase in the solubility coefficient and in a decrease in the diffusion coefficient. Although the diffusion coefficient D and the solubility coefficient S were found to be dependent on the cooling rate, their combined effects canceled out, and the permeability coefficient P (which corresponds to the product of D and S) appeared to remain constant. The relative constancy of P with an increase in free volume for all the gases studied was in

contradiction with common expectations. The free volume arguments, however, seem to hold well when comparing polymers of different structures with gross differences in free volume [1, 2]. The data obtained in this research did not uphold the free volume arguments used to explain diffusion coefficients in polymers [1-14]. Contrary to the Doolittle equation, a decrease in the diffusion coefficient with an increase in the free volume content was experimentally observed. The free volume theory may grossly apply to different polymer structures, but may not discern the subtle differences of a given polymer at different thermal histories. Furthermore, the activation energy of diffusion was found to be greater for the fast cooled samples possessing the greater free volume content, indicating that the free volume concepts alone cannot explain the gas transport mechanism.

The previous results show that the free volume concepts do not apply to gas transport. In order to explain the gas transport process, one can manipulate the processing parameters. The free volume content for instance can be changed by aging polymers. As the polycarbonate cooled under well-defined conditions was aged at 120^{o}C, its density increased linearly with the logarithm of time. Quite interestingly, the changes seen in the density values with sub-T_g annealing had the same order of magnitude as those observed in the cooling rate studies summarized above. Therefore if the permeability coefficient is indeed related to the free volume content as postulated in the literature [1, 2], the permeability coefficient should have been affected the same way in the cooling rate as in the aging studies. However, no changes in the values of the permeability coefficients were observed in the cooling rate studies involving fresh samples, while the permeability coefficient of a sample cooled at a fixed rate was reduced with sub-T_g annealing. The decrease in the permeability coefficient with physical aging was consistent with the literature. The permeability of the larger size gas molecules decreased at a faster rate than that of the smaller size gas molecules, reflecting possible changes in the free volume distribution or changes in molecular chain dynamics. On one hand, the diffusion coefficient of N_2 was observed to be enhanced at short aging times and to decrease with further sub-T_g annealing. On the other hand, the solubility coefficient of N_2 tended to increase with aging time, but the data points were too scattered to draw conclusions.

Changes in the diffusion and solubility coefficients of O_2 with aging time were however rather small. The activation energy of diffusion of N_2 was determined to increase with aging time, in contrast with the recent literature [15].

Polycarbonate samples were also cooled at different rates and aged for 10h at 120^{o}C. The greater the initial cooling rate, i.e. the greater the initial amount of free volume in the materials, the greater was the decrease in tan δ with sub-T_g annealing time. A greater densification rate has also been reported in the literature for samples containing initially a greater amount of free volume [16, 17]. If the permeability coefficient is indeed related to the amount of free volume, as commonly stated in the literature, the permeability coefficient should have decreased the most for the rapidly-cooled sample. However, this was not what was observed experimentally. The permeability coefficient decreased the most for the sample containing initially a lowest free volume content, despite of the lower densification rate. Again, this observation demonstrated that free volume and permeation cannot be directly correlated. Sample containing initially a lower free volume content, corresponding to extended aging time, demonstrated a significantly reduced diffusion coefficient, whereas an enhanced solubility coefficient was observed for N_2. This seems to suggest that the free volume distribution may become narrower with sub-T_g annealing and favor the formation of cavities of a size equal or slightly greater than that of the nitrogen N_2 gas molecule (3.64Å). We postulate that this process occurs when the smaller size cavities group together to form larger size cavities. A reduction in the amount of larger free volume sites is likely to occur with aging in order to account for the increase in density. Alternatively, fast cooling rates may lead to highly restricted conformations, which limit segmental mobility and lower the rate of diffusion. Further aging can reduce the segmental mobility, but much more slowly than in relaxed systems.

The results obtained in the cooling and in the aging studies, apparently in contradiction with one another, lead us to believe that other mechanisms control diffusion besides the free volume content. The experimental results were explained in terms of the conformational rearrangements and the dynamics of the local motions. With slower cooling or at initial aging times the population of trans-trans conformations may increase,

eventually facilitating the temporary opening of the molecular channels, and enhancing the diffusion process. With further annealing the degrees of freedom may be progressively lost. The closing and opening of gaps should depend on the stiffness of the local segments. This process may take a longer time for polymers which have been physically aged, and affects most the gases with greater kinetic diameters. A minimum amount of free volume may be necessary for segmental motions to take place. The increase in the polymer relaxation times with physical aging [18] is believed to hinder the local chain motions. The importance of the chain dynamics in the gas transport phenomenon has actually been pointed out in a recent theoretical paper [19]. By allowing the polymer degrees of freedom in polypropylene the diffusion coefficient could be enhanced by as much as four orders of magnitude.

Since the temperature of the permeation experiments or the interactions between the gas and the polymer remained constant, any changes in the solubility coefficient could only be attributed to a redistribution of the free volume.

Unfortunately we were not able to see any influence of orientation on the gas transport properties. The data points were too scattered to draw confident conclusions. The experimental conditions could not be controlled as well as in the cooling and physical aging studies. The degree of orientation was not found to be constant all over the large area necessary for permeation measurements. In addition, the fact that permeation experiments were performed perpendicularly to the orientation of the chains and not along the orientation axis limited the sensitivity of transport properties to the orientation. Overall, the density remained constant with hot-drawing, and so did the permeability coefficient. Due to experimental problems encountered while attempting the measurements the orientation / physical aging studies were not completed. It was also noticed that such a study would be very complex, since deorientation and shrinkage may take place during sub-T_g annealing.

9.2. Recommendations for future work

1 - We have succeeded in answering the following questions that were opened:

- The free volume concepts alone cannot explain the gas transport mechanism.
- The data points suggest that all the cavity sizes in polycarbonate do not appear to be affected equally by the aging process.
- The activation energy of diffusion increases with aging time.

In this research work, the free volume amount was changed by varying the cooling rate or the physical aging time. Another way to change the amount of free volume inside the amorphous polycarbonate material would be to vary the molecular weight. This would represent one more parameter, which can verify that the relationship between the free volume content and the gas transport properties does not hold true. The lower the molecular weight, the greater is the number of chain ends, the greater is the number of defects, and thus the higher is the amount of free volume inside the material [20, 21]. Imperfect packing is indeed believed to be concentrated near the chain ends that are more mobile than the other polymer segments. The T_g and the density are expected to decrease with a decrease in molecular weight [22, 23]. Studies have to be carried out to evaluate the effect of the molecular weight on the gas transport properties of various polymers since the literature remains relatively sparse on the subject. It would be interesting to study molecular weights in a range covering both below and above the entanglement molecular weight M_e. Lin [24] has indeed shown that three characteristic slopes can be distinguished in the plots of T_g versus molecular weight. The intercepting points were found at M_e and at about 8 M_e. The study was performed on nearly monodisperse samples of polystyrene and polybutadiene. One needs to verify if any characteristic slopes are seen for polycarbonate as well, and if so, if the gas transport parameters do exhibit a change in slope at those particular molecular weights. For example, the entanglement molecular weight of polycarbonate has been determined to be 4,800 g/mol [25]. Of course, while studying the influence of the polycarbonate molecular weight on the gas transport properties, the polydispersity index of the various molecular weights

could be exactly the same since the polydispersity index should affect the properties tremendously. The standard deviation in molecular weight should be mentioned as well for statistical reasons. Indeed, monodisperse polymers for instance do not always have a standard deviation of zero [22]. At an ideal polydispersity of 1 (as what is observed in nature for proteins, nucleic acids, and some polysaccharides, although molecular forces play an important role [26]), the T_g of polycarbonate is expected to be higher than for a polycarbonate with an economical grade having a typical polydispersity index of about 2. An increase in the value of the T_g with a narrowness of the molecular weight distribution has actually been reported in the literature [27, 28].

The permeability coefficient of freshly processed polycarbonate appeared to be unaffected by the cooling rate. Such a fact suggests that the processing conditions (such as the cooling rate) may not need to be optimized. Although bisphenol-A polycarbonate is commonly taken as a reference in the polymer field, it does present some particularities (those particularities have been discussed in Chapter 3). Polycarbonate may actually be a special polymer, not to be generalized or compared with other systems. Further studies have to be conducted to determine whether or not the permeability coefficient remains constant with the cooling rate for other linear amorphous polymers as well. It would also be interesting to change the polymer topology (branches, crosslinks) or the chemical composition (copolymers, blends) while investigating the cooling rate / gas transport relationship. Although the cooling rate may not be a critical parameter for polycarbonate, it should affect the microphase separation in block copolymers that form domains on cooling for instance. Although the chemical structure and the overall free volume content may be constant, a change in morphology occurring with cooling is likely to affect the values of the permeability coefficient. Such an observation would confirm the fact that the free volume concept alone is not sufficient to fully explain the gas transport phenomenon.

The data presented in the current work involving orientation and gas transport do not show clear trends. The main problem encountered in the study dealing with orientation was that the surface area of the film was too large to maintain a constant level

of orientation throughout the whole permeation area. A much smaller permeation area should be probed in order to reduce the error in the degree of orientation and in the thickness determinations, and therefore improve the resolution of the gas transport properties. The permeation cell should be modified accordingly. A more sensitive pressure transducer with a lower closed volume should have been used in the permeation apparatus. In addition, the samples should be stretched and cooled directly after stretching inside an internal-fan oven. Moreover, since the gas transport properties of isotropic samples were found to depend on the cooling rate, the cooling rate of oriented samples should be readjusted for each sample depending on the thickness since thinner samples cool faster. Once the experimental conditions have been improved, studies should determine how the physical aging rate of polycarbonate is affected by orientation. Indeed, data presented in the literature have reported an enhanced aging rate for oriented samples, despite of the lower free volume content [29-35].

The results of orientation studies obtained on a particular polymer are unlikely to be generalized to other polymers. Properties such as density and birefringence taken at the same draw ratio have been shown to highly depend on the nature of the amorphous polymer, as reported in a study comparing polycarbonate and PET [36]. It would have been however better to report the results as a function of the Hermans' orientation function rather than as a function of the draw ratio. It is well known, nevertheless, that all the molecular groups do not orient themselves to the same extent [37-40]. And therefore the effect of orientation on the gas transport properties of amorphous polymers may also depend on the structure of the polymer. This remains to be proven.

Further studies dealing with orientation could be carried out. If one could orient the polymer chains parallel to the gas transport direction, clear changes in the gas transport properties may be observed with orientation. The gas molecules may be capable in this case of moving preferentially along the polymer chains. Such a process should require less energy. As a consequence the diffusion coefficient is expected to be increased in those studies while compared with diffusion results obtained with polymer chains oriented perpendicularly to the gas transport direction. Results of biaxial orientation could be compared with those concerning uniaxial orientation. It is well-

established that the physical properties are not affected identically with those two procedures [41].

2 – Other important aspects arise that remain to be answered.

For instance, how are the sizes and the shapes of the free volume cavities affected by the aging process? In the physical aging studies the solubility coefficient of N_2 had a tendency to increase with aging time, whereas that of O_2 remained relatively constant for the same period. However the overall density was observed to increase with aging time in the same observation period, hence indicated a loss of free volume with aging. The experimental data suggest that the solubility coefficient of N_2 was enhanced with aging time, despite of the overall decrease in the free volume content. The results are believed to reflect the dynamics of the redistribution of free volume, and the size and shape of the free volume voids. One explanation would be that large cavities are formed by cavity coalescence (in order to explain the increase in the solubility coefficient of N_2), whereas the free volume sites larger than the size of the N_2 gas molecule and those smaller than the size of the O_2 gas molecule may decrease with aging time. Since the density increases with aging time, the solubility coefficient of N_2 is unlikely to continuously increase with aging time as well. S_{N2} may remain constant or even decrease after a particular time. In order to have a better picture of the aging process after prolonged times, one should study what happens ultimately to the solubility of N_2 (assuming that no crystals develop in the material). Moreover, in order to understand what happens to the redistribution of free volume with time, the polymeric matrix should be probed with gases having a greater kinetic diameter than that of the nitrogen N_2 gas molecule (kinetic diameter of 3.64Å). Possible candidates include methane CH_4 (kinetic diameter of 3.8Å), ethane C_2H_6 (3.9Å), xenon Xe (3.96Å), or propane C_3H_8 (4.3Å). The larger free volume sites may either keep increasing in size or be divided into smaller cavities. On one hand, one would expect that it would be more difficult to maintain large free volume pockets in the material. On the other hand, the physical aging process may apparent itself to the crystallization process. Indeed, the polymer chains adopt the trans-trans conformation with aging [42, 43] and decrease progressively their degrees of freedom, since the diffusion coefficient of N_2 was

clearly reduced with aging time. This could correspond to the pre-stages of the crystallization phenomenon. In semi-crystalline polymers, such as polyolefins with different types and contents of branches, the defects become concentrated in the amorphous regions as the polymer crystallizes. The question as to whether or not the physical aging process resembles the early stages of the crystallization phenomenon remains opened. Knowledge of the redistribution of the free volume sizes and shapes with aging time is important since it may explain the behavior of mechanical properties with aging time, such as the ductile/brittle transition in impact testing for instance.

To our knowledge, only a few papers have dealt with physical aging and the influence of the cooling rate in general. It is necessary to carry out more extensive studies. Our work has shown that the permeability coefficient decreased more for the slowly-cooled sample despite of the lower densification rate. Experiments such as dilatometry, creep or stress relaxation could show opposite behaviors, as observed in aging studies of anisotropic materials [29-35].

The effects of temperature jumps on the gas transport properties should be investigated since changes in temperature can happen industrially on aged samples. The memory effects discovered by Kovacs [44] may also be discernable in permeation experiments.

Physical aging studies could be carried out both below and within the glass transition region for polycarbonate since the SAXS electron density fluctuations were observed to have two different behaviors in those two zones [27]. The free volume distribution could be affected differently depending on whether the aging is performed outside or within the glass transition region.

Furthermore, aging could affect the gas transport properties in a temperature range where other properties such as the density seem invariant. This remains to be proven.

It would also be interesting to determine how pressure densified samples are affected by physical aging. Acceleration of physical aging has been reported in the literature for pressure-densified samples [45]. A reduced local ordering or more

disordered state was noticed by SAXS measurements on additive-free polystyrene samples densified by application of pressure above T_g and its release at room temperature. Despite of the much higher density those samples appeared to have a greater segmental mobility. Enhancement of the aging of the gas transport properties could be possibly observed for pressure-densified samples.

Physically aged instead of fresh polymers could be stretched and the resulting changes in gas transport examined. Knowledge of the effect of stretching on aged samples is important in food packaging for instance since polymeric films are sometimes stored for months before use. Aging could be erased by applying a stress after aging [46].

Since the permeation properties are of commercial interest mainly at room temperature, one needs to have an estimate of the time it takes to see a change in the permeability coefficient. Aging studies are usually carried out at elevated temperatures (but still in the glassy state) in order to predict how the material is going to behave with time at much lower temperatures by extrapolation of the data. However, the densification rate of polycarbonate has been found to increase tremendously after an aging period of about six months at room temperature [16]. Studies need to be carried out to evaluate how (and if) the gas transport parameters are affected by aging at room temperature after about six months. By comparing the permeation results with the density results, any difference between the two would prove once again that there is no direct correlation between the free volume content and the gas transport properties. The absence of crystallinity would have to be verified though.

In order to reproduce the conditions found in industry, aging should also be performed under hydrolytic conditions in order to determine how the performances of the polymeric membranes are affected. Humidity has indeed been shown to highly affect the mechanical properties of polycarbonate [47]. Hydrolytic chain scissions have also been found to occur in polycarbonate [48]. The effect of sunlight on aging could also maybe be investigated if membranes are directly exposed to sunlight.

Studies need to be carried out to investigate the effects of polymer additives (nature, content, distribution) on the gas transport properties, as this may influence the interactions between the polymeric matrix and the gas molecules [49], and hence affect the solubility coefficient and consequently the overall permeability coefficient. The influence of soluble additives such as plasticizers should be radically different from that of non-soluble ones such as fillers.

3 – The nature of the gas transport process in polymers remains so far opened and arises directly from our work.

Since knowledge of the free volume content alone is not sufficient to predict the gas transport properties, one needs to examine all the factors that may influence the gas transport phenomenon. Those factors could be the followings:

- the free volume content
- the free volume distribution
- the polymer chain dynamics
- the polymer chain conformations
- the intra- and the intermolecular distances between polymer chains
- the interactions between the gas and the polymer
- the polymer chemical structure
- the polymer molecular weight and molecular weight distribution

While considering a particular polymer, the polymer local chain dynamics or the local mobility of the polymer chains are likely to be the key factor in predicting the gas transport properties. This suggests to us that dynamic rather than static models should be considered. Computer simulations should be carried out to estimate how the gas transport properties are affected as the conformations of the chains vary, and/or as the polymer degrees of freedom are progressively lost. Nevertheless such simulations are restricted so far by the algorithm chosen to model the transport phenomemon, as well as by the time increments.

Finally, this research work emphasized the fact that free volume and gas transport properties may not be directly correlated. Nevertheless several studies have shown that this relationship is verified when various polymer structures are considered (see Chapter 2 for details). The overall free volume content is calculated from group contribution methods for the various chemical structures and the resulting gas transport coefficients appear to be correlated to this free volume content. However the data points (plotted on a logarithmic scale) tend to be too scattered to draw confident conclusions. In addition, the correlation remains problematic for polymers containing fluorinated groups or polar constituents.

A sufficient amount of free volume may be necessary to allow local motions to take place. We expect that local motions, rather than the free volume content, may be better correlated with the gas properties when one considers various polymer structures. Some literature-based research could be done to verify if the gas transport properties correlate better with the β-relaxation than with the free volume amount calculated from group contribution methods for instance.

Our work has set the basis for the above questions. It could be expected to guide the way for future research directions.

9.3. References

1. J. Y. Park, D. R. Paul, Correlation and prediction of gas permeability in glassy polymer membrane materials via a modified free volume based group contribution method, *Journal of Membrane Science*, 125, 23-39 (1997).
2. Y. Yampolskii, S. Shishatskii, A. Alentiev, K. Loza, Correlations with and prediction of activation energies of gas permeation and diffusion in glassy polymers, *Journal of Membrane Science*, 148, 59-69 (1998).
3. M. H. Cohen and D. Turnbull, *J. Chem. Phys.*, 31, 1164 (1959).
4. J. S. Vrentas and J. L. Duda, *J. Polym. Sci.*, 15, 403 (1977).
5. J. S. Vrentas and J. L. Duda, *J. Polym. Sci.*, 15, 417 (1977).
6. J. L. Duda and J. M. Zielinski, Free-Volume Theory, *Plastics Engineering*, 32, 143 (1996).
7. H. Fujita, *Fortschr. Hochpolym. Forsch.*, 3, 1 (1961).
8. W. M. Lee, Selection of barrier materials from molecular structure, *Polym. Eng. Sci.*, 20, 65-69 (1980).

9. E. R. Hensema, M. H. V. Mulder and C. A. Smolders, On the Mechanism of Gas Transport in Rigid Polymer Membranes, *Journal of Applied Polymer Science,* 49, 2081 (1993).
10. D. R. Paul, Yuri P. Yampol'skii, editors, *Polymeric gas separation membranes*, CRC Press, Boca Raton, 1994.
11. Y. Kobayashi, K. Haraya, S. Hattori, *Polymer*, 35, 925-928 (1994).
12. S. Trohalaki, L. C. DeBolt, J. E. Mark, H. L. Frisch, *Macromolecules,* 23, 813-816 (1990).
13. Y. Maeda and D. R. Paul, Effect of AntiPlasticization on Gas Sorption and Transport. III. Free Volume Interpretation, *Journal of Polymer Science: Part B: Polymer Physics,* 25, 1005 (1987).
14. A. Thran, G. Kroll, F. Faupel, Correlation between fractional free volume and diffusivity of gas molecules in glassy polymers, *Journal of Polymer Science: Part B: Polymer Physics*, 37, 3344-3358 (1999).
15. P. Pekarski, J. Hampe, I Böhm, H.-G. Brion, and R. Kirchheim, Effect of aging and conditioning on diffusion and sorption of small molecules in polymer glasses, *Macromolecules*, 33, 2192-2199 (2000).
16. R. Wimberger-Friedl and J. G. de Bruin, The very long-term volume recovery of polycarbonate: is self-retardation finite? *Macromolecules,* 29, 4992-4997 (1996).
17. U. Kriesten and J. M. Hutchinson, On the use of a density gradient column to monitor the physical ageing of polystyrene, *Polymer*, 33, 22, 4875-4877 (1992).
18. L. C. E. Struik, Physical aging in amorphous polymers and other materials, Elsevier, New York, 1978.
19. P. S. Rallabandi, A. P. Thompson, and D. M. Ford, A molecular modeling study of entropic and energic selectivities in air separation with glassy polymers, *Macromolecules*, 33, 3142-3152 (2000).
20. M. Hedenqvist, A. Angelstok, L. Edsberg, P. T. Larsson and U. Q. Gedde, Diffusion of Small - Molecule Penetrants in Polyethylene: Free Volume and Morphology, *Polymer*, 37, #14, 2887 (1996).
21. W. C. Yu, C. S. P. Sung, R. E. Robertson, *Macromolecules,* 21, 355 (1988).
22. Dr. Hervé Marand, lecture notes.
23. L. H. Sperling, *Introduction to physical polymer science,* Second edition, John Wiley and Sons, 1992.
24. Y.-H. Lin, Entanglement and the molecular weight dependence of polymer glass transition temperature, *Macromolecules*,23, 5292-5294 (1990).
25. Richard P. Wool, *Polymer Interfaces- Structure and Strength*, Hanser Publishers, 1995.
26. H. S. Chan and K. A. Dill, The protein folding problem, *Physics Today*, 24-32, February (1993).
27. J. J. Curro and R.-J. Roe, Isothermal relaxation of specific volume and density fluctuation in poly(methyl methacrylate) and polycarbonate, *Polymer*, 25, 1424 (1984).
28. R.-J. Roe and J. J. Curro, Small-angle X-ray scattering study of density fluctuation in polystyrene annealed below the glass transition temperature, *Macromolecules*, 16, 428 (1983).

29. J. Bartos, J. Muller, J. H. Wendorff, Physical ageing of isotropic and anisotropic polycarbonate, *Polymer*, 31, 1678 (1990).
30. M. D. Shelby and G. L. Wilkes, Thermodynamic characterization of the oriented state of bisphenol A polycarbonate as it pertains to enhanced physical aging, *Journal of Polymer Science: Part B: Polymer Physics*, 36, 2111 (1998).
31. R. Pixa, B. Grisoni, T. Gay, and D. Froelich, Influence of deformation on physical aging of polycarbonate- 2 - Volume recovery near ambient temperature, *Polymer Bulletin*, 16, 381-387 (1986).
32. M.-S. S. Wu, Intrinsic birefringence of amorphous poly(bisphenol-A carbonate), *Journal of Applied Polymer Science*, 32, 3263-3275 (1986).
33. M. D. Shelby and G. L. Wilkes, The effect of molecular orientation on the physical ageing of amorphous polymers - dilatometric and mechanical creep behaviour, *Polymer*, 39, 26, 6767-6779 (1998).
34. J. Muller, J. H. Wendorff, Thermal density- Fluctuations in rejuvenated and aged polycarbonate, *Journal of Polymer Science: Part C: Polymer Letters*, 26, 421 (1988).
35. J.-J. Pesce and G. B. McKenna, Prediction of the subyield extension and compression responses of glassy polycarbonate from torsional measurements, *J. Rheol*., 41, 5, 929-942 (1997).
36. E. Ito, K. Sawamura and S. Saito, Effects of drawing on molecular motions in polycarbonate, *Colloid & Polymer Sci.*, 253, 480-484 (1975).
37. A. Ameri, S. Ekgasit, C. Hendann, S. Michel, P. Wu, S. Okretic, F. Pfeifer, I. Zebger and H. W. Siesler, Towards a better understanding of segmental mobility in polymers under external perturbations: time-resolved FTIR studies, *ACS, Polymeric Materials Science and Engineering, Conference Proceedings*, San Francisco, Spring 1997, 76, 191-2.
38. E. Ito, T. Hatakeyama, Studies of the amorphous region of polymers- II - Relationship between change of structure and glass-transition temperature in polycarbonate, *Journal of Polymer Science: Polymer Physics Edition*, 13, 2313-2320 (1975).
39. A. C. Lunn and I. V. Yannas, Chain-backbone motion in glassy polycarbonate studied by polarized infrared spectroscopy, *Journal of Polymer Science: Polymer Physics Edition*, 10, 2189-2208 (1972).
40. U. S. Despande, G. Thyagarajan, *Indian J. Pure Appl. Phys.*, 20, 846 (1982).
41. Dr. G. L. Wilkes, lecture notes.
42. J. Lu, Y. Wang, and D. Chen, Infrared spectroscopic and modulated differential scanning calorimetry study of physical aging in bisphenol-A polycarbonate, *Polymer Journal*, 32, 7, 610-615 (2000).
43. N. Heymans, FTIR investigation of structural modification of polycarbonate during thermodynamical treatments, *Polymer*, 38, 14, 3435 (1997).
44. A. J. Kovacs, Transition vitreuse dans les polymeres amorphes- Etude phenomenologique, *Fortschr. Hochpolym.- Forsch.*, 394-507 (1963).
45. H. H. Song and R.-J. Roe, Structural change accompanying volume change in amorphous polystyrene as studied by small and intermediate angle X-ray scattering, *Macromolecules*, 20, 2723-2732 (1987).

46. R. P. Chartoff, Thermoplastic polymers, in Thermal characterization of polymeric materials, E. A. Turi, edt, Academic Press, NY, 548-573 (1997).
47. C.-H. Wang, The effect of humidity and temperature on mechanical properties of PC and PC/ABS, *ANTEC'95*, 1946 (1995).
48. I. Ghorbel, F. Thominette, P. Spiteri, J. Verdu, Hydrolytic aging of polycarbonate. I-physical aspects, *Journal of Applied Polymer Science*, 55, 163 (1995).
49. W. R. Vieth, L. H. Dao, and H. Pedersen, Non-equilibrium microstructural and transport characteristics of glassy poly(ethylene terephthalate), *Journal of Membrane Science*, 60, 41-62 (1991).

Vita

Christelle Marie Laot was born on April 4, 1973, in Provins, France. She grew up in the Celtic region of France, in rural Brittany. She was raised with French as her mother tongue rather than Breton as was common for previous generations.

Christelle graduated from high school in 1991 with a Baccalauréat in Mathematics and Physics. She then entered the five-year engineering program at UTC Compiègne in the north-east of Paris, France.

As an undergraduate student, Christelle spent most of her summer vacations working for various companies, mainly in the food industry. Besides her studies, she volunteered for two years to teach Mathematics to children living in poor neighborhoods where French was not the primary language. She also went to Russia for a short period of time thanks to an exchange program with her Engineering School. While working on a six-month European confidential research project (Fall 1994) in R&D for Sicof Inc., France, she got involved in measuring the properties of conductive polymeric coatings. Finally, she was selected by her Engineering School among fourth year students to complete her fifth and last year of her undergraduate education as an exchange student in the United States. She participated in the UTC- VPI&SU exchange program and enrolled in August 1995 in the Master of Science program in Chemical Engineering at Virginia Tech, USA.

After Christelle had successfully defended her Master of Science degree in August 1997, she started to work towards her PhD degree in Chemical Engineering at Virginia Tech with a specialization in polymer science and engineering. She received her Diplôme d'Ingénieur UTC in Process Engineering in November 1997. In July 2000, she left the United States to finish writing her dissertation in Europe. She briefly came back in April 2001 to give her required departmental seminar.

Christelle has been employed since May 2001 as a research scientist at Bayer AG (Leverkusen, Germany) in the Polymer Physics Group.